U.S.N.A. --- Trident Scholar project report; no. 334 (2005)

AN HISTORICAL AND APPLIED AERODYNAMIC STUDY OF THE WRIGHT BROTHERS' WIND TUNNEL TEST PROGRAM AND APPLICATION TO SUCCESSFUL MANNED FLIGHT

by

Midshipman 1/c Michael G. Dodson, Class of 2005
United States Naval Academy
Annapolis, Maryland

_____
(signature)

Certification of Adviser Approval

Assistant Professor David S. Miklosovic
Aerospace Engineering Department

_____
(signature)

_____
(date)

Acceptance for the Trident Scholar Committee

Professor Joyce E. Shade
Deputy Director of Research & Scholarship

_____
(signature)

_____
(date)

USNA-1531-2

REPORT DOCUMENTATION PAGE

Form Approved
OMB No. 074-0188

1. AGENCY USE ONLY (Leave blank)	2. REPORT DATE	3. REPORT TYPE AND DATE COVERED
	18 May 2005	

4. TITLE AND SUBTITLE
An historical and applied aerodynamic study of the Wright Brothers' wind tunnel test program and application to successful manned flight

5. FUNDING NUMBERS

6. AUTHOR(S)
Dodson, Michael G. (Michael Gary), 1983-

7. PERFORMING ORGANIZATION NAME(S) AND ADDRESS(ES)

8. PERFORMING ORGANIZATION REPORT NUMBER

9. SPONSORING/MONITORING AGENCY NAME(S) AND ADDRESS(ES)
US Naval Academy
Annapolis, MD 21402

10. SPONSORING/MONITORING AGENCY REPORT NUMBER
Trident Scholar project report no. 335 (2005)

11. SUPPLEMENTARY NOTES

12a. DISTRIBUTION/AVAILABILITY STATEMENT
This document has been approved for public release; its distribution is UNLIMITED.

12b. DISTRIBUTION CODE

13. ABSTRACT: An active area of research in the robotics community is "swarm control," where many simple robots work together to execute tasks which are beyond the capability of any single robot acting alone. Yet in order for the swarm members to work together effectively they must maintain a reliable and robust wireless communication network among themselves. The goal of this project was to create a motion control law which could fulfill the dual and sometimes conflicting requirements of executing a primary mission (e.g., search and rescue), while maintaining a robust mobile wireless communication network among the swarm members. The success or failure in sending or receiving a wireless message is inherently probabilistic, but the odds of successfully relaying a message increase considerably based upon the spatial arrangement of the swarm members. This imposes a variety of constraints on each robot's motion. Each robot sending a message should: 1. maintain a line of sight to the receiving robot (esp. in an environment like a cave or bunker with dense walls); 2. stay within close proximity of the receiving robot (the range is dictated by the power of the transmitter); and 3. increase the overall redundancy of the swarm by maintaining requirements 1 and 2 for two or more receiving robots simultaneously. To this end, several artificial potential field controllers - a popular method of robotic control - have been developed in this project and simulated to determine their success in controlling the swarm. At a higher level, the project addressed the challenge of composing a motion control law to achieve the primary mission, while maintaining as many communication constraints as possible. This project included a proof-of-concept implementation of the motion control law on real robots. In addition, this project simulated and statistically analyzed the controller to determine its effectiveness at achieving the primary mission and maintaining a robust communication network. The effectiveness of the control law was seen both in simulation and experiment. Overall the robustness of the swarm was increased 200-300% in the scenarios considered.
.
.

14. SUBJECT TERMS:
Swarm robotics, Communication Networks, Artificial potential fields, Line of Sight, Redundancy

15. NUMBER OF PAGES
127

16. PRICE CODE

17. SECURITY CLASSIFICATION OF REPORT	18. SECURITY CLASSIFICATION OF THIS PAGE	19. SECURITY CLASSIFICATION OF ABSTRACT	20. LIMITATION OF ABSTRACT

ABSTRACT

Based on the most accurate surviving description of the Wright Brothers' wind tunnel, a replica was constructed and used to determine the effect flow quality and experimental method had on the Brothers' results, and whether those results were useful in a quantitative sense. The research incorporated static and total pressure measurements, velocity surveys across the jet, and quantitative flow visualization. Velocity surveys involved high resolution dynamic pressure measurements along the horizontal and vertical test section axes. Particle image velocimetry provided velocity magnitudes, turbulence intensities, and vorticity measurements in the test section. Force measurements on an airfoil model supported the conclusions regarding the effect of flow characteristics on aerodynamic measurements.

Testing revealed boundary layers extending 2.5″ from each wall. In the center of the tunnel was a 5″ diameter "dead zone" in which the flow velocity was 20% lower than the maximum tunnel velocity. Isolated pockets of high velocity flow reaching 35 mph existed outside the "dead zone". PIV data revealed asymmetric load distributions on the airfoil due to velocity and vorticity gradients, and indicated the Wrights' lift measurements were at least 7% low due to flow interactions with the lift balance. Direct force measurements showed the Wrights' lift measurements were at least 6% and as much as 15% low depending on the Wrights' true tunnel velocity. Scaling from the tunnel to the Wright Flyer increased the C_L discrepancy by an additional 14% and showed the Wrights' drag prediction to be 300% too high, resulting in highly inaccurate efficiency predictions. Thus, though they learned a great deal from their wind tunnel experiments, the Wrights' quantitative data was not applicable to full scale design.

The conclusions provide insight into the birth of aviation and the men who were the first to succeed despite limitations and deficiencies with their equipment, experience, and knowledge.

Keywords: Wright, Flyer, Wind Tunnel, Kitty Hawk

ACKNOWLEDGEMENTS

First I would like to thank my advisor, Assistant Professor David Miklosovic, whose attention, expertise, and guidance keeps us driving toward our goal. The hours he commits to the project are invaluable to its successful completion. I would also like to thank Professor Joyce Shade for the time and effort she puts in to supporting and promoting the Trident Scholars, and the rest my Trident Sub-Committee, Professor Robert Ferrante, Lieutenant Brett St. George, USN, and Professor Peter Andre, for their input and for the opportunity to continue my research.

A special thanks goes to Admiral Frank Bowman, USN, and the C.J. Mack Family Foundation for their support and funding of Midshipman research.

Without the help of the technical staff in the Low Speed Aerospace Laboratory my research would be impossible. Mr. Richard Garman is always willing to take time away from rebuilding his facilities to support my testing. Mr. Rusty Foard provides valuable aide and suggestions for construction and testing. Mrs. Louise Becnel makes all my purchasing easy, and puts any equipment in her fluids lab at my disposal.

Many thanks go to the technical staff in the machine shop who built my wind tunnel while simultaneously trying to recover equipment and power after Hurricane Isabel. The shop supervisor, Mr. Tom Price, was very helpful, and would always make someone available to fill my work orders. Mr. Earl Fox built the tunnel box, and was infinitely patient with my continuous changes and additions. Mr. George Burton shaped the tunnel contraction, and spent hours building the metal honeycomb by hand since his equipment was out-of-commission. Finally, Mr. Michael Superczynski was a constant source of ideas, improvements, and education.

The input and enthusiasm from Drs. John Anderson and Peter Jakab at the National Air and Space Museum, Smithsonian Institution, was a great aide to my historical research. The contrast of their backgrounds provided me with a unique and broad perspective on the Wright Brothers' work.

I would also like to thank Professor Daryl Boden and Associate Professor Gary Fowler who kept the Trident Scholars focused on our long term goals and provided insight and perspective we otherwise would not have obtained.

TABLE OF CONTENTS

LIST OF FIGURES

LIST OF TABLES

LIST OF EQUATIONS

1 INTRODUCTION

On December 17th, 1903 a telegraph arrived at the Wright household:

SUCCESS FOUR FLIGHTS THURSDAY MORNING ALL AGAINST TWENTY ONE MILE WIND STARTED FROM LEVEL WITH ENGINE POWER ALONE AVERAGE SPEED THROUGH AIR THIRTY-ONE MILES LONGEST 57 SECONDS INFORM PRESS HOME CHRISTMAS[1]

This short and seemingly insignificant message was the first announcement of an event which changed the world forever. Orville and Wilbur Wright had successfully achieved sustained, manned flight for the first time in human history[2]. Though excited, they were not surprised. The Brothers were confident that they had carefully planned, designed, and tested every aspect of their Flyer, and that success was imminent.[3]

In designing the first successful airplane, the Wright Brothers were on the leading edge of one of the greatest technological paradigm shifts in modern times. Their intuitive engineering approach allowed them to develop innovations to solve an old problem. However, they made several critical design decisions based on partial information, imprecise results, and even complete misunderstanding,[4] leading to the two possible conclusions:

i) They were extremely lucky in making the right decisions at crucial points in the design evolution, or
ii) They were extremely astute in recognizing the limitations of their experiments and the shortcomings or their results, and compensated accordingly.

Though the latter potentially says far more about the Wrights' engineering expertise than if they had all the technical information required to design and build an effective airplane, their success is endorsed by both conclusions: they put themselves in a position to be lucky based on diligence in performing detailed aerodynamic measurements, intuition in interpreting their results, and application of the results in an appropriate manner.

The Brothers made significant strides in advancing the state of the art, even going so far as to develop and compile their own aerodynamic data base from wind tunnel measurements. This wind tunnel research was the key to the Wrights' success. From this research they gained all the

---

[1] Marvin W. McFarland, ed., The Papers of Wilbur and Orville Wright, vol. 1 (New York: McGraw-Hill Book Company, Inc., 1953), 397.
[2] Charles H. Gibbs-Smith, Aviation: An Historical Survey from its Origins to the end of World War II, (London: Her Majesty's Stationary Office, 1970), 101.
[3] McFarland, Papers, 393.
[4] John D. Anderson, Jr., A History of Aerodynamics and Its Impact on Flying Machines, (New York: Cambridge University Press, 1997), 209: Anderson notes the Wrights' initial errors in their glider calculations were due to the use of an incorrect value of the Smeaton Coefficient, a misunderstanding of the effects of camber location, and a general lack of knowledge regarding aspect ratio, scaling, and Reynolds number.

qualitative tools they needed to successfully design and fly a manned airplane. However, due to numerous design flaws and a general lack of understanding of fluid flow fundamentals, the configuration of the Wrights' wind tunnel and the flow quality it engendered were poor. Additionally, since the Wrights were not aware of the tunnel's flaws, their testing method further detracted from the quality of their results. Therefore, the present historical and applied aerodynamics study of the Wrights' wind tunnel test program will show that the applicability of their results was limited to qualitative trends, rather than a quantitative basis for aerodynamic design.

1.1 Basic Wind Tunnel Testing

1.1.1 Purpose

The purpose of a wind tunnel is to test aerodynamic concepts in a controlled environment using visualization and/or measurement techniques. A quality wind tunnel moves a uniform flow of air over a model while minimizing interference and turbulence which can adversely affect results. There is usually some means of measuring and recording the aerodynamic forces and moments on the test model, and these will be corrected for known imperfections in the tunnel.[5] Furthermore, visualization equipment, such as smoke or micro tufts, can be used to gain a visual representation of the motion and effect of the flow.[6]

1.1.2 Description of a Modern High Quality Wind Tunnel

Wind tunnels generally have five distinct regions: an inlet and settling chamber, a contraction, a test section, a diffuser, and a driver section. Figure 1.1 gives the basic layout of a modern tunnel. Design of the inlet and settling chamber involves bringing air into the tunnel with the least turbulence. Usually the edges of the inlet are rounded to prevent flow disturbances caused by a sharp leading edge. Just after the inlet, the settling chamber conditions the flow before it enters the contraction. The inlet takes large turbulent vortices present in the air and divides it into smaller and smaller turbulent vortices through the honeycomb, screens, and straightening vanes which make up the inlet.

[5] Jewel B. Barlow, William H. Rae, Jr., and Alan Pope, Low-Speed Wind Tunnel Testing: Third Edition, (New York: John Wiley & Sons, Inc., 1999), 62.
[6] Barlow, Testing, 35.

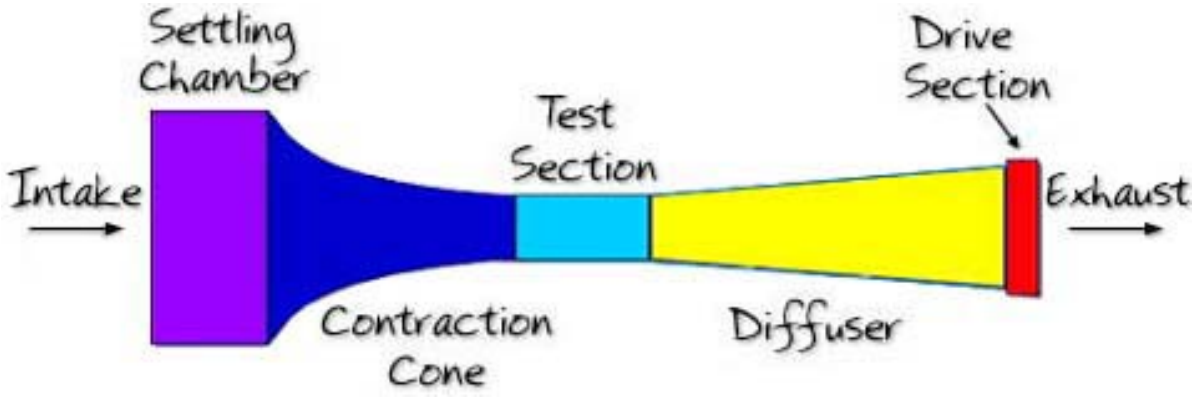

Figure 1.1. Diagram of the major sections of a modern wind tunnel

Once the vortices are reduced by an acceptable amount, the contraction uniformly accelerates and straightens the flow to the desired velocity. Barlow, Pope and Rae, in *Low Speed Wind Tunnel Testing* specify that a contraction should have a uniform cross section, and that the settling chamber before it should be at least as long as half the diameter of the contraction.[7]

Following the contraction is the test section which contains the test article and measurement equipment. Ideally, the test section will have a uniform, steady velocity profile, no up or cross-flow, and minimal turbulence. To compensate for boundary layer and buoyancy effects, the cross section should be slightly increased along the test section. Barlow, Pope and Rae recommend the walls canted outward approximately 1/2° each to provide this increase. Additionally, the test article should be less than 80% the width of the test section to minimize wall interference effects, and the test section should be about 50% wider than it is tall for the same reason.[8]

The diffuser follows the test section and its purpose is to expand the flow and recover the flow pressure by decreasing the flow velocity. A well-designed diffuser will maintain high quality flow upstream by preventing flow separation as the air expands. A high adverse pressure gradient in the diffuser will force the flow to separate causing turbulence and unsteadiness to propagate upstream into the test section.[9]

Finally, the driver section, which consists of a fan and straightening elements, should be downstream of the model and have some means of preventing swirl in the flow. Common methods such as two counter-rotating fans, pre-rotating vanes ahead of the fan, or vertical straightening vanes after the fan are used to keep the flow straight and uniform.[10]

---

[7] Barlow, Testing, 97.
[8] Barlow, Testing, 123.
[9] Barlow, Testing, 120.
[10] Barlow, Testing, 102.

1.2 The Wright Brothers' Wind Tunnel

1.2.1 Wind Tunnel Description

There were at least ten wind tunnels built before the Wrights', starting with Francis Wenham who conducted tests with an "artificial current" in 1870,[11] but the Wrights were the first to attempt accuracy high enough to apply their results directly to design. Despite this, the Wrights' wind tunnel was flawed in many respects due to their lack of understanding of fluid mechanics. Figure 1.2 and Figure 1.3 are photographs of the first replica (1938) of the Wright tunnel at Greenfield Village.

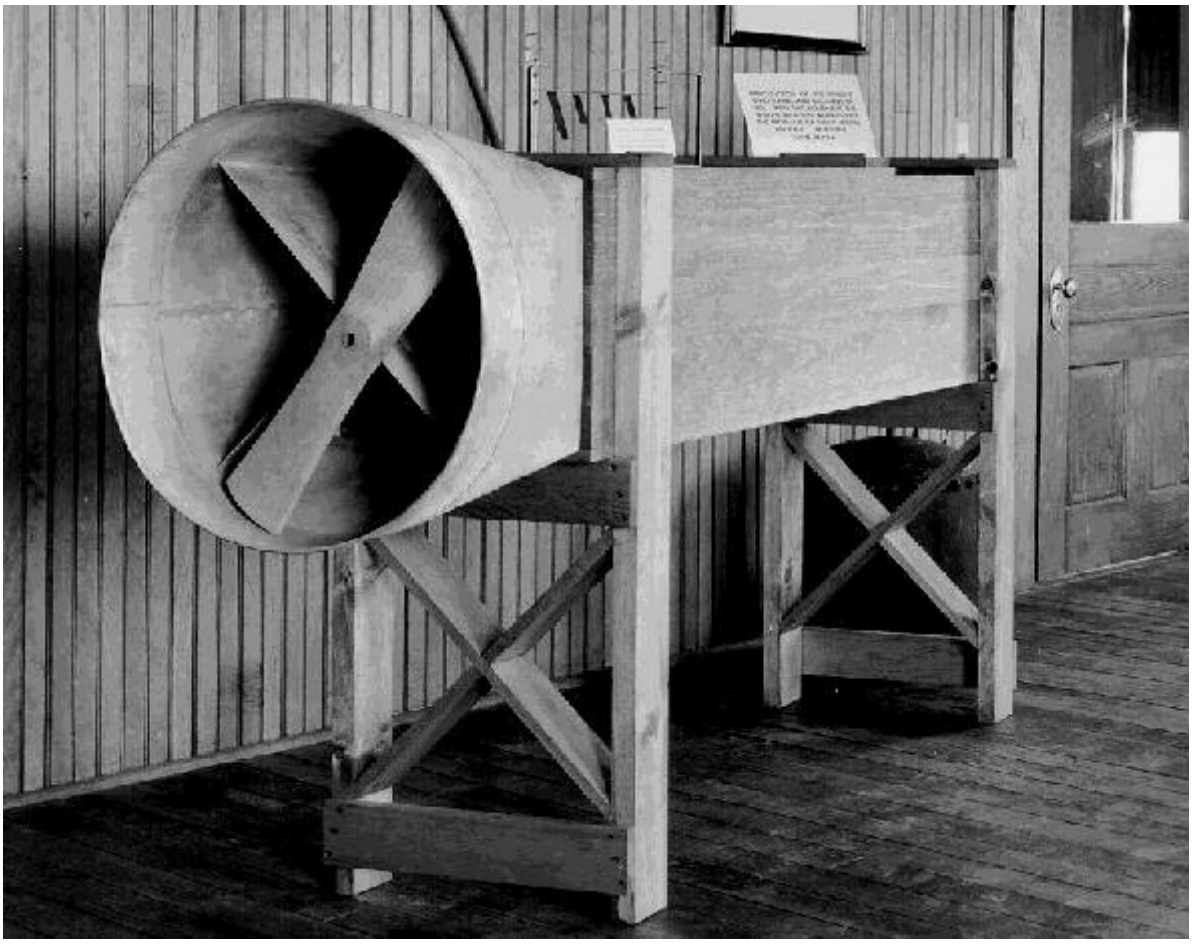

Figure 1.2. View of Wright tunnel replica showing fan location without motor mount[12]

[11] Anderson, History, 122.
[12] "Wind Tunnel Front," Wright Aeroplane Company, n.d., <http://www.first-to-fly.com> (30 Nov 2004).

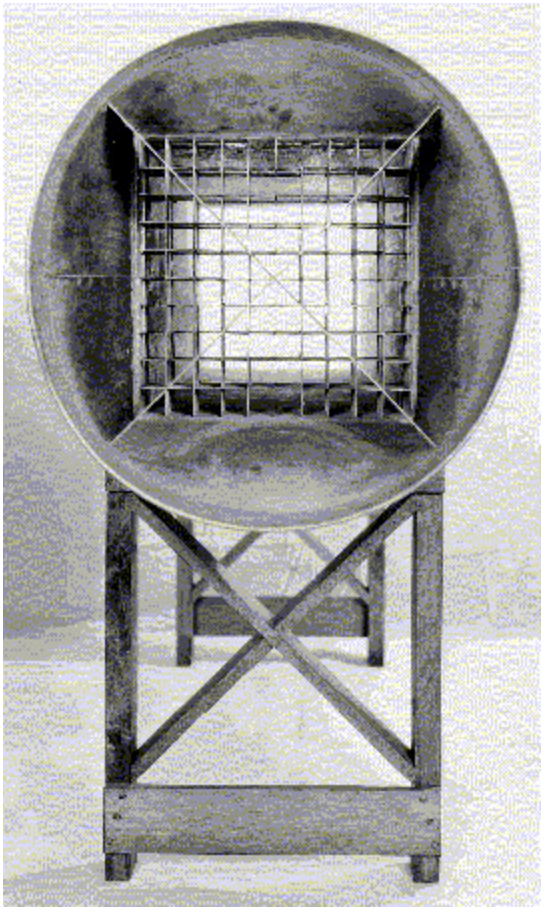

Figure 1.3. Front view of 1938 replica without fan or motor mount[13]

Looking at the front of their tunnel, one of the Brothers' biggest mistakes is apparent: the driver section blows air into the tunnel. The propeller, mounted to a box in front of the tunnel, is shrouded by a collar on the contraction. The box itself presents a problem. As each blade passes in front of the box, there is no longer a source of air for it to blow into the tunnel. Not only will this generate non-uniform flow entering the tunnel, but will result in oscillations as the blade in free air generates thrust while the blade in front of the box does not.[14] Additionally, the flow is pulled around the outside of the shroud which, according to research conducted at Old Dominion University, results in separated flow as the air passes through the propeller into the contraction. [15]

The contraction is made up of a circular inlet with a square exit. Flow conditioning occurs within the contraction, rather than before, thus all means of straightening or improving the flow uniformity occur while the flow is being accelerated. The conditioning is accomplished by a

---

[13] "Wind Tunnel End View," Wright Aeroplane Company, n.d., <http://www.first-to-fly.com> (30 Nov 2004).
[14] Kurt Wolko, "Wright 1901 Wind Tunnel," Plans drawn for the National Air and Space Museum, Smithsonian Institution (1983).
[15] Colin P. Britcher, Rafaello Mariani, Pat Craig, Jill Gillespie, Mudit Monsi, Darius Luna, and Mark Sykes, "Analysis of the Wright Brothers Wind Tunnel and Design of an Educational Derivative," AIAA Paper 2004-1141, Jan. 2004.)

short honeycomb and crossed vanes which straighten the flow but do not necessarily improve flow uniformity. In fact, as non-uniform flow is pushed into the contraction from the propeller, the crossed vanes will sectionalize the flow, preventing it from becoming uniform before entering the test section.

The test section is a constant cross section, 16″x16″ square which continues 60 inches from the end of the contraction and ends abruptly. The tunnel does not have a diffuser; the flow passes through the test section and returns immediately to atmospheric pressure.[16]

1.2.2 Wright Brothers' Wind Tunnel Testing Methods

Besides flaws in the tunnel design, the Wrights' methods also inadvertently contributed to the poor flow and results.

Though the Wrights did not record their method for determining the quality of their flow, one can assume what means they used with reasonable accuracy since those means available to them were limited. To measure velocity, the Wrights most likely used a hand held anemometer: essentially a fan blade and a dial which showed how fast the fan was turning when acted on by a flow.[17] They could have used this to ensure uniformity of the exit flow by testing velocities at different points in the exit plane. However, the anemometer would have produced inherently skewed results of which the Wrights were not aware. The presence of the anemometer in the flow would have resulted in interference, changing the flow properties in all directions and causing the velocity reading to be inaccurate. This effect would be amplified if the Wrights either reached into the test section or mounted the anemometer in the test section, rather than just testing the exit velocity. Because the Wrights misunderstood fluid mechanics and the propagation of "information" throughout a subsonic flow, they could not have understood the consequences of their anemometer use.

To test flow directionality the Wrights most likely used tufts: small pieces of light string which could be mounted to the walls of the tunnel, or moved to different points in the flow at the end of a "tuft wand". The Wrights could observe if the tufts were flying straight back, indicating straight flow, or off to one side or the other, indicating directional flow. The Wrights spent a fair amount of time trying to straighten the flow[18] through their tunnel and may have achieved their goal, but with only these test methods at their disposal, straight flow was by no means quality flow.[19]

The Wrights measurement and data collection also presented problems. The Wrights used large balances to which their airfoils were mounted (Figure 1.4), and these interfered with the

---

[16] Kurt Wolko, "Wright 1901 Wind Tunnel," Plans drawn for the National Air and Space Museum, Smithsonian Institution (1983).
[17] McFarland, Papers, 55.
[18] Wilbur Wright, "Letter to George C. Spratt," 19 Oct 1901, Personal correspondence (05 Aug 04).
[19] Colin P. Britcher, Rafaello Mariani, Pat Craig, Jill Gillespie, Mudit Monsi, Darius Luna, and Mark Sykes, "Analysis of the Wright Brothers Wind Tunnel and Design of an Educational Derivative," AIAA Paper 2004-1141, Jan. 2004.)

uniformity of the flow in the same manner as would an anemometer. The sheet metal and bicycle spokes used in constructing the balances would create large disturbances, generating drag and affecting the flow upstream. Consequently, this would result in turbulent, non-uniform flow over the airfoil being tested.

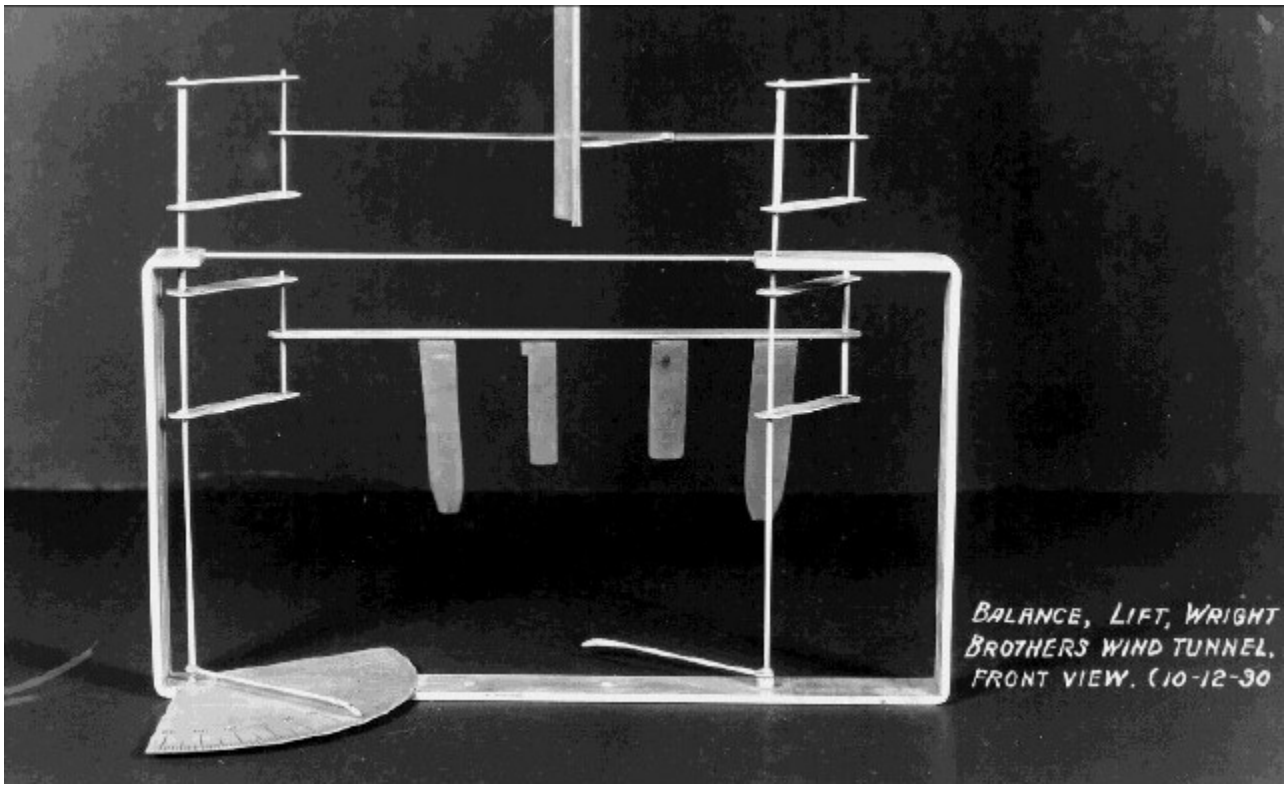

Figure 1.4. Front view of Wrights' lift balance with mounted airfoil[20]

Additionally, the airfoils tested were mounted high in the tunnel, partially immersed in the upper boundary layer generated by frictional effects. So, in addition to the flow being perturbed by the balances, the boundary layer would create uneven velocity and pressure distributions over the airfoil. Finally, the lack of a diffuser would generate turbulence and non-uniformity upstream as high velocity flow impacted the still air outside the exit plane. The Wrights chose to mount their airfoils only inches ahead of the exit plane, putting them in the region most affected by the propagation of turbulence forward from the exit plane.

1.3 Anticipated Effect on Wind Tunnel Results

Many of the design aspects of the wind tunnel are detrimental to the quality of the flow. The fan, upstream of the test section, generated turbulence and swirl. The poorly designed contraction would contribute to turbulent rather than uniform flow. The honeycomb helped remove the

[20] "1901 Lift Balance," Wright Aeroplane Company, n.d., <http://www.first-to-fly.com> (30 Nov 2004).

radial motion caused by the fan, but the crossed vanes sectionalized an already non-uniform flow. With no further means to improve the flow before the test section, this non-uniform, unsteady, turbulent flow interacted with the test model.

Additionally, the design generated large frictional effects, creating a large boundary layer which increased axially along the tunnel. The increasing boundary layer would decrease the effective cross sectional area of the tunnel, affecting the uniformity of flow. The lack of a diffuser generated turbulence, separation, and non-uniformity in the test section as well.

Further contributing to the potential for poor results is the method of test. The intrusive nature of the Wrights' balances decreased the quality of flow in the test section by generating turbulent, non-uniform, directional flow. By mounting the airfoils high in the tunnel, there would be a non-uniform velocity profile over the span of the wing.

Considering the design and method of test, the quantitative results from the tunnel will not be accurate enough for direct application to full scale flight. This does not rule out the immense amount of qualitative knowledge gained from this tunnel, and the impact it had on the Wrights' designs. However these inadequacies seriously inhibit the direct application of any results, in any reliable manner, to the quantitative design of a successful flying machine.

2 HISTORICAL BACKGROUND

2.1 Approach to design

The wind tunnel research conducted by the Wrights was the greatest reason for their ultimate success; however, the systematic engineering approach the Wrights used in all of their work, rather than the quantitative merits of their experiments, was what allowed them to gain so much from that research.

2.1.1 Aircraft Development/Progression

Looking at the big picture, the Wrights' progression from an 1899 kite to the 1903 Flyer followed an evolution which other would-be-aviators did not consider: they kept the configuration largely the same.[21] While the 1903 Flyer was not a mirror image of the 1899 glider, their relationship is clear and the major aspects, such as the biplane configuration, Pratt truss, canard, and wing warping controls, remained relatively constant (Figure 2.1 through Figure 2.5).

At the time, experimenters in aerodynamics would test a design, it would fail, and they would develop a whole new design; it was almost entirely a random trial-and-error process. The Wrights, on the other hand, applied each new lesson in aeronautics to their original design, making small adjustments and changes, and eventually converged on a successful airplane. For example, as they began to understand adverse yaw they added a rudder to counteract the effect. When their wind tunnel research made the benefits of aspect ratio apparent to them, they changed the scale of their wings. Similarly, as they learned how the center of gravity affected the stability and control of the aircraft they redistributed weight accordingly.[22] Through this evolution, which Dr. Peter Jakab calls a "continuity of design," the Wrights were able to succeed where others had failed.[23]

---

[21] Peter Jakab, Visions of a Flying Machine (Washington: Smithsonian Institution Press, 1990), 5.
[22] Frederick J. Hooven, "The Wright Brothers' Flight-Control System," Scientific American, November 1978, 166.
[23] Jakab, Visions, 5.

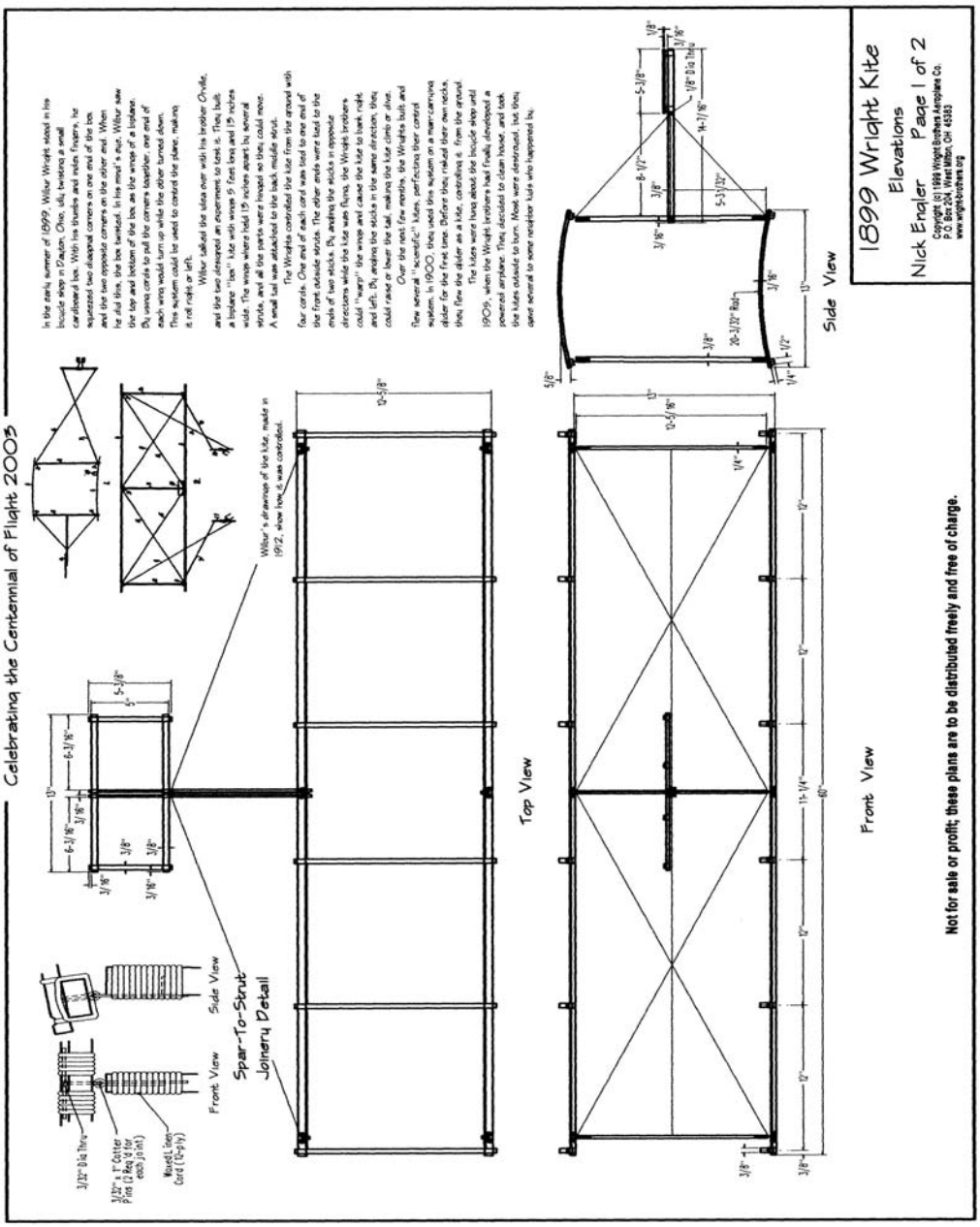

Figure 2.1. Three-view of 1899 kite[24]

[24] "The 1899 Wright Kite," Wright Aeroplane Company, n.d., <http://www.first-to-fly.com> (30 Nov 2004).

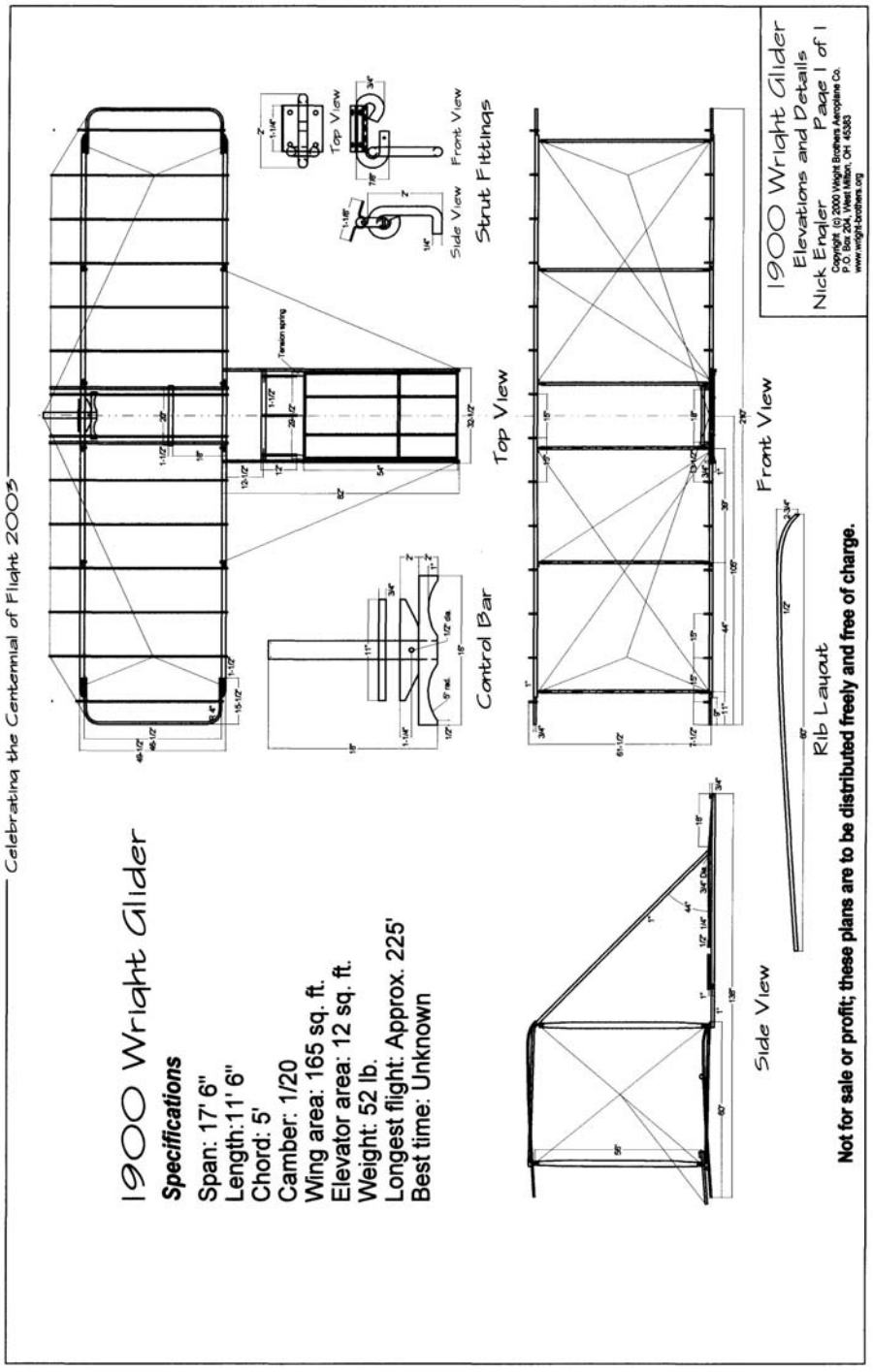

Figure 2.2. Three-view of 1900 glider and airfoil cross section[25]

[25] "The 1900 Wright Glider," Wright Aeroplane Company, n.d., <http://www.first-to-fly.com> (30 Nov 2004).

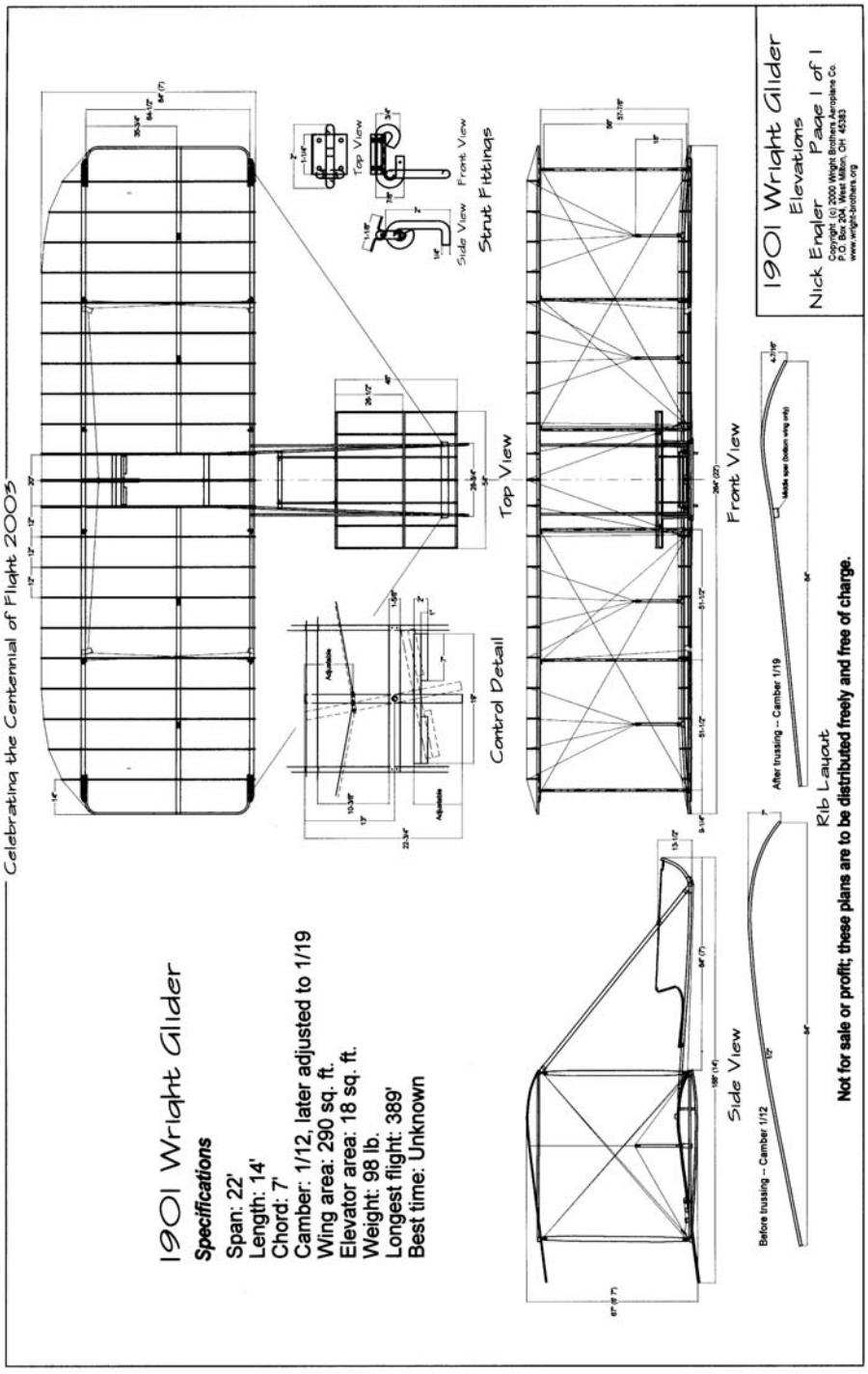

Figure 2.3. Three-view of 1901 glider and airfoil cross sections[26]

[26] "The 1901 Wright Glider," Wright Aeroplane Company, n.d., <http://www.first-to-fly.com> (30 Nov 2004).

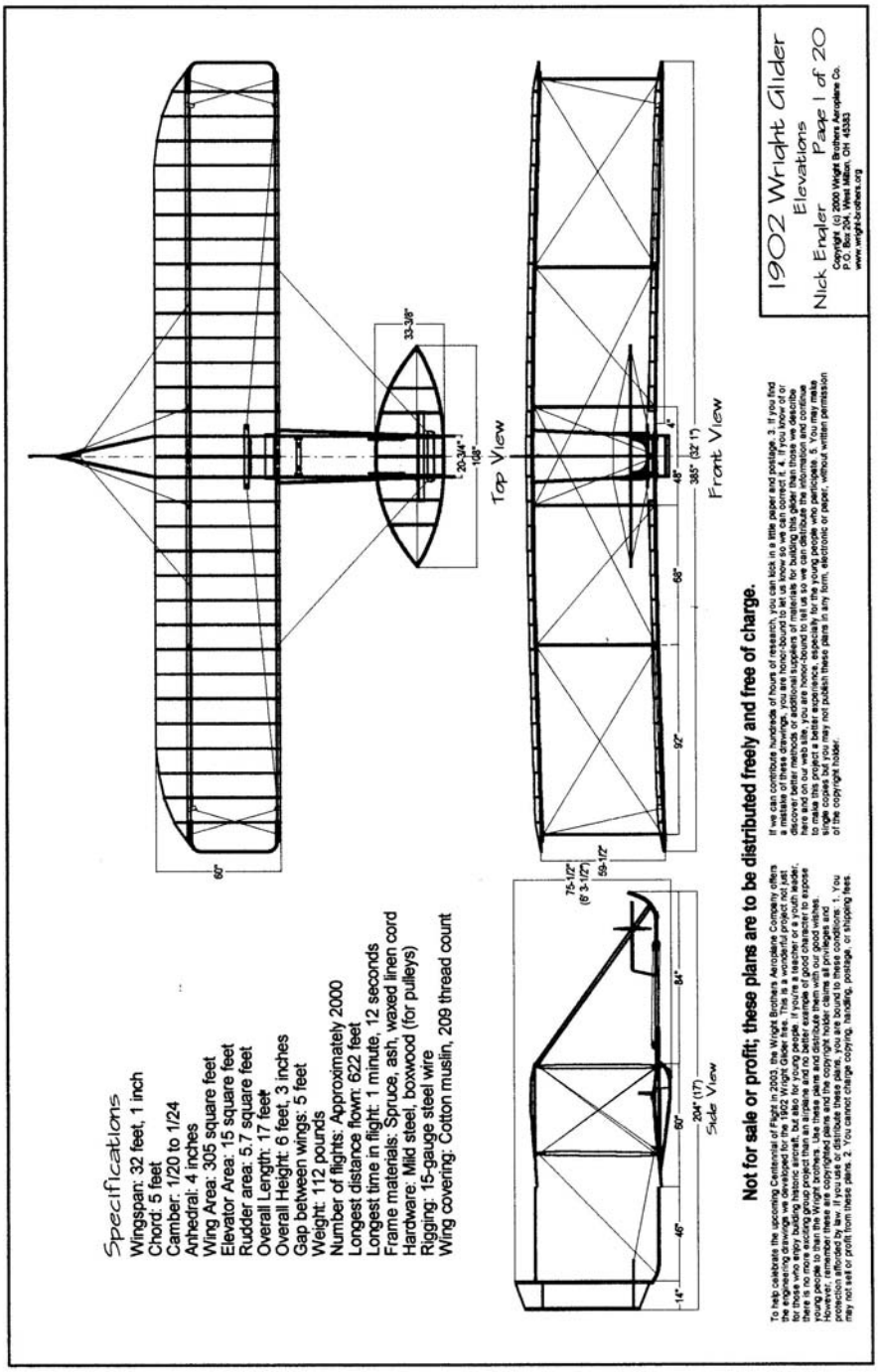

Figure 2.4. Three-view of 1902 glider and airfoil cross section[27]

[27] "The 1903 Wright Flyer 1," Wright Aeroplane Company, n.d., <http://www.first-to-fly.com> (30 Nov 2004).

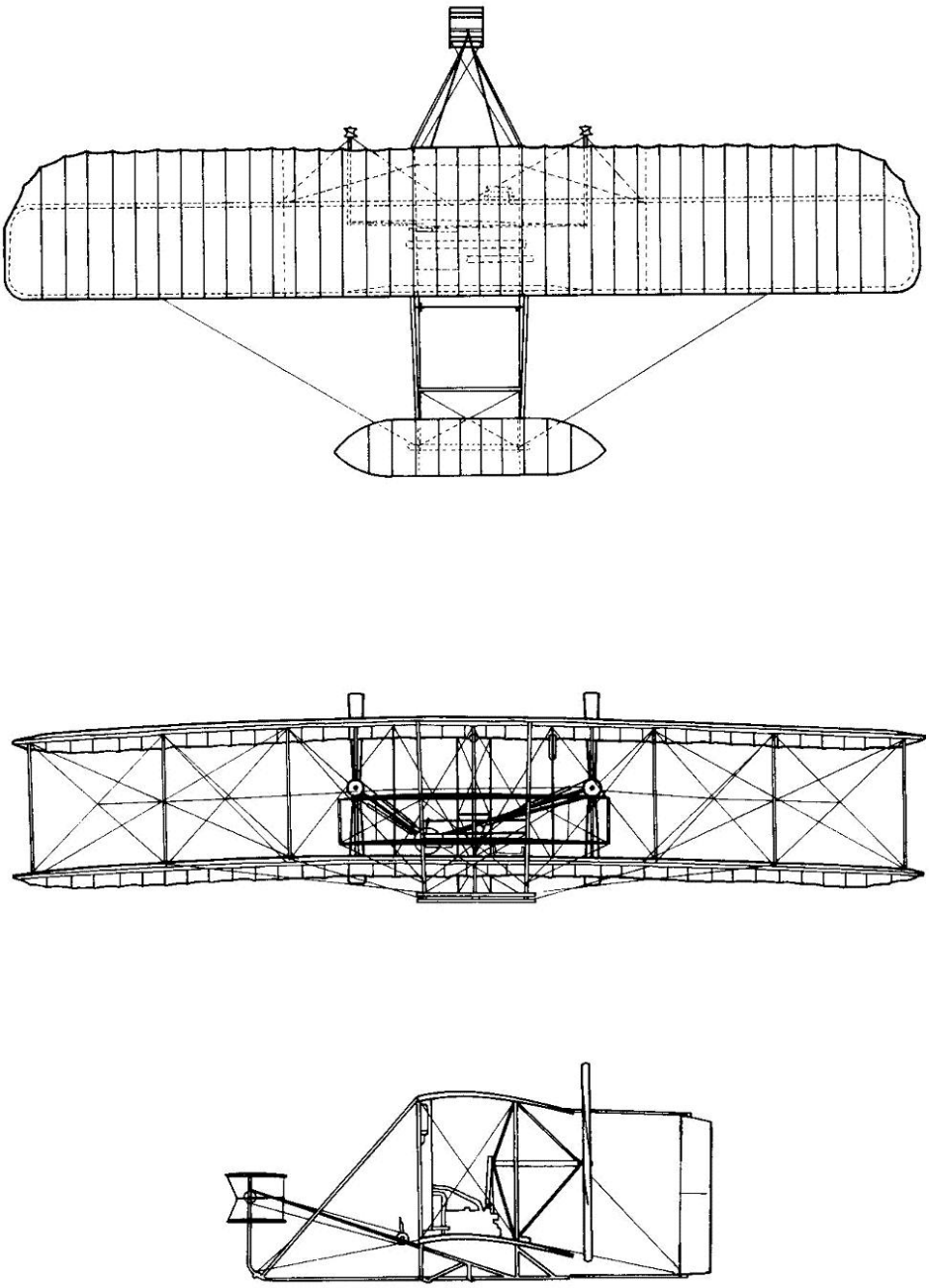

Figure 2.5. Three-view of 1903 Wright Flyer 1[28]

The figures of the Wrights' kites, gliders, and Flyer clearly show the consistency of their overall design. The 1899 glider (Figure 2.1), made to test the concept of wing warping, initiated the idea of a biplane design which remained throughout the four year evolution. The 1900 glider (Figure 2.2) is the first to show the characteristics which marked the Wrights' experiments for years: the

[28] "The 1903 Wright Flyer 1," Wright Aeroplane Company, n.d., <http://www.first-to-fly.com> (30 Nov 2004).

Pratt truss, and the canard. The Pratt truss used the vertical struts and diagonal cables to provide rigidity to a biplane configuration. They modified the truss to allow for wing warping, and maintained the design through the Flyer and beyond.[29] The Wrights chose a canard design in hopes of avoiding the fate of Lilienthal who was killed when his glider stalled and plummeted nose first into the ground. Though they did not understand the aerodynamics behind their success with the canard, they used variations of the canard until well after their 1903 success.[30] Additionally, the Wrights designed their 1900 glider for a pilot who lay prone instead of one who sat up, [31] which the Wrights reasoned would reduce drag; they maintained this aspect of the design through the 1903 Flyer as well.[32]

The actual changes from one year to the next were small but notable, since each indicated some new bit of knowledge or understanding. Very little changed between 1900 and 1901 (Figure 2.3) except the glider was larger and had greater camber. The Wrights were attempting to increase the lift produced by the glider, so while they maintained the overall design, they changed certain variables (i.e. camber and planform area) to generate an anticipated result.[33]

1902 (Figure 2.4) was a huge leap for the Brothers because of the information they gleaned from their wind tunnel experiments. They now understood the factors that affected lift distribution and designed their glider accordingly. Notably, the visual design remains very similar to the previous designs: the biplane configuration with canard, supported by a modified Pratt truss. Visually, one notices a vertical rudder was added which counters the effects of adverse yaw, discovered in the 1901 flight tests. Some other modifications were less obvious and involved increased aspect ratio, decreased camber, and a larger canard with tapered edges, the effects of which they finally understood after their wind tunnel tests.[34]

Finally, the 1903 Wright Flyer (Figure 2.5), which achieved success on 17 December 1903, still maintained many of the design characteristics of the 1900 glider, along with the modifications made along the way. Again, the biplane with the canard and Pratt truss is unchanged. A second surface has been added to the rudder and canard to improve their control authority, and certain modifications have been made to compensate for the motor, linkage, and propellers, but the overall design is the same as their first glider.[35] This consistency through their design process, isolating problems and making small modifications, carried them to the success they achieved in 1903.

2.1.2 Influences

---

[29] Jakab, Visions, 5.
[30] Fred E.C. Culick, "What the Wright Brothers Did and Did Not Understand About Flight Mechanics—In Modern Terms," AIAA Paper 2001-3385, Jul. 2001,21
[31] McFarland, Papers, 61.
[32] Fred E.C. Culick, "What the Wright Brothers Did and Did Not Understand About Flight Mechanics—In Modern Terms," AIAA Paper 2001-3385, Jul. 2001, 21
[33] Jakab, Visions, 5.
[34] McFarland, Papers, 174.
[35] "The 1903 Wright Flyer 1," Wright Aeroplane Company, n.d., <http://www.first-to-fly.com> (30 Nov 2004).

There were many individuals who influenced the work and success of the Wrights, either through their own work, their ideas, their criticism, or simply their support.

2.1.2.1 Lilienthal

The man responsible, indirectly, for sparking the Wrights' interest in aerodynamics was Otto Lilienthal. Known as the "Glider Man," Lilienthal was the first to realize men must understand the dynamics of flight before powered flight could succeed. He believed such understanding would come from testing the medium. To improve his own understanding he made thousands of glides in machines of his own design until a crash in 1896 ended his life.[36] Despite the tragedy, his aerial exploits piqued the interest of the Brothers and in 1899 they began their quest to finish what Lilienthal had begun, and they began building gliders of their own in order to understand the medium.

In addition to sparking their interest, Lilienthal's work was also the basis for the Wrights' early experiments. They used his extensive tables for lift and drag to design and build their 1900 and 1901 gliders and predict their performance.[37] Similarly, they followed his lead in realizing the need for a horizontal surface to maintain a constant angle of attack, but decided to design it as a canard rather than a tail in an attempt to avoid the nose down plummet which killed Lilienthal.[38]

Finally, it was in part due to their enormous respect for Lilienthal's work that they ignored the work of other aerodynamicists who contradicted Lilienthal in any way, such as Samuel Langley. Langley was a well respected scientist and aerodynamicist, but the Wrights had no faith in his published works. Contrary to Lilienthal's experiments and publications, Langley steadfastly refused to state the superiority of cambered airfoils though he used them on his models. Many aerodynamicists, including the Wrights, felt this obvious inconsistency was a reflection on the quality of all his work and conclusions.[39] Additionally, Langley did not believe gliding was a necessary precursor to flight which was the entire philosophy behind Lilienthal's work. These disputes, among others, drove the Wrights away from Langley and the aerodynamic knowledge he had to offer.

2.1.2.2 Langley

Samuel P. Langley's influence on the Wrights, as mentioned above, is based on their inattention, rather than attention to his work. In 1891 Langley had published information about center of pressure travel on cambered airfoils, the benefits of high aspect ratio,[40] and the proper value of the Smeaton coefficient.[41] The Brothers had access to his works, and had they applied this knowledge they would have had much greater success with their 1900 and 1901 gliders. They had used the wrong value of the Smeaton coefficient to predict the lift and drag of their gliders,

---

[36] Anderson, History, 155.
[37] Anderson, History, 148.
[38] Jakab, Visions, 69.
[39] Anderson, History, 180.
[40] Anderson, History, 171.
[41] Anderson, History, 168.

and had no concept of aspect ratio resulting in the poor lifting characteristics of their gliders.[42] However, Langley also touted "Langley's Law," and refused to state the superiority of cambered airfoils over flat plates, both of which caused many interested aerodynamicists to doubt the usefulness of his results and conclusions.[43] Fortunately, the Wrights were part of this group who ignored Langley's experiments;[44] had the Wrights thought Langley was a valuable source of aerodynamic data, they would have had much greater success with their early gliders, but may never have conducted their wind tunnel experiments. Though it cannot be known for certain, without the qualitative knowledge gained from their wind tunnel tests, the Brothers may never have successfully achieved manned flight.

2.1.2.3 Chanute

Octave Chanute had greater influence on the Wright Brothers than any other person and was the catalyst which drove them to success. He contributed information, ideas, money, and constructive criticism, but his primary influence was in dictating they way in which the Brothers received their education in aerodynamics.

The Brothers began receiving initial information from the Smithsonian before contacting Chanute, such as certain pamphlets along with Langley's *Experiments in Aerodynamics.*[45] They even conducted their first flight test in 1899, applying their wing warping technique, before making direct contact with Chanute.[46] Despite the initial lack of direct contact, they were well aware of Chanute's work, and read his book, *Progress in Flying Machines,* as well as his contributions to the *Aeronautical Annual*, before they decided to contact him.[47] In fact their initial designs for the 1899 kite were based on his biplane design,[48] and their wing warping technique may have been adapted from a discussion in the *Aeronautical Annual* on bird flight.[49] In early 1900, when the Wrights began their regular correspondence with Chanute, his first influence was to emphasize certain material, such as his own writings in the *Aeronautical Annuals,* and the *Aeronautical Journal.*[50]

Chanute had a direct influence not only on what the Wrights considered good information, but also what they did not bother to study. For example Chanute was the other major influence which directed the Brothers away from Langley. The Wrights related to a fellow experimentalist, George C. Spratt, in a June 1903 letter that Chanute and the Brothers agreed Langley's works were not of great value.[51] Chanute's de-emphasis of Langley's *Experiments in Aerodynamics* meant the Wrights were not exposed to Langley's understanding of aspect ratio, and his accurate

---

[42] Anderson, History, 210.
[43] Anderson, History, 179.
[44] Anderson, History, 179.
[45] McFarland, Papers, 5.
[46] McFarland, Papers, 9.
[47] McFarland, Papers, 5.
[48] McFarland, Papers, 7.
[49] James Means, ed., The Aeronautical Annuals – 1896, (Boston: W. B. Clarke & Co., 1896), 73.
[50] McFarland, Papers, 19.
[51] Wilbur Wright, "Letter to George C. Spratt," 28 Jun 1903, Personal correspondence (05 Aug 04).

value of the Smeaton coefficient,[52] both of which plagued the Wrights gliders in 1900 and 1901, and forced them to accumulate their own tunnel data in 1901. Chanute's mistrust of Langley's research may have involved an element of competition, but was more likely due to Langley's constant touting of "Langley's Law," which made a conclusion about the velocity-power relationship that most scientists found absurd.[53]

Beside his initial contribution to and guidance of their education, Octave Chanute also provided invaluable support, confidence, and occasional financial backing to the Brothers. While this seems trivial initially, it is important to remember the Wrights were conducting their experiments for their own personal gratification, and often could not take time away from the bicycle shop,[54] or did not have the money to progress further with experiments.[55] Even when the Wrights' aeronautical understanding advanced beyond what Chanute could follow, he still provided an invaluable push to the Brothers,[56] and kept them moving toward successful flight.

2.1.2.4 Others

There are certain people who had a smaller, but notable impact on the Wrights' aerodynamic success, primarily George Spratt and Edwin Huffaker.

Spratt was an aerodynamicist, and was in contact with Chanute well before the Wrights began correspondence.[57] Huffaker was a scientist who had worked for Langley at the Smithsonian for a time, and was designing and building gliders for Chanute when Chanute suggested he visit the Wrights' camp.[58]

Both men were visitors to the Wrights' camp at Kitty Hawk in 1900. They observed the first marginally successful tests of the 1900 glider, and together suggested the problems with the Wright's stability involved the reversal of travel of the center of pressure at low angles of attack. It was well known that the center of pressure on a flat plate would travel toward the leading edge as the angle of attack decreased. These men suggested that the center of pressure on a cambered wing would begin traveling toward the leading edge with decreasing angle of attack, but reverse direction at a certain point and travel aft, toward the trailing edge. Spratt had studied this phenomenon some in his own experiments,[59] and Huffaker had worked on the problem when he was under Langley's purview at the Smithsonian.[60] Since the Brothers had not anticipated the problem, it had severe consequences on their stability and control.

Huffaker fell out of contact with the Wrights after the visit, but the Brothers continued contact with Dr. Spratt. For years they discussed center of pressure, camber, and other characteristics,

---

[52] Anderson, History, 168.
[53] Anderson, History, 180.
[54] McFarland, Papers, 180.
[55] McFarland, Papers, 66.
[56] Jakab, Visions, 160.
[57] Octave Chanute, "Letter to George C. Spratt," 24 Dec 1898, Personal correspondence (05 Aug 04).
[58] McFarland, Papers, 57.
[59] George C. Spratt, "Letter to Octave Chanute," 20 Apr 1900, Personal correspondence (05 Aug 04).
[60] McFarland, Papers, 108.

but his major contribution to the Wrights' research was his suggestion to measure the drag to lift ratio rather than drag alone.[61] Based on his suggestion the Wrights developed the balance to measure the ratio, which allowed them to determine the most efficient of the airfoils they tested as well as determine the actual drag value based on lift values acquired earlier.[62]

2.2 Approach to Aerodynamics

2.2.1 Systematic Wind Tunnel Testing

On a smaller scale, but equally important, was the systematic approach the Wrights used in their wind tunnel research. Starting with the tunnel itself, they realized proper experimentation required everything to remain constant except the variable being analyzed. Though they were experimenting in the middle of their bicycle shop, they were meticulous about keeping the organization of the room constant so the flow would move though the room and their tunnel in the same manner each time they ran a test. Additionally, they had the foresight to make their data immediately applicable. Whether or not the quality of the tunnel permitted actual quantitative use of their data, the brilliant design of their balances provided insight no other wind tunnel had been able to provide. There balances were simple, but generated data which required little reduction to obtain useful results (Figure 2.6), and could be plotted directly to use in comparison, such as the plots in Figure 2.7. It took the Wrights only a few minutes to generate plots for an airfoil which they could compare to plots for other airfoils to determine which had better lifting properties, the least drag, and the best overall efficiency.[63]

They also applied a systematic approach to the actual testing. They used "families" of airfoils, which had the same general characteristic, such as camber or planform shape, but all varied in a particular aspect. Testing and comparing within the family gave the Wrights a clear understanding of how that variable affected the performance of an airfoil. For example, a "family" would all have the same rectangular planform shape and camber, but would vary in aspect ratio. By comparing the lift curves and the lift to drag ratios, both of which could be read directly from the balances, the Wrights learned that high aspect ratio wings were much more efficient, and applied that knowledge after their wind tunnel tests.[64] The two most obvious changes after the wind tunnel testing were the aspect ratio, more than doubling from 3.3 in the 1901 glider to 6.7 in the 1902 glider, and the camber which decreased from 1/12 in 1901 to between 1/24 and 1/30 (it was variable) in 1902.[65]

---

[61] Jakab, Visions, 134.
[62] Jakab, Visions, 134.
[63] McFarland, Papers, 174.
[64] McFarland, Papers, 177.
[65] Anderson, History, 241.

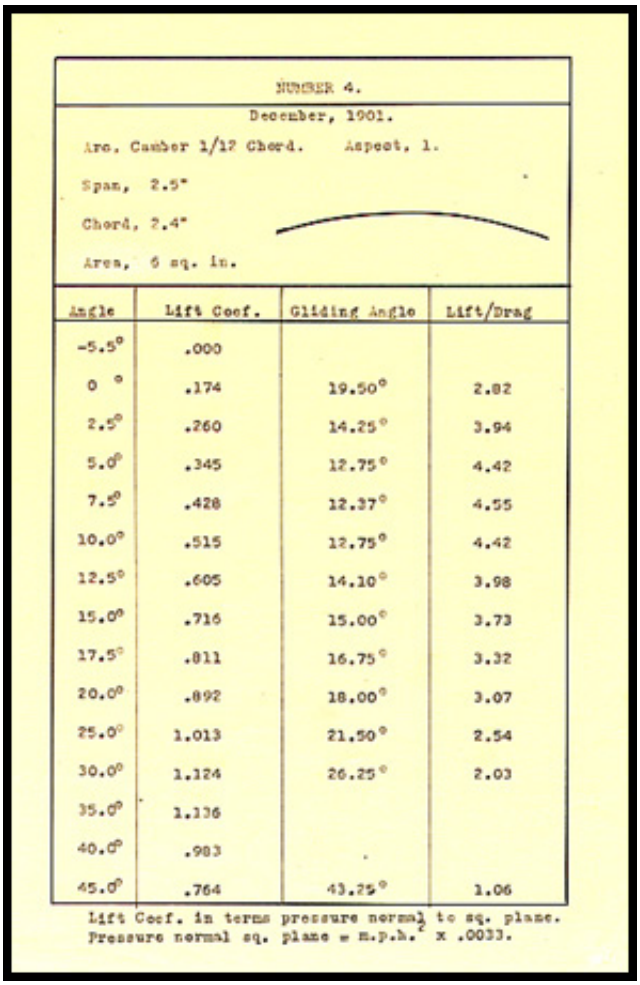

NUMBER 4.

December, 1901.

Arc. Camber 1/12 Chord. Aspect, 1.

Span, 2.5"

Chord, 2.4"

Area, 6 sq. in.

Angle	Lift Coef.	Gliding Angle	Lift/Drag
-5.5°	.000		
0 °	.174	19.50°	2.82
2.5°	.260	14.25°	3.94
5.0°	.345	12.75°	4.42
7.5°	.428	12.37°	4.55
10.0°	.515	12.75°	4.42
12.5°	.605	14.10°	3.98
15.0°	.716	15.00°	3.73
17.5°	.811	16.75°	3.32
20.0°	.892	18.00°	3.07
25.0°	1.013	21.50°	2.54
30.0°	1.124	26.25°	2.03
35.0°	1.136		
40.0°	.983		
45.0°	.764	43.25°	1.06

Lift Coef. in terms pressure normal to sq. plane.
Pressure normal sq. plane = m.p.h.^{2} x .0033.

Figure 2.6. Wright Brothers table of results for number 4 airfoil[66]

[66] "Image – Wind Tunnel Data Graph," Franklin Institute Aeronautical Engineering Collection, n.d., <http://sln.fi.edu/> (30 Nov 2004).

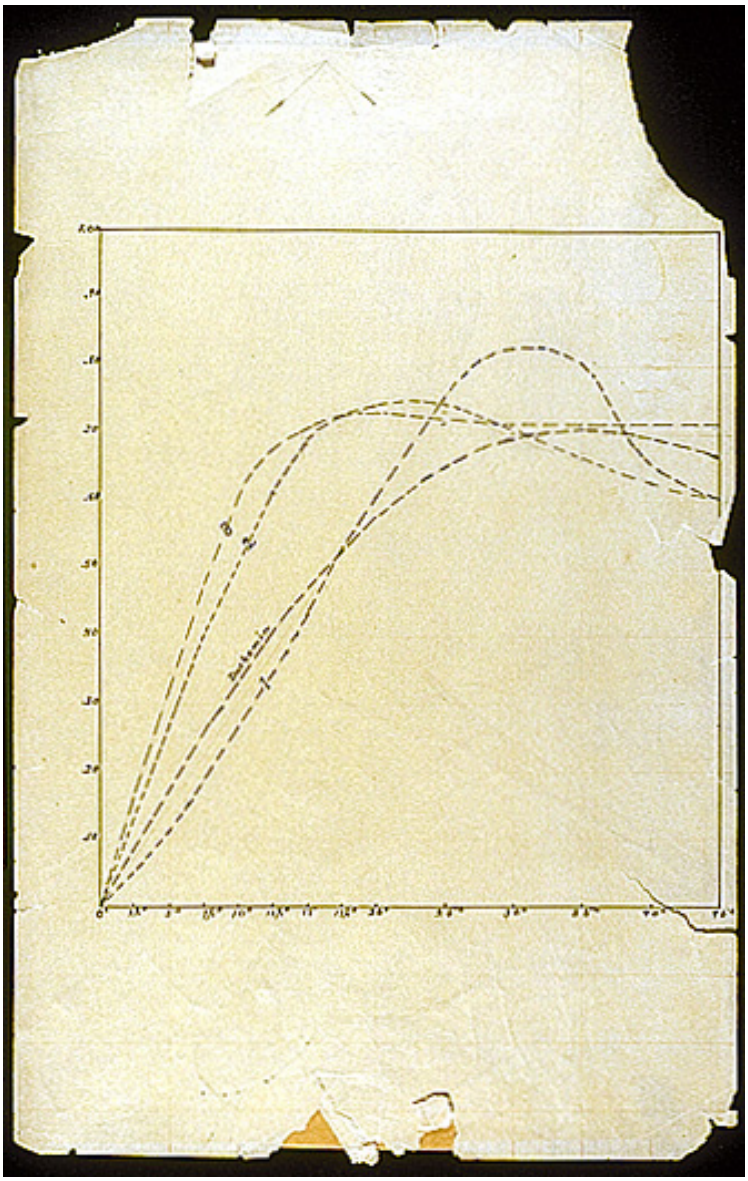

Figure 2.7. Page from Wrights' notebooks showing a comparison of lift curves[67]

The systematic method of testing allowed the Wrights to evaluate a large number of airfoils, over 200, in a short period of time. They used the basic knowledge from these broad tests to reduce their test group to 48 airfoils and configurations (such as biplane combinations).[68] These were the airfoils which had performed the best, and the Wrights wanted to test them more extensively, tabulating lift and "drift" (drag) data and generating graphical data such as lift curves.[69] From these curves they found trends, such as the decrease in lift past a certain angle of attack (they

[67] "Image – Wind Tunnel Data Graph," Franklin Institute Aeronautical Engineering Collection, n.d., <http://sln.fi.edu/> (30 Nov 2004).
[68] Anderson, History, 227.
[69] Anderson, History, 227.

were witnessing stall phenomena without recognizing its significance), the improvement in lift with increased aspect ratio, and that camber greater than 1/20 resulted in poor efficiency.[70]

2.2.2 Analytic Research versus Trial and Error

Regarding the Wrights' use of their quantitative wind tunnel data in their full scale designs, it is tempting to point to the Wrights' extensive analytical work as proof that they would not have gone ahead with full scale designs without using hard numbers gained in experiment. There are many instances, however, where the Wrights either felt that data was not important, or that they had a strong intuition on an issue, and thus moved ahead without the detailed calculations which characterized so much of their work.

Their analytic ability is well documented. For example they were the first to accurately measure the lift and drag forces on a glider.[71] Also, they consistently tested ideas with small scale models first. This was apparent both with the 1899 glider and with their wind tunnel testing in general. Their meticulous analysis allowed them to isolate and fix problems, such as applying a rudder to counter the adverse yaw they discovered.[72] Their systematic wind tunnel approach was intuitive and brilliant with respect to their balance design, method of recording and plotting data, as well as their use of "families" of airfoils to understand concepts.[73] Even their forward camber design, though based on faulty logic, was an excellent example of their attempts to conceptualize before they conducted experiments.[74]

In many instances, though, they abandoned their analytic approach and slowed themselves with trial and error. From the beginning their canard design was a guess based mostly on personal reassurance.[75] Had they been aware of the canard's adverse effects on stability and control, they most likely would have used a different configuration. Similarly, they never bothered to experimentally understand the pitching moment. They were aware that a longitudinal moment existed, and had even discussed with Spratt that it was affecting their stability, but did not bother to examine it during their wind tunnel experiments.[76] They continued to guess in 1901 when they went back and forth sizing their canard. They first made it smaller, then much larger, trying to stabilize their glider.[77] They were hoping for a quick fix rather than a conceptual understanding.

Even their wind tunnel testing, which supplied them with the greatest body of aerodynamic knowledge available at the time, resulted in instances of trial and error. For example, they built the 1902 glider in a manner which allowed them to vary the camber dramatically on scene from

---

[70] Jakab, Visions, 151.
[71] Anderson, History, 208.
[72] Jakab, Visions, 158.
[73] McFarland, Papers, 177.
[74] McFarland, Papers, 110.
[75] Jakab, Visions, 69: The Wrights were extremely afraid of the nose dive which killed both Lilienthal and Pilcher. They understood a tail was used to maintain longitudinal stability, and decided it would work just as well in front. This way they could see it, watch the changes in its orientation, and be assured it was keeping their nose in the air.
[76] Wilbur Wright, "Letter to George C. Spratt," 15 Dec 1901, Personal correspondence (05 Aug 04).
[77] McFarland, Papers, 71.

as little as 1/30 to as much as 1/24.[78] They had not tested anything less than 1/20 in their tunnel,[79] so the camber of the 1902 glider was based purely on extrapolation and qualitative knowledge. Even after their 1903 success they guessed on issues they did not fully understand, such as the relationship between center of gravity location and stability. In 1904 they tried to improve stability by shifting the center of gravity, first moving it aft, which greatly degraded the stability of the glider, then forward as they began to understand its influence.[80]

Overall, analytic ability was a great aide to the Brothers, but these short excursions away from analytical understanding, often detrimental to their progress, show the Wrights did not always need or want quantitative data to conduct their experiments, and that they felt their intuitive reasoning or trial-and-error would suffice.

2.3 Interpretation

2.3.1 Wind Tunnel Quality

The Wrights were very confident in the capabilities of their own wind tunnel, and, rightly, were critical of the experimental results of other wind tunnels and whirling arms, such as those of Langley and Lilienthal. While explaining their wind tunnel to Chanute in a November 1901 letter, the Wrights first explain why previous experiments were inaccurate, and that previous results deviated by at least 100% from true values.[81] They claimed their own results were much more accurate. As such, they were much more useful. The Wrights insisted their results were within one to two percent of true values for higher angles of attack, from 5°-15°. At lower angles of attack, fewer than 5°, their results were still within 10% of the "absolute truth."[82] Based on this statement they must have believed their results to be much better than any predecessor, and also believed, at least initially, their data would accurately predict full scale flight performance.

The Wrights would have had good reason to believe their wind tunnel flow was of high quality. Besides the fact that they did not understand the flow they were testing, they took great care in setting up their wind tunnel and their experiments so the results would be accurate. In a letter to fellow aerodynamicist George Spratt the Wrights related their means of straightening the flow from the fan using vanes and honeycomb. They said the process took almost a month, but they were confident they had perfectly uniform flow direction in their tunnel.[83]

---

[78] Anderson, History, 236.
[79] Anderson, History, 236.
[80] Frederick J. Hooven, "The Wright Brothers' Flight-Control System," Scientific American, November 1978, 166.
[81] McFarland, Papers, 164.
[82] McFarland, Papers, 164.
[83] Wilbur Wright, "Letter to George C. Spratt," 19 Oct 1901, Personal correspondence (05 Aug 04).

Believing their flow to be of high quality, the only variable left in the overall quality of results was their balance. A recent study by David Pinella and Richard Branch[84] proved conclusively that the Wrights painstakingly calibrated their balances so the readings were accurate. Additionally, the Brothers deliberately tried to minimize error caused by their large balances interfering with the flow. They documented their procedure for quantifying and correcting the interference and drag caused by different parts of their balance, and were confident their results were unaffected once corrections had been made.

It is also significant to note what the Wrights did *not* discuss with respect to their wind tunnel. In correspondence with Chanute, the Wrights were not hesitant about discussing failure. They related failed attempts and experiments, discussed potential remedies, and asked for advice. For example, they related the poor performance of their 1900 glider to Chanute[85] and expressed their frustration. They also listed potential reasons for their failure, such as the accuracy of Lilienthal's data, the unknown effect of air passing through the cloth of their wings, or that their camber was too shallow.[86] In contrast there is never any mention to Chanute, or even in their personal journals, of any failed experiment in the wind tunnel or of any doubt regarding the quality of their flow or data.

2.3.2 Basic Aerodynamics

Though the Wrights advanced the understanding of aerodynamics beyond anything that preceded them, they never completely or accurately grasped fluid mechanics: the interactions of air flowing over objects, the origins of forces and moments, the causes and consequences of flow separation, and the resulting concepts of stability and control.

Beyond the confusion apparent in the design and use of their wind tunnel, the Wrights' initial experiments in aerodynamics showed a misunderstanding of basic aeronautical principles. Their kite and first two gliders reveal that the Wrights had no concept of the effect of aspect ratio. They believed planform area alone was the variable with which they needed to concern themselves, increasing it 75% from the 1900 to the 1901 glider in an attempt to increase the glider's lift production.[87] In the same tests they show a misunderstanding of camber with respect to both magnitude and location. Since they had no appreciation for the pitching moment induced by an airfoil,[88] they felt they could continually increase their camber and, thus, increase the lift generated.[89] Between 1900 and 1901 they increased the camber from 1/23 to 1/12, attempting to improve the lift. They realized such a large amount of camber was affecting the flying qualities of the glider, and decreased the camber to 1/19, but continued to misunderstand the relationship between camber and lift, and camber and stability.[90] Similarly, though their decision to have

---

[84] David Pinella, and Richard Branch, "Calibration of the Wright Brothers' 1901 Lift Balance," Presentation made at the National Air and Space Museum, Smithsonian Institution, 2004.
[85] McFarland, Papers, 42.
[86] McFarland, Papers, 106.
[87] Anderson, History, 209.
[88] Howard S. Wolko, ed. The Wright Flyer: An Engineering Perspective, (Washington: Smithsonian Institution, 1987), 30.
[89] Anderson, History, 209.
[90] Anderson, History, 209.

forward-located camber versus a circular arc was correct, the attempt to describe the flow over an airfoil in a 1901 paper showed they had no concept of streamlines over an airfoil, and thought aerodynamics was based on the angles of incidence and reflection of air impacting the airfoil (a Newtonian view of fluid motion).[91] Based on this description, their correct decision to use forward-located camber was a coincidence.

After their wind tunnel experiments they had developed an understanding of many aspects of aerodynamics and fluid flow, but still misunderstood many applicable concepts. After experimenting with camber in the wind tunnel, their 1902 glider showed they still were not confident with their understanding of its effects. Due to their lack of confidence, they had foresight to build the glider with adjustable camber, allowing them to improve the flight quality through experiment by varying between a camber of 1/24 and 1/30.[92] Additionally, their 1902 designs and tests indicate they still did not understand stall phenomena, despite the fact that they saw its effects in the tunnel, conducted different tests to verify the results, and specifically noted them to Chanute.[93]

Finally, the Wrights never showed any understanding of ground effect. Recent full scale wind tunnel tests and analysis show the Wright Flyer would not have flown without the lift boost and drag decrease provided by flying in ground effect.[94] At one point the Brothers indicate they recognize the potential effects in a tunnel, but specifically tell Chanute it would not be applicable to gliders or powered flight.[95] This raises some interesting questions about the Wrights' results. The Wrights continually stated that they used their wind tunnel data to predict the forces on their 1902 glider and 1903 Flyer, and that their predictions were extremely accurate.[96] Beside the fact that they did not directly scale up any of their airfoils, if they did not anticipate and test for ground effect, which were apparently necessary for the Flyer to succeed, how could any prediction be accurate?

2.4 Contradictions: Claims and Inconsistencies

The Wrights claimed to have used their wind tunnel data to predict the performance of their gliders and Flyer with great accuracy. There are many inconsistencies with the claim, however, along with facts which seem to refute it altogether.

The primary inconsistency is that the Wrights did not model their full scale wings after any of their wind tunnel models.[97] Some historians claim the Wrights were able to extrapolate data beyond what they gained directly from the tunnel,[98] and others state that all the Brothers needed from the tunnel was the qualitative understanding of aerodynamics, and that they could make

---

[91] Jakab, Visions, 67.
[92] Anderson, History, 236.
[93] McFarland, Papers, 170.
[94] Colin P. Britcher, Drew Landman, Robert Ash, Kevin Kochersberger, and Ken Hyde, "Predicted Flight Performance of the Wright 'Flyer' Based on Full-Scale Tunnel Data," AIAA Paper 2004-0104, Jan. 2004.
[95] McFarland, Papers, 333.
[96] McFarland, Papers, 403.
[97] Jakab, Visions, 151.
[98] Anderson, History, 236.

accurate predictions based on that knowledge.[99] There is no evidence that the Wrights used either of these methods, and the analytical methods required to make these computations, such as Prandtl's thin-airfoil theory, were not available at the time.[100] Additionally, their 1902 glider, which was a direct product of their wind tunnel results, was built so the Wrights could modify the camber without too much trouble.[101] Had they fully understood the concepts and been able to accurately predict performance, they would not need to vary their wing geometry on site at Kitty Hawk.

Similarly, the 1902 glider and 1903 Flyer involved complicated flow interactions. The canard and the wings each affected the flow over the other. Additionally, the biplane effect decreases the performance of the individual wings. The Wrights understood these phenomena and qualitatively tested them in their wind tunnel.[102] Again, however, the exact combinations they tested never appeared in their designs,[103] and even if they could extrapolate data for a single airfoil, predictions for multiple airfoils are infinitely more complicated and would certainly have been beyond their understanding.

The most convincing inconsistency, mentioned earlier, is the apparent ignorance of ground effect, without which the 1903 Flyer could not have succeeded.[104] The Wrights were not aware of the phenomenon yet their predictions obviously convinced them they would be successful, otherwise they would not have made the attempt. Thus, either the data they were using to predict performance was incorrect, their method of scaling data was incorrect, or they were not making quantitative predictions as they claimed, but rather making general predictions based on broad, qualitative knowledge.

---

[99] Anderson, History, 236.
[100] Anderson, History, 257: Prandtl developed his thin-airfoil theory during WWI. The theory was the first to provide analytical calculations of airfoil properties.
[101] Anderson, History, 236.
[102] McFarland, Papers, 179.
[103] Jakab, Visions, 151.
[104] Colin P. Britcher, Drew Landman, Robert Ash, Kevin Kochersberger, and Ken Hyde, "Predicted Flight Performance of the Wright 'Flyer' Based on Full-Scale Tunnel Data," AIAA Paper 2004-0104, Jan. 2004.

3 CONTEMPORARY RESEARCH

Since the Wrights' success in 1903, there have been numerous research efforts to analyze their equipment, abilities, and level of aerodynamic knowledge. Much of this research occurred in the few years preceding the 2003 Centennial of Flight celebration, commemorating the 100th anniversary of the Wright Brothers' success at Kitty Hawk. Most of the studies focused on the Wright Flyer itself, or the gliders which preceded the Flyer, but there have also been studies which focused on the wind tunnel directly and the flow quality it produced. A group at Old Dominion University headed by Dr. Colin Britcher stumbled on the poor flow quality of the tunnel while trying to create an educational derivative of the Wrights' tunnel.[105] They discuss the main reasons for the poor flow, namely the fan upstream of the test section and the lack of a diffuser before the flow exits the tunnel. Preliminary tests with an inadequate propeller revealed highly non-uniform flow, with dynamic pressure differences as great as 50% between two regions which should be equal by symmetry.

Detailed flow surveys with a total pressure rake, as well as hot wire tests to measure the turbulence intensity were conducted once the fan was replaced with a five-bladed, variable-pitch fan capable of producing the velocities claimed by the Wrights. Notably the uniformity and turbulence were affected very little by the change in fan indicating the poor flow was not a function of fan design. The detailed tests revealed a region of low velocity flow in the center of the tunnel surrounded by high velocity flow which peaked in the corners of the tunnel. The turbulence intensities were measured at between 4% and 5% of the average tunnel flow velocity, and most likely were due to the test section being downstream of the fan.

Although many studies did not directly pertain to the Wrights' wind tunnel, analysis of the gliders and Flyer reveal a great deal about the Wrights' understanding of aerodynamics and the role their wind tunnel test played in that understanding. Several studies provide indications about what the Wrights' *did not* study or understand, but incorporated in the 1902 glider and 1903 Flyer. Dr. Fred Culick at the California Institute of Technology wrote a complete analysis on the Wrights' understanding of flight mechanics in which he revealed one of the Brothers' main problems was lack of appreciation for the adverse effects of the zero lift pitching moment.[106] Thus they were unaware of the problems with highly cambered airfoils which plagued their attempts to stabilize and control their aircraft. Similarly, Culick notes the 1903 canard stalled before reaching the trim lift coefficient. This is significant because it is something the Wrights could have discovered in their wind tunnel testing. They tested superposed wings and should have recognized the effects of upwash on the forward surface. This is especially true since the Wrights claim to have used their quantitative data from the tunnel to design and accurately predict the performance of the 1902 glider and 1903 Flyer.

---

[105] Colin P. Britcher, Rafaello Mariani, Pat Craig, Jill Gillespie, Mudit Monsi, Darius Luna, and Mark Sykes, "Analysis of the Wright Brothers Wind Tunnel and Design of an Educational Derivative," AIAA Paper 2004-1141, Jan. 2004.

[106] Fred E.C. Culick, "What the Wright Brothers Did and Did Not Understand About Flight Mechanics—In Modern Terms," AIAA Paper 2001-3385, Jul. 2001.

Data from full scale wind tunnel tests of a 1902 glider replica, acquired by Kochersberger, Landman, Player, and Hyde, similarly reveal defects which the Wrights should have anticipated from wind tunnel testing. In this case, the sharp leading edge of the glider airfoil resulted in separation, causing a severe nose down pitching moment. Because of this moment, the glider was unstable in pitch between 0° and 10° angle of attack.[107]

The 1903 Flyer, similarly, had problems due to leading edge separation. Britcher, Landman, Ash, Kochersberger, and Hyde conducted full scale wind tunnel tests on a Flyer replica revealing a large leading edge separation bubble which resulted in an increase in profile drag.[108] The tests also showed the Flyer would not take off without a stiff headwind on the short rails the Wrights constructed. This could be a result of brilliant calculation, or gross miscalculation. Similarly, the Wrights estimated the lift-to-drag ratio of the 1903 Flyer to be 8 based mostly on their wind tunnel data. Full scale tests outside ground effect show the ratio to be just over 6, but within ground effect the ratio would be significantly higher. Again, either the Wrights were well aware of ground effect and accounted for it, though they never discussed it having an effect on full scale tests, or they miscalculated and were lucky to leave a large enough margin of error to still succeed.

Many studies have researched more deeply into the question of ground effect on the Wright Flyer. Kochersberger, Britcher, Crabill, Dominguez, Player, and Hyde analyzed data from full scale wind tunnel tests of a Wright Flyer replica, and concluded take-off performance was enhanced by a 20% increase in lift curve slope due to the ground effect. They noted qualitatively that ground effect increased the lift curve slope to a smaller extent throughout the flight profile.[109] Further study by Britcher, Ash, and Hyde found ground effect reduced the induced drag on the Flyer by 35% during take off and 10% up to an altitude of 12 feet.[110] Finally, the earlier study by Britcher, Landman, Ash, Kochersberger, and Hyde showed conclusively that take off and flight by the 1903 Flyer was practically impossible without the benefits of ground effect.[111]

Almost all studies of the Wrights reveal admiration for their intuition and analytic ability. Full scale wind tunnel tests of a 1901 glider replica by Kochersberger, Ash, Britcher, Landman, and Hyde reveal the Wrights ability to conduct accurate measurements of glider performance, a feat never before accomplished. The Wrights estimated the lift-to-drag ratio of their glider to be 6. Initial wind tunnel tests showed the ratio to be only 3.9. When ground effect was considered,

---

[107] Kevin Kochersberger, Drew Landman, Jenn Player, and Ken Hyde, "An Evaluation of the Wright 1902 Glider Using Full Scale Wind Tunnel Data," AIAA Paper 2003-0096, Jan. 2003.
[108] Colin P. Britcher, Drew Landman, Robert Ash, Kevin Kochersberger, and Ken Hyde, "Predicted Flight Performance of the Wright 'Flyer' Based on Full-Scale Tunnel Data," AIAA Paper 2004-0104, Jan. 2004.
[109] Kevin Kochersberger, Colin P. Britcher, N. Crabill, K. Dominguez, Jenn Player, and Ken Hyde, "Flying Qualities of the Wright 1903 Flyer: From Simulation to Flight Test," AIAA Paper 2004-0105, Jan. 2004.
[110] Colin P. Britcher, Robert L. Ash, and Ken Hyde, "An Analysis of Flight Number 4: December 17, 1903," Presentation made by Department of Aerospace Engineering at Old Dominion University in conjunction with The Wright Experience, n.d.
[111] Colin P. Britcher, Drew Landman, Robert Ash, Kevin Kochersberger, and Ken Hyde, "Predicted Flight Performance of the Wright 'Flyer' Based on Full-Scale Tunnel Data," AIAA Paper 2004-0104, Jan. 2004.

however, the ratio increased to 4.2, and the ratio increased to 5.8 when the cloth was treated to reduce permeability to air, which compared favorably to the Wrights prediction.[112]

Similarly, a study by Pinella and Branch found evidence which conclusively proved the Wrights quantified the errors with their lift balance and calibrated the balance to compensate. The calibration resulted in the 40° incline of the drag fingers on the balance.[113] Wind tunnel tests with a full scale model of the Wrights' Model B Airfoil by Landman, Alvarez, Ash, Blackburn, and Hyde further emphasize the Wrights' engineering prowess. The airfoil was found to closely resemble the #12 airfoil tested by the Wrights in their wind tunnel. Surprisingly, the data from the full scale tests of the Model B airfoil corresponded excellently with the lift data from the Wrights' test of the #12, and corresponded fairly well with the Wrights' drag data from the same airfoil.[114]

[112] Kevin Kochersberger, Robert Ash, Colin Britcher, Drew Landman, and Ken Hyde, "Evaluation of the Wright 1901 Glider Using Full-Scale Wind-Tunnel Data," Journal of Aircraft 40, no. 3 (2003): 417.
[113] David Pinella, and Richard Branch, "Calibration of the Wright Brothers' 1901 Lift Balance," Presentation made at the National Air and Space Museum, Smithsonian Institution, 2004.
[114] Drew Landman, Julian Alvarez, Robert Ash, Spiros Blackburn, and Ken Hyde, "Wind-Tunnel Testing of the Wright Brothers' Moder B Airfoil," Journal of Aircraft 39, no. 1 (2002): 30.

4 EXPERIMENTAL SETUP

4.1 Wind Tunnel and Driver Section

The replica wind tunnel was based on the engineering sketches by Kurt Wolko, made for the Smithsonian in 1983,[115] as well as designs supplied by the Wright Aeroplane Company, a company which provides Wright Brothers educational material.[116] It was essentially based on descriptions in the Wrights' correspondence and notebooks, but the tunnel did not survive and no picture of the real tunnel exists, so any replica is an approximation of what the Wright Brothers had at their disposal.[117]

4.1.1 Wind Tunnel

The replica tunnel is shown in Figure 4.1, Figure 4.2, and Figure 4.3. It was constructed of ¾″ birch plywood based on the plans shown in Figure 4.4 as well as plans from the Smithsonian Institution Archives. It was 60″ long and the interior dimension of the cross section was 16.18″x16.18″. Similar to the Wrights' tunnel, the replica had a window above the test section for observing experiments. The plexiglass window was secured to the tunnel with six easily-removable screws which thread into brass inserts in the tunnel wall. The contraction was a square-to-round transition made of 1/16″ sheet metal. The contraction's upstream cross-section was a 24″ diameter circle with a four-inch collar acting as a shroud for the propeller. The circle converged to match the 16.18″x16.18″ square interior cross section. The transition from circle to square took place over 10 ¾″.

In the square-to-round transition there were two crossed vanes used to straighten the flow. The vanes were perpendicular to each other, starting at the inside edge of the collar and stopping ¾″ before the honeycomb which was secured precisely where the transition ended and the square cross section began. The honeycomb consisted of 1 ½″ x 1 ½″ x 1 ½″ cells, 10 to a side. The cells around the edge were slightly smaller to accommodate the thickness of the metal and the inner dimension of the cross section. Due to fabrication issues, the cells had to be individually bent and welded together, thus there were some small gaps and imperfections. Though the exact impact of these imperfections was unknown, it was expected to be small compared to the magnitude of other flow quality flaws in the tunnel.

---

[115] Kurt Wolko, "Wright 1901 Wind Tunnel," Plans drawn for the National Air and Space Museum, Smithsonian Institution (1983).
[116] "The 1901 Wind Tunnel and balances" Wright Aeroplane Company, n.d., <http://www.first-to-fly.com> (30 Nov 2004).
[117] Colin P. Britcher, Rafaello Mariani, Pat Craig, Jill Gillespie, Mudit Monsi, Darius Luna, and Mark Sykes, "Analysis of the Wright Brothers Wind Tunnel and Design of an Educational Derivative," AIAA Paper 2004-1141, Jan. 2004.)

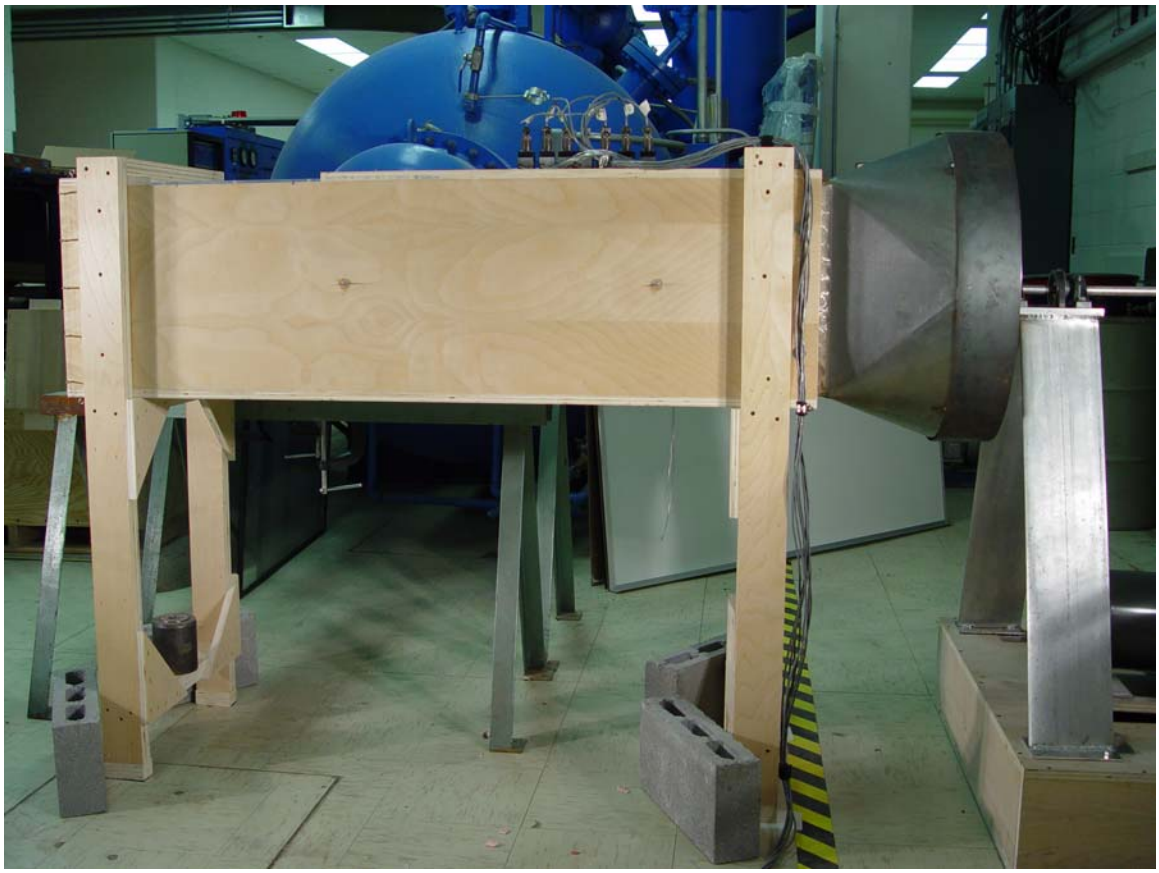

Figure 4.1. Side view of replica tunnel

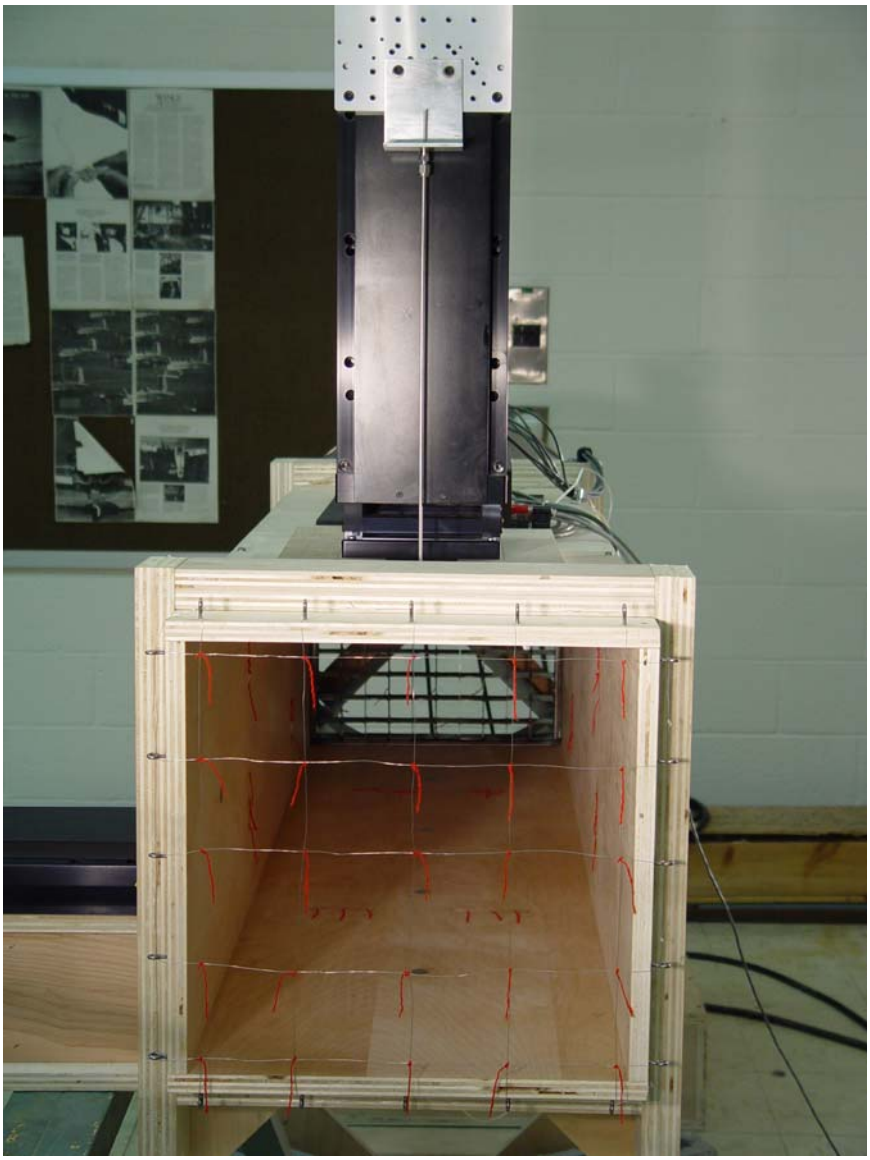

Figure 4.2. Rear view of replica tunnel and traverse

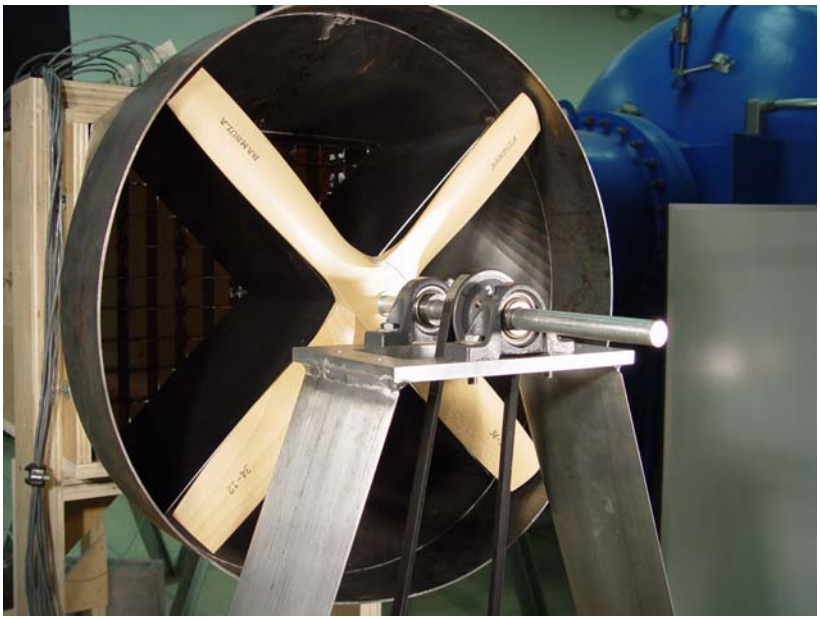

Figure 4.3. Front view of replica tunnel and fan

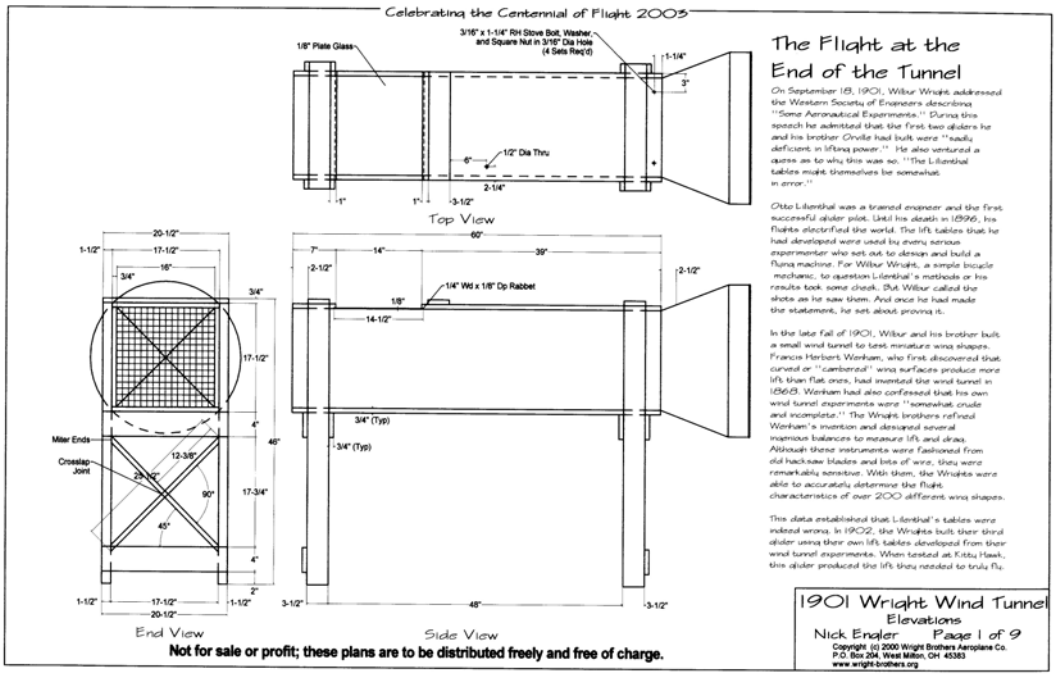

Figure 4.4. Wright Aeroplane Company plans for building a replica Wright wind tunnel[118]

[118] "The 1901 Wind Tunnel and balances" Wright Aeroplane Company, n.d., <http://www.first-to-fly.com> (30 Nov 2004).

4.1.2 Driver Section

The original Wright design was known to have involved a large wood box to which the propeller shaft and propeller were mounted. The shaft was driven by a belt from the ceiling, which was powered by a gasoline engine.[119] The wood box covered roughly 40% of the tunnel contraction and likely detracted greatly from the flow quality.

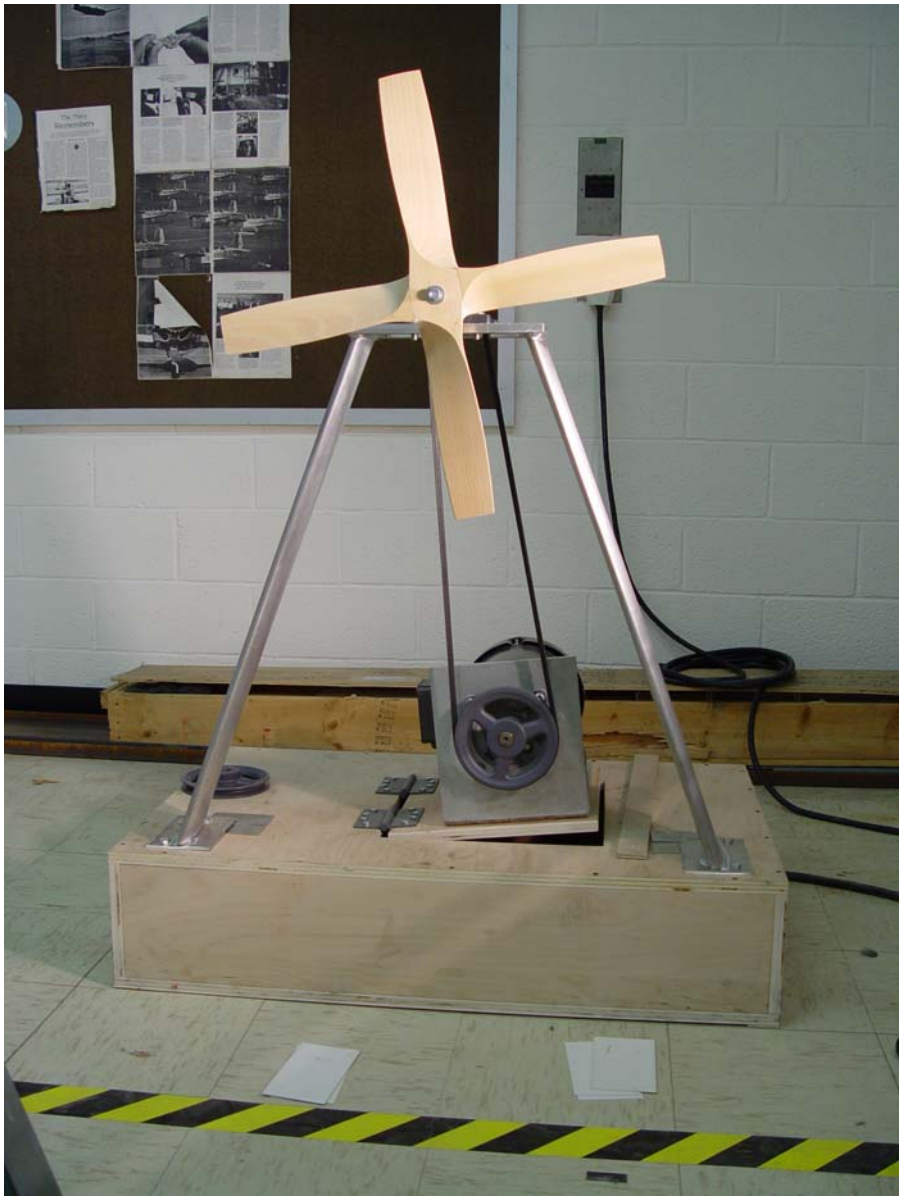

Figure 4.5. Front view of driver section

[119] Jakab, Visions, 124.

The motor/propeller setup for this experiment is shown in Figure 4.5, and Figure 4.6, and was designed to provide the best possible flow with least interference and flow blockage. The flow could be degraded to match the Wrights' flow using various methods such as securing plywood to the struts, forward of the propeller. The base consisted of a short, floor mounted box constructed of ¾″ plywood to which the motor and propeller struts were mounted. The propeller struts extended up roughly 30″. To provide the least interference to the flow they were constructed of airfoil sections whcih had a 6″ chord length. Atop the struts, two bearing assemblies held the propeller shaft, between which was the pulley, and at the end of which was the propeller. The pulley was connected by V-belt to another pulley on the shaft of the motor. The propeller shaft pulley was 3″ in diameter while the motor shaft pulley was 6″, allowing the propeller to spin twice as fast as the motor shaft.

The motor was a two-horsepower, three-phase, 230 VAC electric motor. The motor was face-mounted to a bracket which secured it to a hinged door between the propeller struts (Figure 4.7). The hinged door essentially used the weight of the motor to tension the belt, as well as act as a clutch if anything were to interfere with the propeller. The maximum RPM of the motor was 1,784 making the maximum propeller RPM equal to 3,568.

Figure 4.6. Close up view of fan mount and pulley connection

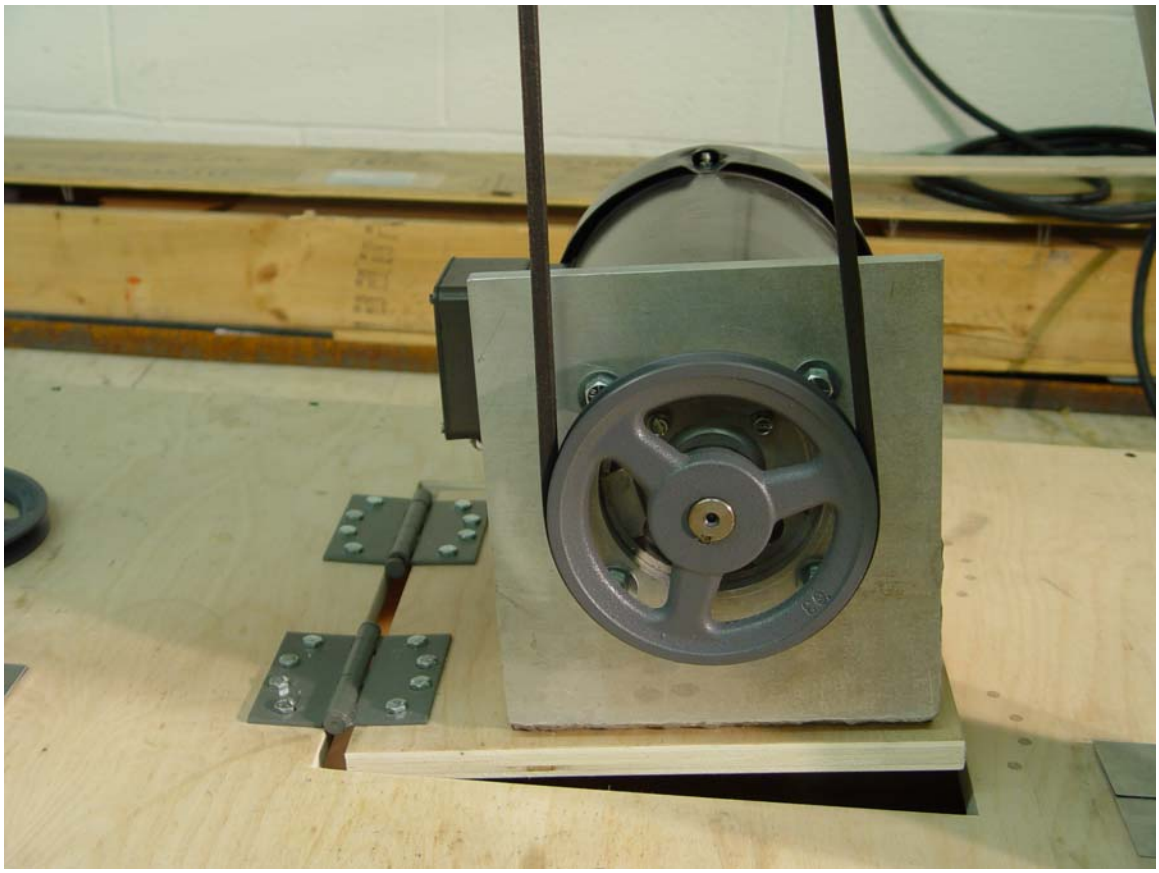

Figure 4.7. Close up view of hinged motor mount

4.1.3 Propellers

There is no accurate description of the propellers used by the Wrights in their wind tunnel, but they did record their RPM and flow velocity. Their claimed propeller RPM was about 3000,[120] and their flow velocity was between 30 and 35 mph.[121] By trying to replicate these conditions, one can assume the general flow characteristics generated by the spinning propeller (i.e. swirl and turbulence levels) are equivalent. Therefore many propellers were to be tested using the current setup. Originally, two-bladed propellers were tested to determine which would meet the specifications of the Wrights' tunnel (see Preliminary Results). All were between 30″ and 34″ in diameter and were cut down to fit the 24″ diameter collar of the contraction. The propellers were statically balanced on two knife edges which was important because a small imbalance at 3500 RPM would result in large vibrations and oscillations, and could have potentially destroyed the entire mount.

---

[120] Colin P. Britcher, Rafaello Mariani, Pat Craig, Jill Gillespie, Mudit Monsi, Darius Luna, and Mark Sykes, "Analysis of the Wright Brothers Wind Tunnel and Design of an Educational Derivative," AIAA Paper 2004-1141, Jan. 2004.

[121] Wilbur Wright, "Letter to George C. Spratt," 12 Nov 1902, Personal correspondence (05 Aug 04).

Once tested, however, it was apparent two-bladed propellers would not provide sufficient flow velocity. To achieve the necessary flow velocity, duplicates of the largest propeller, measuring 34″x12, were bonded together to form a four-bladed propeller. This was then cut and balanced in the same way as the two-bladed propellers, and provided sufficient flow velocity at the desired RPM. Figure 4 compares the two-bladed 34″x12 propeller and the four-bladed propeller constructed of two 34″x12 propellers.

Figure 4.8 Comparison of two and four bladed propellers

4.2 Instrumentation

4.2.1 Static Pressure Ports

The tunnel was modified to accommodate instrumentation such as static pressure ports in the walls, and Pitot-static probes. Ten static ports were installed in the tunnel. Four ports along the bottom wall, spaced an even one foot apart, measured the axial boundary layer growth through the tunnel. The axial ports, fore to aft, were labeled 1 through 4. Additionally, two “rings” of

static ports, the first being two feet from the exit plane of the tunnel, and the second two feet ahead of that (referred to as the aft and forward cross sectional static ports), measured the cross sectional uniformity of the boundary layer. These rings consisted of one port in the center of each side wall and the top wall, and used the axial static port from the bottom wall (in the same cross section) to complete the ring. Figure 4.9 and Figure 4.10 provide interior and exterior close up views of a static port. Figure 4.11 shows the axial ports and the forward ring. Table 4.1 provides the axial location of each port referenced to the inlet of the tunnel, aft of the contraction.

Figure 4.9. Oblique interior view of a static pressure port (note small opening in the center)

Figure 4.10. Exterior view of a static pressure port plumbed to a transducer

Figure 4.11. View from forward end of the tunnel showing axial ports and part of the forward ring (red strings are tufts)

Table 4.1. Axial location of static pressure ports

Pressure Port	Location (inches)	Angular Location[122] (deg.)
1	12	0°
2	24	0°
3	36	0°
4	48	0°
5f (forward cross-sectional "ring")	12	90°
6f (forward cross-sectional "ring")	12	180°
7f (forward cross-sectional "ring")	12	270°
5a (aft cross-sectional "ring")	36	90°
6a (aft cross-sectional "ring")	36	180°
7a (aft cross-sectional "ring")	36	270°

[122] Zero degrees references the bottom wall, and the angles increase in the clockwise direction looking in from the opening of the tunnel (as viewed in Figure 4.11)

Each port was a ¾″ aluminum insert with a 0.040″ diameter hole. Outside the tunnel, each port had a connector which attached to a pressure measurement device. Each was epoxied into tight-fitting holes, with about 0.001″ of the insert exposed on the inside of the tunnel. They were then sanded flush with the tunnel wall to minimize interference. Machining the hole in the aluminum port avoided the splinters, cracks, etc. which would have deteriorated measurements if pressure was being measured directly through a "square hole" drilled through the plywood. Additionally, the aluminum itself did not affect the flow in a different manner than would a clean wood surface.

4.2.2 Total Pressure Probes and Traverse

The tunnel also supporedt either a total pressure probe or a Pitot-static tube. The total pressure probe had a 1/16″ opening in the front which measured the stagnation, or total pressure at a point. The small diameter of the opening was ideal for measuring the pressure close to the tunnel wall to determine boundary layer magnitude and profile. The measurement obtained from the total pressure probe was the differential between total pressure at the point and ambient pressure outside the tunnel. The Pitot-static probe had both the total pressure port in front as well as ports in the side which, like the static pressure ports in the tunnel walls, measure the static pressure at a given point. The Pitot-static probe provided the differential between the total pressure and the static pressure at that point resulting in the dynamic pressure, 'q,' from which velocity could be calculated. Additionally, the total pressure hole in both probes was aligned with a static port at the bottom of the tunnel (port 4). For the total pressure probe, this allowed a comparison between total and static pressure at a point, which, like the Pitot-static probe, resulted in the dynamic pressure. For the Pitot-static probe, alignment with this port was a benchmark and a standard of comparison for accuracy. Figure 4.12 compares the two probes, and Figure 4.13 shows the probe connections.

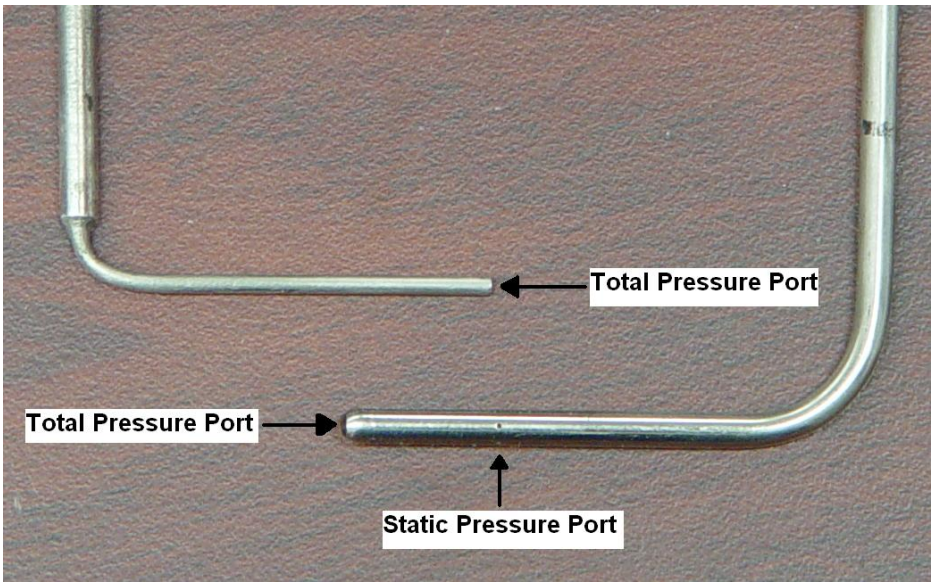

Figure 4.12. Close up of total (left) and Pitot-static (right) pressure probes

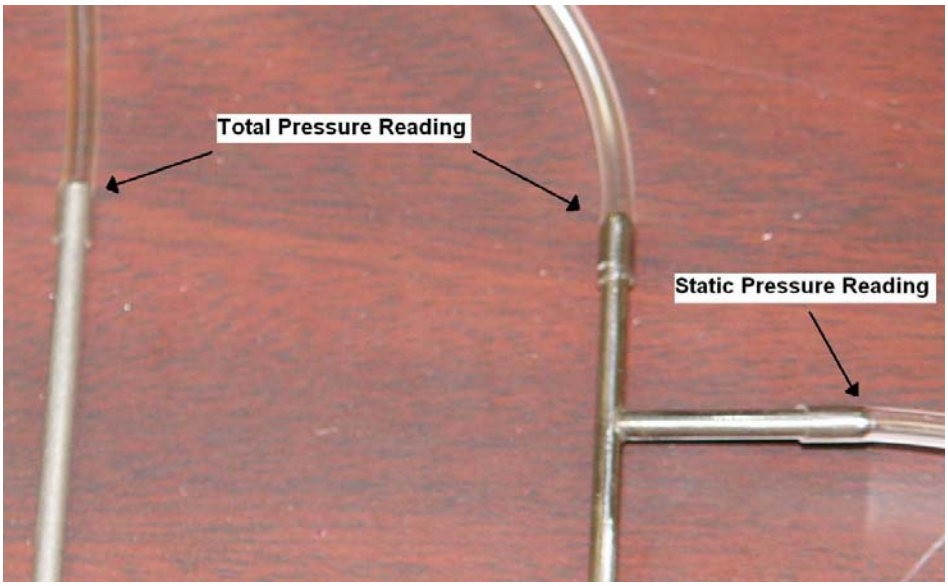

Figure 4.13. Close up of total (left) and Pitot-static (right) connections

Additionally, the plexiglass window on the tunnel could be removed and replaced with mock "windows" which supported instrumentation. One such "window" was made of ¾″ plywood, reinforced with parallel, 3″ strips of the same plywood running lengthwise. The reinforced strips provided a mounting point and added stiffness which kept the window from bowing into the tunnel and interfering with the flow under heavy loads. This window supported the heavy vertical traverse which was used to accurately and precisely change the position of the Pitot-static or total pressure probe, either of which could connect to the traverse from the test section through a small hole in the window. The traverse was accurate to better than one thousandth of a millimeter and was controlled either directly from the controller front panel, or by remote control. The traverse could move either probe along almost the entire height of the tunnel, from bottom to top, while the pressure was measured. However, the travel on the traverse was two centimeters short of the internal height of the tunnel. The probe could be shifted in the mount so the full range of the traverse included either the top or bottom two centimeters. Thus a full vertical survey required two sweeps, one including the top two centimeters, and the other including the bottom two centimeters of the tunnel.

4.2.3 Data Acquisition

Pressures from the static ports and total pressure probes were measured by Validine DP15 Variable Reluctance Differential Pressure Transducers. These transducers measured the difference between two pressure inputs. These DP15's had a full scale range from -0.5 psia to +0.5 psia, and a resolution of 0.00125 psi. Each static pressure port was connected to a transducer which output the difference between the static pressure measured and the ambient pressure outside the tunnel. The total pressure probe connected to a transducer which output the difference between the total pressure and ambient pressure. The Pitot-static tube connected to a transducer which output the difference between the total and static pressure.

Each transducer was connected to a carrier/demodulator which showed a voltage output based on the pressure differential measured by the transducer. The static ports were connected to a bank of seven CD18 demodulators and the Pitot-static probe and the total pressure tube were connected to a portable CD23 demodulator. The only significant difference between the two demodulators was the mobility: the CD18's were fixed in a bank of instruments while the CD23 could be carried, moved, and mounted at the user's discretion.

Both the CD23 and CD18 had a voltage output in addition to the LCD readout. The voltage output was connected to an Agilent 34970A Digital Multiplexing Datalogger which interfaced with the computer. The datalogger read the voltage from a demodulator and averaged its value over a specified time, recording the average voltage and saving it to a spreadsheet. Once the pressure differential/voltage output relationship for each transducer was known, that value could be input as the GAIN of the transducer. For different tests, the acquisition settings were fixed for an integration aperture between 10 and 100 powerline cycles and between 5 and 30 scans per channel. The datalogger multiplied the transducer's average voltage output by the gain, and, thus, record the pressure differential measured by the transducer.

4.2.4 Transducer Calibration and Testing

The output of each transducer was a voltage which corresponded to the pressure differential measured. Reduction of the data to units of pressure required accurate knowledge of the linear relationship between pressure differential and voltage output.

By applying known pressures to each transducer and recording the output over a range of pressures, a linear fit could be applied which provided the pressure/voltage relationship. The pressure supply was a Druck DPI 515 Precision Pressure Controller/Calibrator which provided a precise, constant pressure to an observed accuracy of ±0.0005 psi. The DPI515 was connected to each transducer, and the output from each transducer was recorded by the Agilent datalogger. The datalogger was set to scan all eight channels (one for each static port and one for the total pressure probe), and repeated the scan five times. Thus, at each pressure, there were five readings from every transducer.

Since the expected operating range for the tests should not exceed 0.035 psi, the transducers were calibrated from 0.000 psi to 0.045 psi, thus the calibrated resolution of the transducers was greater than the published resolution. The pressure was increased from 0.000 psi to 0.045 psi in 0.005 psi increments, and then brought back to 0.000 in the same increments. At each pressure up to and down from 0.045 psi, five scans were completed.

Figure 4.14 is an example of a calibration graph. The five voltage values recorded at each pressure were plotted against the pressure applied. Since there were five values for each pressure going from 0.000 to 0.045, and five on the way down, each pressure had ten voltage data points associated with it. The data coincided so closely, however, the ten data points seem to converge into one large point. Once the data from all the pressures were plotted, a line was fit to the data.

The slope of that line was the V/psi relationship. The inverse of that relationship, psi/V, was the gain which could be used directly to attain the pressure differential based on the voltage output.

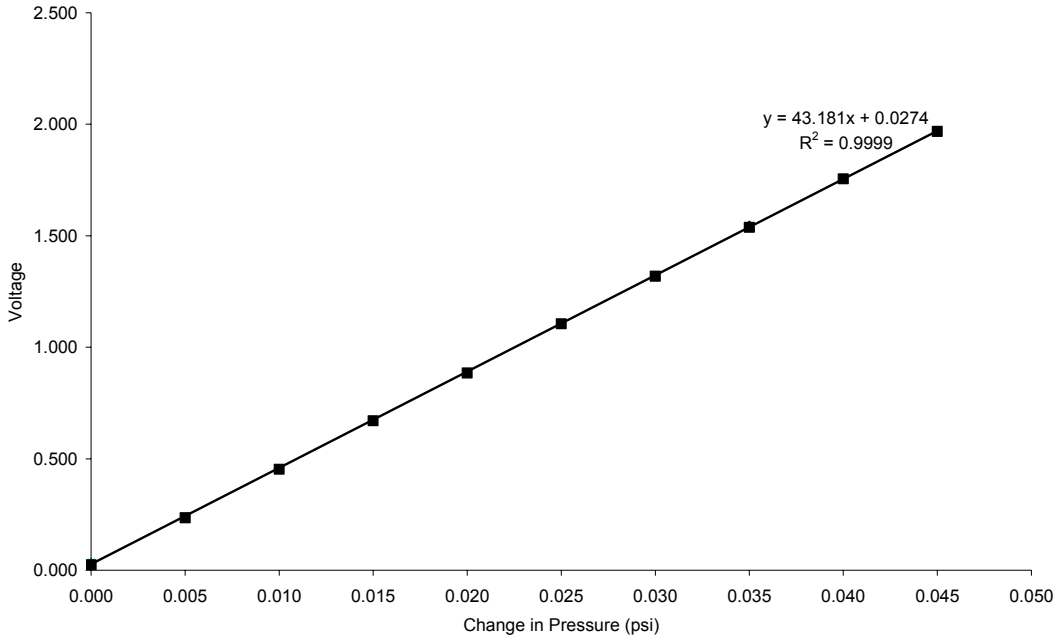

Figure 4.14. Sample calibration for transducer # 1

Notably, the sensors were calibrated to a precision which exceeded the factory specification. The calibrations all had an error (R-squared) value of 0.9999 or 1.000 which confirmed the accuracy of the linear fit. Also important, the offset of the line (the y-intercept) was a function of the zero setting before the calibration and was not a part of the pressure/voltage relationship. The relationship for each transducer can be found in Table 4.2, and the graphs for each transducer calibration can be found in APPENDIX B. Finally, the transducers were calibrated in the same orientation, location, and position in which they were used, so there was no error induced by a change in any of these variables.

Table 4.2. Pressure/Voltage relationships for transducers 1-8

Transducer	psi/V	Serial #	R-squared
1	0.0232	122328	0.9999
2	0.0221	122329	0.9999
3	0.0223	122330	1.0000
4	0.0250	122335	1.0000
5	0.0196	122336	1.0000
6	0.0193	122337	1.0000
7	0.0239	122338	1.0000
8	0.0248	94173	0.9999

4.2.5 Calibration Validation Test

The transducers were then tested to see if their psi/V relationships were accurate. Once the gain for each transducer was input into the multiplexer, the multiplexer directly recorded the pressure differential measured by each transducer. Thus, the pressure applied could be compared to the output to verify the accuracy of the psi/V relationship.

The DPI 515 was again used to apply a constant pressure. For this test the pressures were increased from 0.000 psi to 0.040 psi in 0.010 psi increments. The data was collected and plotted against the pressure applied, thus the graph was pressure applied versus pressure recorded. A line was fit to the data, and the slope of the line indicated whether the gain was accurate. Figure 4.15 is a sample of the test results.

Ideally, the slope of the line should be 1.000 which would indicate the multiplexer was recording the exact pressure applied. Though the slopes were not exactly 1.000, they were all within 2%, and all but one were within 0.6%. The largest error was with the total pressure transducer which was connected to the older CD23, and the results from this demodulator were less steady, though still within acceptable bounds of error.

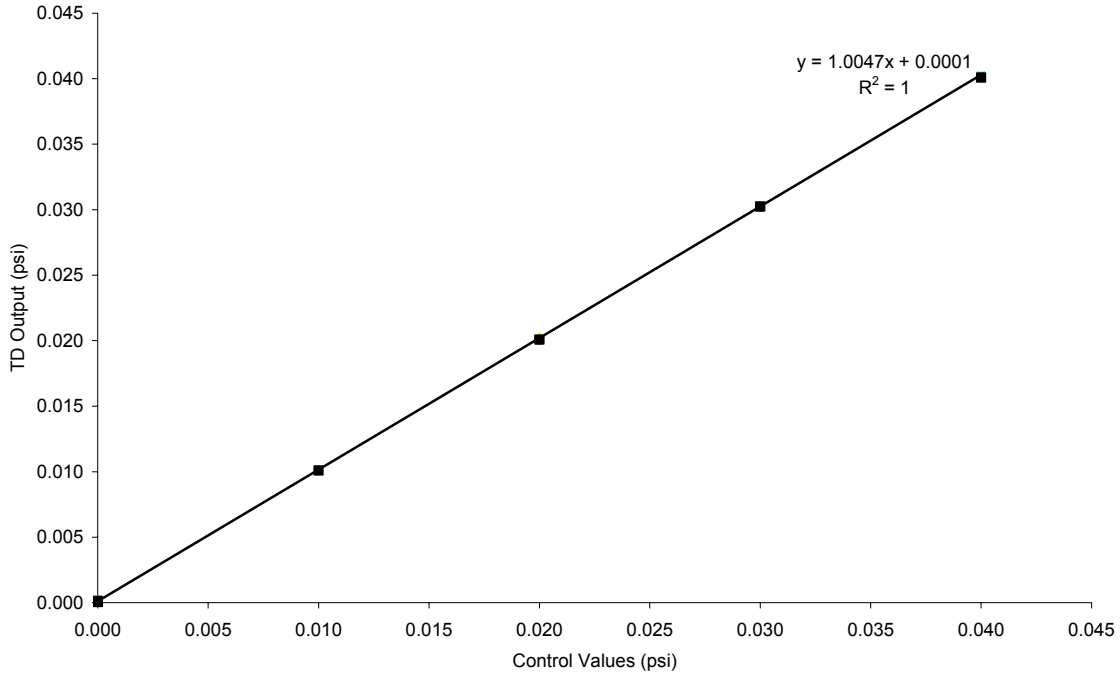

Figure 4.15. Sample of calibration test for transducer # 1

4.3 Preliminary Results and Tunnel Validation

4.3.1 Initial Flow Surveys and Fan Sizing

Before all the instruments were installed and validated, tests were needed to size the fan blade and gain an initial appreciation for the flow quality. Five propellers of various pitch and length were cut and balanced to fit the tunnel inlet, and were tested at the maximum RPM of 3,568. A Pitot-static probe was used to measure the velocity at the center of the tunnel, then 4″ (101.6mm), 2″ (50.8mm), 1″ (25.4mm), and ½″ (12.7mm) from the upper wall to generate a vertical velocity gradient for the top half of the vertical tunnel axis. The data from the five propellers is reflected in Figure 4.16.

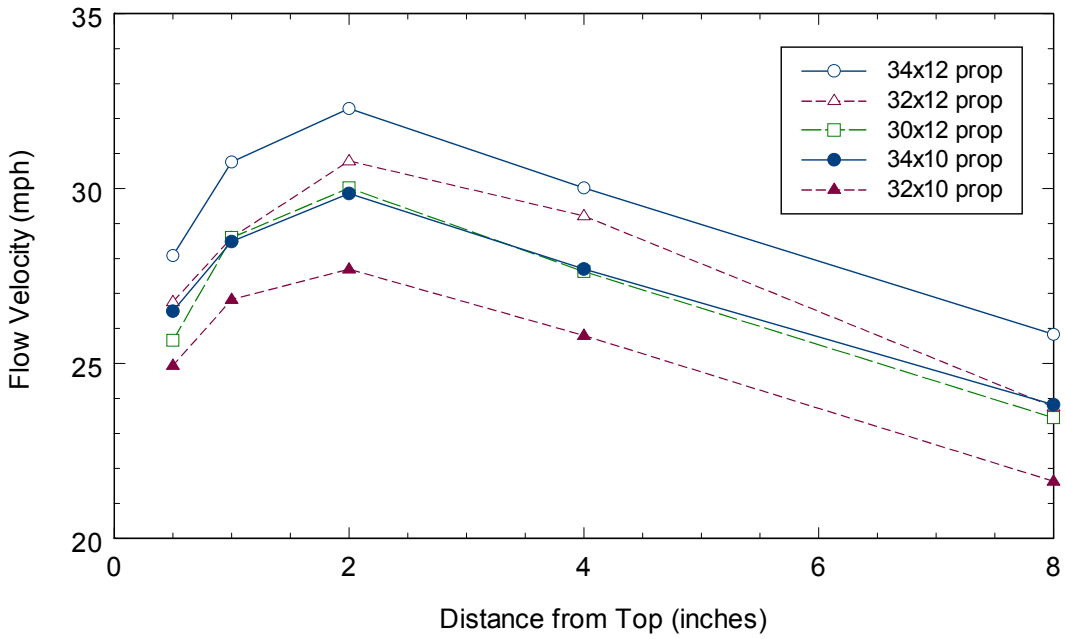

Figure 4.16. Vertical velocity profile for each propeller configuration

The data showed non-uniform flow in the vertical axis, and a boundary layer extending as much as 2″ (50.8mm) from the tunnel wall. There was a “dead zone” in the center of the tunnel surrounded by flow 25% faster, in turn surrounded by the boundary layer.

The tests showed the largest propeller, 34″x12 (34” in diameter, with a travel of 12” per rotation at 100% efficiency), produced the greatest velocity, averaging about 29 mph, but was still short of the Wrights’ claim of 30 to 35 mph. Based on these results a four-bladed fan was constructed and used in subsequent tests to achieve the desired velocity at the given RPM.

The data recorded from the static pressure ports, both axial and cross sectional, was simply used to verify the ports and transducers were functioning properly. The data showed there was no blockage in any of the static pressure ports, and that there were no major discrepancies, such as pressure readings varying by an order of magnitude or more.

These tests also showed the need for a more detailed flow survey. The Wrights mounted their airfoils vertically, and the non-uniformity measured would certainly have influenced their results. Thus, understanding the pressure distribution in the vertical axis was essential to realize its effect on their results.

Before a more detailed test was conducted, the four-bladed fan was installed. The transducers were recalibrated using the method described above. The total pressure probe replaced the Pitot-static probe so high resolution tests close to the wall could be conducted accurately. The traverse moved the total pressure probe along the vertical axis in two sweeps: one from the top down, and the other from the bottom up, both sweeps stopping within a few centimeters of the opposite wall. Table 4.3 shows the resolution used in the movement of the total pressure probe.

Table 4.3. Resolutions for different flow regions

Distance from wall (mm)	Δy resolution (mm)
0-20	1
22-50	2
55-100	5
110-400	10

The highest resolution was in the boundary layers where the velocity gradient was greatest. The resolution was less in the middle of the tunnel where the velocity varied the least.

The total pressure was used in conjunction with static pressure port four (in the test section) to calculate the dynamic pressure after both the total and static pressure were corrected with zeros recorded before and after the test. From the dynamic pressure the velocity was calculated at each vertical location, generating a velocity distribution along the entire vertical axis (Figure 4.17).

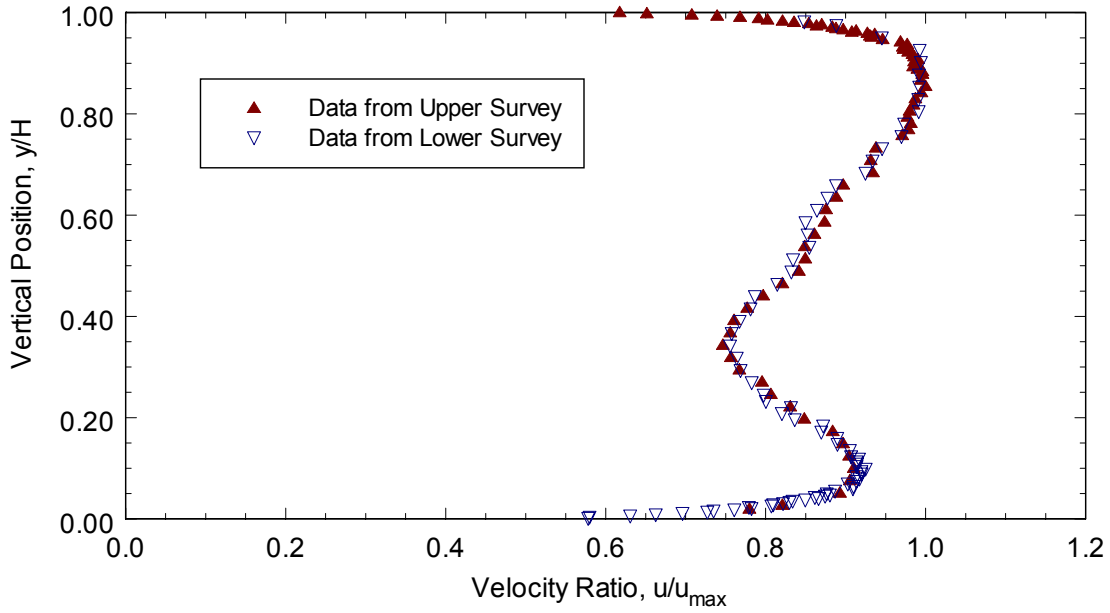

Figure 4.17. Non-dimensional vertical flow survey

The data was non-dimensionalized by dividing through by the total height (411mm) and the maximum velocity (35.75 mph).

The non-uniformity was consistent with the first test showing all three regions: "dead zone," high velocity zone, and boundary layer. Significantly, the Wrights mounted their airfoils in the top half of the tunnel, spanning all three regions. The spanwise pressure distribution would change based on the airfoil's shape and size, generating inconsistent results from one airfoil to another.

Figure 4.18 shows the upper and lower boundary layers in more detail. Though the boundary layers were smaller than originally anticipated, they still extended 8.5% of the total height from each wall, resulting in a large buoyancy effect as the effective area decreased from the tunnel opening to the test section.

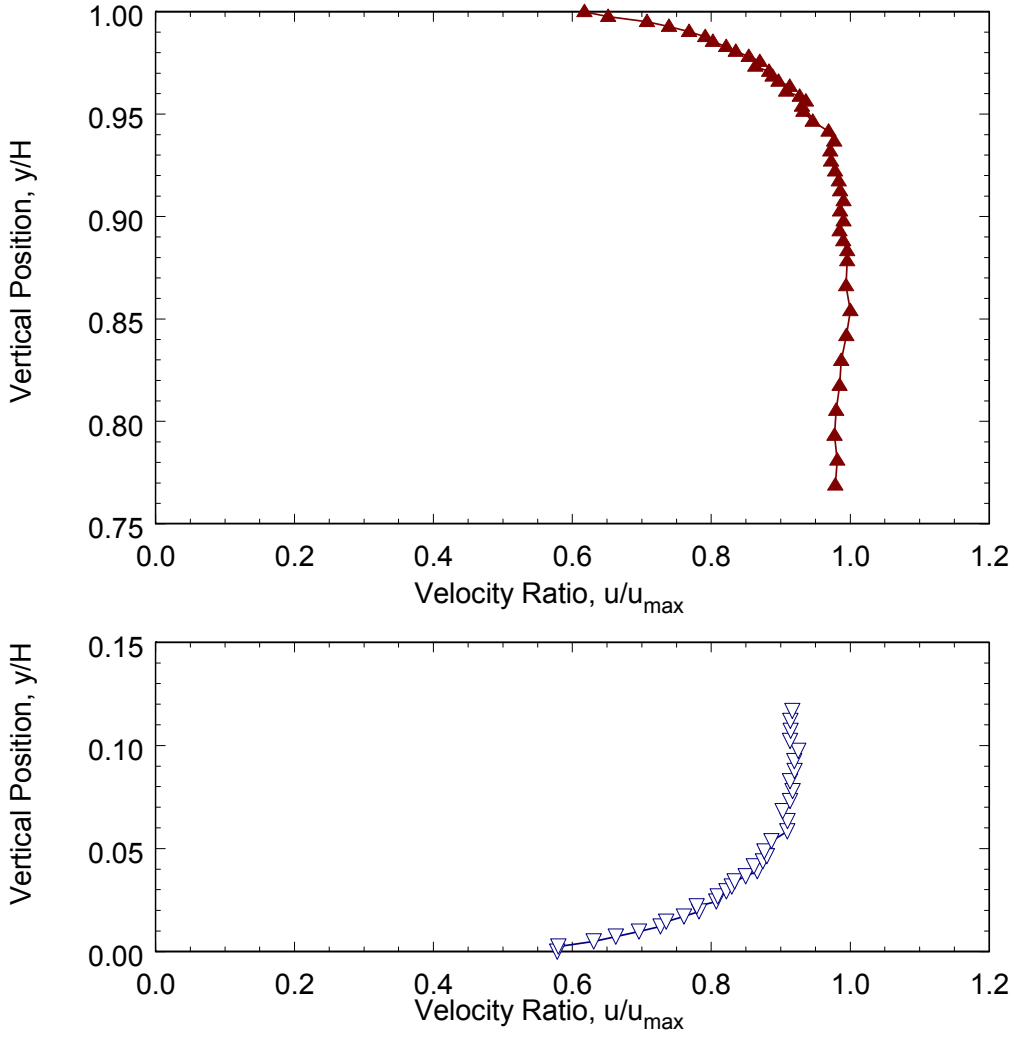

Figure 4.18. Non-dimensional upper and lower boundary layer velocity profiles

The vertical survey also revealed asymmetry between the upper and lower half of the replica tunnel. The asymmetry was due to misalignment of the fan. Corrections were made to align the propeller hub with the tunnel centerline, and ensure the fan was perpendicular to the centerline axis of the tunnel. Despite the asymmetry, the qualitative conclusions regarding the uniformity and boundary layer were still valid. The next step would be to retest the vertical axis, conduct a horizontal survey, and measure the velocity in the corners.

4.3.2 Repeatability Evaluation

After the fan was correctly aligned, it was important to establish the time dependence of the data based on the repeatability of total and static pressure measurements. This data would establish the accuracy of all subsequent results.

The tunnel was set up with the total pressure probe firmly mounted just outside the boundary layer, 40 mm from the upper wall, with the axial and forward cross-sectional static pressure ports connected to transducers. The pressure from each port and probe was recorded thirty times over roughly 1½ minutes. The scan sequence was conducted at 25%, 50%, 75%, and 100% of the maximum fan RPM, and the data was corrected by zeros taken before and after the tests. The set of tests was then repeated with the aft cross-section connected.

The average and standard deviation from each port and probe were calculated, and the standard deviation was divided by the average resulting in a percent variation for each probe and port over the 30 scans. The percent variation was a non-dimensional value allowing ease of comparison of the data. Figure 4.19 shows the variation in the axial data while Figure 4.20 and Figure 4.21 show the forward and aft cross sectional data.

The large variations in the static were due to the extremely low pressures being recorded. However, with the exception of the ¼ RPM run, the data showed as RPM increased the percent variation decreased. The pressure measured was increasing with RPM faster than the fluctuations increased, resulting in data which showed accurate trends. At 25% of max RPM the static pressures were simply too small compared to the magnitude of the noise disturbances.

The axial data was recorded twice, once with the forward and once with the aft cross-section connected, and was therefore redundant. The data with the forward cross section connected is shown in Figure 4.19. The variations decreased dramatically as fan RPM increased. Since the pressures increased with RPM, the "noise," or fluctuations in the pressure became smaller relative to the pressure magnitude. Variations in the two tests compared favorably which showed the ports generated consistent values over time.

The cross-sectional data in Figure 4.20 and Figure 4.21 indicated greater turbulence in the aft cross section of the tunnel, most likely due to the lack of a diffuser. The result was a greater unsteadiness which must be considered when analyzing data from these ports. Notably, the average values were still close enough to consider the ports useful and valid.

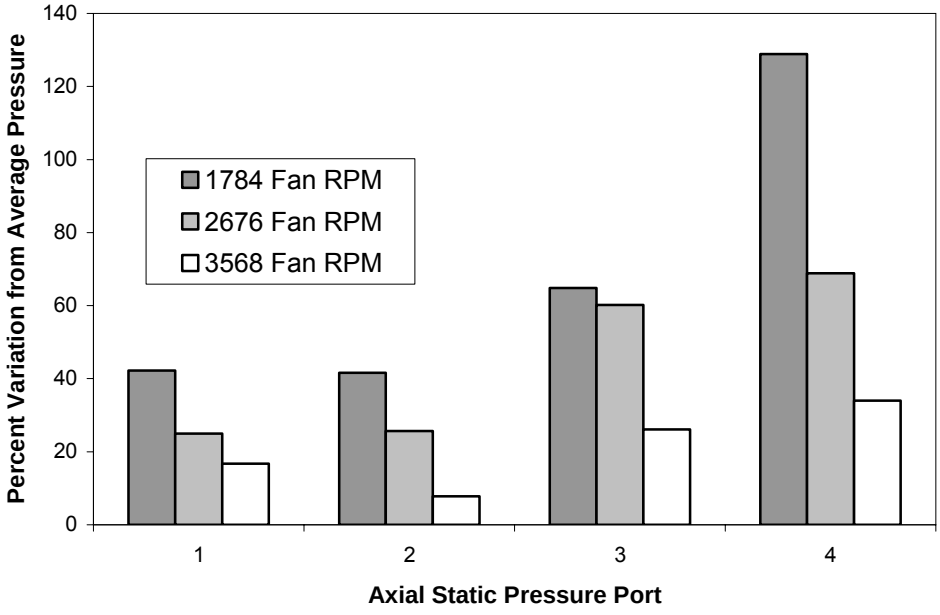

Figure 4.19 Comparison of axial pressure percent variation with forward static ring connected

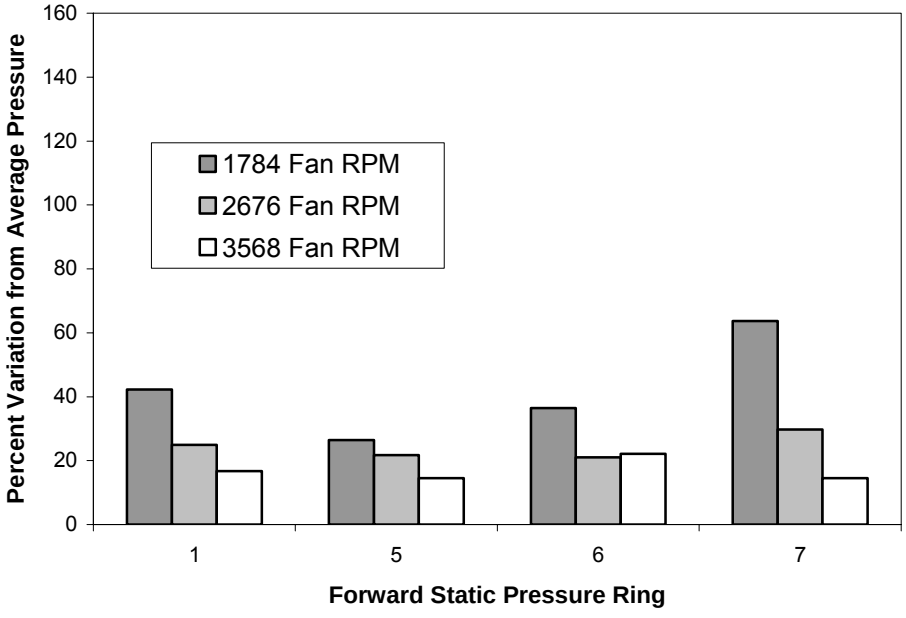

Figure 4.20 Comparison of cross sectional pressure percent variations for the forward ring

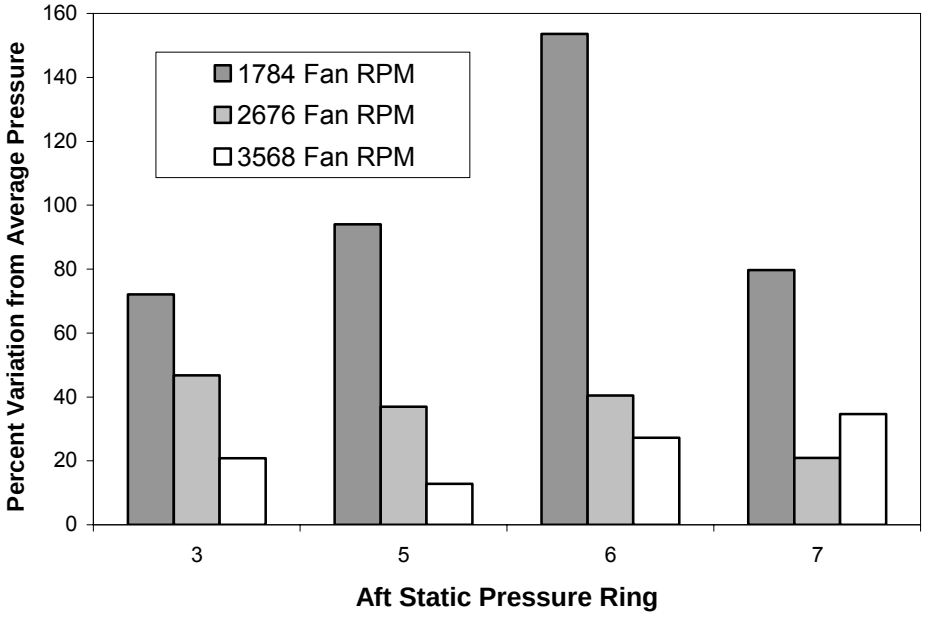

Figure 4.21 Comparison of cross sectional pressure percent variations for the aft ring

The percent variations in the total pressure were much lower than the static pressure because the pressures measured were much greater (two orders of magnitude greater than the static pressures) while the magnitude of the disturbances remained the same. Table 4.4 shows the percent variation of the total pressure during test 1 with the forward cross section connected. The data from test one and test two compared favorably which further showed the pressure measurements were repeatable.

Table 4.4. Percent variation of the total pressure

RPM	% variation (test 1)	% variation (test 2)
892	2.21	4.13
1784	1.84	2.39
2676	1.56	1.48
3568	1.39	1.23

4.4 Particle Image Velocimetry Setup

4.4.1 Theory

Particle Image Velocimetry (PIV) is a quantitative flow visualization technique. It is based on dividing planar region or cross section of a flow into small, discrete, elements and quantitatively

measuring the flow properties in each element to obtain a high resolution picture of the flow properties and dynamics in the whole region. The smallest element in which the flow properties can be accurately measured results in the greatest resolution, and, thus, the most complete measurement of the region's properties. The resulting data includes three-dimensional velocities, turbulence intensities, vorticity, and Reynolds stresses for the region.

The process involves taking a series of two image "captures" over a period of time. The two images in each capture are taken in rapid succession, with a Δt of between 40 and 100 μs between images for the velocities in this study. The computer then processes these images by correlation. The images are divided into interrogation spots and the small groups of particles within each grid element are analyzed independently. Correlation determines how each group of particles in the flow shifted during the Δt between images (see Figure 4.22). Based on the shift, the computer generates a two-dimensional velocity vector for that group of particles. Each image is made up of hundreds of these groups of particles, so each capture results in hundreds of vectors based on the two images of that capture. By taking several hundred captures at a rate of one per second, the computer generates accurate, high-resolution, quantitative data for the flow in the observed region. The quality of the data is dependent on the capture peak-to-noise ratio. A high peak-to-noise ratio allows the computer to correlate more data points producing quality data, while a low ratio results in fewer correlations and poor data.

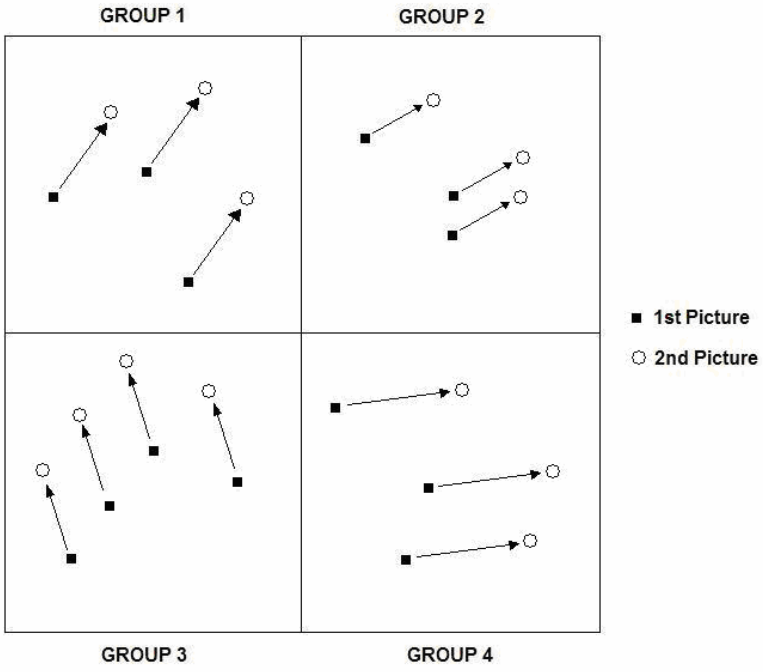

Figure 4.22 Sample PIV correlation for two images in a capture

The particles were "seeded" into the flow using an organic oil droplet generator. The droplets exiting the generator were 10 microns or less in diameter, and the density of the droplets in the tunnel was controlled by an air supply and a pressure regulator at the source. A rake (Figure

4.23) was built from PVC piping to evenly distribute the stream of oil droplets entering the contraction of the tunnel. Figure 4.24 shows the distribution openings in more detail.

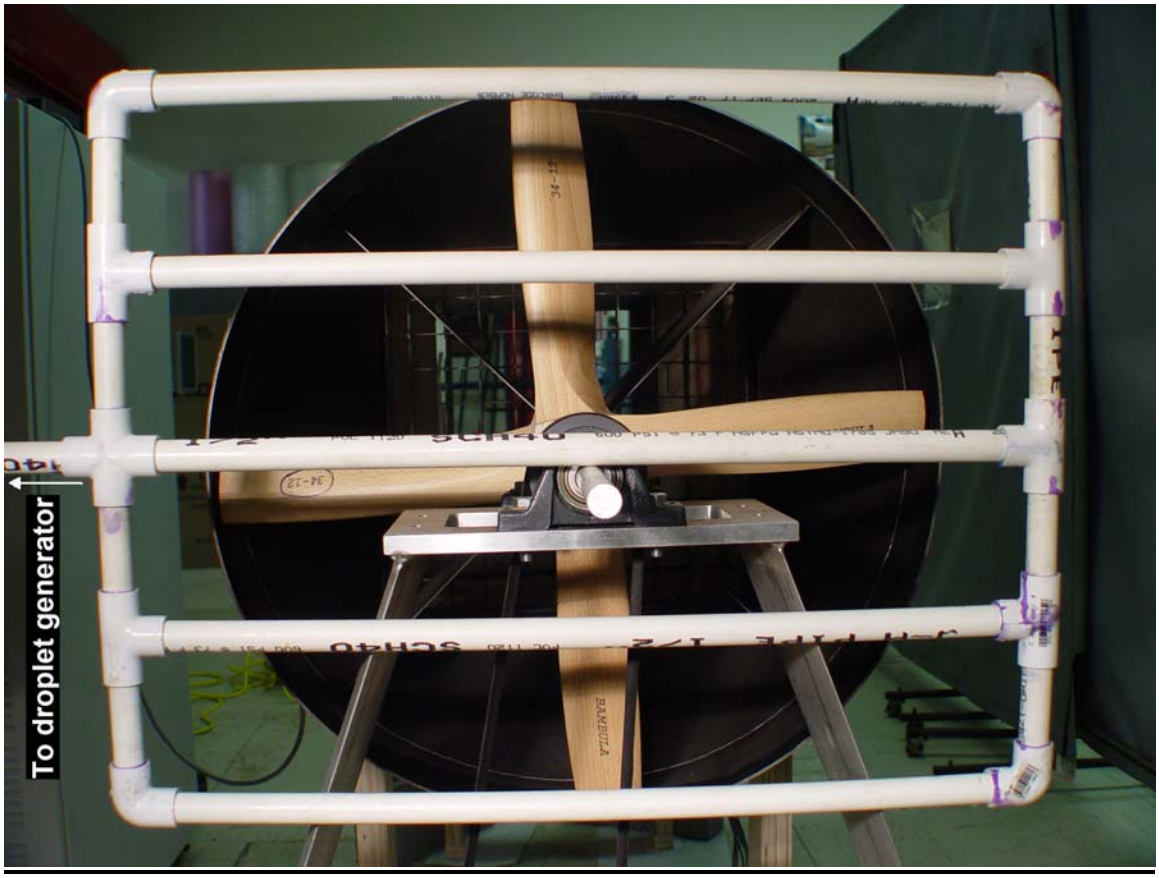

Figure 4.23 Rake for even distribution of oil droplet streams

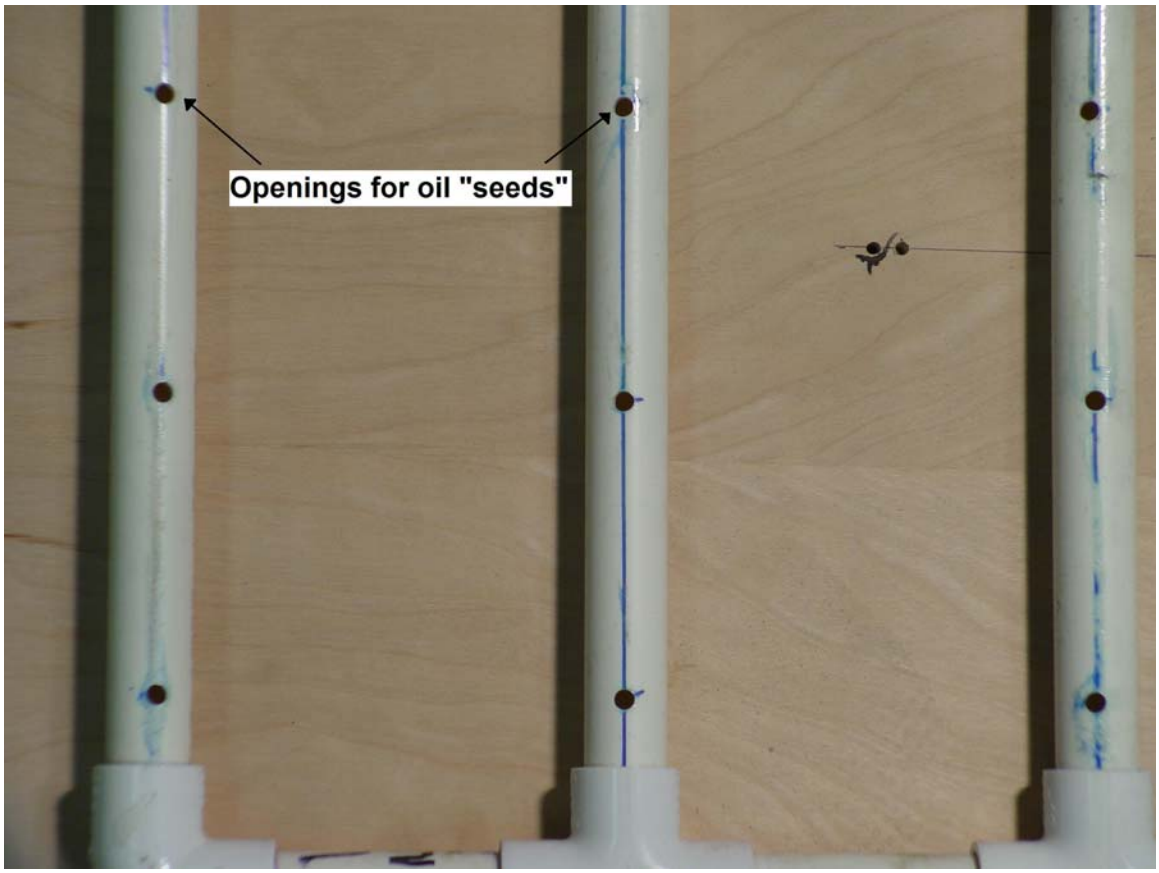

Figure 4.24 Zoom on openings which evenly distribute oil “seeds”

In order for the cameras to image these particles as they passed through the region of interest, a high powered laser was used to generate a sheet of laser light in the plane of observation. The laser is synchronized with the cameras and emits a high powered pulse just as each image of each capture is being recorded. The particles scatter the laser light as they pass through the instantaneous sheet. The result is a plane of bright dots recorded by the camera. Two such images in each capture are then correlated producing the vector data for the plane.

This correlation produces quantitative, two-dimensional velocity data. To produce three-dimensional data two cameras are necessary. The cameras are synchronized together with the laser so they observe the same particles passing through the laser sheet during a given pulse, but they observe from slightly different angles. The angle between the cameras allows the computer to analyze the 2D vectors from both cameras and produce three-dimensional velocity data.

There are six rules of thumb which promote good PIV data. First, the size of the grid element must be small enough that the vector describes the motion of the particles within the spot. Second, there should be more than ten particle image pairs per interrogation spot. Third, the maximum in-plane displacement of a particle should be less than ¼ of the size of the grid element. Fourth, the maximum out of plane displacement should be less than ¼ the thickness of

the light sheet. Fifth, the minimum in-plane displacement should be at least two particle-image diameters. Sixth, the exposure must be large enough to clearly show the particles.

The velocity data is similar to the flow survey results, but is conducted on a much broader scale providing a plane of high resolution data rather than the limited linear survey of velocities. The PIV results also allowed the flow unsteadiness to be quantified by measuring the turbulence intensities in the view area. Qualitatively, the unsteadiness was addressed in the Repeatability Survey, but PIV expanded greatly on those results providing accurate data across the plane. Additionally, the PIV results provided vorticity measurements which were not possible by any other available testing method.

The nature of PIV testing was also well suited for image subtraction. Essentially the effects of one element in the flow were isolated by subtracting out the known effects of another element. For example, the effect of the balance on the flow around the airfoil was determined by subtracting PIV data obtained with just a balance in the tunnel from PIV data taken with a balance and airfoil mounted in the tunnel, resulting in the airfoil by itself. Figure 4.25 is a simplified demonstration of how this subtraction would occur. The velocities, turbulence intensities, and vorticities of this subtracted image were then compared to the original image, with airfoil and balance mounted, to determine the net effect by the balance on the airfoil. It should be noted, however, that interference effects are non-linear and must be determined by other methods.

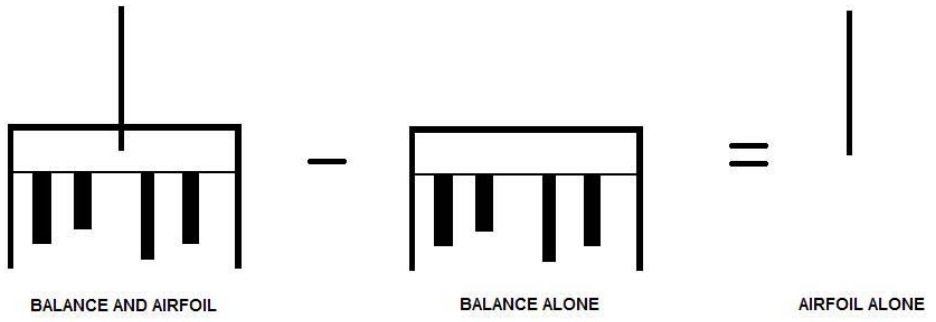

Figure 4.25 Demonstration of how image subtraction isolates the effects of a single element

4.4.2 Equipment

The laser was a New Wave Research Gemini I. Specifically it was a dual-head, flashlamp-pumped, 200 mJ, Nd: YAG laser. The flashlamp frequency was 15 Hz and the light wavelength was 532 nm.

Each camera was a PIVCam 14-10 produced by TSI, Inc. The cameras had a resolution of 1374x1024 pixels with a maximum framerate of 10 Hz and a shutter open time of 255 μs. The cameras used 50 mm Nikon lenses.

The synchronizer, which coordinated the laser pulses with the camera captures, was set to "frame straddle" mode which would allow the capture of two images within the Δt of 40 μs used for some of the tests.

Depending on the velocity being tested, the Δt for each capture was between 40 and 100 μs. The pulse delay was constant at 0.25 ms. The pulse repetition rate was 1 Hz. The Q-switch delay was also constant at 175 μs which was the high power setting for the laser.

4.4.3 Positioning and Orientation

4.4.3.1 Wind Tunnel

The window which the Wrights installed over their test section provided a convenient access through which the laser sheet could be pulsed. To avoid having to mount the laser securely several feet above the tunnel, the tunnel was rotated 90° clockwise (viewed from behind the tunnel) so the laser could be mounted to a table and produce a horizontal beam into the tunnel. Figure 4.26 shows the configuration from above. Abridged horizontal and vertical flow surveys were conducted to confirm rotating the tunnel had not greatly affected the characteristics of the flow.

4.4.3.2 Laser

The laser was positioned so the "waist," or thinnest section, of the laser sheet was located in the middle of the region being observed. A spherical and cylindrical lens combination was used which focused the sheet one meter from the laser aperture and generated a sheet just wide enough to meet both sides of the test section. This ensured there was sufficient laser energy in the entire region of observation with minimal power loss from refraction. The height of the laser matched the height of the centerline of the tunnel so the power distribution of the laser light would be symmetric throughout the test section. Axially, the laser was positioned so the sheet would fall *behind* where the airfoil was mounted by about 2″. This allowed the balance and the airfoil to be inserted into the tunnel without interfering with the laser sheet and allowing the effects of both objects to be measured.

4.4.3.3 Cameras

The ideal setup for two-camera, stereoscopic PIV suggests a 25° angle between the lines-of-sight of the two cameras to obtain an accurate calibration. Also, through trial-and-error, it was discovered the data recorded by the cameras is improved if the cameras were positioned to pick up forward-scattered energy from the laser rather than back-scattered energy. To best meet these criteria the cameras were placed downstream of the tunnel, but outside the jet to avoid interfering with the flow (see Figure 4.26). The cameras were mounted on a steel frame which was secured

to the floor and the apertures were aligned at the same height as the tunnel centerline. The lines-of-sight were 27.5°, rather than 25°, apart, but there was no apparent effect on the calibration. This configuration also avoided the problem caused by laser light reflecting off the tunnel window saturating the camera capture, which was experienced during an early attempt to mount the cameras such that they viewed the target area through the window (the cameras were next to the laser rather than aft of the tunnel).

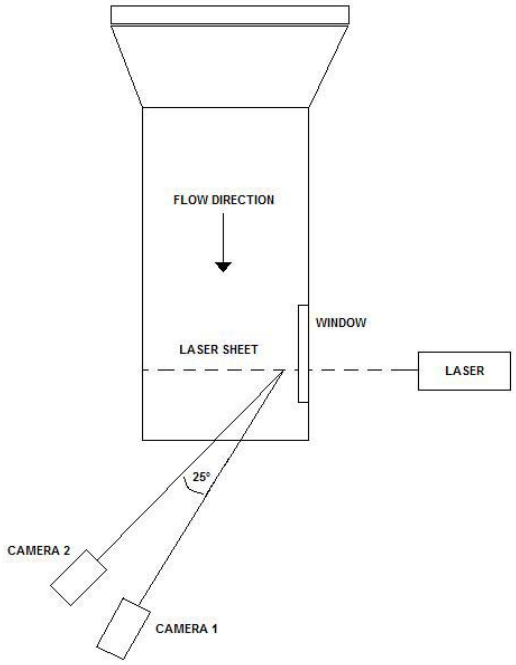

Figure 4.26 Tunnel, laser, and camera orientation for PIV testing (viewed from above)

The cameras each had a 50mm lens and a 532nm filter. The filter cut out any light which did not match the frequency of the laser light. This improved the peak-to-noise ratio significantly since the noise of ambient light was removed.

4.4.4 Calibration

In standard processing the computer generates vectors in the 2D plane of the camera image. To calculate 3D velocities, a geometric relationship between the 2D plane of each camera must be determined.

The key to the procedure is the calibration target pictured in Figure 4.27. The target's surface is made up of a series of dots spaced 10 mm apart with a larger cross in the center known as the fiducial point. The diagonals are offset by a depth of 1.0 mm. The spacing, including the depth difference, provides a reference in all three axes for the calibration. The target was mounted in the tunnel so the fiducial mark was at the same height as the center of the camera and laser

apertures. The target was located directly behind where the airfoil would have been mounted in the tunnel since this was the region of interest.

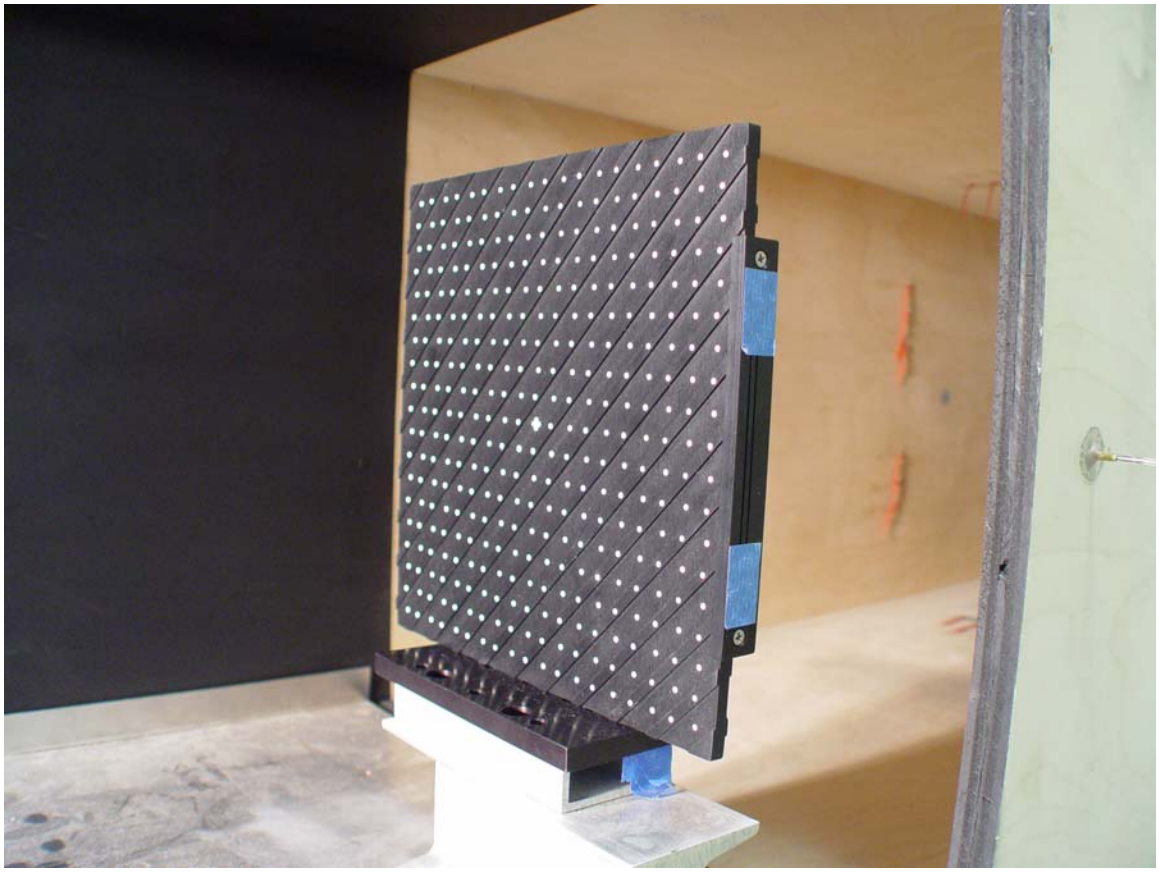

Figure 4.27 Calibration target

To ensure the target as aligned with the laser, the edge of the target contains a mirror which reflected laser pulses back at the laser. Positioning the target involved careful adjustments until the reflected laser light from the mirror perfectly split the aperture of the laser. Once the target was aligned, the cameras were adjusted until the crosshairs fell on the fiducial point, resulting in the 27.5°angle between the two cameras.

The next step involved bringing the plane into focus, which is difficult since the plane is not perpendicular to the cameras' lines-of-sight. The solution is to angle the camera with respect to its lens. The angle, known as the Scheimpflüg Angle, allows the camera to focus on a plane which is not perpendicular to its line-of-sight. To set the angle, the camera was focused to infinity and slowly brought into focus. Once it was apparent which side focused first, the angle was adjusted slightly and the process repeated until the plane came into focus evenly.

With the target and cameras aligned and focused appropriately, the next step involved generating the geometric relationship between the camera planes in order to obtain 3D data. Each camera captured an image of the calibration target (Figure 4.28) with the saturation points showing up as red and darker background represented by blue. The computer then determined where the calibration dots and fiducial point were located based on its criteria of the size and shape of those items. Since there are regions of saturation other than the calibration points, the criteria were adjusted until the computer only selected the calibration points and fiducial mark.

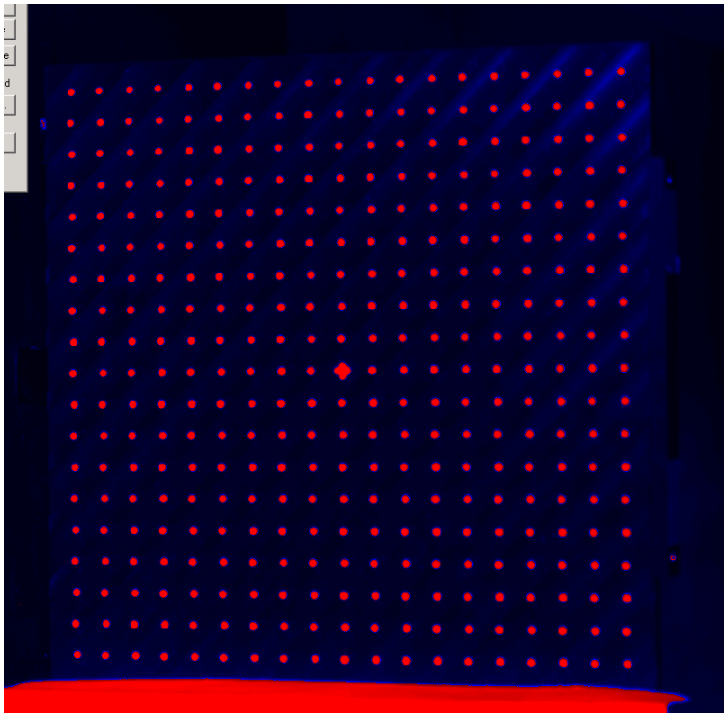

Figure 4.28. Sample capture of the calibration target

Once a calibration image was generated from each camera, the computer generated a 3D map (Figure 4.29) by analyzing the location of the calibration dots in both pictures and correlating the two. This map resulted in the geometric relationship used by the computer to obtain three-dimensional data for the tunnel flow based on images from the two cameras.

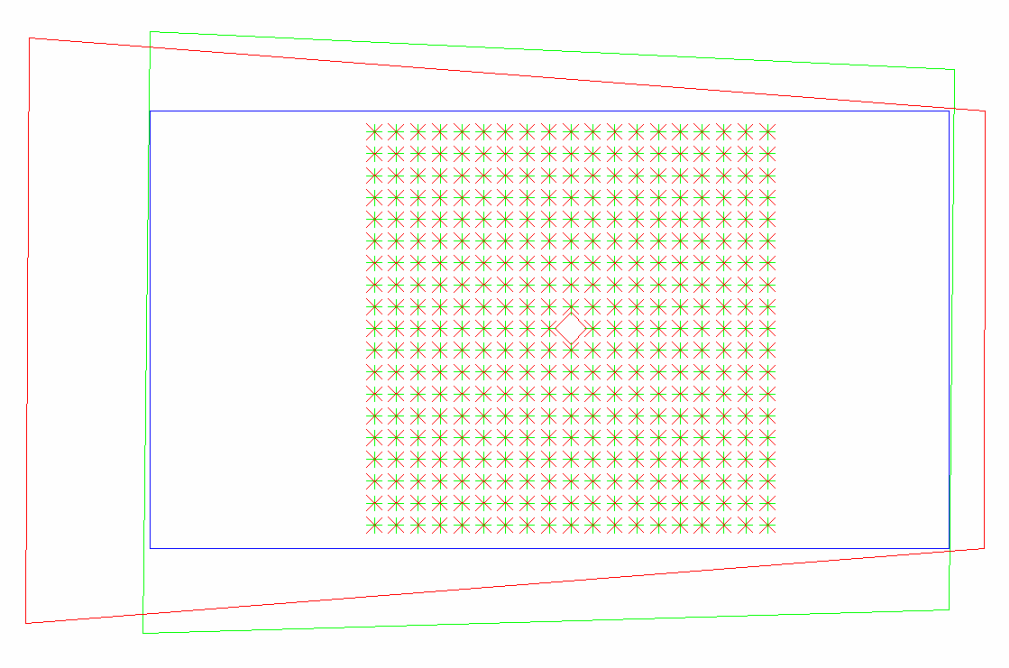

Figure 4.29 3D map generated by calibration

4.4.5 Test Procedure

Before acquiring data, the peak-to-noise ratio was maximized for the best processing performance. This involved adjusting multiple variables including the laser power, the seeder pressure, the camera f-stop and focus, and the Δt between laser pulses. Since window reflection was not an issue, the laser power was left at HIGH to maximize the amount of light scattered by the oil droplets. The seeder pressure was highly dependent on the velocity of the tunnel. Higher velocities required a slightly greater seeder pressure to increase the droplet density, as the particles were moving through the tunnel faster. Similarly, the higher velocities required a lower Δt because the oil droplets were moving faster, thus a lower delta was necessary to capture the droplets moving the same distance.

Once a satisfactory peak-to-noise level was achieved, the setup was ready to capture PIV images. Acceptable peak-to-noise ratios are anything greater than 1.5, though a ratio greater than 10 is desirable for good results. These tests achieved a ratio between 8 and 15. Each capture consisted of four high-resolution images: two images from each camera taken in rapid succession. The captures were obtained at a rate of 1 Hz. For each test, 1000 captures were recorded and saved to file.

Once captured, the images were analyzed to determine if background removal would be an effective means of further improving the peak-to-noise ratio before processing. Background subtraction was a pre-processing technique which removed the pixels below a minimum brightness tolerance. This effectively left the brightest pixels which contained reflected light

from the oil droplets, and removed most of the background generating a larger contrast which improved the peak-to-noise ratio. In some cases, however, this removed a significant portion of the actual data along with the background and, thus, could not be used for every test.

The images were then processed to obtain 2D and 3D vectors for every capture. The processing proceeded through two steps, known as recursive grid processing. First it processed each image in 64x64 pixel elements, and then divided each into four 32x32 pixel elements to refine the processing and correlate the images to produce 2D vectors. At each stage in the processing, aggressive filters were applied to remove outlying data, and in some cases were used to interpolate data to fill small holes. Each filter ran through a four point check to remove erroneous data. The filters worked by making comparisons to the local group, defined by the grid elements in the surrounding 5x5 element region. The first gate was a Double Correlation filter which removed any vectors generated from obvious noise peaks. The second was a Standard Deviation filter, removing vectors whose standard deviation varied from neighboring vectors' by more than a set tolerance. The third was a Median filter, again removing vectors that deviated from the local median by more than a set allowance. The Mean filter worked the same way, comparing and removing vectors deviating by a given amount from the local mean. Finally, provided that any gaps in the interrogation space were only missing 2 or 3 vectors, the filter interpolated from local data to fill the gaps. The interpolation was turned off in certain cases where the test conditions (such as blockage from the balance) generated large gaps in the data in which case interpolation would be grossly inaccurate.

The result was a series of 1000 vector files containing the u-, v-, and w-velocities, standard deviations, and Reynolds stresses. A visualization program, TecPlot, then analyzed these 1000 files to generate an average vector file containing the same categories. The average vector files from each run were the basis for the remainder of the PIV data analysis.

4.4.6 Post Processing

4.4.6.1 Image Processing

The PIV software processed the images and stored data in files which contain x, y, and z coordinates for each data point. The coordinates were based on the initial calibration and were referenced to the fiducial point on the calibration target. The coordinates were floating point numbers which made them difficult to work with, especially when processing two or more files simultaneously. The processing became more complicated when trying to shift all data points to the universal coordinate system with (0,0) along the centerline of the tunnel. The solution was interpolating each set of vectors onto a new, uniform grid. The same grid was used for every image which made comparison and simultaneous processing easy, and the grid locations were finite integers which were less complicated to process. In MATLAB the process involved generating a grid based on the desired size and resolution (i.e. 180 mm x 185 mm with each element being 1 sq. mm). The vector file from the PIV software processing was then read into MATLAB and the data points interpolated onto the grid based on the x and y coordinates stored in the vector file. The result was a uniform grid, stored in matrix form, which could be easily manipulated or processed as needed for various applications.

4.4.6.2 Processing Codes

Several codes were written in MATLAB in order to process the large amount of PIV data for various applications. They are all essentially derivatives of the same code, reading in raw vector files, and interpolating them onto a uniform grid, but the processing and output are different in each. The scripts can be found in APPENDIX C.

"PIVprocessing.m" was the main code used to process the data. A raw vector file was read into MATLAB and interpolated onto a uniform grid. The program then conducted three processing operations. First, it extracted the data from directly behind the region where the airfoil was (or would have been) mounted. The region was essentially a rectangle the length of the Wright's #12 airfoil (about 150 mm) and 16 mm wide. The velocities at each station along the span were averaged to generate a spanwise velocity distribution. The code also determined the minimum and maximum velocity along the span and the spanwise location of the minimum and maximum points. The second half of the code evaluated the global effects in the region of the airfoil. The code extracted a square region with a height and width equal to the airfoil span. The region was located with the airfoil splitting the box in half. The region was processed to determine minimum and maximum velocity and turbulence intensity along with their locations as well as the average velocity and turbulence intensity for that region. The turbulence intensity was calculated by dividing the velocity standard deviation for each element in the grid by the average velocity for that element. The third element of the code plotted the vorticity in the region processed by part two. The vorticity was calculated by taking the curl of the velocity vector at each element of the grid. Finally, the code output a plot of the spanwise velocity distribution and the vorticity.

"PIVsubtraction.m" was a slight modification to "PIVprocessing.m". Instead of a single file, the code read in two vector files, interpolated both to uniform, identical grids, and subtracted one from the other. The remainder of the code followed "PIVprocessing.m" using the result of the image subtraction. The output consisted of a spanwise velocity distribution in the airfoil region along with the data from the global region stored to Excel files.

"PIVcenterline.m" was one of the primary means of validating the PIV data. It was used to make comparisons to the flow survey data. This code read in a vector file from one of the empty tunnel PIV runs (all flow survey tests were conducted with an empty tunnel) and interpolated it onto a uniform grid. The code then conducted a similar operation to the spanwise velocity distribution in "PIVprocessing.m", except it processed the data along the entire vertical centerline of the image, not just the region behind the airfoil. The code output this data to an Excel file which was then used for a direct comparison to the vertical flow surveys. Since the horizontal flow survey only contained 2 or 3 data points within the PIV view area, the horizontal data was not compared.

4.5 Force Testing Setup: Load Cell Analysis

4.5.1 Load Cell

The load cell pictured in Figure 4.30 is a Honeywell-Sensotec MBH minigram balance. Essentially, it is a cantilevered beam sensor which measures a force, or a component of a force, in a specific axis. Though the load cell will output force measurements for out-of-axis forces, the output will not be an accurate representation of the force magnitude. To accurately measure a force, the load must be aligned with the load cell's measurement (bias) axis.

The flat aluminum block is perpendicular to the measurement axis and used to accurately position the angle of the axis. At the end of the load cell, a tapered adapter with a set screw is used to secure a rod which, in turn, is the mounting point for an airfoil. The load cell is wired to a Honeywell-Sensotec Model SC2000 transducer indicator/conditioner which provides load cell excitation and output. The output is calibrated to an accuracy of ±0.0015 lbs over a range of ±5 lbs.

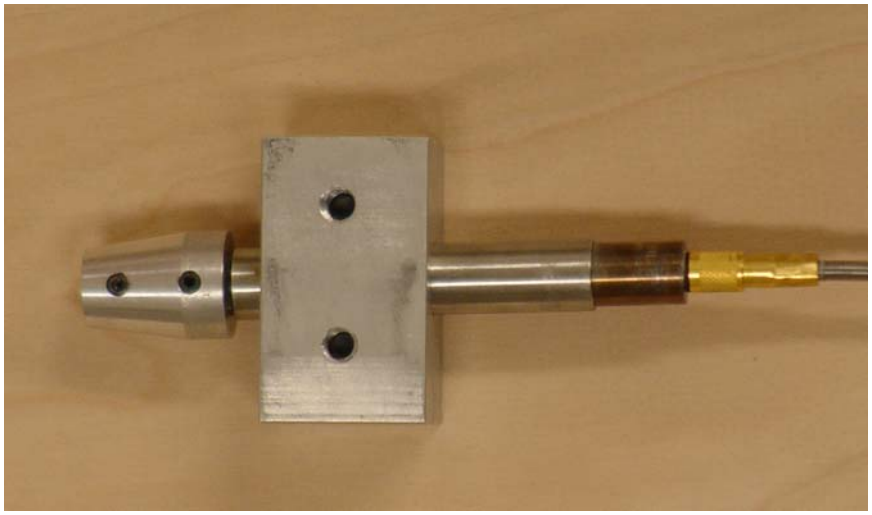

Figure 4.30 Cantilever type load cell

4.5.2 Mounting Bracket

Figure 4.31 shows the mounting unit to which the load cell is secured. The unit is mounted to the tunnel and allows the load cell to be rotated and secured in position so the measurement axis can be positioned at different angles relative to the tunnel flow direction.

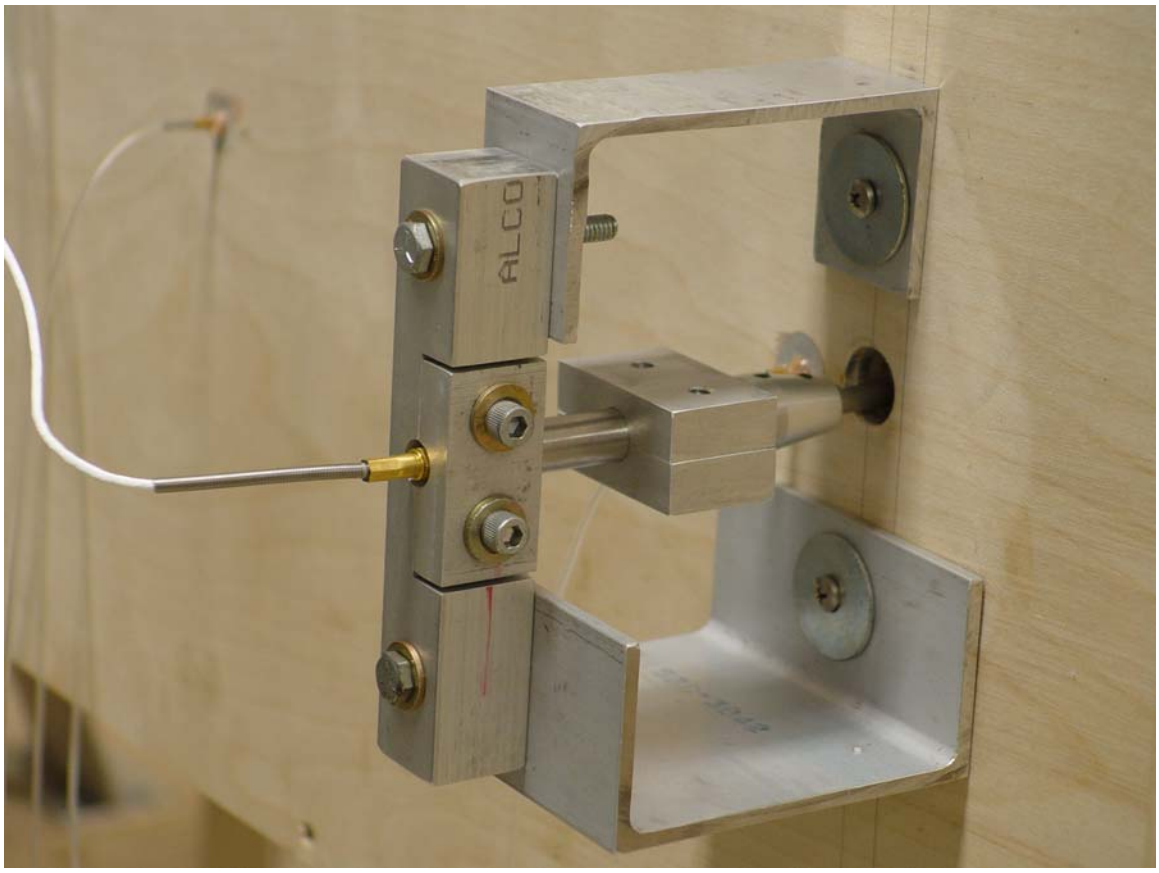

Figure 4.31 Mounting bracket which secures the load cell against the bottom of the tunnel

The bracket is mounted to the bottom wall of the tunnel. However, since the tunnel was rotated 90° to simplify the process of aligning the load cell, it appears the unit is mounted to the left side. The rod, which enters through a small circular opening in the bottom wall of the tunnel, positions the airfoil in the same location the Wrights' mounted their airfoils (see Figure 4.32). This is also the location, mounting method, and test section orientation used for the PIV testing.

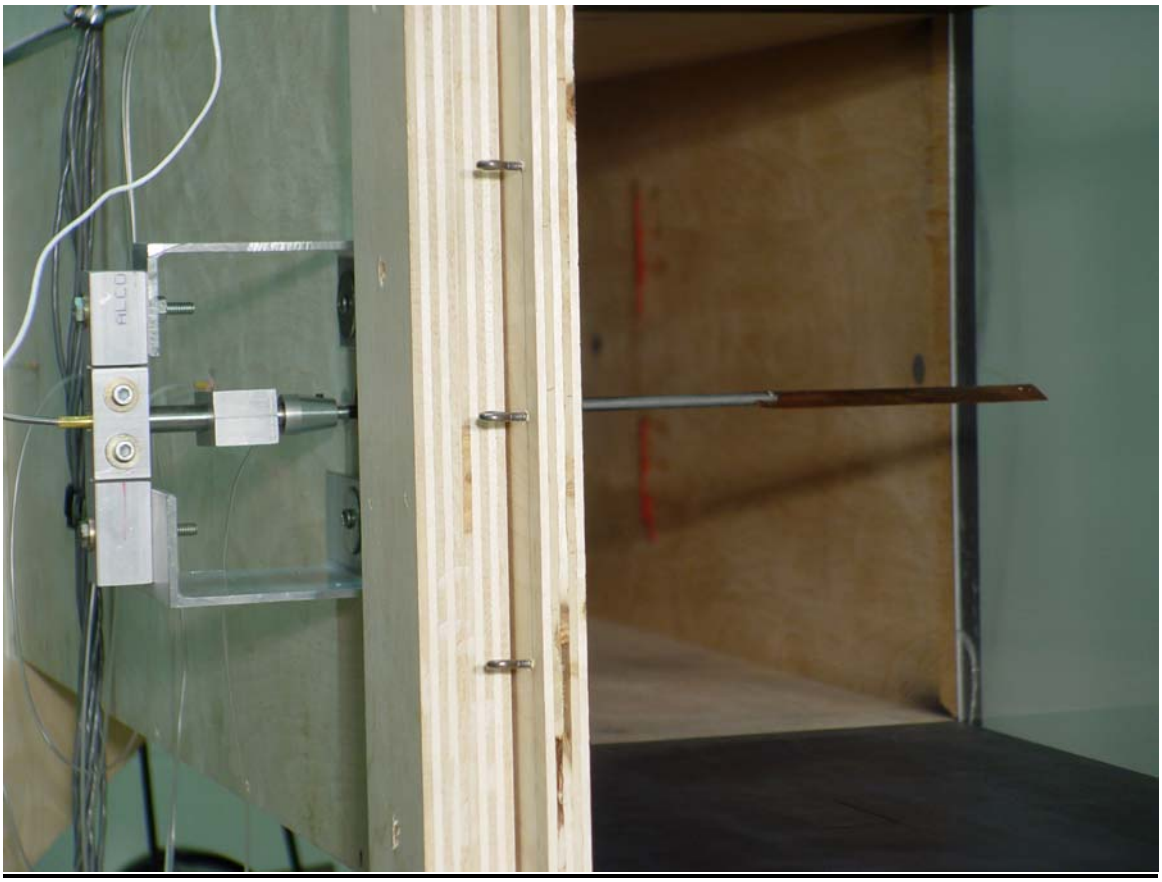

Figure 4.32 Load cell/airfoil configuration

4.5.3 Data Acquisition

Several previous tests indicated the unsteady nature of the tunnel flow. Because of this, an instantaneous value read from the output of the load cell would not be an accurate representation of the force applied. A more accurate method, provided by the same Agilent datalogger used in the pressure surveys, is a time-integrated average. To accomplish this, the output from the calibration instrument, which was wired to the LCD screen, was also wired to the Agilent datalogger.

Since the input to the datalogger is a voltage, a relationship between load applied and voltage recorded was obtained so the force could be determined from the voltage recorded by the datalogger. The LCD output was steady and accurate with the tunnel off, and could be used to accomplish the calibration. Once the biased axis was identified and oriented vertically, several different weights were applied to the load cell by hanging an increasing number of hex nuts from the end of the cantilevered beam. For each nut added, the force was recorded from the LCD along with the time average voltage from the Agilent datalogger. Figure 4.33 shows the calibration plot. The trend is perfectly linear, indicated by the R^2 value of 1.000. The slope on the plot converts the output voltage to pounds applied to the load cell. The intercept is a function

of the weight of the configuration, not the applied load, and is not used to convert from voltage to pounds. Equation 4.1 displays the conversion from recorded voltage (in millivolts) to pounds.

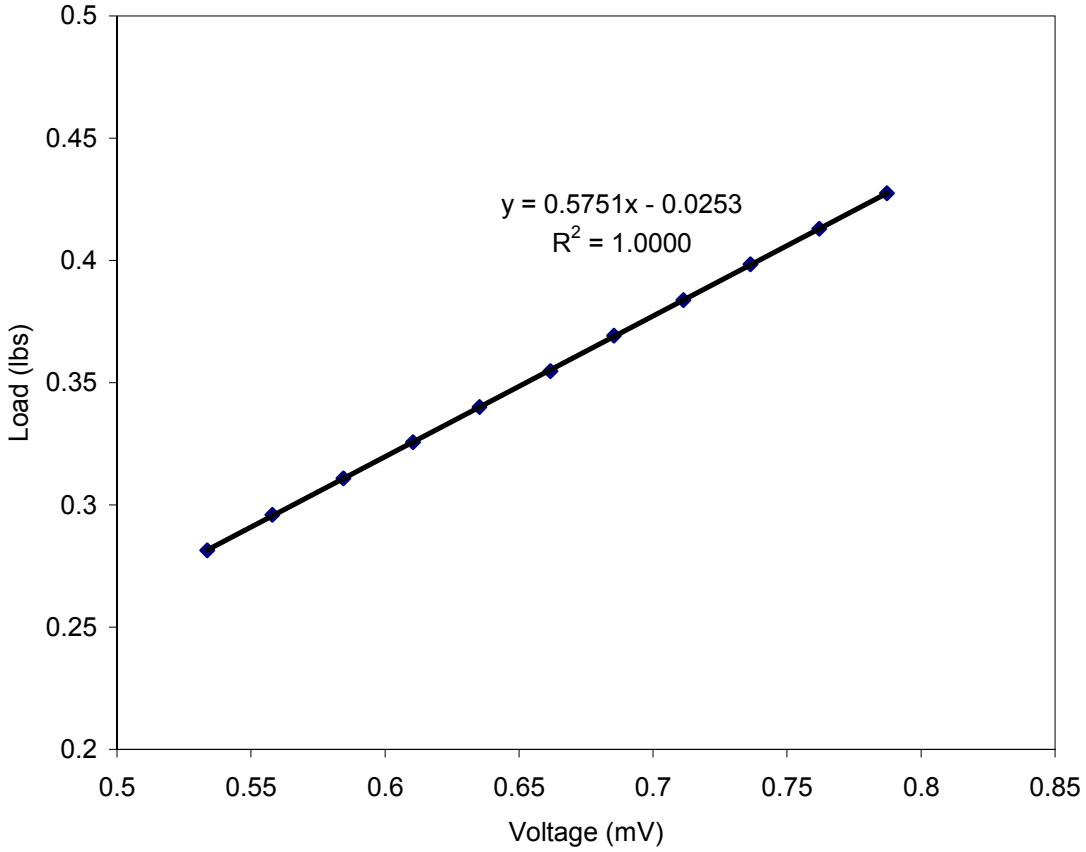

Figure 4.33 Calibration plot relating voltage to pounds applied to the load cell

$$Load(lbs) = 0.5751 \cdot Voltage(mV)$$

Equation 4.1

4.5.4 Load Cell Operation and Data Processing

To simplify the process of adjusting the load cell, the tunnel was rotated 90° to its side. Because of this, the resultant force measured by the load cell is not simply a vector sum of the aerodynamic forces, but also includes the weight of the model and mounting hardware. To

obtain the actual aerodynamic resultant force of the lift and drag, the weight must be recorded and accounted for using vector subtraction. Figure 4.34 shows a schematic of the measured forces and then the subtraction which results in the actual resultant force.

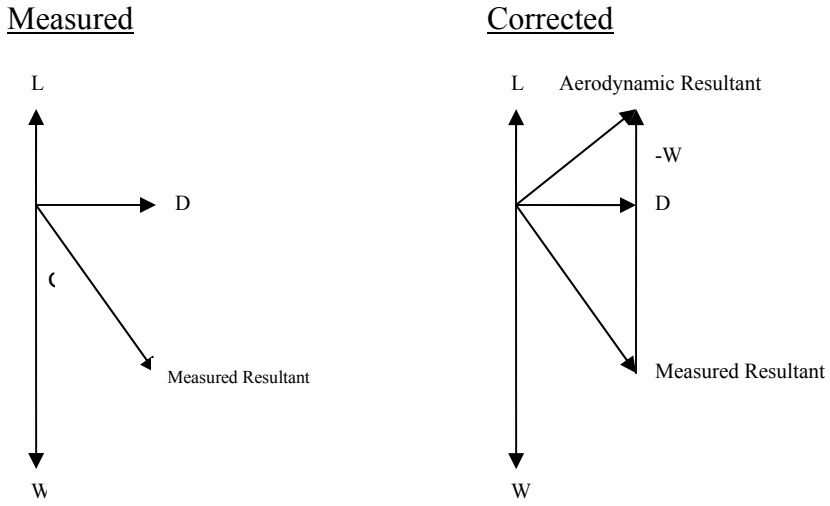

Figure 4.34 Vector math showing how the weight is subtracted to obtain the actual resultant force

The direction of the resultant force, initially, was an unknown and was found empirically. The load cell output was only accurate when the measurement axis was aligned with the load. Therefore, the angle of the resultant could be obtained by rotating the load cell until the output was maximized. At this point the measurement axis was aligned with the resultant force.

Since the weight of the configuration was significantly larger than the predicted lift on a six square inch airfoil, the measured resultant must have been located in the fourth quadrant, most likely close to straight down, which was defined as 0°. The first measurement recorded the weight: the load cell axis was aligned with 0°, and the tunnel remained off. The tunnel was then set to the desired RPM and measurements were obtained every 2.5° until a peak was recorded and confirmed with decreasing loads measured 2.5° and 5° past the peak (i.e. if the peak was recorded at 7.5°, measurements were taken at 10° and 12.5° to ensure a downward trend past the peak).

For each measurement, the tunnel was shut down and the load cell and airfoil repositioned. To position the load cell axis a digital protractor was set on the flat aluminum block mounted on the load cell. The protractor angle, φ, indicated how far the measurement axis deviated from 0°, which was defined as straight down. Once the load cell was secured at the desired angle, the set screw holding the rod was loosened and a wood guide was inserted into the tunnel to ensure the airfoil sat at 5° (the angle at which the Wrights' claimed greatest efficiency for the #12 airfoil). Once positioned, the set screw was tightened, the guide removed, and the tunnel started.

At each 2.5° increment the Agilent was set to scan the load cell 10 times for approximately three seconds per scan. Each scan generated a time average value for the voltage output of the load cell, and the average of the 10 scans provided an accurate measurement of the load, despite the unsteadiness of the measurements. Once the peak was determined, 100 scans were conducted and averaged to obtain a very accurate representation of the measured resultant force.

Once the peak magnitude and direction were recorded, vector arithmetic was applied (according to Figure 4.34) to obtain the true resultant of the lift and drag forces. The relationship between voltage and pounds was then used to obtain the magnitude of the resultant force in pounds. Simple trigonometry then resolved the force into the lift and drag components.

Additionally, the qualitative effect of the interference between the rod and the airfoil was measured by inserting a dummy rod from the top of the tunnel. The rod was mounted as close as possible to the airfoil tip without actually touching the airfoil. 10 scans were conducted in this configuration to determine whether the interference from a rod would affect the measured resultant force.

As the resultant force magnitude and direction were dependent on RPM, the entire battery of tests was repeated for the driver section running at half, three-quarter, and maximum RPM. Earlier experiments had determined data at one-quarter RPM were unreliable, thus the tests were not conducted at that RPM.

5 ANALYTIC TRADE STUDY RESULTS

5.1 Numerical Analysis Setup: MSES

MSES, which stands for Multi-element Airfoil Design/Analysis Software, is a numerical airfoil development code. It has analytic, design, and optimization capabilities, but was only used to analyze a single element airfoil across a range of Reynolds numbers and angles of attack. The code is capable of solving for low Reynolds number flows, separation bubbles, and trailing edge separation, all of which were necessary in the evaluations of the Wrights' airfoil. Aerodynamic force predictions were accurate just past the stall point, and the code was able to predict transition from laminar to turbulent flow.

MSES is not computational fluid dynamics software in which a grid would be applied to an entire three dimensional space and evaluated according to approximations of the Euler equations. Instead it uses "finite volume discretizations of the steady Euler equations on an intrinsic streamline grid."[123] An intrinsic streamline grid is an 'H' grid similar to Figure 5.1. Finite volume discretization refers to the discretized equations of motion which are solved at the mass centroid of each grid element (as opposed to being solved at the gridline intersections as they are in finite element analysis). The code uses two equations to model the boundary layers and the trailing wakes, and solves them iteratively by applying certain boundary conditions set by the airfoil surface. The system is a two-equation momentum integral and is solved using a "full Newton method."

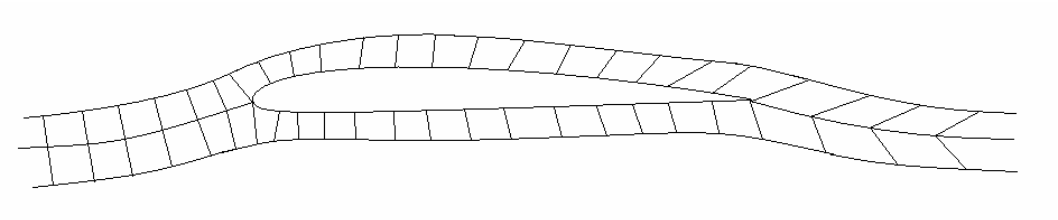

Figure 5.1 Example of an intrinsic 'H' grid

5.2 Purpose and Method

The Reynolds number within the Wrights' wind tunnel was extremely low, roughly 20,000, while the Reynolds number for the flow over the Wright Flyer was closer to 1,800,000, more than two order of magnitudes larger[124]. It is important to understand the effects of this Reynolds number variation on lift, drag, pitching moment, and efficiency, defined as the lift-to-drag ratio.

[123] Mark Drela, *MSES User's Manual*, 16 May 1994.
[124] Colin P. Britcher, Drew Landman, Robert Ash, Kevin Kochersberger, and Ken Hyde, "Predicted Flight Performance of the Wright 'Flyer' Based on Full-Scale Tunnel Data," AIAA Paper 2004-0104, Jan. 2004.

In most wind tunnels matching both a Reynolds and Mach number is a near impossible task. Because of this, it is far easier to study Reynolds and Mach effects through analytic methods.

The airfoil studied was a modified model 10 Eiffel airfoil design found in the UIUC Airfoil Database[125]. The database claims the airfoil was close to the Wrights' #12 airfoil and the airfoil used on the Wright Flyer and the Wright Model B. The leading edge of the airfoil was rounded with a circular contour so the analysis code could process it.

The code, MSES, is an airfoil development and analysis program. It conducts viscous approximations and can be used to conduct analysis over a range of angles of attack, evaluate Reynolds number effects, and determine flow transition points. Since the code is a 2D analysis program, the values will be different from the Wrights 3D wind tunnel measurements (lift will be higher, drag and moment lower), but the qualitative comparison remains valid for Reynolds number effects.

5.3 Reynolds Number Sweep

The first set of runs involved a Reynolds sweep from the wind tunnel Reynolds number of 20,000 to 2,000,000 while maintaining a constant angle of attack of 5° (which the Wright data showed as the most efficient, and which was used in these and the PIV experiments for that reason). The code was used to evaluate the effects of increasing Reynolds number on lift, drag, pitching moment, and efficiency.

Using a logarithmic scale, there was a coherent trend apparent with all forces and moments as Reynolds number increased. Figure 5.2, Figure 5.3, and Figure 5.4 show the variation of the forces and moments with Reynolds number, while Figure 5.5 shows how efficiency was affected by the increase in Reynolds number. The plots make it clear that an increase in Reynolds number results in a greater lift coefficient and lift-to-drag ratio, and results in a decrease in the drag and pitching moment coefficients.

[125] UIUC Airfoil Database – Version 2.0, <http://www.aae.uiuc.edu/m-selig/ads/coord_database.html>

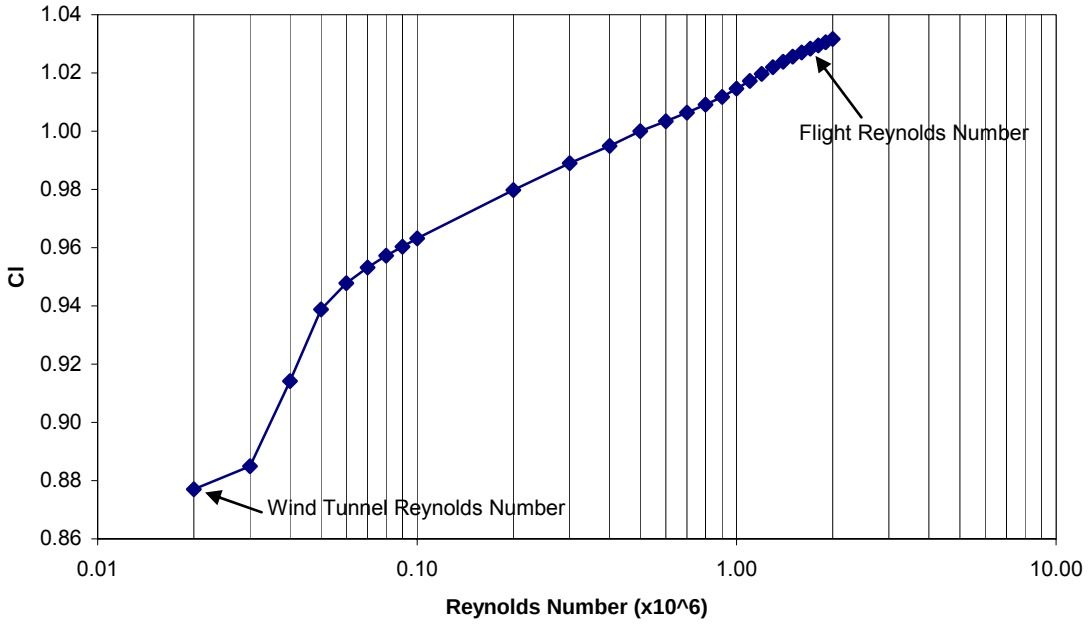

Figure 5.2 Variation of lift coefficient with Reynolds number

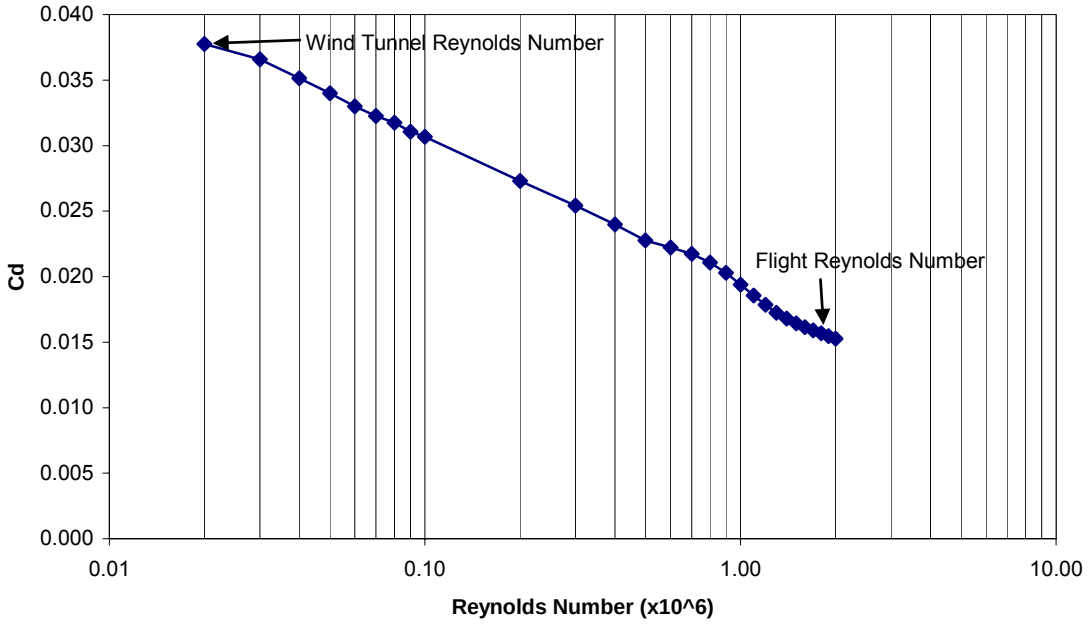

Figure 5.3 Variation of drag coefficient with Reynolds number

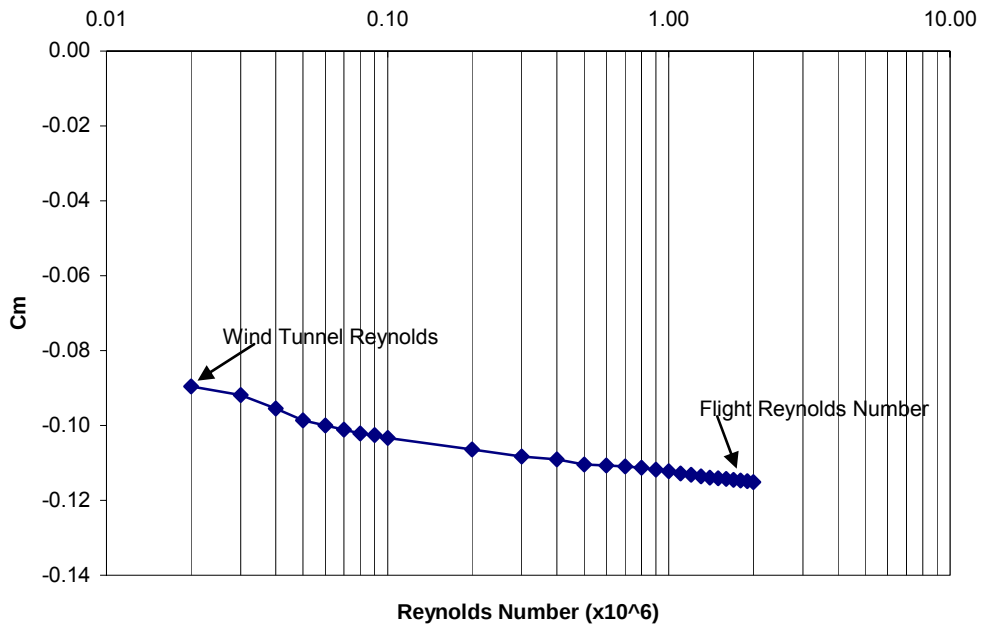

Figure 5.4 Variation of moment coefficient with Reynolds number

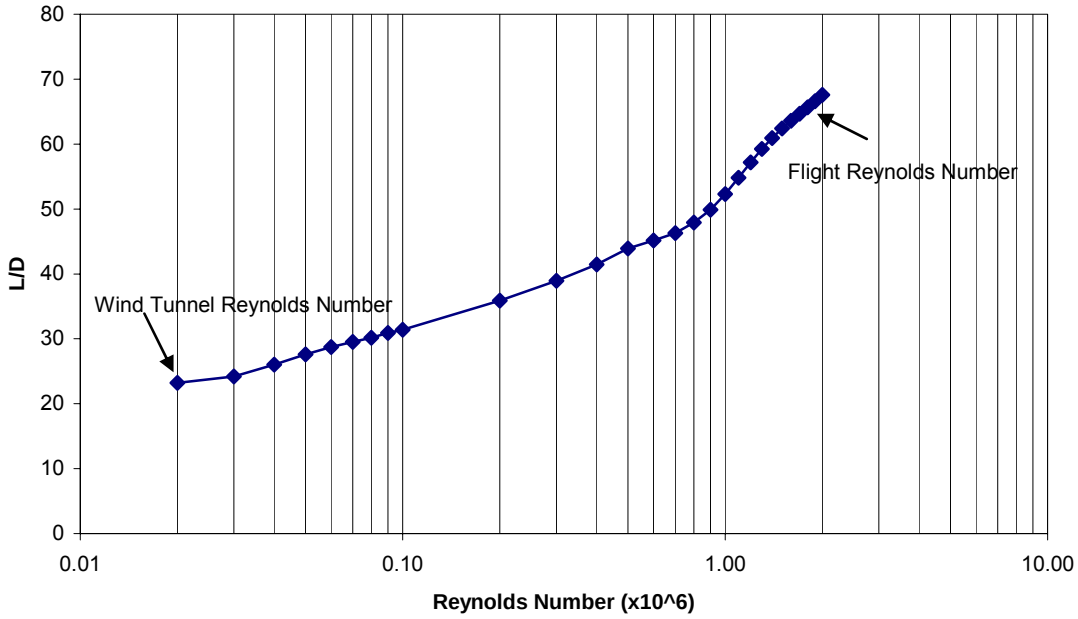

Figure 5.5 Variation of lift-to-drag ratio with Reynolds number

The graphs show how drastic an effect the Reynolds number had on the major characteristics of the airfoil. Table 5.1 provides a more direct comparison of the airfoil characteristics at the wind tunnel and flight Reynolds numbers. All the changes were substantial but those that stand out most were the drag and efficiency (L/D) which are inherently related. Essentially, increasing Reynolds number by a factor of 90 resulted in a 280% boost in efficiency by increasing lift and decreasing drag. As a side effect, the magnitude of the pitching moment also increased; however the Wrights were not quantitatively aware of pitching moment effects.

Table 5.1 Comparison of wind tunnel and flight Reynolds number at 5°

	C_l	C_d	C_m	L/D
20,000 (Wind Tunnel)	0.877	0.0378	-0.0896	23.23
1,800,000 (Flight)	1.029	0.0157	-0.115	65.65
Percent Increase	17.38%	-58.46%	28.01%	182.59%

These results show that dependence on the small-scale wind tunnel results would have resulted in an over-designed wing, and a power plant generating more than twice the thrust necessary to overcome the drag. The subsequent performance would have been high even by today's general aviation standards.

5.4 Alpha Sweeps

The second set of runs focused on comparing the wind tunnel and flight Reynolds numbers by conducting alpha sweeps at each Reynolds number (20,000 and 1,800,000 respectively). The lift and moment curves, drag curve, and aerodynamic efficiency across a range of angles of attack were then compared to determine what performance characteristics the Wrights would have predicted from their wind tunnel tests and what the Wright Flyer would have actually produced.

The alpha sweeps were conducted at the wind tunnel and flight Reynolds numbers in order to compare the airfoil characteristics at the two conditions. The lift and moment curves as well as the drag polar and the lift-to-drag plot at both conditions were superimposed to show the effect on airfoil performance when scaled from wind tunnel to flight Reynolds number.

5.4.1 Scaling Effects on Lift

Figure 5.6 compares the lift curves at the wind tunnel and flight Reynolds number. Despite numerous similarities, there is an obvious difference in the profiles at an alpha of 4°. At the wind tunnel Reynolds number the curve steadily dips, then jumps up at 5°, while the higher Reynolds number curve remains smooth across the sweep. Figure 5.7 directly compares the pressure distributions for both Reynolds numbers at the angle where they deviate the most: 4°. At the low Reynolds number there is almost no pressure spike indicating leading edge flow separation which never fully attaches. The high Reynolds number shows a distinct pressure spike at the leading edge indicating attached flow along the entire airfoil. The low Reynolds number also shows a transition point at about 22% of the chord. At the high Reynolds number this transition occurs very near the leading edge since the flow is almost all turbulent. Figure 5.8

goes into more depth showing the effect of the leading edge separation at low Reynolds numbers. At 3° and 4° the pressure spike is small and the pressure drops off quickly producing a relatively flat profile along the chord. At 5°, however, the leading edge flow is attached resulting in a more distinct spike and a large pressure differential before the flow transitions at 22% chord. This accounts for the low Reynolds number lift curve becoming more parallel to the high Reynolds number curve at 5° as shown in Figure 5.6.

Comparing the lift curves reveals several other characteristics of the two Reynolds number tests. First, the plots have similar lift curve slopes and stall angles, thus the Wrights could have accurately predicted the stall location as well as the linear relationship between the angle of attack and lift coefficient. However, since the maximum lift coefficient and the zero lift coefficient are larger in the case of the flight Reynolds number, the Wrights would have under predicted the lift produced unless they were aware of this shift.

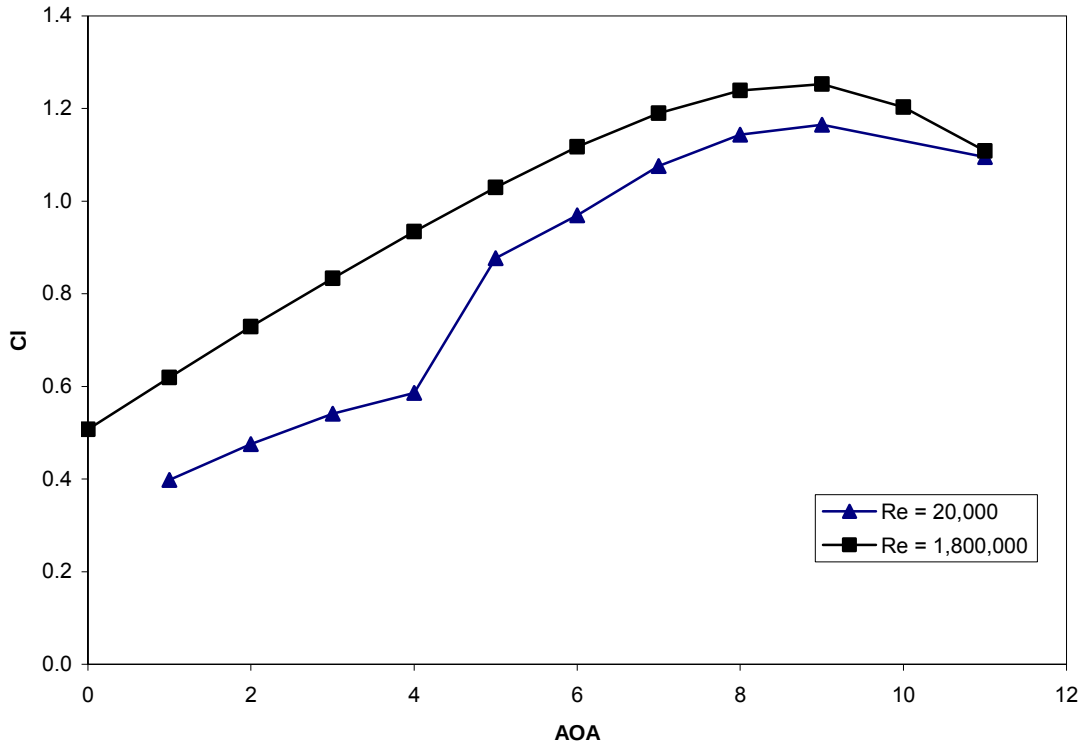

Figure 5.6 Lift curve slope comparison at wind tunnel and flight Reynolds numbers

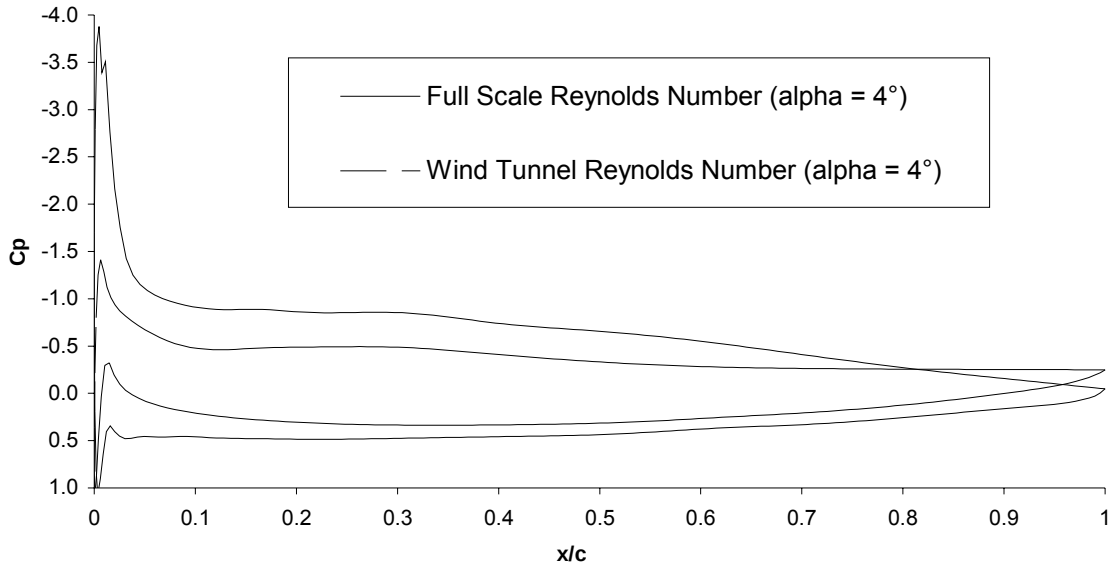

Figure 5.7 Comparison of pressure coefficients at wind tunnel and flight Reynolds numbers at AOA=4°

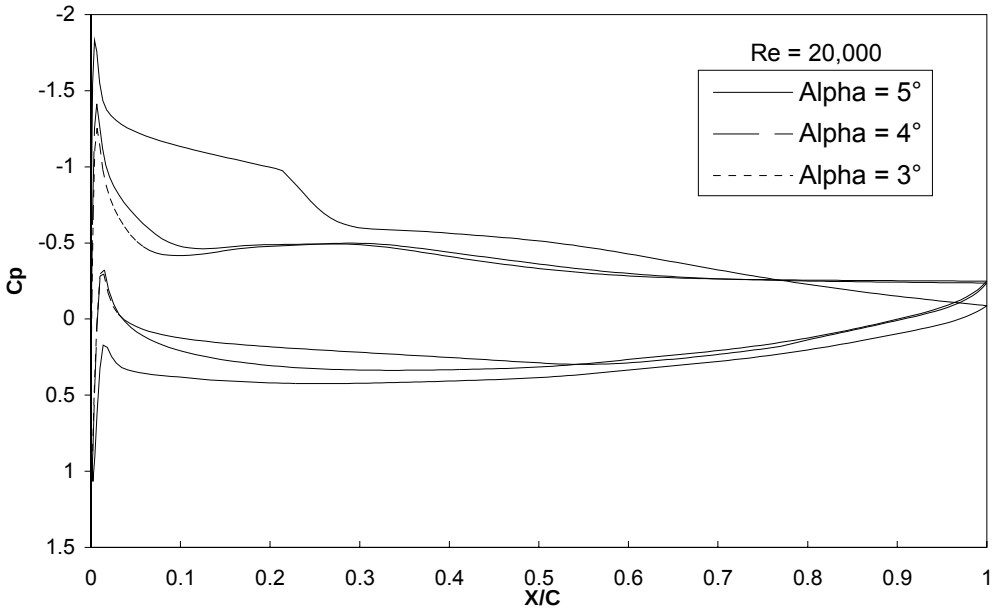

Figure 5.8 Low alpha leading edge separation and attachment at the wind tunnel Reynolds number

5.4.2 Scaling Effects on Drag

Figure 5.9 compares the drag curves (drag polars) at the wind tunnel and flight Reynolds numbers. Similar to the lift curve, the drag polar follows a more consistent trend at the higher Reynolds number, most likely due to the leading edge separation at the wind tunnel Reynolds number causing inconsistency. Despite this, the profiles are very similar with one major difference: the high Reynolds number case is shifted down by a substantial margin. The minimum drag for the high Reynolds number case was 0.01134, while the low Reynolds number case resulted in a minimum drag of 0.03311, a 300% increase. Because of this, the Wrights would have greatly over predicted the drag on their wing. Significantly, this prediction would have forced the Wrights to seek a much greater thrust and much larger engine than actually necessary to overcome the inflated value.

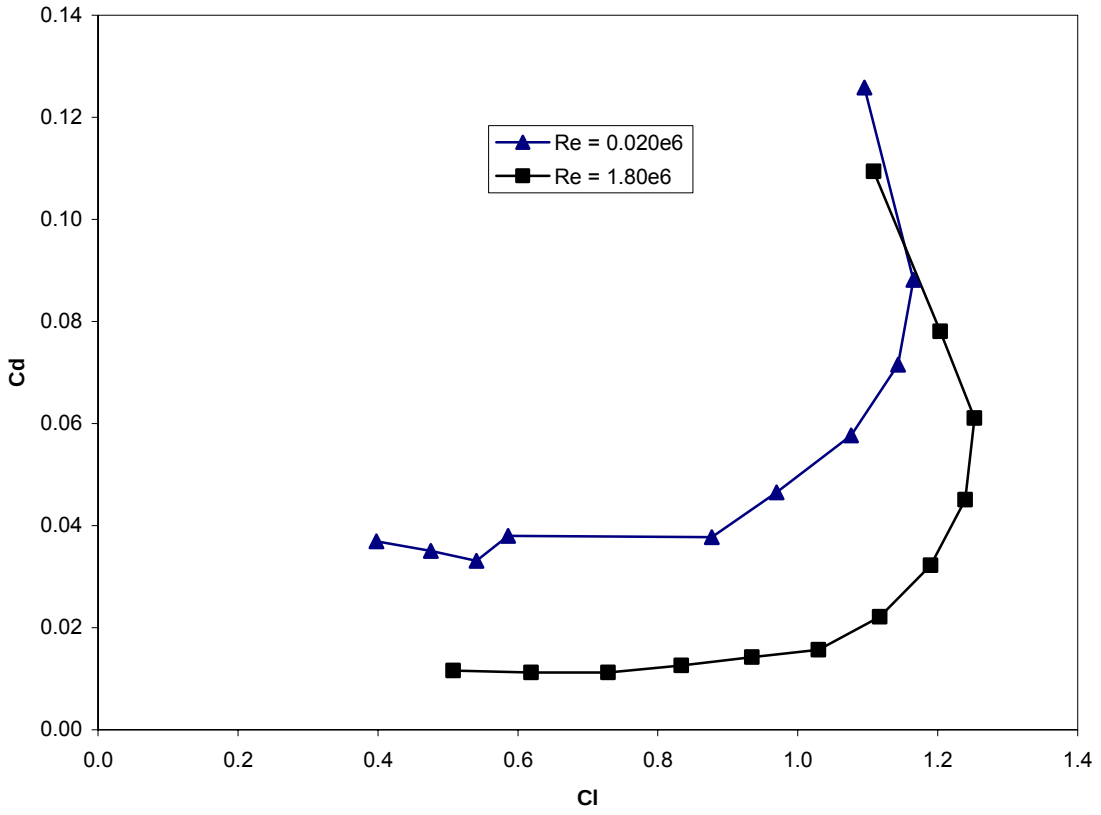

Figure 5.9 Drag polar comparison at wind tunnel and flight Reynolds numbers

5.4.3 Scaling Effects on Pitching Moment

Figure 5.10 compares the pitching moment coefficient at the flight and wind tunnel Reynolds numbers. Of all the performance characteristics this is the only one adversely affected by the

increase in Reynolds number. The magnitude of the moment increases by almost 30% from the wind tunnel to the flight Reynolds number.

The Wrights were not able to measure pitching moments in their wind tunnel and were only slightly aware of its qualitative effects. Because of this, the 30% difference would not have affected their performance predictions, but it does underscore the wholly different performance of the airfoil at the low and high Reynolds numbers. Additionally, it had effects on the aircraft stability and control. Among other things, a larger pitching moment would require a greater countering moment from the canard which, even today, is a difficult element to size.

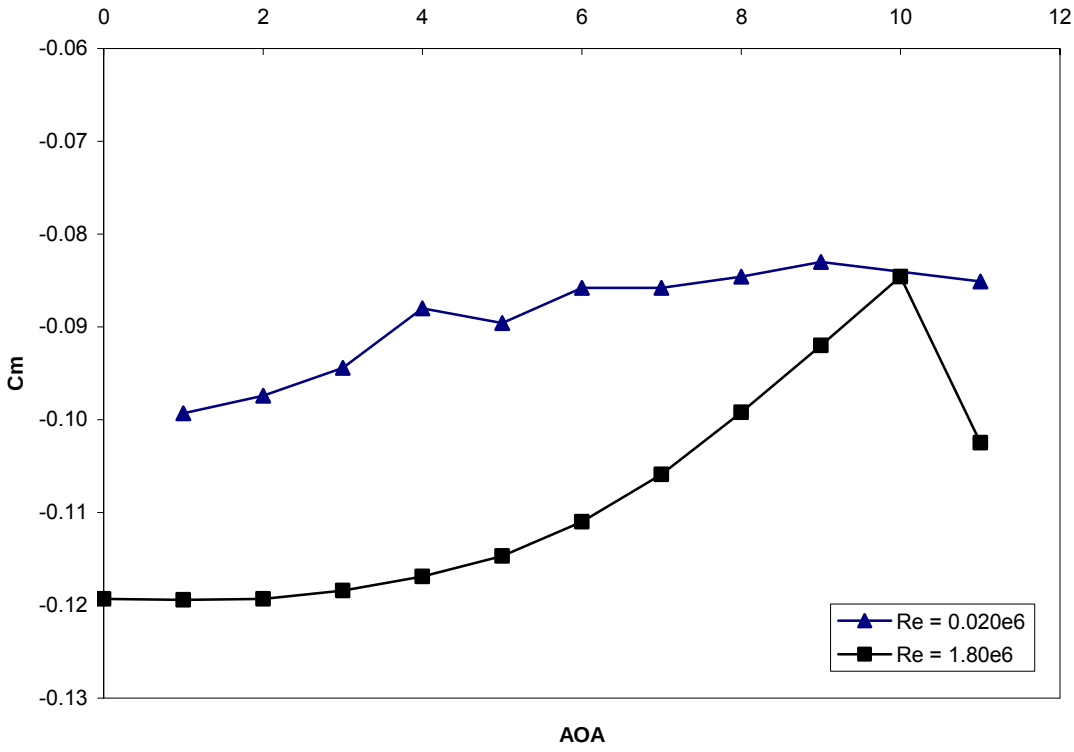

Figure 5.10 Pitching moment comparison at wind tunnel and flight Reynolds numbers

5.4.4 Scaling Effects on Lift-to-Drag Ratio

Figure 5.11 compares the lift-to-drag ratio for the airfoil at the wind tunnel and flight Reynolds numbers. The plot clearly shows the superior efficiency at higher Reynolds number due to the boost in lift and decrease in drag noted earlier. Additionally, the lower Reynolds number condition "peaks" in efficiency at a higher angle of attack than the high Reynolds number case, 5° compared to 2°. This is significant because the Wright Flyer's canard configuration was not

actually stable at its true cruise condition[126]. The Wrights flew it at a higher angle of attack thinking they were flying at the design cruise point. Figure 5.12 shows the Wrights' actual wind tunnel data for the #12 airfoil and confirms the analytical results showing the wind tunnel predicted a higher alpha for "peak" efficiency compared to the flight condition. Note that these are 2D values for lift-to-drag. The 3D values would be significantly lower but would show the same qualitative trends.

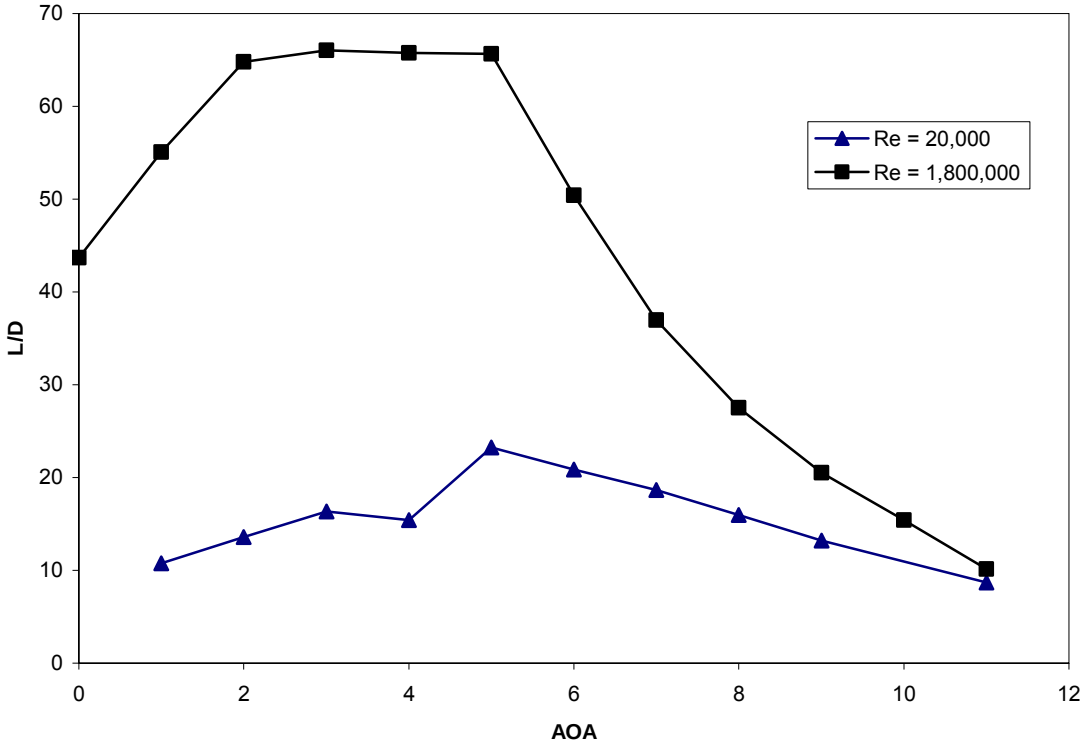

Figure 5.11 Efficiency comparison at wind tunnel and flight Reynolds numbers

[126] Colin P. Britcher, Drew Landman, Robert Ash, Kevin Kochersberger, and Ken Hyde, "Predicted Flight Performance of the Wright 'Flyer' Based on Full-Scale Tunnel Data," AIAA Paper 2004-0104, Jan. 2004.

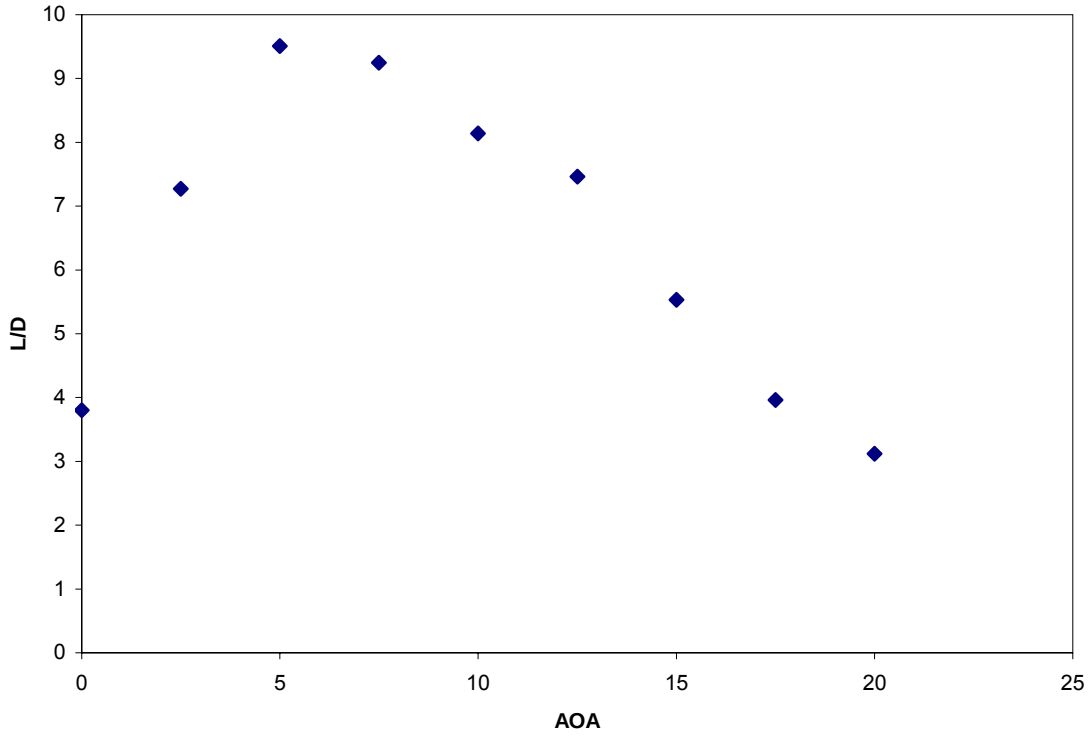

Figure 5.12 Efficiency data recorded by Wright Brothers from wind tunnel tests on #12 airfoil

5.5 Analytic Conclusions

5.5.1 Idealization

Importantly, these analytic tests are ideal, two-dimensional comparisons. They do not take into account the PIV test results which show how spanwise velocity distributions and the effects of the balance on the airfoil would have affected the Wrights' readings from the tunnel.

5.5.2 Scaling Effects

Clearly the Reynolds number has a large impact on all forces and moments over the range from wind tunnel to full scale testing. The data from the wind tunnel deviates so greatly from the full scale data that it may not have been quantitatively useful at all. Under predicting the lift would not have caused their design to fail, however over predicting the drag could have resulted in design aspects which would have prevented flight altogether.

Despite the low quantitative value of the tunnel and the contrast between wind tunnel and full scale Reynolds number data, most of the qualitative comparisons from the wind tunnel data were still extremely valuable to the Wrights and contributed to their ultimate success.

6 EXPERIMENTAL RESULTS

6.1 Axial and Cross Sectional Static Pressure Surveys

6.1.1 Purpose and Method

The static pressures in the cross section and in the axial direction are good indicators of certain flow characteristics. The cross sections are indicators of the directionality, and the axial pressures measure the boundary layer growth as the flow moves through the tunnel. Both sets of pressures are indicators of turbulence and time dependence. These characteristics need to be analyzed to ensure straight flow before more detailed flow analysis, such as dynamic pressure surveys, can be completed.

These surveys used the same data set acquired for the Repeatability Evaluation in the Experimental Setup.

6.1.2 Evaluation of Pressure Coefficients

The static pressures were non-dimensionalized as a pressure coefficient using Equation 6.1.

$$C_{p_s} \equiv \frac{(p_T - p_{s_i})}{(p_T - p_{s_{TS}})} = \frac{(p_T - p_{s_i})}{(q_{TS})}$$

Equation 6.1

where p_T and $p_{s_{TS}}$ are the total and static pressure in the test section (static port 4), p_{s_i} is the static pressure at the port being non-dimensionalized, and q is the dynamic pressure in the test section.

By non-dimensionalizing the data, all the static pressures are measured on the same scale, making comparisons easier, and making trends easier to see.

6.1.2.1 Cross Sectional Data

The cross sectional data was organized into forward and aft cross sections (test 1 and test 2, respectively), and further divided into groups based on RPM. For each cross section the readings from the four static pressure ports[127] were averaged and the standard deviation was calculated. Similar to the Repeatability Evaluation, the standard deviations were non-dimensionalized by

[127] The "reading" from each pressure port is an average of the 30 pressure recordings at a given RPM, the same data set used in the Repeatability Evaluation.

dividing through by the average, resulting in percent variations. The percent variation permits ease of comparison between different RPMs and between the two cross sections.

6.1.2.1.1 Comparison of Forward and Aft Cross Sections

Table 6.1 shows the percent variation in the forward and aft cross section at each propeller RPM.

Table 6.1. Percent variation for forward and aft cross section

RPM	%variation (fwd cross section)	%variation (aft cross section)
892	28.99	485.93
1784	23.93	35.15
2676	16.24	20.16
3568	15.11	11.84

The large variations at the minimum RPM are present here as they were in the Repeatability Evaluation, especially in the aft cross section. Once again, the data will not be considered in this analysis because the pressure differentials were significantly smaller than the disturbance magnitudes. Thus the minimum RPM data is not an accurate representation of the variation at that RPM.

Notably the aft cross section has much larger variations at 1784 RPM, but the variations approach the magnitude of the forward cross section at 2676 RPM. By the maximum RPM the aft cross section variations are smaller than the forward variations. The trends in the variations result from numerous sources of turbulence, and it is important to note that these variations demonstrate a great deal of flow unsteadiness.

6.1.2.1.2 Evaluation of Cross Section Uniformity

Once the accuracy of the cross sectional data has been established, it can be evaluated to determine uniformity of static pressure within a cross section. Within either the forward or aft cross sections, the standard deviation is an indication of the uniformity: the smaller the standard deviation, the more uniform the static pressures are. Establishing the uniformity of the static pressure is important because the dynamic pressure measurements use the total pressure probe and static pressure port 4, often well below the probe. If the static pressures are not uniform, port 4 cannot be used to accurately determine the dynamic pressure.

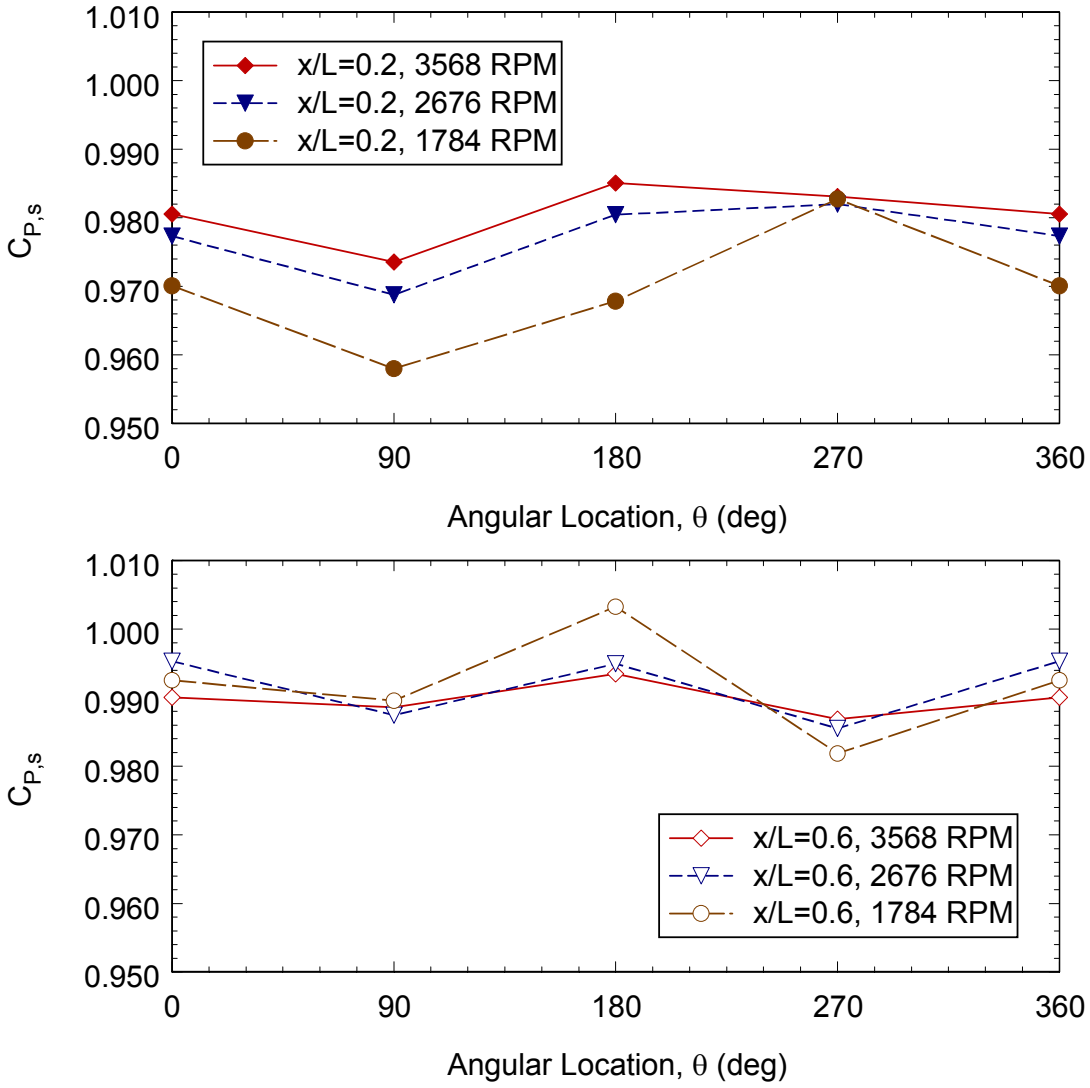

Figure 6.1. Forward (top) and aft (bottom) cross sectional static pressures

The uniformity can also be evaluated by plotting the non-dimensional pressure coefficients which, ideally, would be equal, generating a straight line. Figure 6.1 represents the plots of the cross sectional data with respect to their location on the cross section. The figure represents both the forward (upper plot) and aft (lower plot) cross sectional pressure distributions.

The three RPM settings show surprising uniformity considering the variations recorded in Table 6.1 and discussed in the Repeatability Evaluation. Notably the trends are more organized in the forward cross section than the aft, most likely due to the high turbulence caused as air exits the wind tunnel without any form of pressure recovery. The uniformity further supports the conclusion that the average of a low pressure taken over a long period is accurate despite short term variations. Additionally, static pressure uniformity is one indicator of flow directionality (i.e. smaller variations are the result of flow aligned with the tunnel centerline).

6.1.2.2 Axial Data

The axial data provides a measure of the boundary layer growth in the tunnel, fore to aft. Since the axial group remained constant between test 1 and 2, the results are redundant and allow for comparison to evaluate the repeatability of the data.

The data should show an upward trend fore to aft indicating boundary layer growth. As the boundary layer grows, this buoyancy effect causes the velocity to increase fore to aft which increases the dynamic pressure resulting in a decrease in the static pressure. Therefore the magnitude of the change in static pressure will increase axially as the absolute static pressure drops.

Figure 6.2 shows the results from both test 1 and test 2: the non-dimensional pressure coefficient versus the non-dimensional axial location.

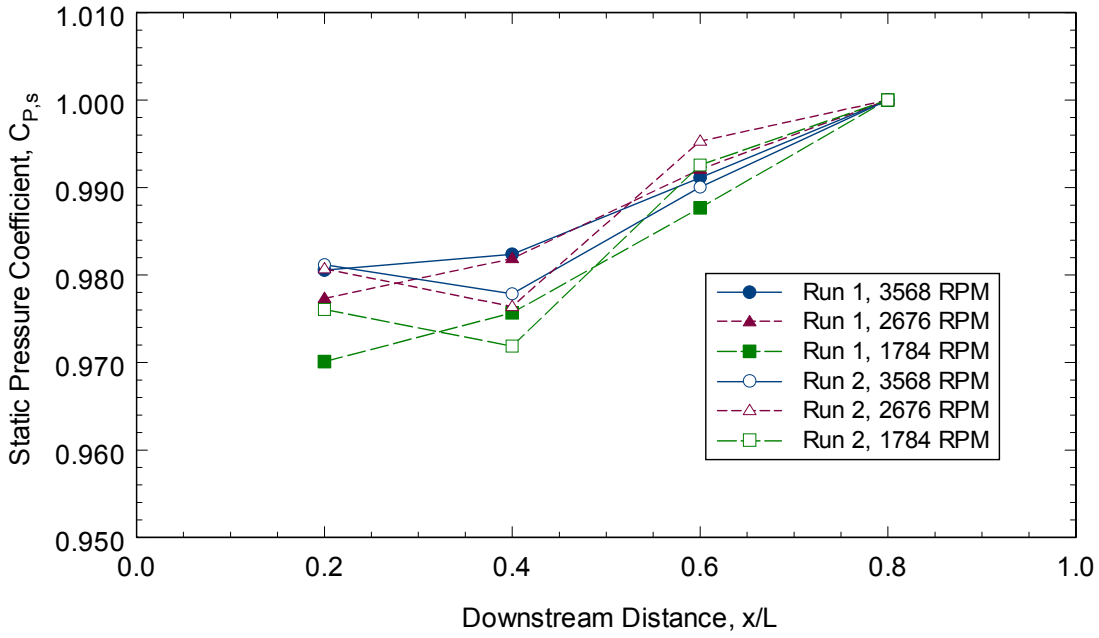

Figure 6.2. Axial static pressure data

The test results show a general upward trend, as expected, indicating the growth of the boundary layer. The fact that all terminate at 1.00 is trivial. The denominator of the non-dimensional equation includes static port 4, which is also the final port in the axial group, therefore the equation reduces to 1.0 at that location. One discrepancy, however, pertains to the three groups which have a drop, rather than a rise, between static port 1 and 2. The discrepancy only occurs in Test 2 which indicates the cause may be a slight movement in the tunnel or the contraction between tests 1 and 2 causing a change in the flow, or even flow separation, which would result in the indicated pressure drop between ports 1 and 2. Despite the small discrepancy, the data

shows the expected trend and a linear curve-fit through the data would yield a reliable pressure gradient.

6.1.3 Static Pressure Conclusions

The most important conclusion which can be drawn from the static pressure analysis is that the average of small pressure differentials over a long period of time is accurate despite short term inconsistencies. The uniformity within each of the cross sections and the anticipated upward trend of the axial groups indicate the results for these pressure ports were accurate, despite the differentials being lower than the resolution of the transducers.

6.1.3.1 Cross Sectional Conclusions

The two cross sections have similar variations but different sources. The aft cross section is mostly affected by the lack of a diffuser while the forward cross section is affected most by the fan blowing directly into the tunnel and the poor design of the inlet and contraction. The uniformity of the cross sectional data indicates the flow is aligned with the tunnel centerline. If the flow was misaligned, generating directionality and swirl, the readings on the four walls would vary to a much larger degree.

6.1.3.2 Axial Conclusions

The data overlap from one axial data set to another shows consistent boundary layer growth at all RPMs which concurs with the anticipated trend.

6.1.3.3 Errors

One source of error is similar to the Repeatability Evaluation: there could be problems with the individual pressure ports. However this is unlikely as the ports have been checked and the data produced follows the anticipated trends.

The other potential error involves the discrepancy in the axial results from test two. Regardless of the reason, redundant data which should be repeatable shows unexpected discrepancies. Despite the discrepancy the data still indicates the expected trend and yields an accurate pressure gradient.

6.2 Vertical and Horizontal Flow Surveys

6.2.1 Purpose and Method

The original vertical flow survey served three distinct purposes. First, it established the gross non-uniform velocity profile of the flow, resulting in a “dead zone,” a high velocity region, and the boundary layer region. The survey also established the approximate magnitude and profile of the upper and lower boundary layers. Finally, the accurate overlap of the top-down and bottom-up data validated the method and resolutions used to obtain the data.

The original survey left much to be desired, however. First, the asymmetry in the results indicated a misalignment of the fan and tunnel which meant, while the qualitative conclusions might still be valid, the quantitative data was not. To gain a quantitative understanding of the uniformity and the boundary layers, the survey had to be repeated once the alignment was corrected. Second, there was no data across the horizontal axis to provide insight into the overall flow symmetry. Finally, since the original survey was only conducted at the maximum RPM, there was no data to establish the dependence of flow characteristics on RPM and velocity. The second set of vertical flow surveys, combined with horizontal surveys, were conducted to address these issues.

The vertical flow surveys were conducted almost identically to those previous (see Experimental Setup). The traverse was secured in place of the tunnel window, and the total pressure probe recorded data according to the resolutions in Table 6.2. Data point spacing was decreased near the walls to obtain better resolution in the boundary layer.

Table 6.2 Resolutions in different flow regions.

Distance from wall (mm)	Δy resolution (mm)
0-20	1
22-50	2
55-100	5
110-400	10

In both the top-down and bottom-up survey, the probe only traversed 250 mm rather than the 400 mm in the original survey. This still provided almost 100 mm of overlap, which was sufficient based on the accuracy of the overlap in the original flow survey.

The horizontal survey was conducted using the same resolution and overlap. In order to use the traverse, however, a hole was drilled in the side of the tunnel, at the centerline, and a traverse was secured to a sawhorse and sat flush with the side of the tunnel so the probe could be moved along the horizontal axis (see Figure 6.3). With the traverse mounted on the side of the tunnel, the survey was taken identically to the vertical survey, first moving from left to right, covering 250 mm, then right to left, covering 250 mm, with almost 100 mm of overlap.

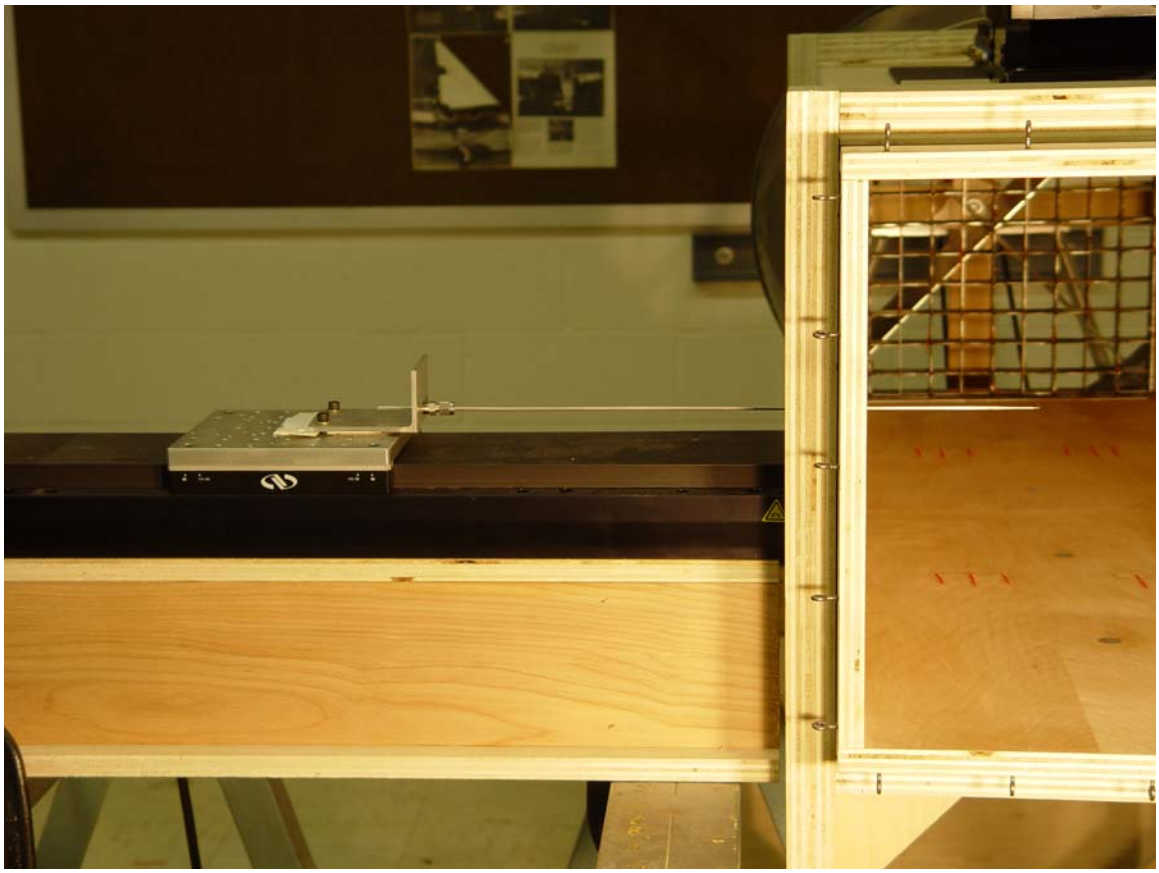

Figure 6.3 Horizontal survey setup with traverse and total pressure probe

6.2.2 Evaluation of Flow Nonuniformity

The first observation made during the flow surveys was to ensure the fan was aligned with the tunnel centerline, and that it was perpendicular to the intended direction of flow. If the fan was aligned the flow would be symmetric, otherwise the "dead zone" would not be in the center and the boundary layers would not have equal magnitude. Figure 6.4 and Figure 6.5 represent the nondimensional horizontal and vertical flow surveys, respectively, and include data from surveys at a fan RPM of 1784 and 3568. In both plots, the origin is the center of the tunnel. The rotation of the plots provides a more intuitive view of each condition.

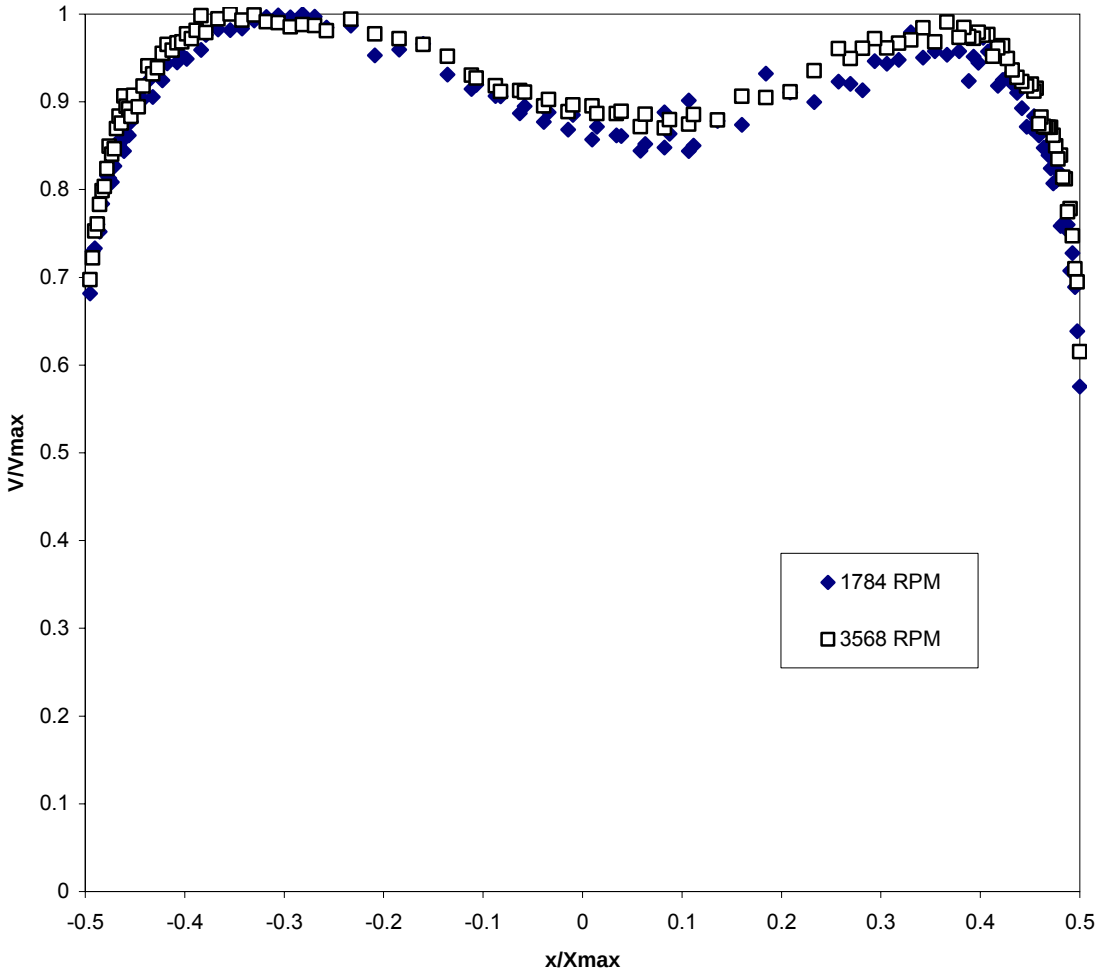

Figure 6.4 Overlay of nondimensional horizontal flow surveys at half and maximum RPM

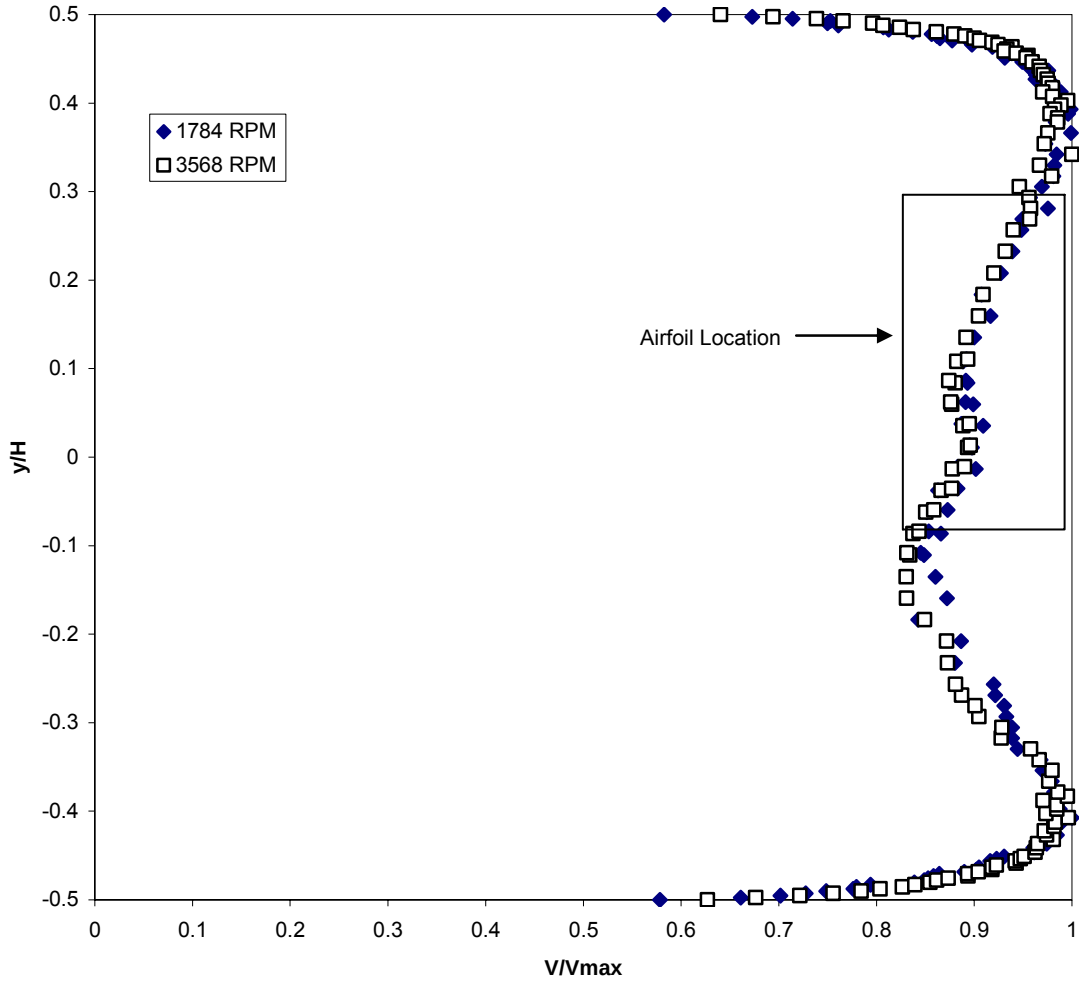

Figure 6.5 Overlay of nondimensional vertical flow surveys at half and maximum RPM

Both sets of surveys show the "dead zone" approximately in the middle of the tunnel. More importantly, the boundary layer magnitudes and profiles are almost identical. The surveys are not perfectly symmetric about the centerline, but the fan was aligned to obtain the best overall symmetry which required some compromise in both the vertical and horizontal orientations.

6.2.2.1 Comparison of Half and Maximum RPM Surveys

The superposition of the maximum and half RPM surveys in Figure 6.5 and Figure 6.4 indicate a great deal about the flow characteristics of the tunnel. The overlay is almost perfect in both the horizontal and vertical survey. Table 6.3 contains the average and maximum difference between the half RPM and maximum RPM survey for both the horizontal and vertical test condition.

Table 6.3 Average and maximum difference between half and maximum RPM in each survey

Test Condition	Average Difference	Maximum Difference
Vertical Survey	1.58%	5.79%
Horizontal Survey	2.28%	8.0%

The small average differences indicate the flow characteristics are statistically very similar in the two RPM conditions.

The similarity continues in comparing the magnitude and profile of the boundary layers. Figure 6.6 and Figure 6.7 show the left and top boundary layers, respectively. Again, the axes are not oriented in the same way. The overlap of the 50% and 100% RPM surveys in these figures show in more detail the similarity in flow characteristics. The boundary layer thickness was about 15% of the tunnel dimension at each wall, resulting in boundary layers almost 2.5″ thick.

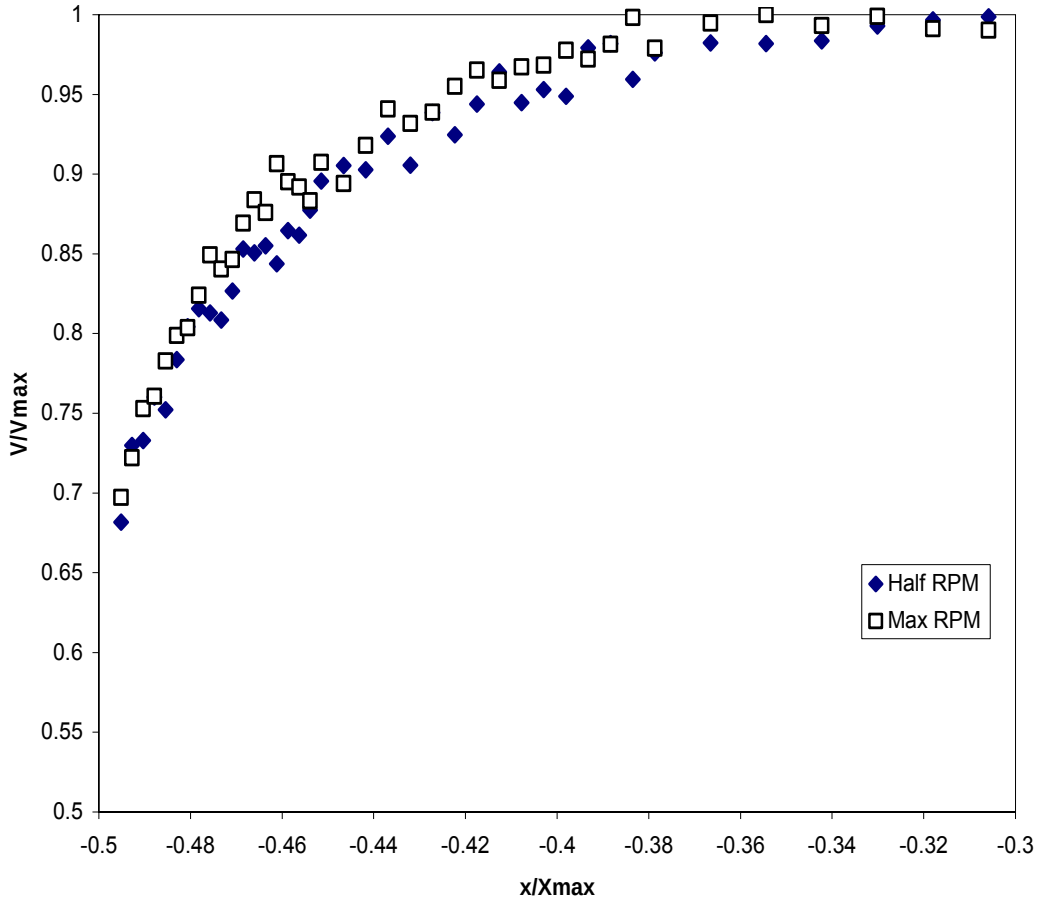

Figure 6.6 Left edge boundary layer from horizontal flow surveys

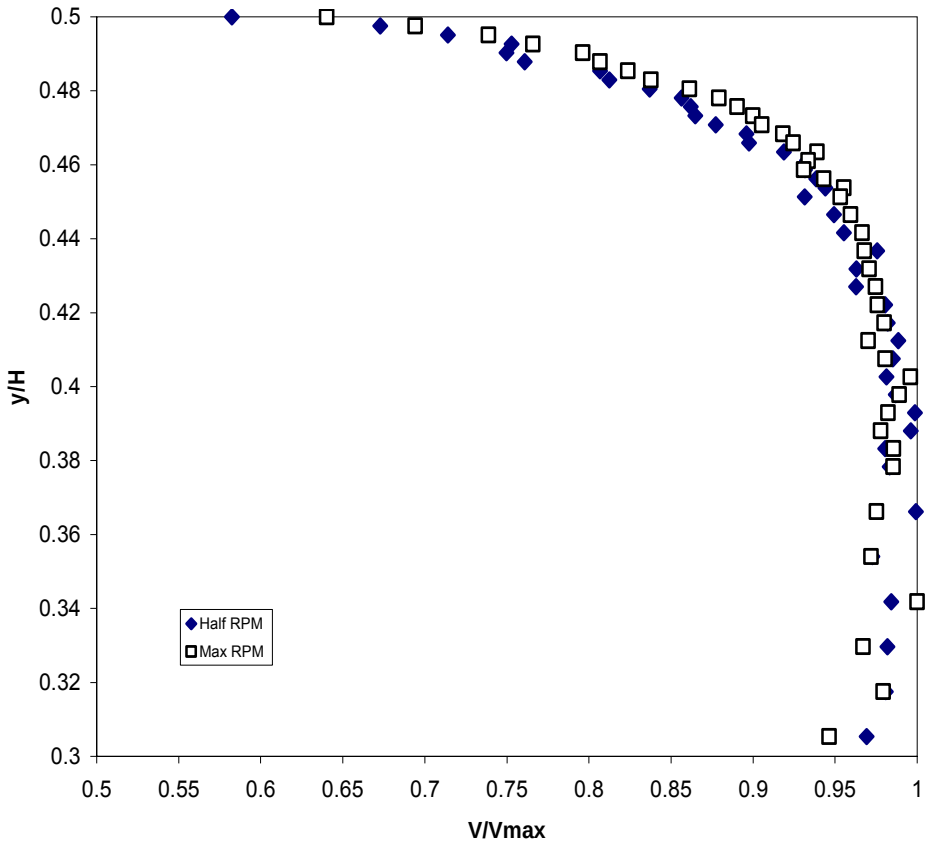

Figure 6.7 Top boundary layer from vertical flow surveys

The full survey comparison and the detailed boundary layer comparison indicate the flow characteristics, including frictional effects, are insensitive to fan RPM and tunnel velocity between 50% and 100% RPM.

6.2.2.2 Comparison of Horizontal and Vertical Flow Surveys

In order to compare the horizontal and vertical surveys, the vertical surveys were rotated and superimposed on the same plot with the horizontal surveys. Figure 6.8 contains all four surveys on the same plot.

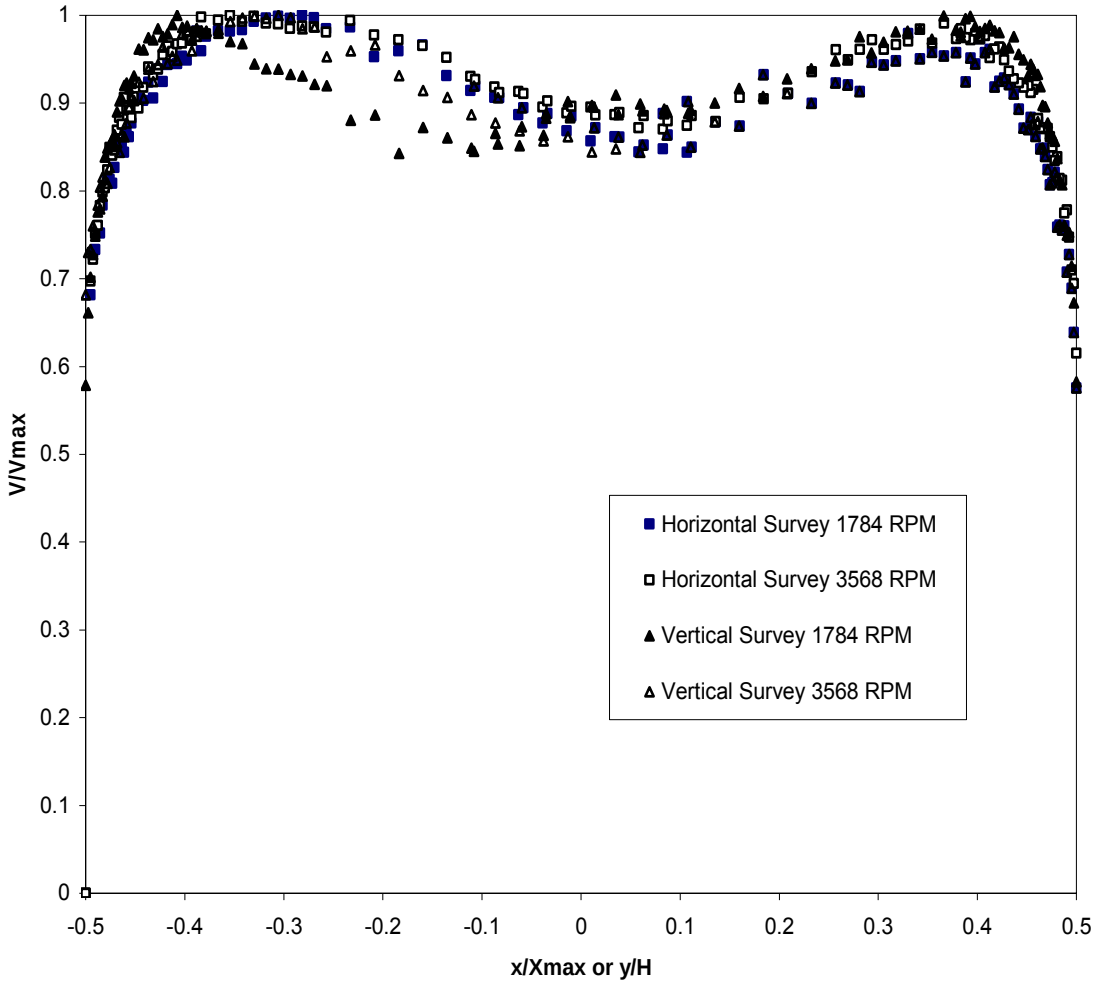

Figure 6.8 Overlay of horizontal and vertical flow surveys

Though the high density of the data makes it difficult to distinguish between the surveys, it shows the similarity between the horizontal and vertical flow characteristics. The general profile, the boundary layer profiles, and the locations of the relative minimum and maximum velocities all correspond, indicating the flow along the horizontal and vertical axes are very similar. The maximum difference between any two surveys is 13%, and at most locations all four surveys are within a 5% to 6% range of nondimensional velocities.

6.2.3 Flow Survey Conclusions

The horizontal and vertical flow surveys provided great insight into three aspects of the tunnel flow characteristics:

First, the comparison between the 50% and 100% RPM surveys indicate the dynamic pressure (and thus velocity) distribution is independent of the fan RPM and average tunnel velocity. Thus it can be assumed that the conclusions drawn from this data regarding non-uniformity and boundary layer magnitude are applicable to any RPM setting within the 50% to 100% RPM range. This is significant because there is some debate regarding the actual velocity generated in the Wright's tunnel, and estimates range from 20 mph to just over 30 mph. Since the RPM's tested bracket this range of velocities, the conclusions drawn from these tests are independent of the velocity actually generated in the Wright's tunnel.

This result becomes even more relevant when combined with the data from a 2004 AIAA article[128] which found the non-uniformity and turbulence intensity of the flow through the Wright's tunnel was largely independent of the propeller configuration. Together, the results indicate the major characteristics of the flow through the Wright's wind tunnel are independent of the driver section, including RPM and propeller configuration. Though this replica was designed to match the conditions of the Wrights' tunnel as much as possible, the conclusions regarding non-uniformity and boundary layer growth are still valid even though the replica may be running at a slightly different velocity with a different fan configuration.

Second, the high degree of similarity between the vertical and horizontal flow surveys provide assurance of the alignment of the tunnel and fan section at least as well as the Wrights, who did not have such means, could have aligned them. The boundary layers develop the same profile and magnitude on each wall, and the "dead zone" in the center of the tunnel is the same size in all surveys. Misalignment in either the vertical or horizontal plane would have resulted in an asymmetry and a poor comparison between the two surveys. However, the characteristics near the corners are still unknown and the actual shape of the three main flow regions, the "dead zone", the high velocity region, and the boundary layer, could not be determined until the off-axis surveys were conducted.

Additionally, these surveys provided more accurate results than the original vertical flow survey. The boundary layers in all cases extended 10% to 12% from the wall, which correlates to 1.5 in to 2 in: slightly larger than the original survey indicated. In the vertical surveys the difference between maximum and minimum velocity was 17%. In the horizontal surveys the difference was 16%. Though still very large, both differences are slightly less than anticipated from the original flow survey. Regardless, the Wrights' airfoils would certainly have spanned the distance from the minimum to the maximum and may have reached the boundary layer, resulting in an unacceptably large spanwise velocity gradient.

[128] Colin P. Britcher, Rafaello Mariani, Pat Craig, Jill Gillespie, Mudit Monsi, Darius Luna, and Mark Sykes, "Analysis of the Wright Brothers Wind Tunnel and Design of an Educational Derivative," AIAA Paper 2004-1141, Jan. 2004.

6.3 Particle Image Velocimetry

6.3.1 Purpose and Method

Particle Image Velocimetry (PIV) provided a means for large scale qualitative and quantitative evaluations of the tunnel flow properties. Unlike the flow survey measurements which could only record data along a single axis, PIV was used to measure flow characteristics in a large field of the test section plane including the region where the Wrights mounted their airfoils. Figure 6.9 shows the location of the PIV view area and the relative location of the airfoil within the view area.

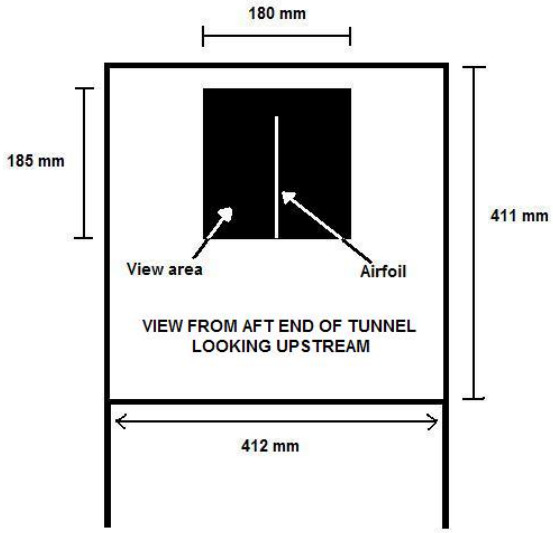

Figure 6.9 Diagram showing PIV field of view within the tunnel test section

6.3.2 Empty Tunnel Evaluation

The MATLAB scripts which processed the vector files also output visual representations of the velocity profile in the plane. Figure 6.10 represents the velocity magnitude contour plots for the tunnel at 3568 RPM and 1784 RPM respectively, also referred to as the high and low speed runs. The center of the tunnel was located at (0 mm, 0 mm).

The asymmetry in these images reveals the centerline data from the flow surveys was not a representation of the entire region, and likely the imperfections of the contraction result in symmetry variations despite alignment attempts. However, these asymmetries were at least as large, if not larger in the Wrights' tunnel as their means of both machining and alignment were inferior to those used in this experiment.

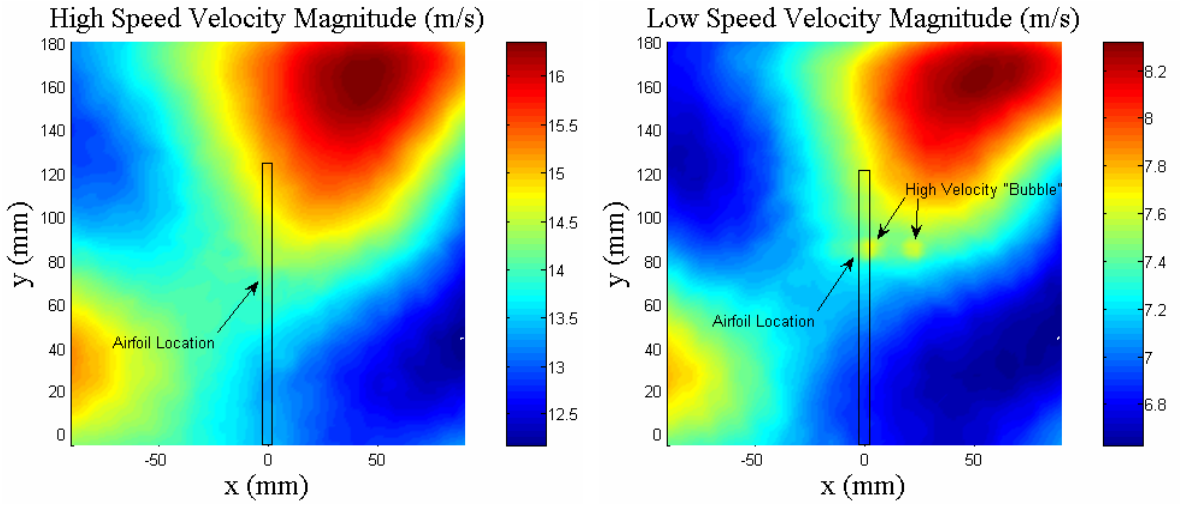

Figure 6.10 Velocity magnitude in the empty tunnel PIV field of view.

6.3.2.1 Comparison of High Speed to Low Speed Tests

A qualitative comparison between the high and low speed tests reveals many similarities. Despite the different velocity scales to the right of each image, the regions of high and low velocity magnitude closely correspond. The highest velocity flow in both tests occurred in a pocket extending horizontally from about the centerline to the rightmost edge of the view area, and vertically from y = 100 mm to the upper boundary. Another region of high velocity flow existed in both tests in the leftmost 30 mm. In the high velocity test the region was located vertically between 10 mm and 50 mm, while in the low speed run it existed between 20 mm and 40 mm. The lowest velocity flow also corresponded. A diagonal band of the slowest flow was revealed in both images starting at the rightmost boundary, at y = 50 mm and continuing to the lower boundary at x = 30 mm. The rectangle representing the location of the airfoil shows that at both run conditions the lower tip of the airfoil was located in one of the slowest regions, while the upper tip breached the highest velocity pocket.

An apparent discrepancy exists near the vertical centerline at about y = 80 mm. In the low speed run there are two high speed “bubbles” roughly 25 mm apart which are not present in the high speed run. These anomalies may be inaccurate data resulting from glare or reflection of laser light during the PIV testing. They could also be the result of tight vortices generated by the honeycomb in the contraction which have maintained strength through the length of the test section. The spacing between them is close to the 1″ spacing of the honeycomb grid. Greater diffusion in the high speed run may have smeared the vortices until they were unrecognizable. It is unclear why only two are present in the data

6.3.2.1.1 Vertical Centerline Comparison

Analyzing the centerline of the high and low speed tests provides a more detailed comparison of the two conditions. For comparison purposes, the vertical position was non-dimensionalized by the tunnel height, y/H = 0.00 denotes the tunnel centerline and y/H = 0.50 represents the top wall. The comparison shows that the velocity profile in the tunnel is largely insensitive to changes in tunnel speed. Figure 6.11 shows the superposition of the high and low speed data revealing the good correlation between the two run conditions. The largest discrepancy occurs in the "dead zone" where the difference is less than 2%.

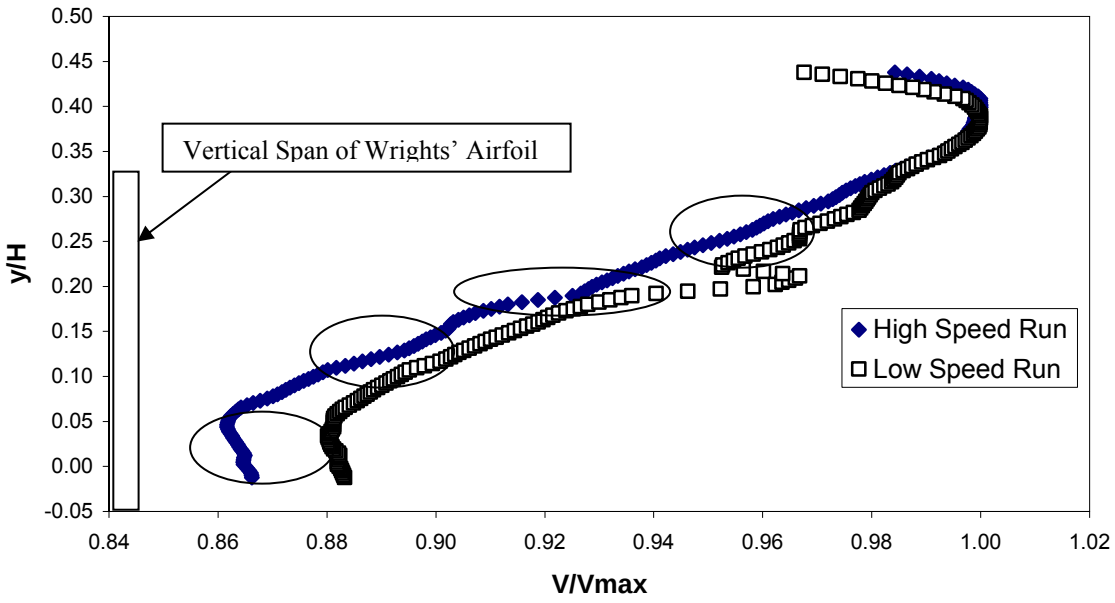

Figure 6.11 Comparison of high and low speed PIV data for the vertical centerline of the empty tunnel

Significantly, the boundary layers overlap almost completely. The two runs begin to deviate closer to the "dead zone" with the largest difference of 2% occurring at the minimum point. The higher velocity "bubble" described earlier in the low speed data manifests itself here close to y/H = 0.2.

A detailed comparison between the local trends in each run show their similarity to a greater extent. The ovals in Figure 6.11 show small local trends which manifest themselves at each speed. Even the "bubble" in the low speed run was paralleled slightly at the high speed run which may indicate a similar vortex smeared out by the higher velocity.

6.3.2.1.2 Global Comparison

The high and low speed runs also compare very favorably in a larger region surrounding the airfoil. The region was defined as a square with dimensions equal to the airfoil span centered behind the airfoil mounting location (-5mm < x < 125mm, -65mm < y < 65mm). Table 6.4 and Table 6.5 provide comparisons of the maxima and minima within this region for the high and low speed empty tunnel runs. The locations of the maxima and minima closely correspond, and the velocities are essentially linearly related to the speed.

Table 6.4 Comparison of maximum velocities near the airfoil location

Tunnel Speed	Avg Vel (m/s)	x location (mm)	y location (mm)	Mag (m/s)
High	13.87	27	125	15.71
Low	7.13	28	125	8.00

Table 6.5 Comparison of minimum velocities near the airfoil location

Tunnel Speed	Avg Vel (m/s)	x location (mm)	y location (mm)	Mag (m/s)
High	13.87	56	31	12.36
Low	7.13	54	35	6.62

6.3.2.2 Comparison to Vertical Flow Surveys

The PIV data provide much greater insight into the qualitative flow characteristics than did the flow surveys. For example, the "dead zone" is apparent (from y/H = 0.00 to 0.10), as is the high velocity region (y/H = 0.37 to 0.42) along the vertical centerline of both the PIV and flow survey data; however the PIV makes clear that the higher velocity region does not completely surround the dead zone, and that flow effects in the corners result in isolated, rather than continuous, high velocity regions.

Quantitative comparisons between the PIV and flow surveys are also valuable. For a quantitative comparison, only the vertical flow survey was used. The horizontal survey only had two points which were within the PIV field of view, so no horizontal comparison was made. Figure 6.12 and Figure 6.13 show the superposition of the PIV and flow survey data at the high and low speeds, respectively. With respect to data range, the PIV data was the limiting case, only spanning part of the tunnel, while the flow survey data went wall to wall. Only the overlapping data was used in comparison.

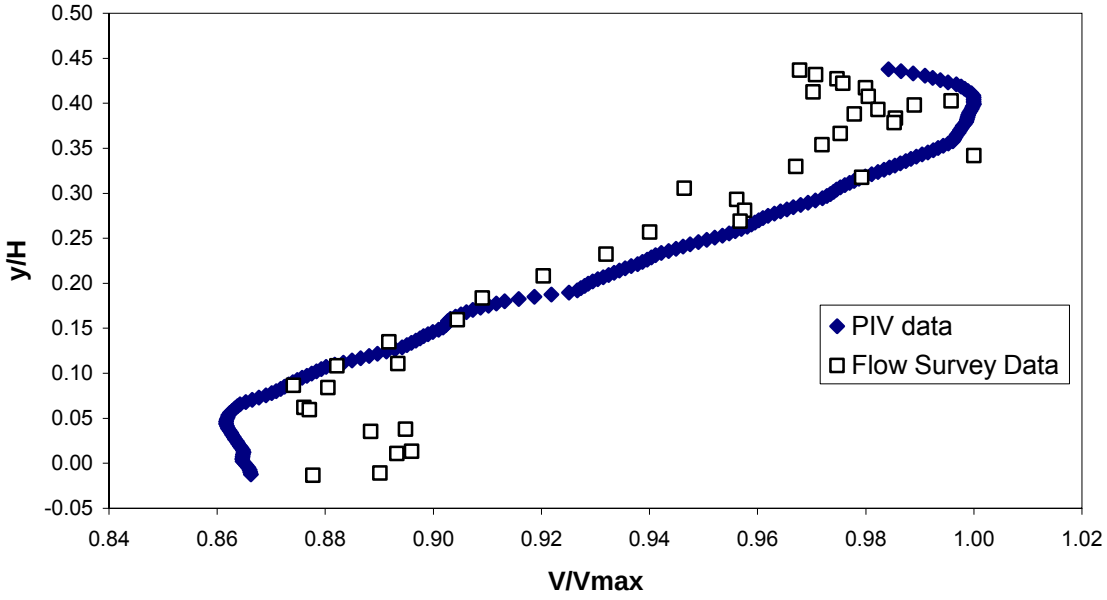

Figure 6.12 High speed comparison of PIV and Flow Survey data

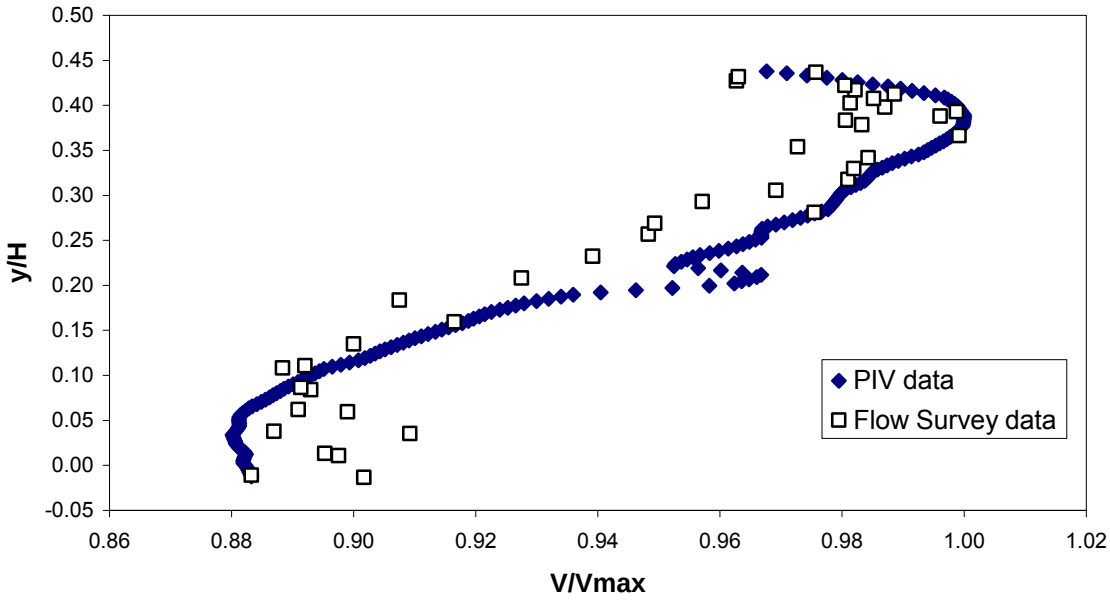

Figure 6.13 Low speed comparison of PIV and Flow Survey data

The two sets of data overlap very well in all three regions: the "dead zone," the high velocity region, and the boundary layer. The maximum difference occurs in the "dead zone" with a 3-4%

discrepancy which decreases to 1-2% in the boundary layer region. The most likely cause for the discrepancy is the short distance between the flow survey cross section and the PIV cross section. The PIV surveys were obtained 85 mm further aft in the tunnel in order to accommodate the balance and airfoil ahead of the laser sheet without causing interference. The flow survey, on the other hand, was meant to obtain data in the exact location of the Wrights' airfoil. Along these 85 mm between the flow survey and PIV planes the boundary layer grew which removed energy from the flow generating a larger boundary layer profile and a greater discrepancy between the boundary layer, the high velocity region, and the "dead zone." This prediction is consistent with the observed results in which the PIV data shows a slower "dead zone" and a more extreme boundary layer profile. The overall agreement between the two sets of data is well illustrated in the tabulated comparison of maximum and minimum velocities and locations for both testing methods in Table 6.6 and Table 6.7.

Table 6.6 Comparison between PIV and flow surveys of maximum velocities and locations

	PIV		Flow Survey	
Tunnel Speed	Vmax (m/s)	Y - Location (mm)	Vmax (m/s)	Y - Location (mm)
High	15.46	164	15.37	140
Low	7.78	159	7.66	151

Table 6.7 Comparison between PIV and flow surveys of minimum velocities and locations

	PIV		Flow Survey	
Tunnel Speed	Vmin (m/s)	Y - Location (mm)	Vmin (m/s)	Y - Location (mm)
High	13.32	18	13.43	36
Low	6.85	14	6.80*	16*

*the actual minimum is an extreme outlier occurring at -4.5mm at a velocity of 6.77 m/s (y/H = -0.2, V/Vmax = 0.884)

The PIV V_{min} was within ±0.8% of flow survey data, while the PIV V_{max} was within ±0.5-1.6% of the flow survey data with the greater error occurring in the low speed run. Though the location varied more in the high speed run, by as much as 24 mm, the trend is accurately matched. These results provide a validation of both the flow survey and PIV results. Using two independent measurement systems, a very similar velocity profile was obtained. Thus all the PIV data, including data for turbulence intensities and vorticities, can be used with confidence to draw conclusions about the flow within the PIV analysis window.

6.3.2.3 Turbulence Intensity in the Empty Tunnel

The PIV data were processed to yield maps of the turbulence intensity in the test section. In this context turbulence intensity was defined by the standard deviation of the axial velocity at a node divided by the average axial velocity at that node for all captures in a test (this defined the scale for the images). Figure 6.14 shows the turbulence intensities in the airfoil region at 3568 RPM (high speed) and 1784 RPM (low speed), respectively. The axes have been cropped so the airfoil

would run the entire vertical span of the image along x = 0.0. The scales are the same for each image which emphasizes the sensitivity of turbulence intensity to tunnel speed.

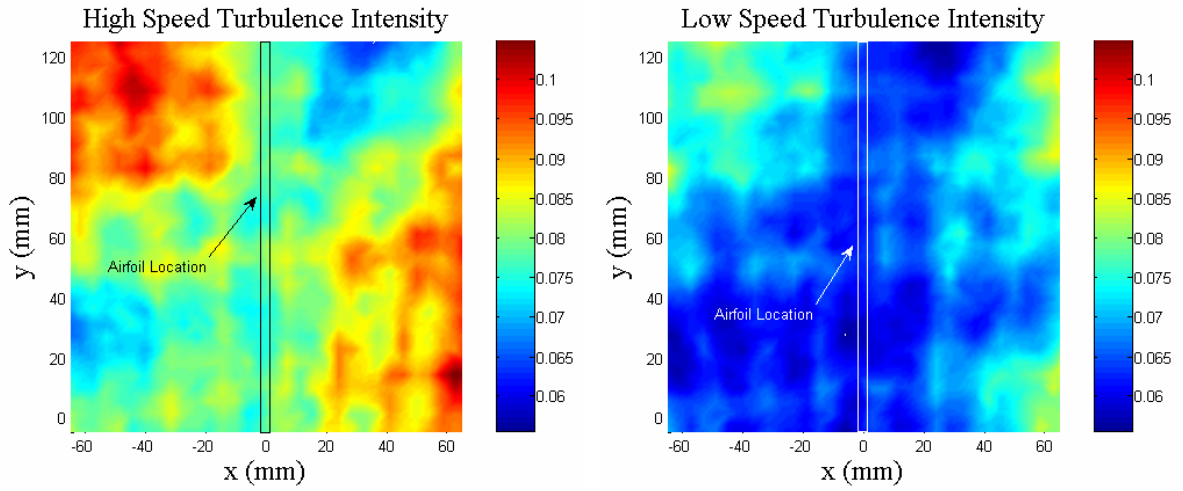

Figure 6.14 Turbulence intensities in the empty tunnel PIV field of view

The turbulence intensity profiles are similar in many respects. Both have regions of high turbulence in the upper left corner, bounded on the right by x = -15 mm, and on the bottom by y = 80 mm. The right side of both fields is also an area of high turbulence from x = 20 mm to the right edge, though in the low speed case the band extends to the top of the image while at high speeds it ends at y = 100 mm. A horizontal low turbulence band exists between y = 20 mm and 40 mm. The band extends into the high turbulence area on the right side of the region, and both runs show reduced turbulence where the bands meet. Another low turbulence pocket is present at the top of the image, from y = 90 mm to the top, between x = 20 mm and 40 mm. The region is larger in the high speed run and interacts with the right side high turbulence band.

The airfoil, located vertically at x = 0.0, did not extend into any of the areas of highest turbulence, but passed through the horizontal low turbulence band. In the high speed run, the airfoil would experience turbulence intensities between 7.25% and 8.75% along the span, while at low speeds the turbulence intensities would have been between 5.00% and 7.00%, a slightly larger variation. Turbulence intensities of this magnitude indicate a large axial velocity variation at each node along the span resulting in proportionally large variations in the local Reynolds number. Analytic data shows the lift coefficient of the Wrights' airfoil was highly dependent on Reynolds number. Thus the velocity and Reynolds number variations would result in a wide variation in the local lift coefficient along the span of the airfoil.

Though the data suggests the turbulence intensity profile is relatively insensitive to tunnel speed, the magnitude of the turbulence intensities is largely dependent on the speed. Table 6.8 shows the minimum, maximum, and average turbulence intensities at each run condition. The average increased by 1.51% from the low to the high speed run condition. The increased turbulence is a result of the fan spinning twice as fast as it pushes air into the tunnel, an effect which would be mediated to some extent if air was sucked through the tunnel. The data provides quantitative

support for the Repeatability Evaluation which qualitatively described the unsteadiness of the flow based on multiple time averaged pressure readings.

Table 6.8 Minimum and maximum turbulence intensities

Fan Speed	Min. Turbulence Intensity	Max. Turbulence Intensity	Avg. Turbulence Intensity
High	6.33%	10.55%	8.25%
Low	5.61%	8.70%	6.74%

6.3.2.4 Vorticity in the Empty Tunnel

There are several potential sources of vorticity in the tunnel including the rotation of the fan and asymmetrical flow. Vorticity in the flow indicates non-axial velocity components in the free stream, which is not an accurate, repeatable flow condition for full scale modeling. Thus, measuring the vorticity is an important aspect of analyzing flow quality.

Figure 6.15 shows the vorticity in the airfoil region at both the high speed and low speed run conditions. There is much greater vorticity, both positive and negative, in the high speed scenario, while the low speed condition has a smaller range and a smoother distribution.

The low speed condition clearly showed striation rings radiating from the center which were a result of swirl from the fan. The alternating rings of positive and negative were products of continuity. The high speed run tended to scatter the vorticity patterns to some extent. The more erratic distribution of the high speed image makes the striations more difficult to see, but the pattern is present there as well.

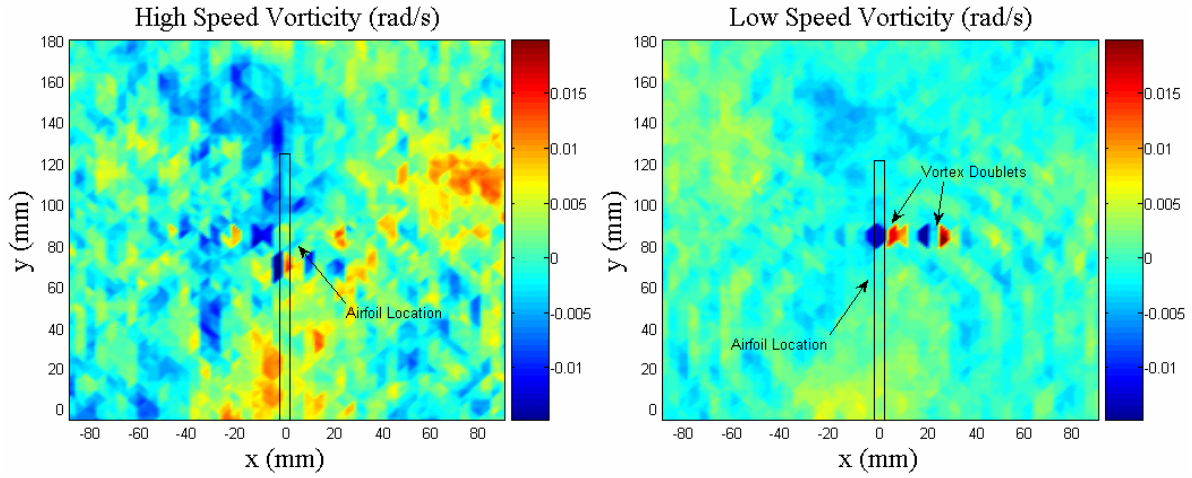

Figure 6.15 Vorticity in the empty tunnel PIV field of view

Though it is most apparent in the high speed data, both runs show the variation of vorticity along the airfoil span. Most significantly, both runs have the lower tip of the airfoil in the region of highest *positive* vorticity, with the upper tip of the airfoil in the region of highest *negative* vorticity. This would result in a large velocity component in the positive x direction at the upper tip and a large component in the negative x direction at the lower tip. Thus, not only does the wind tunnel configuration generate large non-axial velocity components in the region of the airfoil, but there is a large gradient of those non-axial components along the span of the airfoil.

Additionally, the low speed data reveals the true nature of the two high velocity "bubbles" which existed in the low speed and were less apparent at the high speed condition. The low speed run in Figure 6.15 shows a vortex doublet at the location of each "bubble." The data is not an inaccurate anomaly, but rather explains a real flow characteristic. The spacing of 1″ (25 mm) indicates the vortices may have originated at the honeycomb grid in the contraction and propagated into the test section. At the higher velocity the doublets have diffused out, but the centerline velocity data indicates the beginning of a similar trend at that velocity.

6.3.3 Effect of Wrights' Lift Balance on Flow in Airfoil Region

PIV was conducted with a replica of the Wright Brothers' lift balance installed in the tunnel without any airfoil mounted to the balance. Data was recorded with the tunnel running at the high and low speeds defined by 3568 RPM and 1784 RPM. Using image subtraction to isolate the effects of the balance from the effects of the empty tunnel configuration, the data provided a great deal of information regarding the influences of the balance on the velocity magnitude, turbulence intensity, and vorticity in the region occupied by the airfoil. Note, image subtraction results in images which show only the *difference* or change in velocity, turbulence, and vorticity between the two images. For example, a local velocity of -0.2 m/s indicates the flow is 0.2 m/s slower at that point due to the presence of the balance.

6.3.3.1 Velocity Magnitude Effects

Before testing began it was assumed that inserting a large blockage such as the lift balance into the tunnel would cause significant changes in the test section flow. The initial assumption was correct, but the balance affected the flow in a surprising manner. A velocity increase in the airfoil region was predictable: blockage in the lower half of the tunnel from the balance should result in an increased velocity in the top half of the tunnel. This is shown clearly by the high speed run in Figure 6.16 in which the flow in the airfoil region is at least 0.5 m/s greater with the balance installed. The horizontal velocity gradient which is apparent in this figure, however, was not anticipated. The balance clearly generated a horizontal variation in the velocity which can be seen in both runs in Figure 6.16 (high and low speed, respectively). These figures are the result of subtracting the empty tunnel image from the image of the tunnel with the balance, isolating the effects of the balance on the flow. Therefore the values shown are only those effects which are due to the presence of the balance.

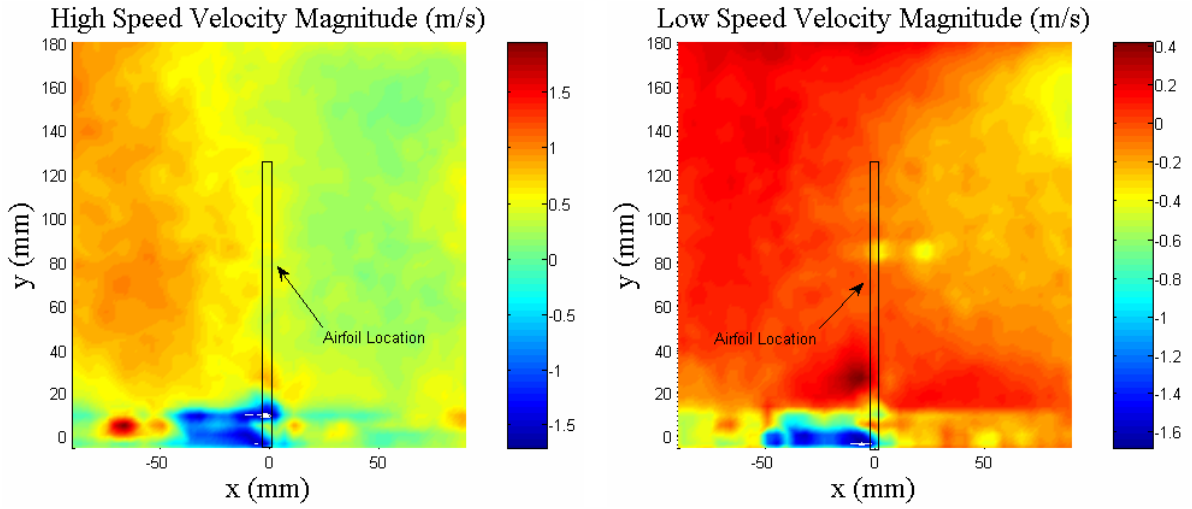

Figure 6.16 Velocity result of image subtraction isolating balance effects from empty tunnel effects.

The difference is more obvious in the high speed case where the left side of the flow has clearly accelerated and the right side has decelerated. The difference between the left and right sides is greater than 3% of the average velocity. The low speed scenario also shows the effect of the balance, though the decelerated region is smaller and the difference in velocity is, predictably, less.

In the low speed run in Figure 6.16, the two velocity "bubbles" from the empty tunnel testing are apparent and represent regions of negative velocity, or regions where the flow is slower with the balance installed than without. The balance likely forces the vortices, which are responsible for the "bubbles," to dissipate, resulting in a more uniform local flow. When the empty tunnel velocity data is subtracted from the velocity data with the balance installed the result is a negative velocity "bubble." The negative pockets show the vortices are not pronounced when the balance is in place, but are not real elements of the flow in this case.

The band at the bottom of both figures, from y = 0 mm to 20 mm, reveals the location of the upper strut of the balance. In both cases the line is significantly slower than the rest of the flow due to the drag effects of the balance. Especially noticeable is the low velocity flow from about -40 to 0 mm on the horizontal axis. This is where the airfoil mount is located. The strut is more than twice as thick in this region, generating more drag. The piece also has two brackets at an angle to the flow resulting in the small bubble of accelerated flow just above the strut near the vertical centerline.

Figure 6.17 emphasizes the velocity effects due to the balance, focusing specifically on the airfoil region. The figure shows the velocities directly behind where the airfoil would be located. It is the result of subtracting the empty tunnel image from the image of the balance and tunnel at full speed, thus the image represents the effect of the balance on the spanwise velocity distribution. As noted before, the balance increased the velocity in the upper airfoil region by

about 0.5 m/s. The vertical, rather than sloped, trend on the plot shows that the balance did not contribute in any way to the spanwise velocity distribution on the airfoil. Thus, any spanwise velocity gradient is due to the wind tunnel configuration alone. In the lower airfoil region the data is sporadic due to the PIV laser sheet interaction with the top strut of the balance.

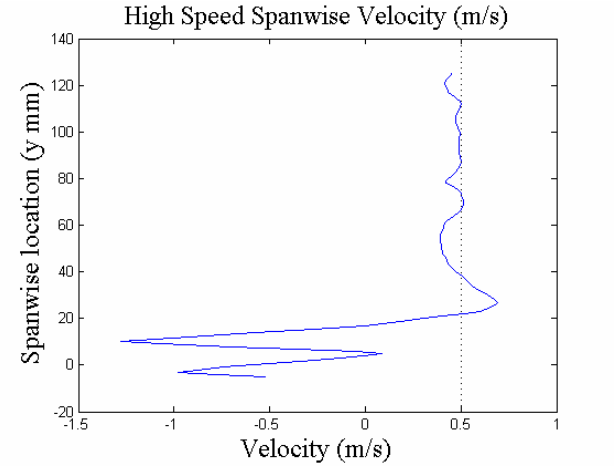

Figure 6.17 High speed test spanwise velocity distribution across airfoil region resulting from image subtraction

6.3.3.2 Turbulence Intensity Effects

Surprisingly, the effects of the balance on turbulence intensity were not consistent between the high and low speed run conditions. Figure 6.18 shows the isolated effects of the balance on turbulence intensity for both run conditions.

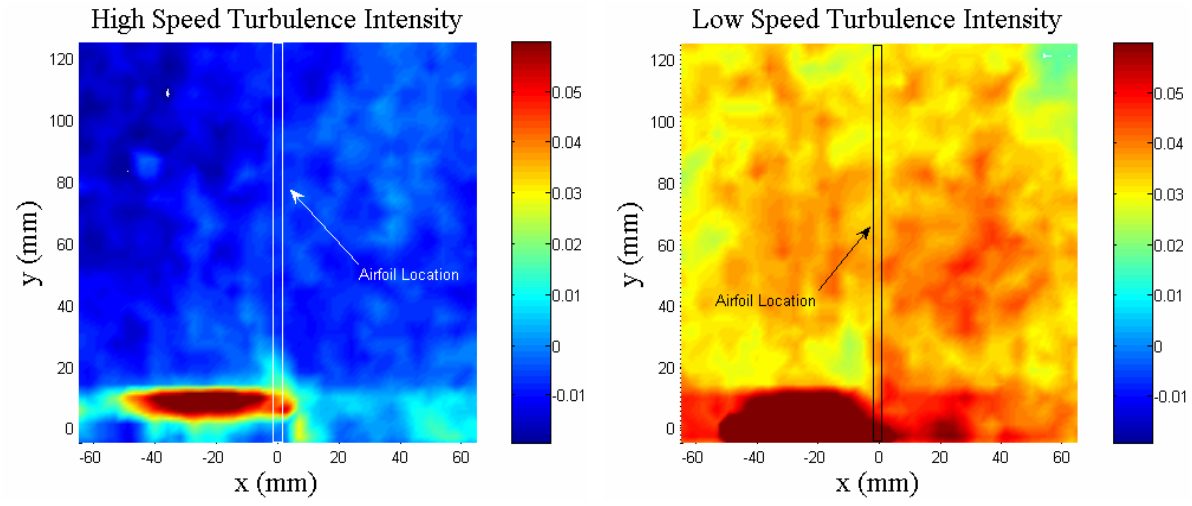

Figure 6.18 Turbulence result of image subtraction isolating balance effects from empty tunnel effects.

The scale is the same on both images making it clear that in the low speed run condition, the balance significantly increased the turbulence by 2%-5%, while in the high speed condition the balance had very little, if any, effect on the turbulence in the airfoil region. The comparison shows the turbulence at higher speeds is less sensitive to inserting blockage in the flow. This is partially due to the empty tunnel generating more average turbulence at higher speed (8.19% at high speed compared to 6.64% at low speed) so the effects of the balance are less apparent.

Again, the bottom of the image shows the effect of the balance strut which has a large, though local, effect on the turbulence.

6.3.3.3 Vorticity Effects

Using image subtraction, Figure 6.19 shows show the isolated effects of the balance on the vorticity in the tunnel at both run conditions. Because of the image subtraction, the striations present in Figure 6.15 (vorticity in the empty tunnel) are not present.

These images show the balance has relatively little effect on the vorticity in the airfoil region. Through most of the region the net influence of the balance is zero. The one major exception is at the airfoil mount, located along the vertical centerline, about 20 mm above the horizontal centerline. The mount includes a vertical bracket which is at an angle to the flow. The bracket acts like a small airfoil causing a strong vortex to wrap around the edge. The opposing vortex in the doublet is also apparent and is labeled on both images.

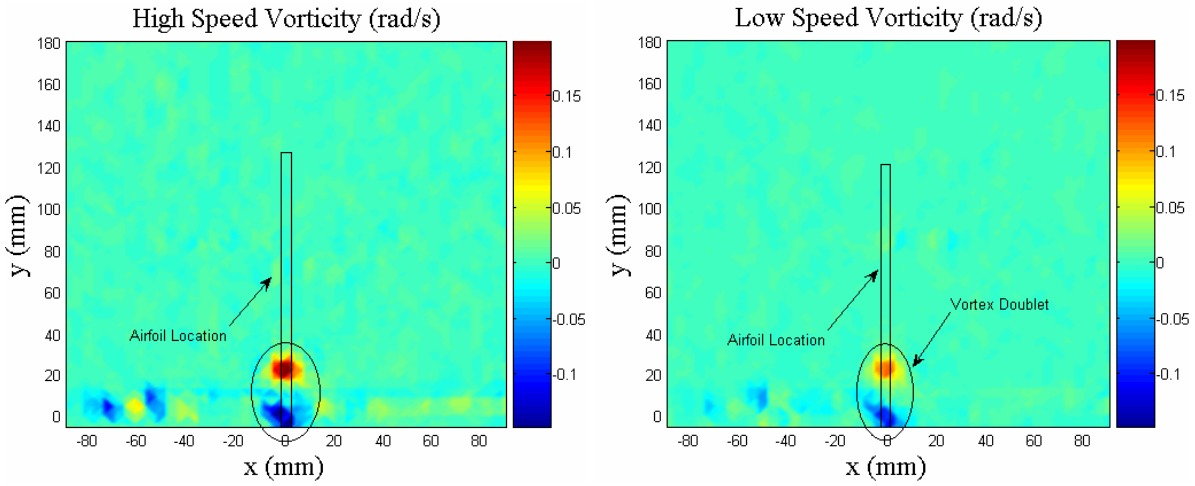

Figure 6.19 Vorticity result of image subtraction isolating balance effects from empty tunnel effects.

When the airfoil is attached to the mount, the bracket is flush with the airfoil surface and no longer has an exposed edge to generate a wingtip-type vortex. It may still shed a vortex where the airfoil and mount intersect which would affect the pressure distribution on the upper surface of the airfoil.

6.3.4 Effect of Wrights' #12 Airfoil on Tunnel Flow Characteristics

In addition to studying the effects of the balance on the flow in the airfoil region, it is also important to analyze the interaction of the airfoil with the flow, especially with respect to interaction and interference between the airfoil and the balance.

The effects of the airfoil by itself were analyzed by attaching a replica of the Wrights' #12 airfoil to a mounting rod and positioning the airfoil at the location it would be mounted if attached to the lift balance. The airfoil was oriented at 5° angle of attack which the Wrights recorded as the most efficient AOA for that airfoil. PIV data was recorded and processed for the setup, then the airfoil was removed and data was recorded for the rod by itself. Using image subtraction, the effects of the rod were removed, isolating the effects of the airfoil. A similar procedure was used with the balance. The balance was installed and data was recorded with the airfoil attached, and then again without the airfoil. Together, the data provides information regarding the interaction between the airfoil and the balance. As was the case with the balance isolation, image subtraction results in images which show only the *difference* or change in velocity, turbulence, and vorticity between the two images.

Since interference effects are not linear, image subtraction does not completely isolate the effects of the airfoil, but rather the effects of the airfoil *and* the effects of interference. Equation 6.2 shows the combination of velocity effects for the test with the balance and airfoil. After subtracting the effects of the balance (Equation 6.3), the effects of interference remain. The same is true for tests using the rod to mount the airfoil rather than the balance.

$$V_{total} = V_{balance} + V_{airfoil} + V_{interference_{B+A}}$$

Equation 6.2

$$V_{total} - V_{balance} = V_{airfoil} + V_{interference_{B+A}}$$

Equation 6.3

6.3.4.1 Velocity Magnitude Effects

6.3.4.1.1 Airfoil without Balance Interference (Rod Tests)

The set of tests which used the airfoil and rod (to isolate the airfoil from the effects of the balance) showed the airfoil alone had very little effect on the flow characteristics in the tunnel. Figure 6.20 shows the isolated effects of the airfoil on velocity in the local region. The velocity range is scaled to the tunnel speed so the images can be compared despite the difference in range. The large dark band in the center of both images results from the airfoil which greatly decelerates the flow. The actual velocity directly behind the airfoil is much lower than the

velocity range shown, but the purpose of these images is to show the velocity effects in the local region, not the momentum deficit behind the airfoil, so the scale was set for that purpose.

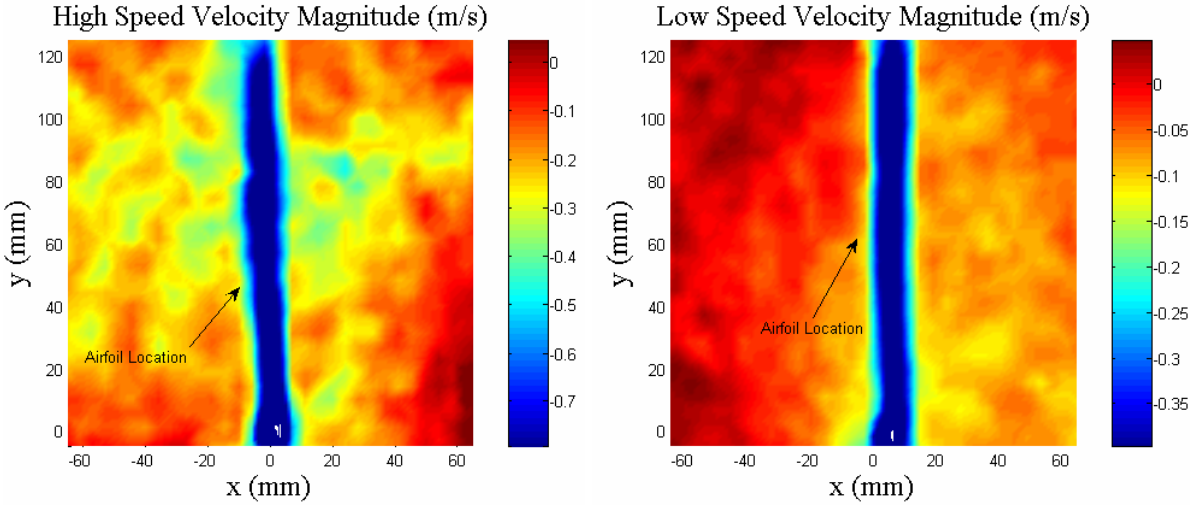

Figure 6.20 Velocity result of image subtraction isolating airfoil effects from rod effects.

Both images show the airfoil removes energy from the local flow region. The negative velocity close to the airfoil indicates the velocity was lower in that region with the airfoil mounted than with the rod by itself. The deficit is larger in the full speed case and extends further from the airfoil on both sides. As distance from the airfoil increases the effects on the flow become less prominent, resulting in the regions of zero velocity change at the edges of both images.

6.3.4.1.2 Airfoil with Balance Interference

The interaction of the airfoil with the balance resulted in flow conditions similar to, but more pronounced than the effects of the balance alone. Figure 6.21 shows the isolated effects of the airfoil on the flow after the effects of the balance have been subtracted.

Like the isolated effects of the balance, flow on the left side of the region was accelerated while flow on the right side was decelerated. However, the effects of the balance have been subtracted in this case, so this horizontal velocity distribution is *in addition to* that distribution produced by the balance. Significantly, such a large distribution was not apparent with the airfoil and rod data, thus this distribution, with a range greater than 0.6 m/s from the left to the right side of the region, was the result of interactions between the airfoil and balance.

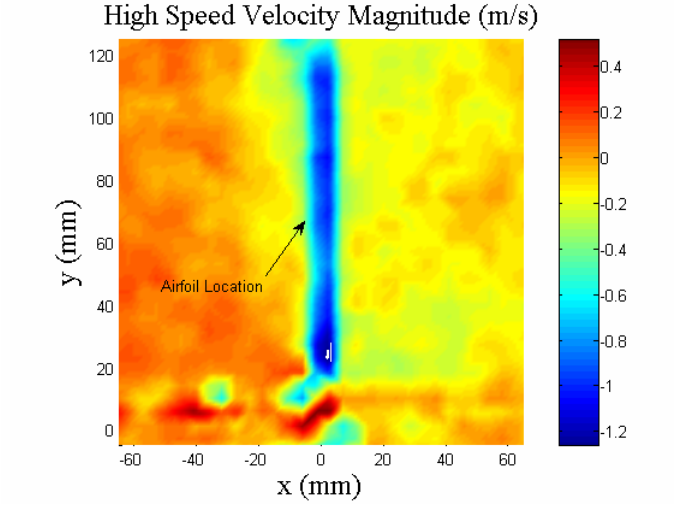

Figure 6.21 Velocity result of image subtraction isolating airfoil effects from balance effects.

6.3.4.2 Turbulence Intensity Effects

The airfoil itself had very little impact on the turbulence in the tunnel. Figure 6.22 shows the isolated effects of the airfoil on the turbulence intensity with the effects of the rod subtracted out. While both images have areas of increased turbulence, both also have areas of decreased turbulence, and the overall range is relatively small. The turbulence in the high speed case was greater than the low speed case which was consistent with the earlier results for the balance alone and the empty tunnel. Table 6.9 contains the average and maximum turbulence intensities for both cases as well as the maximum increase at any grid location due to the airfoil interaction. The airfoil did not have a significant effect on the average turbulence, and in every case the average was actually slightly lower than the empty tunnel average. Additionally, the maximum values were similar to the maximum values for the empty tunnel runs.

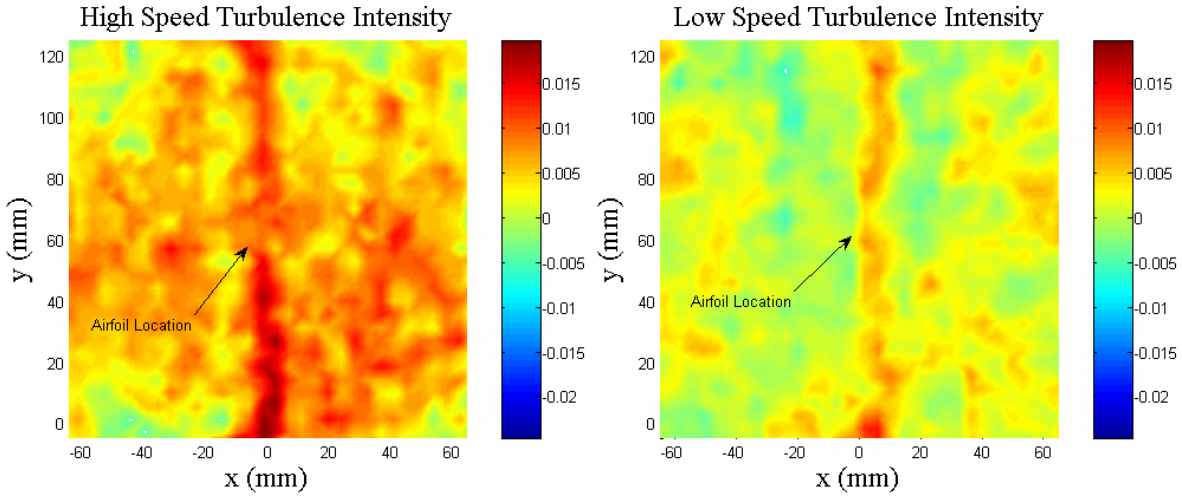

Figure 6.22 Turbulence result of image subtraction isolating airfoil effects from rod effects.

Table 6.9 Turbulence data for three run conditions

Run Condition (Fan speed and setup)	Avg. Turbulence Intensity	Max. Turbulence Intensity	Max Increase at any Node due to Airfoil
Low speed with rod	5.87%	7.34%	1.35%
High speed with rod	7.82%	9.88%	1.92%
High speed with balance	8.01%	17.87%	1.66%

Similarly, the effects on turbulence intensity from the airfoil when mounted to the balance were small. Again, Table 6.9 shows the average for the region was still below the average for the empty tunnel in this scenario. The peak turbulence is much higher, however, and results from the turbulence caused by the balance itself and interference between the balance and airfoil. Figure 6.23 shows the turbulence intensity generated by the airfoil when isolated from the balance. Interestingly there are several areas near the balance strut, at the bottom of the image, with increased turbulence due to the presence of the airfoil, but there are also several areas with decreased turbulence due to that same presence. There is also increased turbulence off the airfoil tip, possibly as a result of shedding the wing tip vortex. Despite this, the largest overall change at any grid location was still relatively small, only 1.66%.

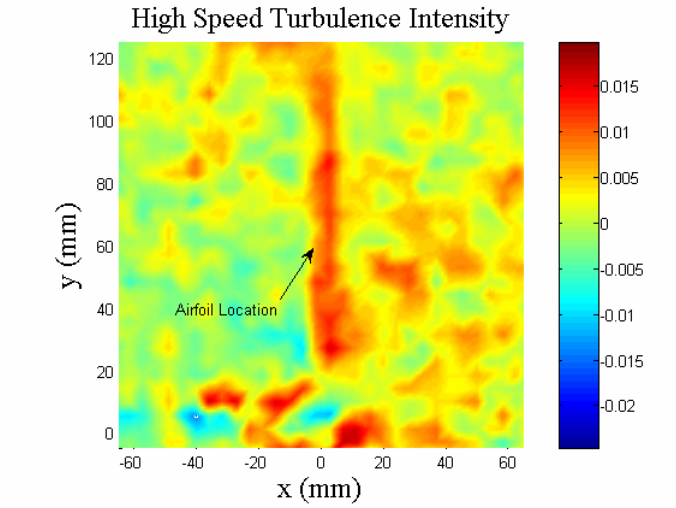

Figure 6.23 Turbulence result of image subtraction isolating airfoil effects from balance effects at high speed

The small variations, highlighted by the lack of variation at any given node (maximum change of less than 2.0%), indicate most of the turbulence present is due to the tunnel design, and not the presence of the balance/wing combination.

6.3.4.3 Vorticity Effects

The airfoil, predictably, produced a significant amount of vorticity at its tip due to its wing tip vortex (only one of the two wing tips was within the viewing area). Compared to the vortices produced by the airfoil, the small vorticity striations apparent in the empty tunnel data are negligible (more than an order of magnitude smaller). Figure 6.24 shows the vorticity effects of the airfoil when isolated from the mounting rod. There is a large vortex apparent at the tip of the airfoil in both images. The scales on the two images are different due to the differences in velocity, but Table 6.10 provides a concise comparison of the maximum vorticity achieved at the center of each vortex. Mounted to the rod, the high speed run produced a predictably stronger vortex, reaching 0.29 rad/s in the center compared to 0.10 rad/s for the low speed test. The slight bank of the airfoil in the high speed run was a mounting error, but did not have a significant effect on the results.

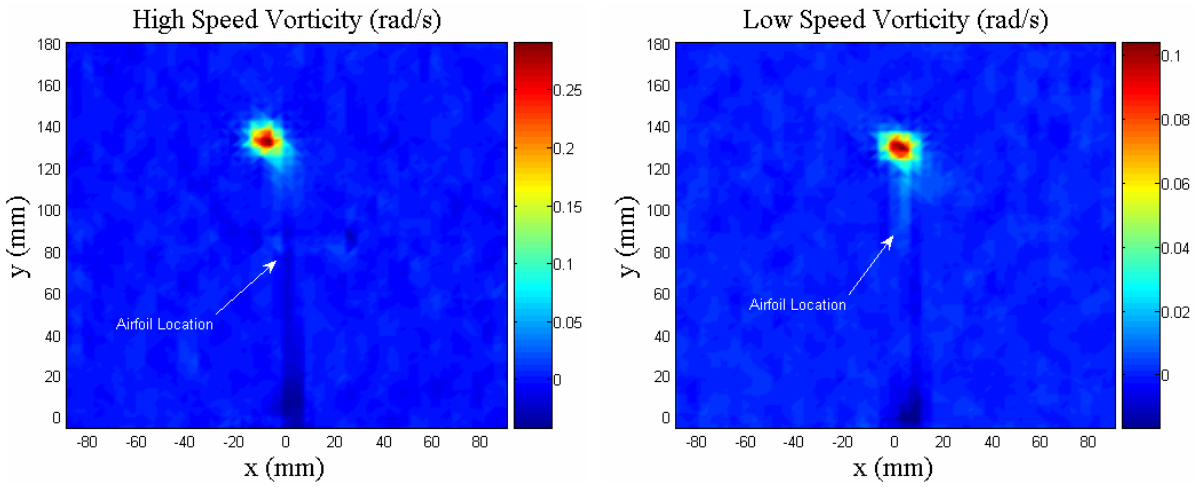

Figure 6.24 Vorticity result of image subtraction isolating airfoil effects from rod effects.

Table 6.10 Maximum vorticity at various run conditions

Run Condition (RPM and setup)	Maximum Vorticity (rad/sec)
50% RPM with rod	0.1048
100% RPM with rod	0.2927
100% RPM with balance	0.3773

With the airfoil mounted to the balance rather than the rod (Figure 6.25) the maximum vorticity at the center of the wing tip vortex increased by almost 30%. The increase may be due to the way the airfoil was mounted to the balance. The rod mount did not significantly interfere with vortex formation, resulting in symmetric wingtip vortices. The balance, on the other hand, may have prevented or retarded a vortex from forming on the lower tip of the airfoil, causing the vortex on the upper tip to strengthen.

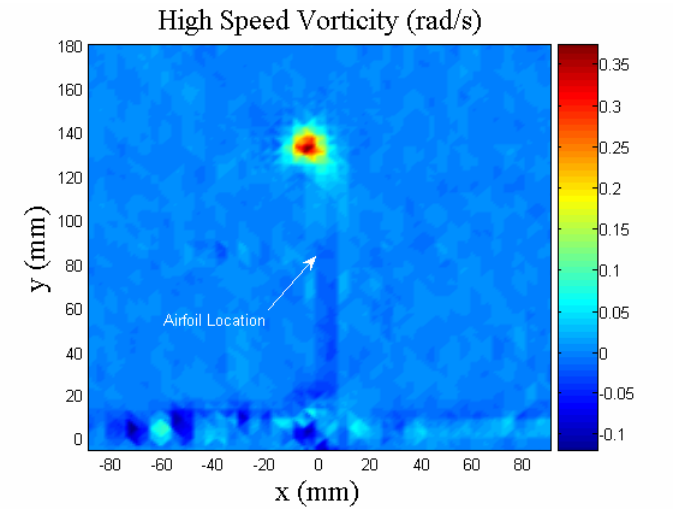

Figure 6.25 Vorticity result of image subtraction isolating airfoil and balance effects from empty tunnel effects at high speed

The lower vortex's interference with the balance has two separate effects. The first, already discussed, is the increased vortex formation at the upper tip. This will result in a downwash greater than the airfoil alone would generate. Increased downwash will exaggerate three-dimensional effects caused by a lower effective angle of attack. The result is decreased lift and increased induced drag. The second effect has the opposite result: by blocking the vortex on the lower tip the downwash will be less and, thus, the effective angle of attack will be greater. Therefore the lower tip would generate greater lift and less induced drag. The overall result is a force gradient along the span of the airfoil which is dependent on the speed of the tunnel, with greater lift generated at the lower tip.

6.3.5 Conclusions

6.3.5.1 Velocity Magnitude

The velocity gradients, both vertical and horizontal, were the most obvious revelations in the PIV data. The vertical gradient was much more significant than the horizontal, and its sole source was the tunnel configuration. The vertical variation in velocity was as large as 3.0 m/s in the high speed case with the maximum at the upper wing tip. At both tunnel speeds, the variation was as much as 10% of the maximum velocity. Since lift is proportional to the square of the velocity, such a large variation from tip to tip would result in an even larger variation in lift across the span.

While the velocity gradients result in a direct force variation (both lift and drag are functions of velocity), they also contribute to an indirect variation due to Reynolds number. Reynolds

number is directly proportional to velocity, thus a velocity gradient also generates a Reynolds number gradient. Analytic testing shows increased Reynolds number results in an increase in the lift coefficient. As Reynolds number increases across the gradient, the lift coefficient also increases. This contributes in the same sense as the increased lift due to the velocity gradient, exaggerating that effect even more.

The velocity magnitude data also indicated the velocity profile was relatively insensitive to speed (and RPM) variations. The pockets and bands of high and low velocity were in similar locations and were of similar relative magnitudes in the high and low speed empty tunnel tests. Comparisons along the vertical centerline indicated even small, local trends were mirrored at the two speeds. The conclusion is further supported by the favorable comparison to flow survey data which showed similar trends, boundary layer profiles, and magnitudes. Based on this conclusion, the qualitative trends and analysis of the region observed are applicable across the velocity range bounded by 1784 RPM and 3568 RPM.

6.3.5.2 Turbulence Intensity

Though the turbulence intensity profiles were minimally affected by the tunnel velocity, the effect on the magnitude was surprising and counterintuitive. Turbulence intensities in the empty tunnel increased with tunnel velocity, which was predicted, but the effect reversed when the balance was mounted in the tunnel. The total change in turbulence intensity with the balance installed was larger for the lower velocity. The implications of the turbulence intensity are mainly related to Reynolds number variations. Although the turbulence was relatively constant along the airfoil span, averaging 6% at low speed and 8% at high speed for the empty tunnel, the turbulence would result in Reynolds number variations of the same magnitude along the span. Again, inconsistent Reynolds numbers would generate inconsistent lift coefficients resulting in poor data accuracy and repeatability.

6.3.5.3 Vorticity

Unlike the velocity magnitude and turbulence intensity, the vorticity profile was highly dependent on the tunnel velocity. For the empty tunnel at low speeds, the profile showed clear striations with alternating positive and negative vorticity. The higher velocity test was much more erratic with pockets of positive and negative vorticity spread throughout the image. Despite this, in both tests the lower airfoil tip was located in the region of greatest positive vorticity and the upper tip was in the region of greatest negative vorticity. The local effect, then, would be a decrease in lift and increase in induced drag at the upper tip, with the opposite occurring at the lower tip. Further exaggerating this gradient, by blocking the lower wing tip vortex, the balance increases the strength of the upper wing tip vortex. The effects coincide producing an even larger lift and induced drag gradient along the span. Interestingly, this effect opposes the force gradient generated by the velocity magnitude variations; therefore one is a moderating influence on the other.

6.4 Force Testing

6.4.1 Purpose and Method

The force testing, accomplished using the cantilever load cell, was conducted to validate conclusions drawn from PIV and other tests about the flow quality. By testing the forces acting on the airfoil alone, the effects of the flow quality, of balance interference, and of the unsteady nature of the flow were measured.

Once the load cell data was corrected for the weight of the configuration, the data was reduced for comparison to the Wrights' wind tunnel lift data. PIV data was used to calculate average velocities along the airfoil span to determine the lift coefficients from the corrected load data.

6.4.2 Lift Coefficient Calculations

Figure 6.26 is a plot of the output voltage measured for each angle orientation of the load cell. The plot indicates the peaks at which the bias axis of the load cell was aligned with the resultant force for each RPM. The voltages were non-dimensionalized by dividing each run by the peak output voltage. At each run condition, there was a repeatable peak trend. At 3,568 RPM, however, a slight dip, which opposed the trend toward the peak, occurred at an angle of 12.5°. The dip is exaggerated by the small scale of the vertical axis, but was a repeatable result which indicated the angle and RPM combination resulted in a decrease in the aerodynamic forces.

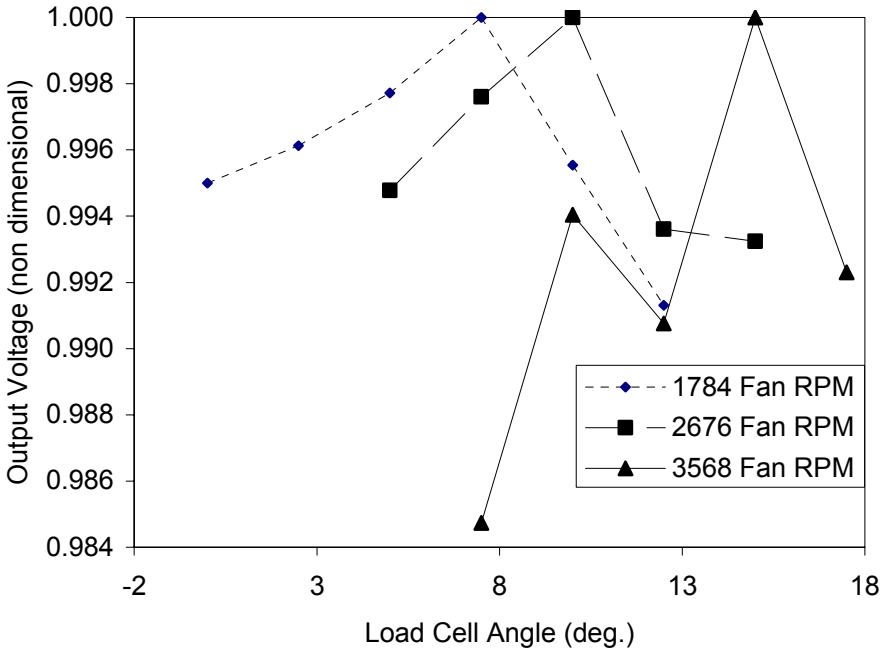

Figure 6.26 Plot showing the location of the peak voltages which indicated the angle of the resultant force

Both the flow surveys and the PIV data proved the existence of a large spanwise velocity gradient in the wind tunnel which affected the airfoil. Equation 6.4 shows the relationship between lift coefficient and velocity. Since the velocity is squared, the lift coefficient is especially sensitive to changes in the velocity. The large velocity gradient across the airfoil span means selecting the reference velocity is not very straightforward, and, thus, there is potential for a broad range of lift coefficients. The difficulty is determining which velocity, and resulting lift coefficient, was closest to that used by the Wrights.

$$C_L = \frac{L}{\frac{1}{2}\rho V^2 S}$$

Equation 6.4

6.4.2.1 Average Velocity Calculation

The first set of results used the average velocity across the airfoil span as the reference velocity. Table 6.11 contains the pertinent data from the load cell measurements. The peak angle indicates the direction of the *measured* resultant force with respect to the zero reference. Once converted to pounds the lift force was used to calculate the lift coefficient according to Equation 6.4.

Table 6.11 Lift and C_L data for each RPM

Fan RPM	Peak Angle (φ)	Measured Resultant (lbs)	Lift (lbs)	V avg. (fps)	C_L
3568	15.0°	0.225	0.0641	45.62	0.624
2676	10.0°	0.206	0.0368	34.5*	0.629
1784	7.5°	0.182	0.0154	23.38	0.571

*The average velocity at 1338 RPM was based on the assumption of linear variation of velocity with RPM

The density was based on the atmospheric conditions at the time of the test. The velocity was averaged from the velocity distribution along the airfoil span obtained from the PIV results for the empty tunnel running at full and half RPM. The three-quarter RPM result was averaged from the other two based on the assumption of linear variation of velocity with RPM.

The decrease in the peak angle was consistent with expected results. As RPM decreased, the lift force decreased. Since the weight remained constant as RPM decreased, the weight was a greater portion of the vector sum, and, thus, the angle of the measured resultant decreased.

Table 6.12 notes the percent difference between the measured lift coefficients, and the lift coefficient measured by the Wrights of 0.515 for their #12 airfoil at an angle of attack of 5°.

Table 6.12 Percent change in C_L from Wright Brothers' results

	C_L	% greater than Wrights' C_L
Wrights' Result	0.515	0.0%
3568 RPM	0.624	17.5%
2676 RPM	0.629	18.2%
1784 RPM	0.571	9.9%

The data indicates the Wrights' results for the lift coefficient were low by at least 10% and by as much as 18%. Interestingly, the closest result occurred at the half RPM value which only generated half the velocity claimed by the Wrights. This result, however, supports the belief held by some researchers that the Wrights could not have generated the velocity they claim, and that the true tunnel velocity was closer to 20 mph[129]. Although the Wrights did not use velocity in their lift coefficient calculations, the lift coefficient is a function of Reynolds number which is velocity dependent. These results provided limited evidence that the Wrights' tests were conducted at a Reynolds number less than that generated at 30 mph, and the Reynolds number at 20 mph results in a lift coefficient closer to the Wrights' recorded data.

Corrections for interference brought the calculated lift coefficients closer to the Wrights' result. Since the interference was determined by placing a "dummy" rod next to the airfoil, the corrections most likely do not account for the full interference of the attached rod. Based on the decrease in lift coefficient from the partial correction, however, corrections for the full interference might bring the calculated values even closer to the Wrights' data. Table 6.13 shows the partially corrected coefficients and the percent change from the Wrights' result.

Table 6.13 Percent change in C_L corrected for interference from Wright Brothers' results

	C_L	% greater than Wrights' C_L
Wrights' Result	0.515	0.0%
3568 RPM	0.609	15.4%
2676 RPM	0.612	15.9%
1784 RPM	0.550	6.4%

Interference corrections brought the calculated coefficient at half RPM even closer to the Wrights' results, further supporting the claim that the Wrights' tunnel ran at a lower Reynolds number than would be the case for the velocity they claimed.

[129] Wright Aeroplane Company, *Lift and Drift*, < http://www.first-to-fly.com/Adventure/Workshop/lift_and_drift.htm>.

6.4.2.2 Alternate Velocity Calculations

The calculations which used the average spanwise velocity, along with the Wrights' own calculations, assume that the velocity, and thus the dynamic pressure, over the drag fingers of their balance was equal to that over the airfoil. Equation 6.4 showed the dependence of lift coefficient on the lift force, the dynamic pressure, and the planform area. The Wrights' lift balance worked by balancing the force on the drag fingers with the lift on the airfoil, essentially setting the force coefficient on the drag fingers equal to the lift coefficient on the airfoil. However, if the dynamic pressure was not equal, the force coefficient on the drag fingers would no longer equal the lift coefficient of the airfoil. Equation 6.5 is a simplification of the equation mentioned, setting the two forces (drag on fingers, and lift on airfoil) equal to each other. Since the planform areas are equivalent, if the ratio of the dynamic pressures is not equal to 1 (i.e. the pressures are not equal) then the force coefficients would not be equal. If the Wrights were reading the force coefficient from the drag fingers, assuming it to be the same as the lift coefficient on the airfoil, they would have read a value either too high or too low depending on the dynamic pressure ratio.

$$C_{f_{drag}} \cdot \left(\frac{1}{2}\rho V^2\right)_{drag} \cdot S_{drag} = C_{f_{airfoil}} \cdot \left(\frac{1}{2}\rho V^2\right)_{airfoil} \cdot S_{airfoil}$$

Equation 6.5

Variations in the dynamic pressure ratio could have been the result of the impedance of the lift balance in the tunnel. PIV data showed such a large obstruction had a significant effect on the velocities in the flow, and though the effect was inconsistent, the changes should be taken into account. As an example, at 3568 RPM the balance in the tunnel increased the flow velocity by 0.5 m/s along the airfoil span. This increase must have been accompanied by a decrease in the bottom half of the tunnel, around the drag fingers. The velocity difference between the airfoil and drag fingers would have resulted in a large dynamic pressure ratio.

Table 6.14 shows the potential effect on lift coefficient from the presence of the balance as well as the deviation from the Wrights' lift coefficient. The velocity used to generate these coefficients was the average of the spanwise velocity calculated from PIV data with the balance in the tunnel. With the tunnel running at the maximum RPM, the average spanwise velocity was greater than the average for the empty tunnel by 0.6 mph. Conversely, the average for the half RPM case was less than that for the empty tunnel by 0.3 mph (The PIV data was inconsistent between the full and half RPM tests). According to Equation 6.5, if the dynamic pressure of the airfoil is greater than that of the drag fingers, the lift coefficient measured will be less than the true value. This was the case for the maximum RPM test, and the opposite occurred with the half RPM test.

Table 6.14 Percent change in C_L from Wright Brothers' results calculated with balance mounted in tunnel

	C_L	% greater than Wrights' C_L
Wrights' Result	0.515	0.0%
3568 RPM	0.599	14.1%
2676 RPM	0.620	17.0%
1784 RPM	0.593	13.2%

Though the PIV data showed inconsistency with the variation in dynamic pressure, it showed there was likely a difference in the dynamic pressures resulting in a change in the lift coefficient. A large enough difference in the drag and airfoil dynamic pressures could have been responsible for the Wrights' low lift coefficient. A significant decrease in dynamic pressure about the drag fingers is a possibility, generating a large gap between the two dynamic pressures. This would have further decreased the Wrights' measured lift coefficient. Unfortunately, the PIV system was not set up to accurately measure the velocity near the drag fingers to verify this possibility.

6.4.3 Force Testing Conclusions

It is clear the Wrights' calculations for the lift coefficient were below the true C_L for the airfoil. The lift coefficients generated by the Wrights were between 6% and 18% lower than the true value depending on the effects of interference and the velocity of the tunnel.

Though this testing did not clearly reveal the reason for the Wrights' low C_L values, a few possibilities were evident. First, if the dynamic pressure ratio between the drag fingers and the airfoil was something other than one, the force coefficient measured from the drag fingers will not be equal to the lift coefficient of the airfoil. PIV data showed the ratio to be other than one, but the data was inconsistent with RPM. Thus, depending on the ratio, the result would either lower the lift coefficient obtained in the force testing, bringing it closer to the Wrights' measured value, or increase the coefficient which would increase the deviation from the Wrights' data.

In addition to causing variations in the dynamic pressure, the balance would also have generated a large amount of interference. The airfoil was mounted with the bottom 1″ extending below the top strut of the balance. Though the PIV system was not able to analyze this region, the strut would likely have affected the local lift in that region of the airfoil. If the affect was negative, the measured lift coefficient would have been less than the true value, which may have contributed to the Wrights' low measurement.

7 CONCLUSIONS

7.1 Replica Tunnel Validation

The flow through the replica tunnel used in this research was at least the same quality as the flow through the Wright Brothers' tunnel, and most likely better. The design of the tunnel was based on the best approximations available of the Wrights' original tunnel. Since the tunnel itself was not maintained and no photographs exist, the replica design was the best educated guess at the Wrights' design. However the major elements, such as the size of the cross section and the contraction with vanes and honeycomb were based on descriptions by the Wrights in correspondence with Chanute and Spratt. Even if the Smithsonian and Wright Aeroplane Company plans used for the replica were not perfect, the approximation of these main elements resulted in similar flow characteristics and effects.

Initially, the tunnel was set up using the same methods available to the Wrights for validation and alignment such as tufts and an anemometer. Methods unavailable to the Wrights were then used to augment these basic tools. The Wrights had no means of high resolution, unobtrusive velocity measurements. Flow surveys were used in the replica to test and correct for flow asymmetry. Particle Image Velocimetry was then used to examine overall flow uniformity and symmetry. These tests showed how easy it was to induce asymmetry in the flow and ensured the replica tunnel had the best possible flow symmetry.

Beyond the Wrights inability to conduct detailed measurements and validations of their flow, other tunnel characteristics not present in the replica would further degrade their flow. The replica produced roughly the same flow velocity (between 30 and 35 mph) as the Wrights at similar RPM (3,000 to 3,500), but there was no evidence for the type of fan the Wrights used, therefore no method of ensuring identical flow properties. The fan they used was less efficient than that used in the replica since the Wrights had yet to develop their propeller theory, and the propellers of the day were 50% efficient at best. Similarly, the Wrights mounted their fan on a large box which blocked the propeller during part of each rotation. This would asymmetrically load the propeller causing oscillations as well as forcing asymmetric flow though the contraction. The replica tunnel lacked this obstruction and was set up for the best possible flow from the driver section.

7.2 Boundary Layer Evaluation

The preliminary testing indicated the boundary layers in the tunnel were approximately 2″ from each tunnel wall. The detailed flow surveys, conducted in the horizontal and vertical centerlines of the test section, supported the preliminary tests and extended the magnitude to 2.5″. The PIV data further indicated that the boundary layers on each wall were of very similar magnitude and profile.

These boundary layer evaluations were "best case" scenarios. With asymmetric flow caused by misalignment and the blockage in the driver section, the boundary layers would lose their similarity and grow even larger. Even with the "best case" flow the airfoils breached the boundary layer. If the boundary layers grew even larger they would act on a significant portion of the airfoil span, further reducing the accuracy of lift and drag measurements.

7.3 Spanwise Airfoil Gradients

Several gradients influenced the Wright Brothers' airfoils which introduced uncertainty into the measurements of lift and drag. The PIV testing indicated a spanwise velocity variation along the airfoil of up to 1.5 m/s for the low speed run (1784 RPM) and up to 3.0 m/s for the high speed run (3568 fan RPM). The velocity gradient generated an asymmetric lift distribution which could have been as large as 20% from tip to tip. Further contributing to the asymmetric lift, the variation in velocity generated a Reynolds number variation. According to analytic testing the Reynolds number gradient would generate an asymmetric distribution of lift coefficient along the span on the order of hundredths. This C_L gradient operated in the same sense as the velocity gradient, generating more lift at the upper wingtip.

The vorticity also contributed to a spanwise force gradient, though acting opposite to the velocity gradient. Both the empty tunnel vorticity and the influence of the balance on wing tip vortices generated a downwash gradient which resulted in a lift and induced drag variation along the span. Though the downwash gradient acted counter to the axial velocity gradient, it is significantly smaller and only provided a slight moderating influence.

The impedance of the balance also generated a horizontal gradient throughout the tunnel. The distributed blockage reduced the velocity of the flow over the drag fingers and increased the velocity over the airfoil by as much as 0.5 m/s. This caused dynamic pressures along the airfoil to be significantly larger than the dynamic pressures on the drag fingers. Because of the measurement method of the Wrights' lift balance, the ratio of the dynamic pressures along the airfoil and drag fingers resulted in a measured lift coefficient at least 7.0% lower than the actual coefficient of the airfoil. This was a conservative calculation since the actual velocity decrease about the drag fingers could not be accurately measured, and the effects of the horizontal velocity gradient caused by the balance and airfoil, which would increase the dynamic pressure on the upper airfoil surface relative to the lower surface, was not considered. The data was well supported by force test measurements in which the Wrights' data was between 6% and 18% lower than the directly measured lift coefficient for the same airfoil at the same angle of attack.

7.4 Relevance of Wind Tunnel Data to the 1903 Flyer

The historical research provided strong evidence that the Wrights could not have used their wind tunnel data quantitatively. First, they did not scale any of their airfoil shapes to full scale in their gliders or Flyer, and the analytical tools to extrapolate their data, such as Thin Airfoil Theory, had not been developed. Second, recent research indicates the Flyer would not have succeeded without the lift boost and drag decrease provided by flying in ground effect. The Wrights seem to have been unaware of the benefits of ground effect, did not test for it, and most likely could

not predict it. Both indicate that the Wrights could not have used quantitative wind tunnel data to produce the designs for the 1902 glider and 1903 Flyer.

The poor quality of the wind tunnel flow further supports this conclusion. The large force gradients and dynamic pressure ratios resulted in highly inaccurate lift coefficient measurements. As the airfoils tested were of different span, chord, and planform shape, the effects of the gradients and pressure ratios would not have been consistent from one airfoil to another. Thus, not only was the qualitative data flawed due to the poor conditions, but comparisons between airfoils for qualitative purposes lose a certain amount of validity. Additionally, the analytic study showed Reynolds number scaling effects would render the Wrights' wind tunnel data quantitatively useless for application to full scale flight without significant corrections. Even if the Wrights' wind tunnel data had been accurate, lift measurements would still have been 14% lower than the lift at full scale flight conditions at their cruise alpha of 5°.

In measuring the lift coefficient, the Wrights were low by at least 6% and by as much as 15% when compared to direct force measurements of an isolated wing at the same Reynolds number and angle of attack. Considering full scale flight predictions and Reynolds number scaling effects, however, their lift measurement was at least 20% and as much as 30% too low, and their drag prediction was approximately three times greater than full scale. Thus, though they learned a great deal from their tunnel, none of their quantitative data was useful in the design process. However, had they used their wind tunnel as a quantitative tool the Wright Flyer would have been grossly over-designed and may have been too heavy to fly. Therefore the Wrights must have recognized the limits of the tunnel and used it as a qualitative tool, along with the experience they gained in earlier full scale experiments, to engineer and design the first successful manned aircraft.

7.5 Experimental Error

The purpose of the replica tunnel was to model a flawed flow. Due of the nature of the research it was difficult to evaluate the error because the standard of comparison was not perfect flow, but something that was also in error. The assumption was made that building a tunnel as close as possible to the actual designs and generating flow of similar velocity at similar fan speed would result in flow which closely modeled that of the original Wright tunnel.

The unsteadiness of the replicated flow presented some measurement problems. At the maximum fan speed the variation from the average static pressure reading was under 20% in most cases. This is a substantial variation, yet at lower fan speeds this number doubled and tripled as the magnitude of the static pressure change decreased and the unsteady "noise" became a larger component of the pressure measurements.

The flow was not validated by testing a replica balance with a replica airfoil to reproduce the Wrights' data, however this was not an immediate necessity. The purpose of the research was to indicate what the Wrights could and could not have learned from their tunnel, thus exact equivalence was less important than modeling the general flow characteristics which resulted from copying the Wrights' design.

One aspect of the design was not replicated, however, and would have resulted in a certain amount of error. The box on which the Wrights mounted their propeller was replaced with unobtrusive struts which provided much less interference and allowed symmetric loading on the propeller. This actually greatly improved the flow entering the tunnel, thus the conclusions so far are conservative, as the Wrights flow was much degraded by the presence of the mount.

The test location was also a potential source of error. The Wrights noted they never moved any major piece of furniture within their test room, and only the operator was present during tests to minimize disturbances in the flow through the room. Unfortunately the replica was located in a room undergoing renovation and reorganization. There were people moving regularly around the room, though never within 15 feet of the tunnel, and major pieces of machinery are regularly moved into or out of the room. The local area in a 20 foot radius about the tunnel remained unchanged, but the effects of the constant movement and shifting of objects further away were not measured.

7.6 Further Testing Possibilities

The recommended next step in this line of research is to attempt to better model the imperfections in the Wrights' wind tunnel. Primarily, the effects of the Wright Brothers' motor mount should be determined, at least qualitatively. By placing an obstruction forward of the fan, the results of oscillations and flow asymmetry can be determined either with PIV or simply a centerline flow survey. Additionally, repeatability tests should be conducted to determine whether the fan oscillations generate any time dependent effects. If the analysis of the boundary layers and flow uniformity suggest a substantial change in the spanwise velocity gradients along the airfoil, force testing should be used to determine effects of asymmetry on the measured lift coefficient, and PIV data should be obtained to analyze any changes in the horizontal gradient generated by the balance and the airfoil. The PIV data will also reveal the effects of asymmetry on the tunnel vorticity and the development of wing tip vortices.

APPENDIX A. DEFINITION OF TERMS

The purpose of this section is to provide a basic understanding of common aerospace and fluid mechanics terms and expressions.

Alpha Sweep is a set of measurements taken at sequential, increasing **angles of attack**.

Angle of Attack, alpha, or AOA is also defined by the symbol α and represents the angle between the freestream flow and the **chord** line of the wing.

Aspect Ratio (AR) is a ratio of the wing dimensions and affects many of the wing's characteristics. It is defined by the equation below as the ratio of the **span** squared over the **planform area**. This essentially describes the wing slenderness. A high aspect ratio wing is long and slender, while a low aspect ratio wing is short and stubby. In general higher aspect ratio wings are more efficient for lower **Reynolds number** flight because they minimize **three-dimensional effects**, but they have structural limitations and are unsuitable for transonic and supersonic flight.

$$AR = \frac{b^2}{S}$$

Camber is the curvature of an airfoil. It is often defined as a ratio or percent comparing the depth of the curvature to the **chord** of the wing (i.e. 1/20 or 5%). Figure A.1 depicts the elements of a cambered airfoil.

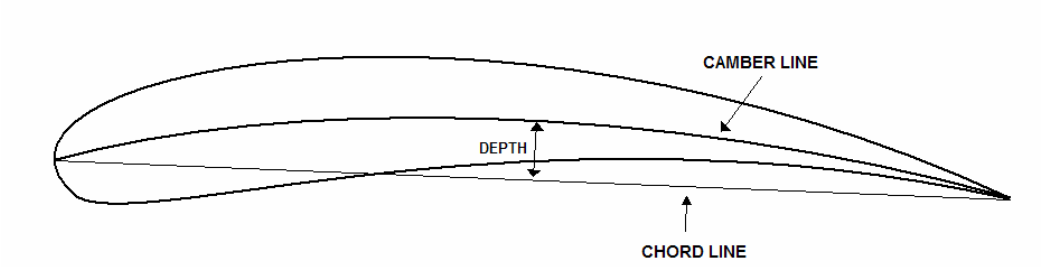

Figure A.1 Representation of a cambered airfoil

Center of Pressure is the point at which the **aerodynamic resultant force** act on an object.

Chord (c) is the distance from the leading edge of a wing to the trailing edge. It is a common reference length used in several equations including the non-dimensionalization of **coefficients** and calculating **Reynolds number**.

Coefficients are representations of a force or moment which are non-dimensionalized according to a certain convention. By non-dimensionalizing the force or moment velocity and size scaling effects are no longer considerations, and the coefficient can be used and compared across a much broader spectrum than the true force or moment which is only applicable to the specific object. The coefficients themselves are functions only of **angle of attack**, **Reynolds number**, **and Mach number**, so if M and Re are matched, the models will produce the same coefficient at the same angle of attack.

The following equations define the most common three-dimensional aerodynamic coefficients. Three-dimensional coefficients are defined with an uppercase subscript while two-dimensional coefficients are represented by lower case subscripts. The three-dimensional coefficients include **three-dimensional effects** in the measurement of the force or moment.

$$C_L = \frac{L}{\frac{1}{2}\rho V^2 S}$$ 3D lift coefficient

$$C_D = \frac{D}{\frac{1}{2}\rho V^2 S}$$ 3D drag coefficient

$$C_M = \frac{M}{\frac{1}{2}\rho V^2 Sc}$$ 3D moment coefficient

Ground Effects are present when an aircraft is flying close to the ground, usually at an altitude less than the **span** of the wing. The ground effectively blocks part of the **wingtip vortices**, reducing the **three-dimensional effects**. The result is an increase in lift and a decrease in **induced drag**.

Induced Drag is drag generated by **three dimensional effects**. Together, **profile drag** and induced drag make up the total drag on a low speed object.

Mach number is a very important concept in wind tunnel testing. It is a dimensionless compressibility parameter. Incompressible flow is mathematically defined as M = 0. The parameter is computed as the ratio of inertia forces to elastic forces in a flow according to the following equation.

$$M = \frac{V}{a}$$

Mach number is directly proportional to the velocity of a flow, and inversely proportional to the speed of sound within the flow.

Mach number is one of two flow similarity, or scaling parameters, the other being **Reynolds number**. If the Reynolds number and Mach number of one flow are equal to that of another, the

two flows are dynamically similar. Thus if the Reynolds number and Mach number of a full scale flow can be matched in a wind tunnel, the forces and moments measured in the wind tunnel can be scaled directly to full scale because the **coefficients** will be identical. Unfortunately, it is near impossible to match both the Reynolds and Mach numbers in most wind tunnel tests and a compromise must be made. For tests which model low Reynolds number flows, it is more important to match the Reynolds number. For high velocity tests, the Mach number should be matched for best equivalency.[130]

Pitching Moment is the tendency of an airfoil or wing to pivot end-over-end. By convention this is defined as positive if the nose is pitching up.

Planform Area is easily pictured as the projected area of an object, or the area of an object's shadow from a light source directly overhead (Figure A.2). The planform area is used as a reference area in calculating most **coefficients** as well as other equations in the fluid mechanics.

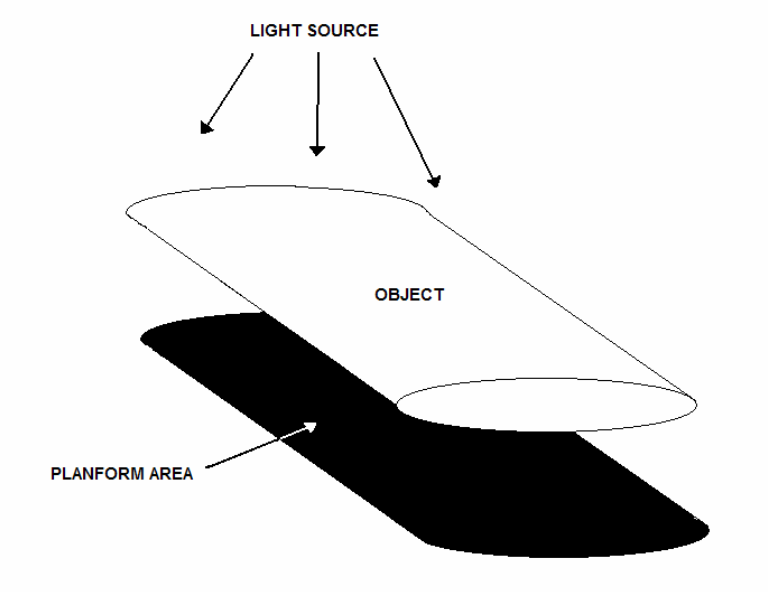

Figure A.2 Image depicting the analogy of an object's shadow to its planform area

Profile Drag is due to skin friction on the surface of a body and pressure drag due to flow **separation** around the body. Together, profile drag and **induced drag** make up the total drag on a low speed object.

Resultant Force (Aerodynamic Resultant Force) is the vector sum of the lift and drag forces.

Reynolds number is one of the most important concepts in wind tunnel testing. It is defined as the ratio of inertia forces to viscous forces in a flow according to the following equation.

[130] Pope and Rae, *Low Speed Wind Tunnel Testing*, (New York: John Wiley and Sons, 1984), 7.

$$\mathrm{Re} = \frac{\rho V c}{\mu}$$

Reynolds number is directly proportional to the fluid density (ρ), velocity (V), and reference length (often the **chord (c)** of a wing or airfoil), and inversely proportional to the viscosity of the flow (μ).

Reynolds number is one of two flow similarity, or scaling parameters, the other being **Mach number**. If the Reynolds number and Mach number of one flow are equal to that of another, the two flows are dynamically similar. Thus, if the Reynolds number and Mach number of a full scale flow can be matched in a wind tunnel, the forces and moments measured in the tunnel can be scaled directly to full scale because the **coefficients** will be identical. Unfortunately, it is near impossible to match both the Reynolds and Mach numbers in most wind tunnel tests and a compromise must be made. For tests which model low Reynolds number flows, it is more important to match the Reynolds number. For high velocity tests, the Mach number should be matched for best equivalency.[131]

Separation occurs when the energy in a flow is not enough to overcome an adverse pressure gradient. For example, flow can generally remain attached to the airfoil surface along the downslope on the back side of the airfoil and further contributes to the lift. However, if the angle becomes too steep, the flow cannot remain attached to the surface and separates from the airfoil at a certain point, no longer generating lift. This can occur at the leading edge, trailing edge, or somewhere in between. The flow can separate at the leading edge then reattach further along the chord, resulting in a separation bubble at the leading edge where a majority of the lift is usually generated when the flow is attached.

Smeaton Coefficient is a coefficient used by early aerodynamicists to scale up non-dimensionalized data. Its modern equivalent is one-half the density. Thus it is a variable coefficient and was the source of much consternation among aerodynamicists. The Wrights used the wrong value for this coefficient to make predictions in their early experiments, and the poor correlation of prediction with observed data drove them to collect their own data with a wind tunnel.

Span (b) is the distance from wingtip to wingtip.

Three-Dimensional Effects are a group of effects which result from the difference between the pressure on the upper and lower surfaces of a wing. The higher pressure on the lower surface naturally wraps around the edges of the wings because of the lower pressure above the wing. As the flow wraps around the wingtip it generates **wingtip vortices** which result in a downward velocity component on the upper surface of the wing. This component reduces the angle of the **aerodynamic resultant force** which decreases the lift produced and increases the drag (creating **induced drag**).

---

[131] Pope and Rae, *Low Speed Wind Tunnel Testing*, (New York: John Wiley and Sons, 1984), 7.

Turbulence Intensity is a percentage which represents perturbations in the axial velocity. It is defined by the following equation.

$$TurbulenceIntensity = \frac{\sqrt{(w(t) - \overline{w})^2}}{\overline{w}}$$

$\overline{w}$ represents the axial velocity, and $w(t)$ is the axial velocity as a function of time.

Wingtip Vortices result from high pressure air below a wing wrapping around the wingtip to fill the void generated by low pressure air on the upper surface. They are the source of **three dimensional effects** and a consequence of circulation.

Zero Lift Pitching Moment is the magnitude of the **pitching moment** defined at the angle where the wing or airfoil is producing zero lift. This is a defining characteristic of a wing and is important in stability and control considerations.

APPENDIX B. SENSOR CALIBRATION DATA

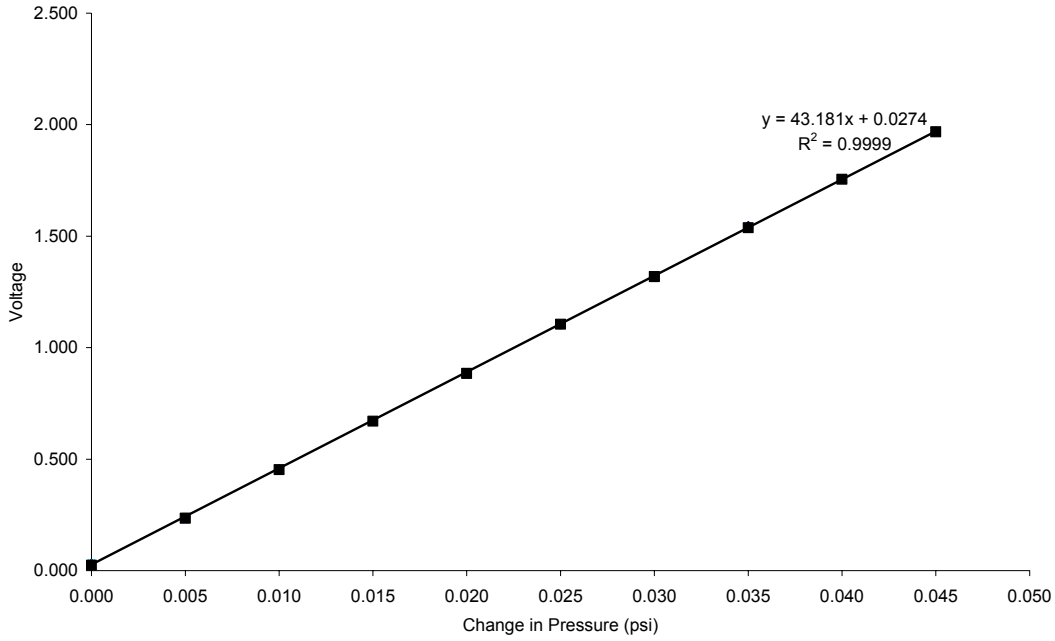

Figure B.1 Calibration of Transducer 1

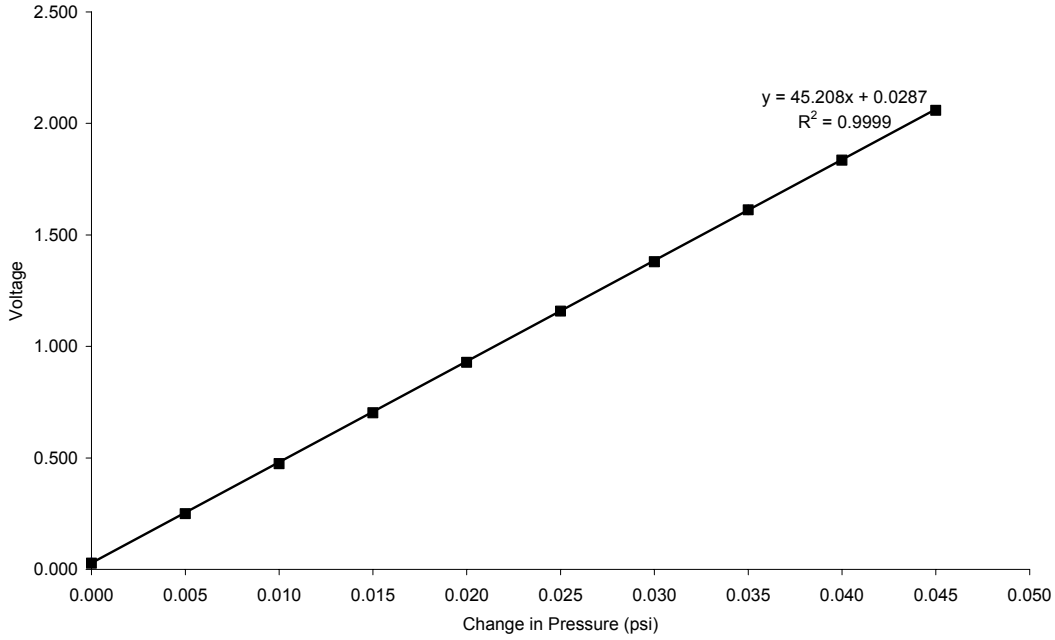

Figure B.2 Calibration of Transducer 2

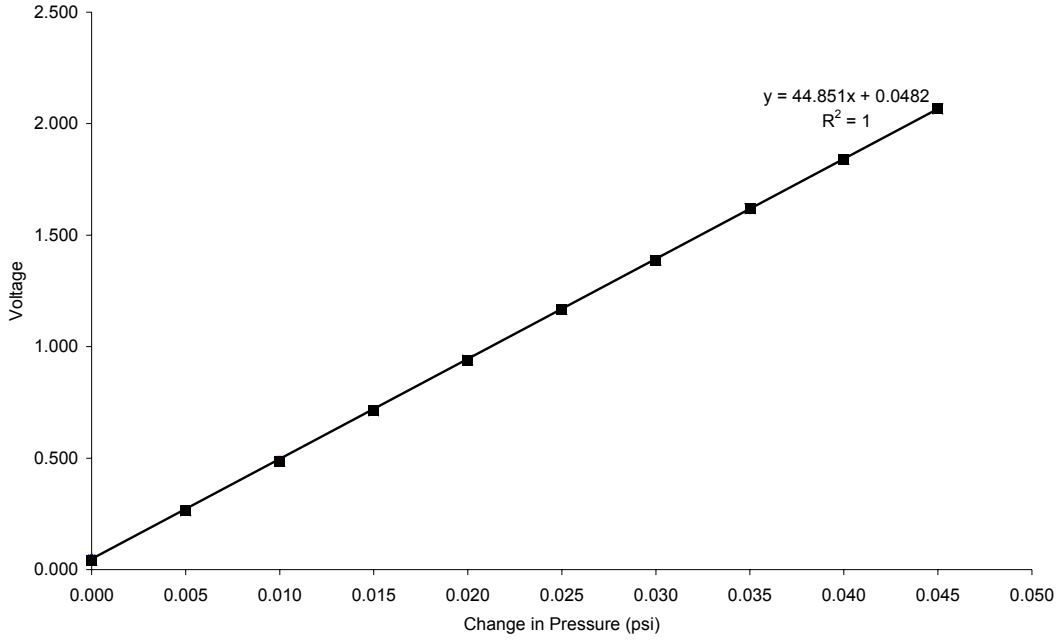

Figure B.3 Calibration of Transducer 3

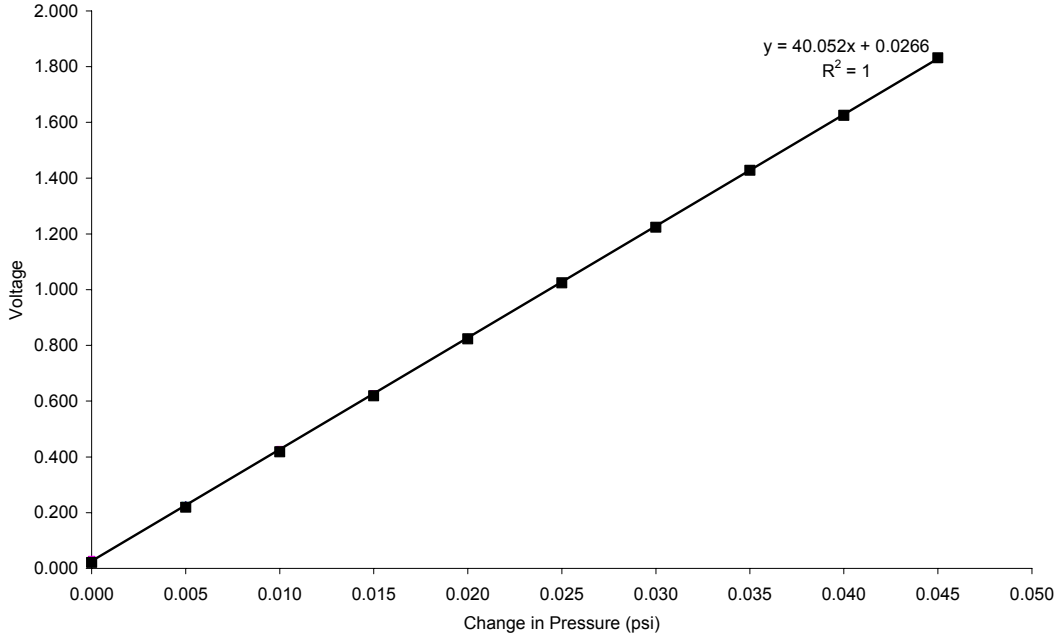

Figure B.4 Calibration of Transducer 4

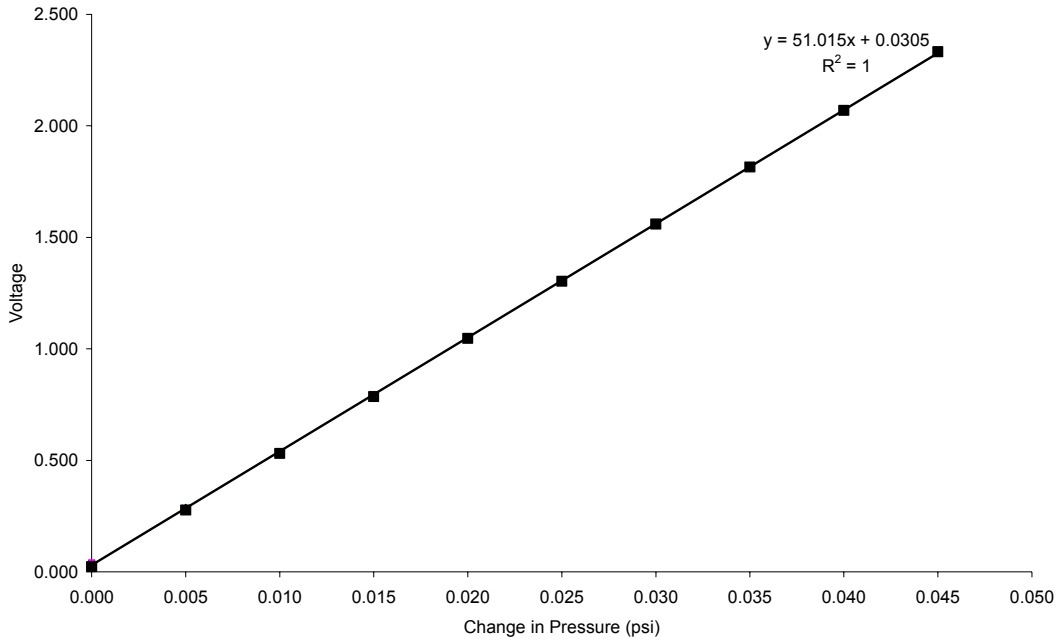

Figure B.5 Calibration of Transducer 5

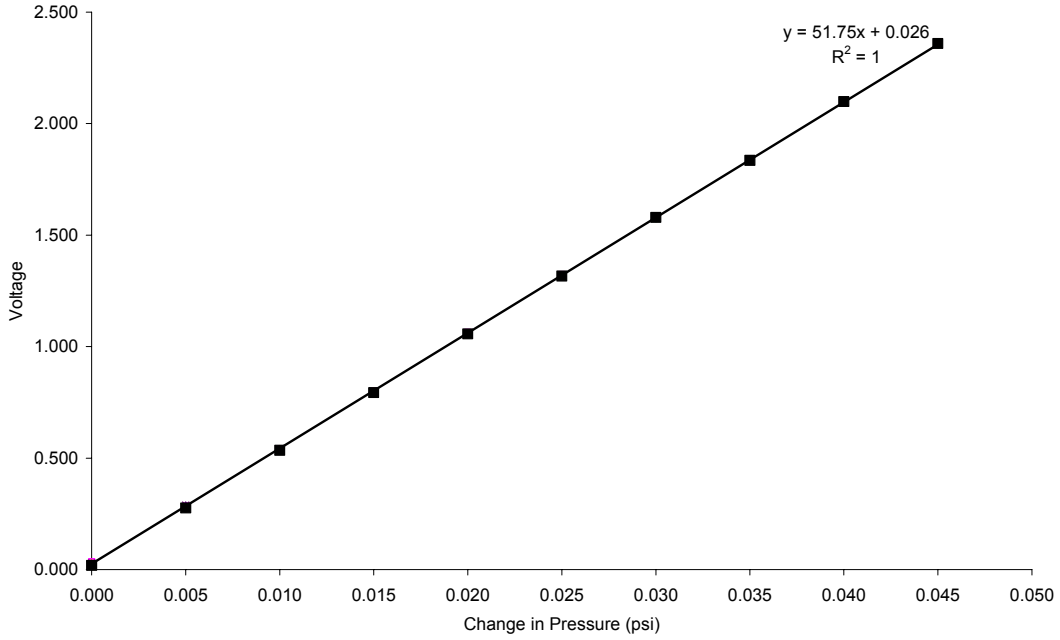

Figure B.6 Calibration of Transducer 6

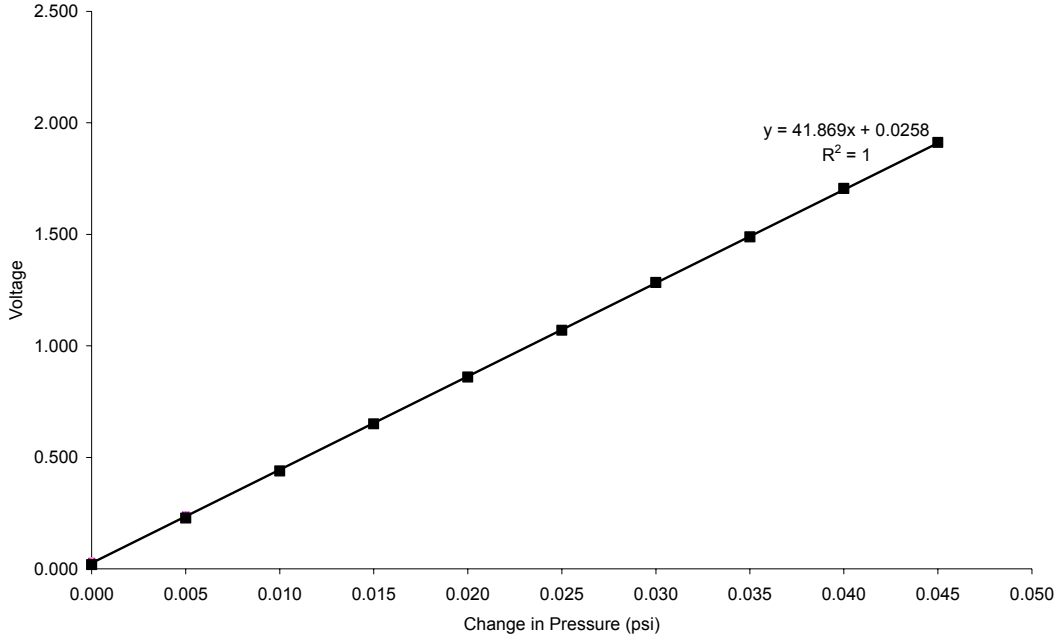

Figure B.7 Calibration of Transducer 7

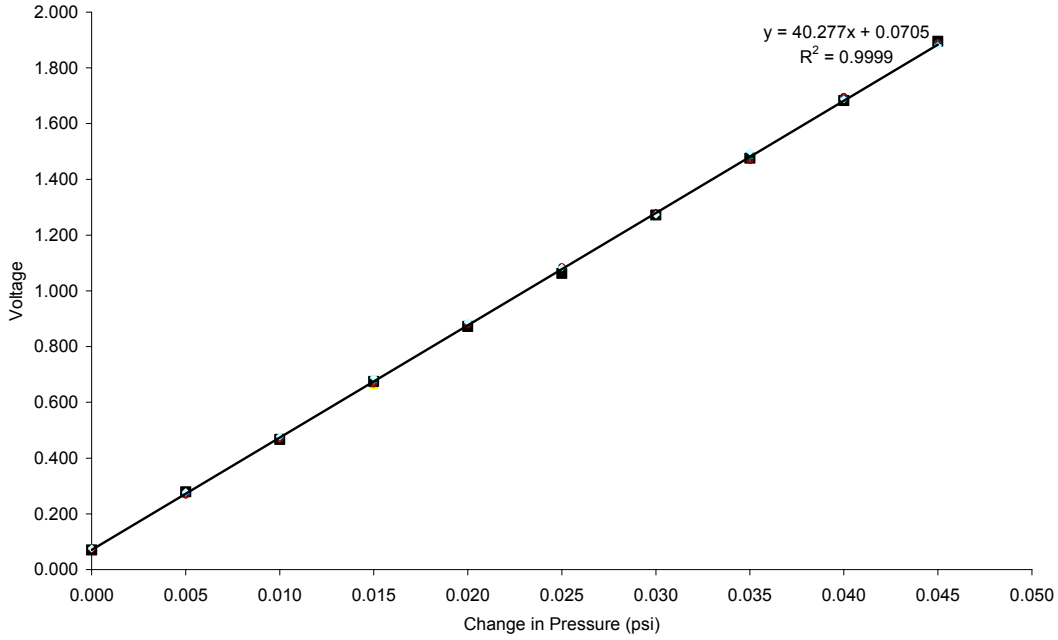

Figure B.8 Calibration of Transducer 8

APPENDIX C. MATLAB SCRIPTS

PIVPROCESSING.M

```
%=========================================================================
function PIVFileCruncher
%=========================================================================

%*************************************************************************
%   PIVProcessing.m     adapted by: Michael Dodson
%
%   Program prompts user for a .v3s PIV file, and interpolates vectors to a
%   uniform grid to allow for ease of processing.  After the files are
%   shifted to the global coordinate system, they are processed in the
%   following ways:
%
%   1.  Spanwise velocity distribution for region directly behind the
%   airfoil
%   2.  Calculate min, max, and average values and locations for velocity
%   magnitude and turbulence intensity for a bxb box in the airfoil region
%   3.  Calculate vorticity for bxb region
%
%   The data for spanwise velocity, and bxb velocity and turbulence
%   intensity are then output to Excel files under the names #_span,
%   #_VelMag, #_TurbInt
%
%   The spanwise velocity, velocity magnitude, turbulence intensity, and
%   vorticity images are then rotated to match the upright tunnel, and
%   output to the screen
%
%   Process is only valid for vectors from the upper region of the wind
%   tunnel (this was the right side of the tunnel when rotated)
%
%   3MAY05
%*************************************************************************

clear all
clc

%******************
% Open and read file
%******************

%"shift" variable stores the distance to shift x to the global coordinate
%system

shift = 85.3848;

% Open dialog to get input filename.
[FileNameIn,PathNameIn] = uigetfile('*.v3s','Input File');
```

```
% Turn input file into array of strings, one per line.
txt_file = textread(FileNameIn,'%s','delimiter','\n');

% Process the first line for information.
[data_run, m, n, tokens] = read_first_line(txt_file{1});

% Read the rest of the file.
for j=2:length(txt_file)
        iline = j;
        text_line = txt_file{iline};
        values = strread(text_line, '%f', 'delimiter', ',')';
        xin(iline-1) = values(1)+shift; yin(iline-1) = values(2); zin(iline-
1) = values(3);
        uin(iline-1) = values(4); vin(iline-1) = values(5); win(iline-1) =
values(6);
        countin(iline-1) = values(7); respixin(iline-1) = values(8);
        Reuvin(iline-1) = values(9); Reuwin(iline-1) = values(10);
Revwin(iline-1) = values(11);
        ustdin(iline-1) = values(12); vstdin(iline-1) = values(13);
wstdin(iline-1) = values(14);
        wturbin(iline-1) = wstdin(iline-1)/win(iline-1);
        if (uin(iline-1)>20)
            uin(iline-1)=0;
        end
        if (vin(iline-1)>20)
            vin(iline-1)=0;
        end
        if (win(iline-1)>20)
            win(iline-1)=0;
        end
end

%**********************
% Begin data processing
%**********************

%generate and interpolate data onto uniform grid
[xg,yg] = meshgrid(-5:1:180, -90:1:90);
uout = griddata(xin,yin,win,xg,yg);
uturb = griddata(xin,yin,wturbin,xg,yg);


%************************************************
% Part 1: Determine spanwise velocity distribution
%************************************************

%extract data from 16mm high rectangle behind the airfoil
%generates grid of area behind the airfoil and interpolates uout onto the
grid
%rectangle spans from -5 to 113 (x) and -8 to 8 (y)

[xw, yw] = meshgrid(-5:1:125, -8:1:8);
wake = griddata(-5:180,-90:90, uout, xw, yw);
```

```
%average each column along the span and save velocities in to Vspan
%Vmin and Vmax hold the min and max velocities and their respective span
%location

Vmin(1) = 0;
Vmax(1) = 0;
Vmin(2) = 100000;
Vmax(2) = 0;

for i=1:length(wake(1,:))
    Vspan(i) = mean(wake(:,i));
    if Vspan(i)>Vmax(2)
        Vmax(2) = Vspan(i);
        Vmax(1) = i-6;      %element 1 in wake corresponds to -5mm
    end
    if Vspan(i)<Vmin(2)
        Vmin(2) = Vspan(i);
        Vmin(1) = i-6;
    end
end

for i=1:length(wake(1,:))
    x(i)=i-6;   %store location in mm into x for plotting use
end

%*************************************************
% Part 2: Evaluate bxb box for min, max and avg values
%         of VelMag, Turbulence Intensity
%*************************************************

%Generate bxb grid with the airfoil in the center
%spanning -5 to 125 in x, 65 to -65 in y

[xb, yb] = meshgrid(-5:1:125, -65:1:65);

%interpolate VelMag and TurbInt data onto grid

Vbox = griddata(-5:180,-90:90, uout, xb, yb);
Turbbox = griddata(-5:180,-90:90, uturb, xb, yb);

%go through each element in box to determine min, max, and avg

count=1;
VsumB=0;
VmaxB(1) = 0;  %initialize xlocation
VmaxB(2) = 0;  %initialize ylocation
VmaxB(3) = 0;  %initialize Magnitude
VminB(1) = 0;
VminB(2) = 0;
VminB(3) = 100000;

TurbsumB=0;
TurbmaxB(1) = 0;  %initialize xlocation
```

```
TurbmaxB(2) = 0;  %initialize ylocation
TurbmaxB(3) = 0;  %initialize Magnitude
TurbminB(1) = 0;
TurbminB(2) = 0;
TurbminB(3) = 100000;

for i=1:length(Vbox(:,1))    %go through each row
    for j=1:length(Vbox(1,:))    %go through each column
        VsumB = VsumB + Vbox(i,j);
        TurbsumB = TurbsumB + Turbbox(i,j);

        if Vbox(i,j)>VmaxB(3)
            VmaxB(3) = Vbox(i,j);
            VmaxB(1) = j-6;      %element 1 in Vbox (x) corresponds to -5mm
and increases
            VmaxB(2) = i-57;     %element 1 in Vbox (y) corresponds to -56mm
and increases
        end
        if Vbox(i,j)<VminB(3)
            VminB(3) = Vbox(i,j);
            VminB(1) = j-6;      %element 1 in box (x) corresponds to -5mm
and increases
            VminB(2) = i-57;     %element 1 in box (y) corresponds to -56mm
and increases
        end

        if Turbbox(i,j)>TurbmaxB(3)
            TurbmaxB(3) = Turbbox(i,j);
            TurbmaxB(1) = j-6;      %element 1 in Turbbox (x) corresponds to
-5mm and increases
            TurbmaxB(2) = i-57;     %element 1 in Turbbox (y) corresponds to
-56mm and increases
        end
        if Turbbox(i,j)<TurbminB(3)
            TurbminB(3) = Turbbox(i,j);
            TurbminB(1) = j-6;      %element 1 in Turbbox (x) corresponds to
-5mm and increases
            TurbminB(2) = i-57;     %element 1 in Turbbox (y) corresponds to
-56mm and increases
        end
        count = count + 1;
    end
end

VavgB = VsumB/count;
TurbavgB = TurbsumB/count;

%*****************************************************
% Part 3: Calculate Vorticity for entire region
%*****************************************************

u = griddata(xin,yin,uin,xg,yg);
v = griddata(xin,yin,vin,xg,yg);
cav = curl(xg,yg,u,v);
```

```
%***************************
% Output to Excel Spreadsheet
%***************************

filenum = strread(FileNameIn,'%s %*s','delimiter','.');


%output spanwise velocity distribution to #_span.xls
spanoutput(1,:) = {'Spanwise Location (mm)', 'Velocity (m/s)','Vmax location
(mm)',...
    'Vmax (m/s)','Vmin location (mm)','Vmin (m/s)'};
for i=1:length(x)
    spanoutput(i+1,1) = num2cell(x(i));   %store spanwise location
    spanoutput(i+1,2) = num2cell(Vspan(i)); %stores spanwise velocity
end
spanoutput(2,3:4) = num2cell(Vmax); %store Vmax
spanoutput(2,5:6) = num2cell(Vmin); %store Vmin

xlswrite(char(strcat(filenum,'_span')),spanoutput);

%output min, max, and average values and locations for VelMag to
%#_VelMag.xls
VelMagoutput(1,:) = {'Avg Vel (m/s)','Vmax x-location (mm)','Vmax y-location
(mm)',...
    'Vmax (m/s)','Vmin x-location (mm)','Vmin y-location (mm)','Vmin (m/s)'};

VelMagoutput(2,1) = num2cell(VavgB);
VelMagoutput(2,2) = num2cell(VmaxB(1));
VelMagoutput(2,3) = num2cell(VmaxB(2));
VelMagoutput(2,4) = num2cell(VmaxB(3));
VelMagoutput(2,5) = num2cell(VminB(1));
VelMagoutput(2,6) = num2cell(VminB(2));
VelMagoutput(2,7) = num2cell(VminB(3));

xlswrite(char(strcat(filenum,'_VelMag')),VelMagoutput);
%xlswrite('10_VelMag',VelMagoutput);

%output min, max, and average values and locations for TurbInt to
%#_TurbInt.xls
TurbIntoutput(1,:) = {'Avg TurbInt','Max x-location (mm)','Max y-location
(mm)',...
    'Max Mag','Min x-location (mm)','Min y-location (mm)','Min Mag'};

TurbIntoutput(2,1) = num2cell(TurbavgB);
TurbIntoutput(2,2) = num2cell(TurbmaxB(1));
TurbIntoutput(2,3) = num2cell(TurbmaxB(2));
TurbIntoutput(2,4) = num2cell(TurbmaxB(3));
TurbIntoutput(2,5) = num2cell(TurbminB(1));
TurbIntoutput(2,6) = num2cell(TurbminB(2));
TurbIntoutput(2,7) = num2cell(TurbminB(3));

xlswrite(char(strcat(filenum,'_TurbInt')),TurbIntoutput);
```

```
%*************************
%  Rotate and Output Images
%*************************

%***************rotate full velocity image

n = length(uout(:,1));
for count=1:n
    urot(count,:) = uout(n+1-count,:);
end

figure(6): surf(yg, xg, urot, urot);
colormap jet;
axis equal tight;
%caxis([11,17]);
colorbar;
title('Full View Velocity (m/s)','FontName','times','FontSize',18)
xlabel('x (mm)','FontName','times','FontSize',18);
ylabel('y (mm)','FontName','times','FontSize',18);
shading interp;
az=0; el=90;
view(az,el);

%***************rotate VelMag image

n = length(Vbox(:,1));
for count=1:n
    Vboxrot(count,:) = Vbox(n+1-count,:);
end

figure(7): surf(yb, xb, Vboxrot, Vboxrot);
colormap jet;
axis equal tight;
%caxis([11,17]);
colorbar;
title('Velocity Magnitude (m/s)','FontName','times','FontSize',18)
xlabel('x (mm)','FontName','times','FontSize',18);
ylabel('y (mm)','FontName','times','FontSize',18);
shading interp;
az=0; el=90;
view(az,el);

%***************rotate Turbulence image

n = length(Turbbox(:,1));
for count=1:n
    Turbboxrot(count,:) = Turbbox(n+1-count,:);
end

figure(8): surf(yb, xb, Turbboxrot, Turbboxrot);
colormap jet;
axis equal tight;
```

```
caxis([.055,.105]);
colorbar;
title('Turbulence Intensity','FontName','times','FontSize',18)
xlabel('x (mm)','FontName','times','FontSize',18);
ylabel('y (mm)','FontName','times','FontSize',18);
shading interp;
az=0; el=90;
view(az,el);

%***************rotate vorticity image

n = length(cav(:,1));
for count=1:n
    cavrot(count,:) = cav(n+1-count,:);
end
figure(9)
pcolor(yg,xg,cavrot); shading interp
title('Vorticity (rad/s)','FontName','times','FontSize',18)
xlabel('x (mm)','FontName','times','FontSize',18);
ylabel('y (mm)','FontName','times','FontSize',18);
caxis([-.015,.02]);
colorbar;
colormap jet;

%***************rotate spanwise velocity image

%plot Vspan v. y location and display min and max V
figure(10)
plot(Vspan, x)
title('Spanwise Velocity (m/s)','FontName','times','FontSize',18)
ylabel('Spanwise location (y mm)','FontName','times','FontSize',18)
xlabel('Velocity (m/s)','FontName','times','FontSize',18)

%=========================================================================
function [data_run, m, n, tokens] = read_first_line(first_line)
%=========================================================================

% Split the first line at the equal signs
tokens = split_string(first_line,'=');

% The 1st token has the word title, don't need that.
% The 2nd token has the file name, and the word variables.
% Extract the file name by splitting the 2nd token at the quotations.
% Then, pull out the run number (specific to DD-963 testing during summer
2004.
tokens_2 = split_string(tokens{2},'"');
run_data_file = tokens_2{2};
ipos = strfind(run_data_file, 'Run');
data_run = run_data_file(ipos:ipos+6);

% The 5th token has the number of rows
tokens_5 = split_string(tokens{5},',');
m = str2num( cell2mat( tokens_5(1) ) );
```

```
% The 6th token has the number of columns
tokens_6 = split_string(tokens{6},',');
n = str2num( cell2mat( tokens_6(1) ) );

% Skip the rest of the information on the first line

%=========================================================================
function first_line = write_first_line(data_run, m, n, tokens)
%=========================================================================

% Paste the first line back together and add the equal signs.
numtokens = length(tokens);
first_line = char(tokens(1));
for it = 2:numtokens
    first_line = strcat( first_line, '=', char(tokens(it)) );
end

%=========================================================================
function tokens = split_string(line, delimiter);
%=========================================================================

% Split a line into tokens seperated by the delimiter
k=strfind(line, delimiter);

ik2=k'-1;
ik1(2:size(ik2,1)+1,1)=k'+1;
ik1(1,1)=1;
ik2(size(ik1,1),1)=size(line,2);

ik=1;
i1 = ik1(ik,1);
i2 = ik2(ik,1);
tokens{1}=deblank(line(i1:i2));
for ik=2:size(ik1,1)
    i1 = ik1(ik,1);
    i2 = ik2(ik,1);
    tokens{ik}=deblank(line(i1:i2));
end
```

PIVSUBTRACTION.M

```
%=========================================================================
function PIVFileCruncher
%=========================================================================

%*************************************************************************
%   PIVSubtraction.m     adapted by: Michael Dodson
%
%   Program prompts user for two .v3s PIV files, and interpolates vectors
%   to a uniform grid to allow for ease of processing.  After the files are
%   shifted to the global coordinate system, the second is subtracted from
%   the first and the resulting vector file is processed in the following
%   ways:
%
%   1.  Spanwise velocity distribution for region directly behind the
%   airfoil
%   2.  Calculate min, max, and average values and locations for velocity
%   magnitude and turbulence intensity for a bxb box in the airfoil region
%   3.  Calculate vorticity for bxb region
%
%   The data for spanwise velocity, and bxb velocity and turbulence
%   intensity are then output to Excel files under the names #_span_subt,
%   #_VelMag_subt, #_TurbInt_subt
%
%   The spanwise velocity, velocity magnitude, turbulence intensity, and
%   vorticity images are then rotated to match the upright tunnel, and
%   output to the screen
%
%   Process is only valid for vectors from the upper region of the wind
%   tunnel (this was the right side of the tunnel when rotated)
%
%   3MAY05
%*************************************************************************

clear all
clc

%******************
% Open and read file
%******************

%"shift" variable stores the distance to shift x to the global coordinate
%system

shift = 85.3848;

% Open dialog to get input filename.
[FileNameIn1,PathNameIn1] = uigetfile('*.v3s','Input File');
[FileNameIn2,PathNameIn2] = uigetfile('*.v3s','Input File');

% Turn input file into array of strings, one per line.
txt_file1 = textread(FileNameIn1,'%s','delimiter','\n');
txt_file2 = textread(FileNameIn2,'%s','delimiter','\n');
```

```
% Process the first line for information.
[data_run1, m1, n1, tokens1] = read_first_line(txt_file1{1});
[data_run2, m2, n2, tokens2] = read_first_line(txt_file2{1});

% Read the rest of the file.
for j=2:length(txt_file1)
        iline = j;
        text_line = txt_file1{iline};
        values = strread(text_line, '%f', 'delimiter', ',')';
        xin1(iline-1) = values(1)+shift; yin1(iline-1) = values(2);
zin1(iline-1) = values(3);
        uin1(iline-1) = values(4); vin1(iline-1) = values(5); win1(iline-1) =
values(6);
        countin1(iline-1) = values(7); respixin1(iline-1) = values(8);
        Reuvin1(iline-1) = values(9); Reuwin1(iline-1) = values(10);
Revwin1(iline-1) = values(11);
        ustdin1(iline-1) = values(12); vstdin1(iline-1) = values(13);
wstdin1(iline-1) = values(14);
        wturbin1(iline-1) = wstdin1(iline-1)/win1(iline-1);
        if (uin1(iline-1)>20)
            uin1(iline-1)=0;
        end
        if (vin1(iline-1)>20)
            vin1(iline-1)=0;
        end
        if (win1(iline-1)>20)
            win1(iline-1)=0;
        end
end

for j=2:length(txt_file2)
        iline = j;
        text_line = txt_file2{iline};
        values = strread(text_line, '%f', 'delimiter', ',')';
        xin2(iline-1) = values(1)+shift; yin2(iline-1) = values(2);
zin2(iline-1) = values(3);
        uin2(iline-1) = values(4); vin2(iline-1) = values(5); win2(iline-1) =
values(6);
        countin2(iline-1) = values(7); respixin2(iline-1) = values(8);
        Reuvin2(iline-1) = values(9); Reuwin2(iline-1) = values(10);
Revwin2(iline-1) = values(11);
        ustdin2(iline-1) = values(12); vstdin2(iline-1) = values(13);
wstdin2(iline-1) = values(14);
        wturbin2(iline-1) = wstdin2(iline-1)/win2(iline-1);
        if (uin2(iline-1)>20)
            uin2(iline-1)=0;
        end
        if (vin2(iline-1)>20)
            vin2(iline-1)=0;
        end
        if (win2(iline-1)>20)
            win2(iline-1)=0;
        end
end
```

```
%**********************
% Begin data processing
%**********************

%generate and interpolate data onto identical grids
[xg1,yg1] = meshgrid(-5:1:180, -90:1:90);
uout1 = griddata(xin1,yin1,win1,xg1,yg1);
uturb1 = griddata(xin1,yin1,wturbin1,xg1,yg1);

[xg2,yg2] = meshgrid(-5:1:180, -90:1:90);
uout2 = griddata(xin2,yin2,win2,xg2,yg2);
uturb2 = griddata(xin2,yin2,wturbin2,xg2,yg2);

%************************************
% Part 1: Subtract image 2 from image 1
%************************************

uout = uout1-uout2;
uturb = uturb1-uturb2;

%************************************************
% Part 2: Determine spanwise velocity distribution
%************************************************

%extract data from 16mm high rectangle behind the airfoil
%generates grid of area behind the airfoil and interpolates uout onto the
grid
%rectangle spans from -5 to 125 (x) and -8 to 8 (y)
[xw, yw] = meshgrid(-5:1:125, -8:1:8);
wake = griddata(-5:180,-90:90, uout, xw, yw);

%average each column along the span and save velocities in to Vspan
%Vmin and Vmax hold the min and max velocities and their respective span
%location

Vmin(1) = 0;
Vmax(1) = 0;
Vmin(2) = 100000;
Vmax(2) = 0;

for i=1:length(wake(1,:))
    Vspan(i) = mean(wake(:,i));
    if (-1*Vspan(i))>Vmax(2)
        Vmax(2) = Vspan(i);
        Vmax(1) = i-6;      %element 1 in wake corresponds to -5mm
    end
    if (-1*Vspan(i))<Vmin(2)
        Vmin(2) = Vspan(i);
        Vmin(1) = i-6;
    end
end
```

```
for i=1:length(wake(1,:))
    x(i)=i-6;   %store location in mm into x for plotting use
end

%*************************************************
% Part 2: Evaluate bxb box for min, max and avg values
%         of VelMag, Turbulence Intensity
%*************************************************

%Generate bxb grid with the airfoil in the center
%spanning -5 to 125 in x, 65 to -65 in y
[xb, yb] = meshgrid(-5:1:125, -65:1:65);

%interpolate VelMag and TurbInt data onto grid
Vbox = griddata(-5:180,-90:90, uout, xb, yb);
Turbbox = griddata(-5:180,-90:90, uturb, xb, yb);

%go through each element in box to determine min, max, and avg

count=1;
VsumB=0;
VmaxB(1) = 0;  %initialize xlocation
VmaxB(2) = 0;  %initialize ylocation
VmaxB(3) = 0;  %initialize Magnitude
VminB(1) = 0;
VminB(2) = 0;
VminB(3) = 100000;

TurbsumB=0;
TurbmaxB(1) = 0;  %initialize xlocation
TurbmaxB(2) = 0;  %initialize ylocation
TurbmaxB(3) = 0;  %initialize Magnitude
TurbminB(1) = 0;
TurbminB(2) = 0;
TurbminB(3) = 100000;

for i=1:length(Vbox(:,1))    %go through each row
    for j=1:length(Vbox(1,:))    %go through each column
        VsumB = VsumB + Vbox(i,j);
        TurbsumB = TurbsumB + Turbbox(i,j);

        if Vbox(i,j)>VmaxB(3)
            VmaxB(3) = Vbox(i,j);
            VmaxB(1) = j-6;      %element 1 in Vbox (x) corresponds to -5mm
and increases
            VmaxB(2) = i-57;     %element 1 in Vbox (y) corresponds to -56mm
and increases
        end
        if Vbox(i,j)<VminB(3)
            VminB(3) = Vbox(i,j);
            VminB(1) = j-6;      %element 1 in box (x) corresponds to -5mm
and increases
            VminB(2) = i-57;     %element 1 in box (y) corresponds to -56mm
and increases
```

```
        end

        if Turbbox(i,j)>TurbmaxB(3)
            TurbmaxB(3) = Turbbox(i,j);
            TurbmaxB(1) = j-6;      %element 1 in Turbbox (x) corresponds to
-5mm and increases
            TurbmaxB(2) = i-57;     %element 1 in Turbbox (y) corresponds to
-56mm and increases
        end
        if Turbbox(i,j)<TurbminB(3)
            TurbminB(3) = Turbbox(i,j);
            TurbminB(1) = j-6;      %element 1 in Turbbox (x) corresponds to
-5mm and increases
            TurbminB(2) = i-57;     %element 1 in Turbbox (y) corresponds to
-56mm and increases
        end
        count = count + 1;
    end
end

VavgB = VsumB/count;
TurbavgB = TurbsumB/count;

%*******************************************************
% Part 3: Calculate and plot Vorticity for entire region
%*******************************************************

uin = uin1-uin2;
vin = vin1-vin2;

u = griddata(xin1,yin1,uin,xg1,yg1);
v = griddata(xin1,yin1,vin,xg1,yg1);
cav = curl(xg1,yg1,u,v);

%***************************
% Output to Excel Spreadsheet
%***************************

filenum1 = strread(FileNameIn1,'%s %*s','delimiter','.');
filenum2 = strread(FileNameIn2,'%s %*s','delimiter','.');


%output spanwise velocity distribution to #_#_span.xls (first number is
%base image)
spanoutput(1,:) = {'Spanwise Location (mm)', 'Velocity (m/s)','Vmax location
(mm)',...
    'Vmax (m/s)','Vmin location (mm)','Vmin (m/s)'};
for i=1:length(x)
    spanoutput(i+1,1) = num2cell(x(i));   %store spanwise location
    spanoutput(i+1,2) = num2cell(Vspan(i)); %stores spanwise velocity
end
spanoutput(2,3:4) = num2cell(Vmax); %store Vmax
spanoutput(2,5:6) = num2cell(Vmin); %store Vmin
```

```
xlswrite(char(strcat(filenum1,'_',filenum2,'_span_subt')),spanoutput);

VelMagoutput(1,:) = {'Avg Vel (m/s)','Vmax x-location (mm)','Vmax y-location
(mm)',...
    'Vmax (m/s)','Vmin x-location (mm)','Vmin y-location (mm)','Vmin
(m/s)'};%

VelMagoutput(2,1) = num2cell(VavgB);
VelMagoutput(2,2) = num2cell(VmaxB(1));
VelMagoutput(2,3) = num2cell(VmaxB(2));
VelMagoutput(2,4) = num2cell(VmaxB(3));
VelMagoutput(2,5) = num2cell(VminB(1));
VelMagoutput(2,6) = num2cell(VminB(2));
VelMagoutput(2,7) = num2cell(VminB(3));

xlswrite(char(strcat(filenum1,'_',filenum2,'_VelMag_subt')),VelMagoutput);

TurbIntoutput(1,:) = {'Avg TurbInt','Max x-location (mm)','Max y-location
(mm)',...
    'Max Mag','Min x-location (mm)','Min y-location (mm)','Min Mag'};

TurbIntoutput(2,1) = num2cell(TurbavgB);
TurbIntoutput(2,2) = num2cell(TurbmaxB(1));
TurbIntoutput(2,3) = num2cell(TurbmaxB(2));
TurbIntoutput(2,4) = num2cell(TurbmaxB(3));
TurbIntoutput(2,5) = num2cell(TurbminB(1));
TurbIntoutput(2,6) = num2cell(TurbminB(2));
TurbIntoutput(2,7) = num2cell(TurbminB(3));

xlswrite(char(strcat(filenum1,'_',filenum2,'_TurbInt_subt')),TurbIntoutput);

%*************************
%  Rotate and Output Images
%*************************

%***************rotate full velocity image

n = length(uout(:,1));
for count=1:n
    urot(count,:) = uout(n+1-count,:);
end

figure(6): surf(yg1, xg1, urot, urot);
colormap jet;
axis equal tight;
%caxis([11,17]);
colorbar;
title('Full View Velocity (m/s)','FontName','times','FontSize',18)
xlabel('x (mm)','FontName','times','FontSize',18);
ylabel('y (mm)','FontName','times','FontSize',18);
shading interp;
az=0; el=90;
```

```
view(az,el);

%***************rotate VelMag image

n = length(Vbox(:,1));
for count=1:n
    Vboxrot(count,:) = Vbox(n+1-count,:);
end

figure(7): surf(yb, xb, Vboxrot, Vboxrot);
colormap jet;
axis equal tight;
caxis([-.8,.05]);
colorbar;
title('Velocity Magnitude (m/s)','FontName','times','FontSize',18)
xlabel('x (mm)','FontName','times','FontSize',18);
ylabel('y (mm)','FontName','times','FontSize',18);
shading interp;
az=0; el=90;
view(az,el);

%***************rotate Turbulence image

n = length(Turbbox(:,1));
for count=1:n
    Turbboxrot(count,:) = Turbbox(n+1-count,:);
end

figure(8): surf(yb, xb, Turbboxrot, Turbboxrot);
colormap jet;
axis equal tight;
caxis([-.025,.02]);
colorbar;
title('Turbulence Intensity','FontName','times','FontSize',18)
xlabel('x (mm)','FontName','times','FontSize',18);
ylabel('y (mm)','FontName','times','FontSize',18);
shading interp;
az=0; el=90;
view(az,el);

%***************rotate vorticity image

n = length(cav(:,1));
for count=1:n
    cavrot(count,:) = cav(n+1-count,:);
end
figure(9)
pcolor(yg1,xg1,cavrot); shading interp
title('Vorticity (rad/s)','FontName','times','FontSize',18)
xlabel('x (mm)','FontName','times','FontSize',18);
ylabel('y (mm)','FontName','times','FontSize',18);
caxis([-.15,.2]);
colorbar;
colormap jet;
```

```
%***************rotate spanwise velocity image

%plot Vspan v. y location and display min and max V
figure(10)
plot(Vspan, x)
title('Spanwise Velocity (m/s)','FontName','times','FontSize',18)
ylabel('Spanwise location (y mm)','FontName','times','FontSize',18)
xlabel('Velocity (m/s)','FontName','times','FontSize',18)

%=========================================================================
function [data_run, m, n, tokens] = read_first_line(first_line)
%=========================================================================

% Split the first line at the equal signs
tokens = split_string(first_line,'=');

% The 1st token has the word title, don't need that.
% The 2nd token has the file name, and the word variables.
% Extract the file name by splitting the 2nd token at the quotations.
% Then, pull out the run number (specific to DD-963 testing during summer
2004.
tokens_2 = split_string(tokens{2},'"');
run_data_file = tokens_2{2};
ipos = strfind(run_data_file, 'Run');
data_run = run_data_file(ipos:ipos+6);

% The 5th token has the number of rows
tokens_5 = split_string(tokens{5},',');
m = str2num( cell2mat( tokens_5(1) ) );

% The 6th token has the number of columns
tokens_6 = split_string(tokens{6},',');
n = str2num( cell2mat( tokens_6(1) ) );

% Skip the rest of the information on the first line

%=========================================================================
function first_line = write_first_line(data_run, m, n, tokens)
%=========================================================================

% Paste the first line back together and add the equal signs.
numtokens = length(tokens);
first_line = char(tokens(1));
for it = 2:numtokens
    first_line = strcat( first_line, '=', char(tokens(it)) );
end

%=========================================================================
function tokens = split_string(line, delimiter);
%=========================================================================

% Split a line into tokens seperated by the delimiter
```

```
k=strfind(line, delimiter);

ik2=k'-1;
ik1(2:size(ik2,1)+1,1)=k'+1;
ik1(1,1)=1;
ik2(size(ik1,1),1)=size(line,2);

ik=1;
i1 = ik1(ik,1);
i2 = ik2(ik,1);
tokens{1}=deblank(line(i1:i2));
for ik=2:size(ik1,1)
    i1 = ik1(ik,1);
    i2 = ik2(ik,1);
    tokens{ik}=deblank(line(i1:i2));
end
```

PIVCENTERLINE.M

```
%=========================================================================
function PIVFileCruncher
%=========================================================================

%*************************************************************************
%   PIVCenterline.m     adapted by: Michael Dodson
%
%   Program prompts user for a .v3s PIV file, and interpolates vectors to a
%   uniform grid to allow for ease of processing.  After the files are
%   shifted to the global coordinate system, the script rips out and
%   processes the vertical and horizontal centerline data for comparison to
%   flow surveys
%
%   The script outputs to #_vertCL.xls and #_horizCL.xls
%
%   NOTE:  The images were obtained with the tunnel rotated on its side, so
%   a vertical survey moves along the image x-axis and a horizontal survey
%   moves along the image y-axis
%
%   3MAY05
%*************************************************************************

clear all
clc

%*******************
% Open and read file
%*******************

%"shift" variable stores the distance to shift x to the global coordinate
%system

shift = 85.3848;

% Open dialog to get input filename.
[FileNameIn,PathNameIn] = uigetfile('*.v3s','Input File');

% Turn input file into array of strings, one per line.
txt_file = textread(FileNameIn,'%s','delimiter','\n');

% Process the first line for information.
[data_run, m, n, tokens] = read_first_line(txt_file{1});

% Read the rest of the file.
for j=2:length(txt_file)
        iline = j;
        text_line = txt_file{iline};
        values = strread(text_line, '%f', 'delimiter', ',')';
        xin(iline-1) = values(1)+shift; yin(iline-1) = values(2); zin(iline-
1) = values(3);
```

```
        uin(iline-1) = values(4); vin(iline-1) = values(5); win(iline-1) =
values(6);
        countin(iline-1) = values(7); respixin(iline-1) = values(8);
        Reuvin(iline-1) = values(9); Reuwin(iline-1) = values(10);
Revwin(iline-1) = values(11);
        ustdin(iline-1) = values(12); vstdin(iline-1) = values(13);
wstdin(iline-1) = values(14);
        if (uin(iline-1)>20)
            uin(iline-1)=0;
        end
        if (vin(iline-1)>20)
            vin(iline-1)=0;
        end
        if (win(iline-1)>20)
            win(iline-1)=0;
        end
end

%**********************
% Begin data processing
%**********************

%generate and interpolate data onto grid
[xg,yg] = meshgrid(-5:1:180, -90:1:90);
uout = griddata(xin,yin,win,xg,yg);

%*********************************************************
% Part 1: Determine vertical spanwise velocity distribution
%*********************************************************

%extract data from 16mm wide rectangle along entire vertical span of image
%generates grid of rectangle and interpolates uout onto the grid
%rectangle spans from -5 to 180 (x) and -8 to 8 (y)
[xw, yw] = meshgrid(-5:1:180, -8:1:8);
wake = griddata(-5:180,-90:90, uout, xw, yw);

%average each column along the span and save velocities in to Vspan
%Vmin and Vmax hold the min and max velocities and their respective span
%location

Vmin(1) = 0;
Vmax(1) = 0;
Vmin(2) = 100000;
Vmax(2) = 0;

for i=1:length(wake(1,:))
    Vspan(i) = mean(wake(:,i));
    if Vspan(i)>Vmax(2)
        Vmax(2) = Vspan(i);
        Vmax(1) = i-6;      %element 1 in wake corresponds to -5mm
    end
    if Vspan(i)<Vmin(2)
        Vmin(2) = Vspan(i);
        Vmin(1) = i-6;
```

```
    end
end

for i=1:length(wake(1,:))
    y(i)=i-6;   %store location in mm into y for plotting use
end

%plot Vspan v. y (to match vertical flow survey)
figure(1)
plot(Vspan, y)
title('Vertical Survey')
xlabel('Velocity (m/s)','FontName','times','FontSize',18)
ylabel('Spanwise location (x mm)','FontName','times','FontSize',18)

%nondimensionalize y and Vspan using ymax = 411mm and Vmax
VspanND = Vspan/Vmax(2);
yND = y/411;

%plot VspanND v. yND (to match vertical flow survey)
figure(2)
plot(VspanND, yND)
title('Non Dimensional Vertical Survey')
xlabel('Velocity (V/Vmax)','FontName','times','FontSize',18)
ylabel('Spanwise location (y/H)','FontName','times','FontSize',18)


%*************************************************************
% Part 2: Determine horizontal spanwise velocity distribution
%*************************************************************

%extract data from 10mm high rectangle across entire horizontal span of image
%generates grid of rectangle and interpolates uout onto the grid
%rectangle spans from -5 to 5 (x) and -90 to 90 (y)

[xh, yh] = meshgrid(-5:1:5, -90:1:90);
wakeh = griddata(-5:180,-90:90, uout, xh, yh);

%average each column along the span and save velocities in to Vspanh
%Vminh and Vmaxh hold the min and max velocities and their respective span
%location

Vminh(1) = 0;
Vmaxh(1) = 0;
Vminh(2) = 100000;
Vmaxh(2) = 0;

for i=1:length(wakeh(1,:))
    Vspanh(i) = mean(wakeh(:,i));
    if Vspanh(i)>Vmaxh(2)
        Vmaxh(2) = Vspanh(i);
        Vmaxh(1) = i-6;      %element 1 in wake corresponds to -5mm
    end
    if Vspanh(i)<Vminh(2)
```

```
        Vminh(2) = Vspanh(i);
        Vminh(1) = i-6;
    end
end

for i=1:length(wakeh(1,:))
    x(i)=i-6;   %store location in mm into x for plotting use
end

%plot x v. Vspanh (to match horizontal flow survey)
figure(3)
plot(x, Vspanh)
title('Horizontal Survey')
xlabel('Spanwise location (x mm)','FontName','times','FontSize',18)
ylabel('Velocity (m/s)','FontName','times','FontSize',18)

%nondimensionalize x and Vspanh using xmax = 412mm and Vmaxh
VspanhND = Vspanh/Vmaxh(2);
xND = x/411;

%plot xND v. VspanhND (to match vertical flow survey)
figure(4)
plot(xND, VspanhND)
title('Non Dimensional Horizontal Survey')
xlabel('Spanwise location (x/Xmax)','FontName','times','FontSize',18)
ylabel('Velocity (V/Vmax)','FontName','times','FontSize',18)

%***************************
% Output to Excel Spreadsheet
%***************************

%output spanwise velocity distribution to #_vertCL.xls and #_horizCL.xls
spanoutput(1,:) = {'Spanwise Location (mm)','ND Spanwise location', 'Velocity
(m/s)'...
    ,'ND Velocity','Vmax location (mm)','Vmax (m/s)','Vmin location
(mm)','Vmin (m/s)'};
spanoutputh(1,:) = spanoutput(1,:);

for i=1:length(y)
    spanoutput(i+1,1) = num2cell(y(i));   %store spanwise location
    spanoutput(i+1,2) = num2cell(yND(i));   %store ND spanwise location
    spanoutput(i+1,3) = num2cell(Vspan(i)); %stores spanwise velocity
    spanoutput(i+1,4) = num2cell(VspanND(i)); %stores ND spanwise velocity
end
spanoutput(2,5:6) = num2cell(Vmax); %store Vmax
spanoutput(2,7:8) = num2cell(Vmin); %store Vmin

filenum = strread(FileNameIn,'%s %*s','delimiter','.');

xlswrite(char(strcat(filenum,'_vertCL')),spanoutput);

for i=1:length(x)
    spanoutputh(i+1,1) = num2cell(x(i));   %store spanwise location
```

```
    spanoutputh(i+1,2) = num2cell(xND(i));   %store ND spanwise location
    spanoutputh(i+1,3) = num2cell(Vspanh(i)); %stores spanwise velocity
    spanoutputh(i+1,4) = num2cell(VspanhND(i)); %stores ND spanwise velocity
end
spanoutputh(2,5:6) = num2cell(Vmaxh); %store Vmax
spanoutputh(2,7:8) = num2cell(Vminh); %store Vmin

xlswrite(char(strcat(filenum,'_horizCL')),spanoutputh);

%=========================================================================
function [data_run, m, n, tokens] = read_first_line(first_line)
%=========================================================================

% Split the first line at the equal signs
tokens = split_string(first_line,'=');

% The 1st token has the word title, don't need that.
% The 2nd token has the file name, and the word variables.
% Extract the file name by splitting the 2nd token at the quotations.
% Then, pull out the run number (specific to DD-963 testing during summer
2004.
tokens_2 = split_string(tokens{2},'"');
run_data_file = tokens_2{2};
ipos = strfind(run_data_file, 'Run');
data_run = run_data_file(ipos:ipos+6);

% The 5th token has the number of rows
tokens_5 = split_string(tokens{5},',');
m = str2num( cell2mat( tokens_5(1) ) );

% The 6th token has the number of columns
tokens_6 = split_string(tokens{6},',');
n = str2num( cell2mat( tokens_6(1) ) );

% Skip the rest of the information on the first line

%=========================================================================
function first_line = write_first_line(data_run, m, n, tokens)
%=========================================================================

% Paste the first line back together and add the equal signs.
numtokens = length(tokens);
first_line = char(tokens(1));
for it = 2:numtokens
    first_line = strcat( first_line, '=', char(tokens(it)) );
end

%=========================================================================
function tokens = split_string(line, delimiter);
%=========================================================================

% Split a line into tokens seperated by the delimiter
k=strfind(line, delimiter);
```

```
ik2=k'-1;
ik1(2:size(ik2,1)+1,1)=k'+1;
ik1(1,1)=1;
ik2(size(ik1,1),1)=size(line,2);

ik=1;
i1 = ik1(ik,1);
i2 = ik2(ik,1);
tokens{1}=deblank(line(i1:i2));
for ik=2:size(ik1,1)
    i1 = ik1(ik,1);
    i2 = ik2(ik,1);
    tokens{ik}=deblank(line(i1:i2));
end
```

REFERENCES

"1901 Lift Balance." Wright Aeroplane Company. n.d.. <http://www.first-to-fly.com> (30 Nov 2004).

"Image – Wind Tunnel Data Graph." Franklin Institute Aeronautical Engineering Collection. n.d. <http://sln.fi.edu/> (30 Nov 2004).

"Image – Wind Tunnel Data Graph." Franklin Institute Aeronautical Engineering Collection. n.d. <http://sln.fi.edu/> (30 Nov 2004).

"The 1899 Wright Kite." Wright Aeroplane Company. n.d. <http://www.first-to-fly.com> (30 Nov 2004).

"The 1900 Wright Glider." Wright Aeroplane Company. n.d. <http://www.first-to-fly.com> (30 Nov 2004).

"The 1901 Wind Tunnel and balances." Wright Aeroplane Company. n.d. <http://www.first-to-fly.com> (30 Nov 2004).

"The 1901 Wright Glider." Wright Aeroplane Company. n.d. <http://www.first-to-fly.com> (30 Nov 2004).

"The 1903 Wright Flyer 1." Wright Aeroplane Company. n.d. <http://www.first-to-fly.com> (30 Nov 2004).

"The 1903 Wright Flyer 1." Wright Aeroplane Company. n.d. <http://www.first-to-fly.com> (30 Nov 2004).

"Wind Tunnel End View." Wright Aeroplane Company. n.d. <http://www.first-to-fly.com> (30 Nov 2004).

"Wind Tunnel Front." Wright Aeroplane Company. n.d. <http://www.first-to-fly.com> (30 Nov 2004).

Anderson, Jr., John D. A History of Aerodynamics and Its Impact on Flying Machines. New York: Cambridge University Press, 1997.

Barlow, Jewel B., William H. Rae, Jr., and Alan Pope. Low-Speed Wind Tunnel Testing: Third Edition. New York: John Wiley & Sons, Inc., 1999.

Britcher, Colin P., Drew Landman, Robert Ash, Kevin Kochersberger, and Ken Hyde. "Predicted Flight Performance of the Wright 'Flyer' Based on Full-Scale Tunnel Data." AIAA Paper 2004-0104, Jan. 2004.

Britcher, Colin P., Rafaello Mariani, Pat Craig, Jill Gillespie, Mudit Monsi, Darius Luna, and Mark Sykes. "Analysis of the Wright Brothers Wind Tunnel and Design of an Educational Derivative." AIAA Paper 2004-1141, Jan. 2004.

Britcher, Colin P., Robert L. Ash, and Ken Hyde. "An Analysis of Flight Number 4: December 17, 1903." Presentation made by Department of Aerospace Engineering at Old Dominion University in conjunction with The Wright Experience, n.d.

Chanute, Octave. "Letter to George C. Spratt." 24 Dec 1898. Library of Congress, Manuscripts Division. Personal correspondence (05 Aug 04).

Chanute, Octave. Progress in Flying Machines. New York: Dover Publications, Inc., 1997.

Cherne, Jack, Fred E. C. Culick, and Pete Zell. "The AIAA 1903 Wright 'Flyer' Project Prior to Full-Scale Tests at NASA Ames Research Center." AIAA Paper 2000-0511, Jan 2000.

Culick, Fred E. C. "The Wright Brothers: First Aeronautical Engineers." AIAA Paper 2001-3385, Jul. 2001.

Culick, Fred E.C. "What the Wright Brothers Did and Did Not Understand About Flight Mechanics—In Modern Terms." AIAA Paper 2001-3385, Jul. 2001.

Dees, Paul. "How Gliders Helped the Wright Brothers Invent the Airplane." AIAA Paper 2003-95, Jan. 2003.

Deters, Robert W., Benjamin A. Broughton, and Michael S. Selig. "A Retrospective: Development of Simulation Models for the 1902 and 1905 Wright Flyers." AIAA Paper 2004-0211, Jan. 2004.

Gibbs-Smith, Charles H.. Aviation: An Historical Survey from its Origins to the end of World War II. London: Her Majesty's Stationary Office, 1970.

Hooven, Frederick J. "The Wright Brothers' Flight-Control System." Scientific American, November 1978, 166.

Jakab, Peter L., and Rick Young, ed. The Published Writings of Wilbur and Orville Wright. Washington: Smithsonian Institute Press, 2000.

Jakab, Peter. Visions of a Flying Machine. Washington: Smithsonian Institution Press, 1990.

Jex, Henry R., Richard Grimm, John Latz, and Craig Hange. "Full-Scale 1903 Wright Flyer Wind Tunnel Test Results from the NASA Ames Research Center." AIAA Paper 2000-0512, Jan. 2000.

Kelly, Fred C., ed. How We Invented The Airplane. New York: David McKay Company, Inc., 1953.

Kochersberger , Kevin, Drew Landman, Jenn Player, and Ken Hyde. "An Evaluation of the Wright 1902 Glider Using Full Scale Wind Tunnel Data." AIAA Paper 2003-0096, Jan. 2003.

Kochersberger, Kevin, Colin P. Britcher, N. Crabill, K. Dominguez, Jenn Player, and Ken Hyde. "Flying Qualities of the Wright 1903 Flyer: From Simulation to Flight Test." AIAA Paper 2004-0105, Jan. 2004.

Kochersberger, Kevin, Robert Ash, Colin Britcher, Drew Landman, and Ken Hyde. "Evaluation of the Wright 1901 Glider Using Full-Scale Wind-Tunnel Data." Journal of Aircraft 40, no. 3 (2003): 417-424.

Kochersberger, Kevin, Robert Ash, Robert Sandusky, and Ken Hyde. "An Evaluation of the Wright 1901 Glider Using Full Scale Wind Tunnel Data." AIAA Paper 2002-1134, Jan. 2002.

Landman, Drew, Julian Alvarez, Robert Ash, Spiros Blackburn, and Ken Hyde. "Wind-Tunnel Testing of the Wright Brothers' Moder B Airfoil." Journal of Aircraft 39, no. 1 (2002): 30-36.

McFarland, Marvin W., ed.. The Papers of Wilbur and Orville Wright. Vol. 1. New York: McGraw-Hill Book Company, Inc., 1953.

McRuer, Duane, and Dunstan Graham. "Flight Control Century: Triumphs of the Systems Approach." Journal of Guidance, Control, and Dynamics 27. No. 2. March-April 2004, 161-173.

Means, James, ed. The Aeronautical Annuals – 1896. Boston: W. B. Clarke & Co., 1896.

Papachristodoulou, A. N., and F. E. C. Culick. "Flight Mechanics of the Wright Aircraft 1903-1912." AIAA Paper 2003-0097. Jan. 2003.

Pinella, David, and Richard Branch. "Calibration of the Wright Brothers' 1901 Lift Balance." Presentation made at the National Air and Space Museum, Smithsonian Institution, 2004.

Spratt, George C. "Letter to Octave Chanute." 20 Apr 1900. Library of Congress, Manuscripts Division. Personal correspondence (05 Aug 04).

Wolko, Howard S., ed. The Wright Flyer: An Engineering Perspective. Washington: Smithsonian Institution, 1987.

Wolko, Kurt. "Wright 1901 Wind Tunnel." Plans drawn for the National Air and Space Museum, Smithsonian Institution (1983).

Wright, Wilbur. "Letter to George C. Spratt." 19 Oct 1901. Library of Congress, Manuscripts Division. Personal correspondence (05 Aug 04).

Wright, Wilbur. "Letter to George C. Spratt." 15 Dec 1901. Library of Congress, Manuscripts Division. Personal correspondence (05 Aug 04).

Wright, Wilbur. "Letter to George C. Spratt." 12 Nov 1902. Library of Congress, Manuscripts Division. Personal correspondence (05 Aug 04).

Wright, Wilbur. "Letter to George C. Spratt." 28 Jun 1903. Library of Congress, Manuscripts Division. Personal correspondence (05 Aug 04).